The recovery of valuable base metals from electronic waste using a biological matrix extracted from Black soldier flies

Thesis submitted for the fulfilment of the degree of Master of Science in Engineering specialising in Chemical engineering

University of Cape Town

2019

Submitted by: Thabo Mabuka

Main Supervisor: Dr. Elaine Govender-Opitz

Co-Supervisor: Prof. Susan T.L. Harrison

Plagiarism declaration

"I know the meaning of plagiarism and declare that all the work in the document, save for that which is properly acknowledged, is my own. This thesis/dissertation has been submitted to the Turnitin module (or equivalent similarity and originality checking software) and I confirm that my supervisor has seen my report and any concerns revealed by such have been resolved with my supervisor."

Signed by candidate

Signature

Acknowledgements

I would like to thank CSIR for the initiative and funding of this project. I would also like to thank Prof Sue Harrison for allowing me to be part of this project and whose consideration gave way to countless growth in the biotechnological field. I thank my parents, Isaac and Katazile Mabuka for their constant support in my journey of education and my brothers, Simon and Rethusaneng for their fellowship. I thank my sister, Pearl Mamabolo whose presence made my stay at UCT feel at home. I would like to thank my main supervisor Dr Elaine Govender-Opitz whose support and supervision I will always treasure. She provided the resources for the accomplishment of this work and gave wholeheartedly to the objectives of this project. Her vision and ideas contributed immensely to the establishment of this dissertation. I thank the Centre for Bioprocessing Engineering (CeBER) staff, whose individual roles played a crucial role in this work. I would like to thank the CeBER laboratory managers at the time, Tichaona Samkange and Emmanuel I-Muaka Ngoma. Lastly, I would like to thank my partner, Tlaleng Lemeke for her constant support and motivation during this dissertation. Her love and support contributed immensely to my mental and social wellbeing. In honour of the contribution by my supervisor, Dr Elaine Govender-Opitz and CeBER, the bio sorbents produced in this dissertation are named after them. This work is submitted in honour of my grandmother, Emma Mabuka whose life I draw inspiration from.

Abstract

Waste streams have increased due to advancements in technology and the increase in the global population, requiring innovative strategies to recover value from them whilst reducing their negative environmental impact and human health hazards. Thus, the increase in waste has led to research focused on circular economies. E-waste is the fastest growing waste stream in the world containing valuable metals that exceed those rich in ore from mines. In Africa, e-waste metal recycling remains largely informal and small scale resulting in inefficient metal recovery, increased negative environmental impact and human health hazards. E-waste metal recycling using pyrometallurgy is limited to secondary smelter feed and there are limited industrial plants dedicated solely for this purpose. While in hydrometallurgy, research in e-waste metal recycling has been largely focused on metal extraction whilst downstream metal recovery processing studies are limited. The strategy often employed in e-waste metal recovery via hydrometallurgy is base metal (BM) extraction before precious metal (PM) recovery due to the high concentration of these metals in e-waste. This results in the production of base metal-rich-leachate solutions. The heterogeneity of these leachate solutions and the high cost of downstream processing requires a multi-disciplinary approach that considers metal recovery selectivity and associated costs. Natural sorbents, chitin and chitosan found in large quantities in industrial food waste and precipitation with sulphides have received much attention due to their high metal recovery efficiencies, metal selectivity, scalable operation and low costs. Chitin and chitosan are mainly sourced from crustacean shell waste and there are limited techno-economic studies on the extraction and production methodology of these polymers. Chitin and chitosan from Black Soldier Fly (BSF) larvae shells, a waste product from BSF farming, is thought to have high adsorptive properties due to their low crystalline index. However, studies on metal adsorption onto chitin and chitosan sourced from BSF larvae and their potential combined application with sulphide precipitation to recover metals from e-waste leachate solutions remains limited. Therefore, the dissertation aimed to develop a cost-effective method of extracting chitin and chitosan from BSF larvae shell waste and investigated the techno-economic feasibility of the application of these polymers in combination with sulphide precipitation for the recovery of base metals from e-waste leachate solutions. The potential application of chitin/chitosan from BSF larvae in e-waste metal recovery may result in a circular economy where solid waste is utilized to produce BSF larvae. While the BSF larvae shell waste generated from BSF larvae production can be used to remediate electronic waste, recovering value from these waste streams while reducing their environmental impact.

The cost-effective method for the extraction of chitin and production of chitosan from BSF larvae was investigated by a study into the effects of demineralisation, deproteination, decolourisation, de-acetylation processes on the chitin and chitosan character, metal adsorption performance and techno-economics. Chitin and chitosan were extracted and produced from BSF larvae (*Hermetia illucens*) using a combination of the processes stated prior. Adsorption studies with the produced chitin and chitosan were conducted on base metals ferrous, ferric, copper and aluminium ions in single and bimetal solutions. The adsorbed metals were then eluted using 0.1 M H_2SO_4.

Precipitation studies were also conducted with various concentrations of copper in a ferrous, copper and aluminium solution. The techno-economic feasibility of the application of the chitin and chitosan and sulphide precipitation with NaHS in PCB leachate solutions was investigated by the development of a model based on the ascertained individual metal recovery performance in the adsorption and precipitation studies.

Extracted chitin from BSF larvae was found to be in the alpha form. 4-hour Deproteination of the BSF larvae after liberation with 4 wt % NaOH and de-acetylation of the deproteinated chitin with 40 wt% NaOH was found to produce chitin and chitosan with the highest metal sorption capacities and lowest cost of production. The maximum adsorption capacity for ferrous, ferric, copper and aluminium ions onto chitin from BSF larvae was 2.29 ± 0.0001 mmol/g, 2.07 ± 0.0001 mmol/g, 1.69 ± 0.0001 mmol/g and 1.82± 0.0001 mmol/g respectively. While for chitosan, the maximum adsorption capacity for ferric, copper and aluminium ions was 0.951 ± 0.0012 mmol/g, 1.16 ± 0.0016 mmol/g and 0.961± 0.0013 mmol/g respectively. The order of metal adsorption selectivity for ferrous, ferric, copper and aluminium on chitin from BSF larvae was determined to be $Fe^{2+}>Fe^{3+}>Al^{3+}>Cu^{2+}$. While for chitosan it was determined to be $Cu^{2+}>Fe^{3+}>Al^{3+}$ and at a low pH (below pH of 2) it was observed to be $Cu^{2+}>Al^{3+}>Fe^{3+}$. Ferrous ion oxidation to ferric ions was observed during the adsorption of ferrous ions onto the chitin and chitosan. Adsorption of the metals onto chitin and chitosan were best modelled by the Freundlich isotherm and Pseudo 2nd order kinetic model. The adsorption on both polymers was found to be spontaneous, favourable, chemisorption and predominantly surface complexation. Sulphide precipitation with NaHS was observed to be selective towards copper precipitation however co-precipitation with aluminium occurred. The application of chitin and chitosan on the multi-metal synthetic PCB leachate solution resulted in the production of two refined streams respectively. The application of NaHS precipitation seems to be more feasible on the refined streams produced by the application of chitin. The combined application of NaHS and chitin from BSF larvae on the multi-metal synthetic PCB leachate solution showed economic feasibility. The recovery costs were $ 116 per kg metal recovered and an overall gross profit of $ 933/ kg metal recovered. However further economic studies which include consideration of capital costs need to be conducted to conclusively determine the economic feasibility of this downstream metal recovery process.

This study shows the potential of chitin and chitosan extracted from BSF larvae to upgrade PCB metal leachate solutions for further downstream processing.

Contents

List of Figures

List of Tables

Glossary of Terms

Circular economics-The reuse of products and waste rather than disposal.

Electronic waste- Formally referred to as WEEE and generally, as e-waste, is disposed of electrical and electronic equipment (EEE).

Extraction/upgrading-In this dissertation refers to the extraction of metals from e-waste into a solution. This is achieved using mechanical, pyrometallurgy, hydrometallurgy and bio-hydrometallurgy.

Hydrometallurgy-The use solution-based chemistry to recover metals from ores and concentrates.

Refining/recovery- In this dissertation, this refers to the recovery of metals from solutions into valuable products.

Pyrometallurgy-The use of high temperatures to extract and recover metals.

Chemical leaching-The process of extracting a soluble constituent from a solid using chemical solvents.

Bio-hydrometallurgy/Bioleaching-The exploitive use of some attributes of micro-organism to facilitate the leaching of metals into solution.

The downstream processing-The final stage in the value recovery process often involving separation and recovery of products to valuable forms.

Sorption-A physio-chemical and metabolic independent process based on mechanisms such as absorption, adsorption, ion exchange, surface complexation and precipitation.

Adsorption-An interface phenomenon which involves the change in concentration of a given substance at the interface with respect to neighbouring phases.

Biosorption-The sorption onto biomass.

Absorption- The process during sorption when sorbate molecules penetrate the bulk of the solid phase.

Commercial Sorbents-Sorbents produced commercially on large scale such as activated carbon, silica gel, magnetic adsorbents and alumina.

Bio sorbents-Biomass capable of sorption processes.

Chitin-A linear basic polysaccharide poly-(1-4)-2-acetamido-2-deoxy-D-glucopyranose (N-acetyl-D-glucosamine) with a molecular formula of $(C_8H_{13}O_5N)_n$, found in fungal cell walls, crustacean shells and insect cuticle.

Chitosan-The deacetylated product of chitin

Acronyms and Abbreviations

BM-Base metal

PM-Precious metal

REE-Rare-earth element

BSF-Black soldier fly

WEEE-Waste electrical and electronic equipment

EEE-Electrical and electronic equipment

PCB-Printed circuit board

CRT-Cathode ray tube

SMME-Small to medium and micro enterprise

HFR-Halogenated flame retardants

CSIR-Council for Scientific and Industrial Research

SX-EW-Solvent extraction and electrowinning

DA-Degree of acetylation

DD-Degree of de-acetylation

pH-Power of hydrogen ions

RoHS-Restriction of hazardous substances

FLS-Fly larvae shell

FTIR-Fourier transform infrared spectroscopy

SD-Standard Deviation

R-Correlation coefficient

r.t.p-Room temperature and pressure

Chapter 1: Introduction

1.1 Background

1.1.1 Waste Streams and Circular Economies

Waste streams such as food industrial waste, solid waste, and waste electrical and electronic equipment (WEEE, e-waste) have increased due to advancements in technology and an increase in the global population (Bourguignon, 2015). Food industrial waste and solid waste is expected to grow by 40.2 % and 50.7 % respectively by 2050 from 887 and 1 050 million tonnes per year in 2016 (Kaza et al., 2018). According to Baldé et al. (2017), the global production of e-waste was about 44.7 million tonnes in 2017 and this amount is expected to reach 52.2 million tonnes in 2021. The common strategy for dealing with waste streams is by reduction, reuse or recycling and disposal (Arushanyan et al., 2017). 40 % of Global waste is disposed of in landfills and open dumps while 11 % is processed by modern incineration. In low-income countries such as those found in Africa, almost 93 % of the waste is burnt or disposed of in open dumps (Kaza et al., 2018). Landfilling and incineration results in loss of value and have negative effects on the environment and human health (World Economic Forum, 2018).

The increase in product consumption and waste has led to a focus towards a circular economy to counteract the effects of this growth, where a circular economy involves the reuse of products and waste rather than disposal. Circular economies are regarded as a sustainable way of producing products (United Nations, 2018). They result in the reduction of waste, environmental impact and recovery value. Circular economies are particularly important for developing economies due to the cost reduction and value recovery from material and energy recycling (Preston et al., 2019). The benefits of viewing waste as resources and considering circular economies in value recovery from waste can be seen from examples such as the production of biogas from municipal waste and food industrial waste; and the production of fish-rock fertiliser from seafood industrial waste. Municipal and food waste disposed of in open dumps and landfills results in the blockage of drainages, mineral-rich leachates that pollute groundwater, cause eutrophication in water sources, breeding of disease carriers such as rats and flies and production of liquid and fumes such as methane and hydrogen sulphide (Ejaz et al., 2010). The minerals in food industrial waste such as in seafood waste can be used to produce fish rock fertiliser by hydrolysis (Knuckey et al., 2004) while the gas production in food industrial waste can be accelerated to generate biogas and bioethanol by anaerobic digestion (Li & Khraisheh, 2007; Kerroum et al., 2012). This allows for value recovery from the waste in the form of material and energy while reducing this waste in landfills and open dumps and its associated environmental impact and human health hazard.

E-waste is disposed of electrical and electronic equipment (EEE) (Khaliq et al., 2014). It is a relatively new waste, emerging in the 20th century due to the innovation and development of EEE. E-waste has received much attention due to it being the fastest growing waste stream in the world and its metal content (Baldé et al., 2017). Africa has the fastest rate of growth of e-waste generation in the world due to the short life span of imported EEE (Schluep et al., 2011; Baldé et

al., 2017). Base metals (BM), precious metals (PM) and rare-earth elements (REEs) in e-waste are highly concentrated and valuable and their concentrations maybe more than that currently extracted from mined ores (Yunus & Sengupta, 2016). For example, the average copper grade in China was 0.8 % in 2016 while the content of copper in printed circuit boards (PCBs) is usually more than 20% (Xu et al., 2016). Printed Circuit Boards (PCBs) contain the highest concentrations of metals in e-waste. Legacy e-waste in landfills produces contaminated leachates, which pollute ground water in poorly managed landfills, whilst the incineration of e-waste results in the emission of toxic fumes and gases (Rao, 2014). Due to the environmental risk they pose and the expected decline in ore grades, aging of mines and depletion of global metals reserves (Lehohla, 2015; Baxter, 2016), e-waste has become a primary focus for metal recycling (Legarth et al., 1995). However, although there is incentive for e-waste recycling, it remains limited due to lack of centralisation and the heterogenous nature of this waste (Cui & Zhang, 2008). In addition, technologies that recover value from e-waste, with minimum resulting waste are limited.

The strategy to deal with e-waste must aim to neutralize the environmental and social impact while recovering economic value. Most African countries are developing economies with low capital investment (Nayyar, 2009; African Development Bank, 2018) and lack the funds and infrastructure to deal with e-waste (Luda, 2011). This has led to poor centralisation of e-waste volumes, with the low volumes only processed in small scale operations such as Small to Medium and Micro Enterprises (SMME) (Schluep, Wasswa, et al., 2008; Amoyaw-Osei et al., 2011; Schluep et al., 2011; Ogungbuyi et al., 2012; Lydall et al., 2017). Centralisation of e-waste to create large scale operations for e-waste metal recovery requires infrastructure development and takes a considerable amount of time to complete (Cui & Zhang, 2008). This also needs a high capital investment. As such, supporting and developing SMMEs in the African waste industry is currently considered to be the cheaper, more practical and socially integrative approach to improve e-waste processing (Schluep, Rochat, et al., 2008). However, this approach requires scalable technological solutions for the treatment of e-waste for value recovery. (Kavitha, 2014).

1.1.2 E-waste Metal Extraction and Recovery

E-waste metal recovery in Africa is largely informal involving the incineration of material to expose the metals (Schluep, Wasswa, et al., 2008; Amoyaw-Osei et al., 2011; Schluep et al., 2011; Ogungbuyi et al., 2012; Lydall et al., 2017) this is largely done in waste dumps such as the one in Accra, Ghana (Kuper & Hojsik, 2008; Amoyaw-Osei et al., 2011). This approach, not only does it involve high occupational hazards (Kuper & Hojsik, 2008) but only has 50 % efficiency in the recovery of base metals. Most of the high-value metals such as gold, palladium and rare earth elements (REE) are left behind (Dahroug, 2004; Schluep, Wasswa, et al., 2008; Amoyaw-Osei et al., 2011; Ogungbuyi et al., 2012).

Metal recycling of e-waste is divided into three categories which are pre-processing/disassembly, extraction/upgrading and refining/recovery. Due to the heterogeneity of e-waste, pre-processing is required to improve metal extraction efficiencies during upgrading. (Kasper et al., 2011). The initial stage of pre-processing is the separation of e-waste into various categories such as PCBs, light bulbs and cathode ray tube (CRT) monitors. In Africa, this is largely done manually and

informally. It is a labour-intensive process employing about 54 million informal workers in the E-waste recycling industry in Africa (Luda, 2011; Lydall et al., 2017). There is a large use of open flames for the separation of the plastics from the metals by burning the plastic and visual inspection for categorisation. Formally, mechanical processes are mainly used in the pre-treatment of e-waste (Cui & Zhang, 2008).

The formal metal extraction/upgrading processes involve the use of mechanical, pyrometallurgy, hydrometallurgy and bio-hydrometallurgy in processing the metal fractions from e-waste. Pyro technology is currently the most utilised technology for metal extraction from e-waste on an industrial scale. In this process, e-waste fractions are mixed with mined ores to form the smelter feed such as in the Noranda process in Quebec, Canada, the Boliden Ltd. Ronnskar smelter in Sweden and the Umicore at Hoboken in Belgium (Luda, 2011). In this process crushed scraps are burned in a furnace or in a molten bath to remove plastic, the refractory oxides form slag with some metal oxides (Cui & Zhang, 2008). In these processes, gas cleaners are utilized to reduce the emissions from the combustion of the plastic fractions. The plastics fractions have a high heating value thus contribute to the reduction in coke used in these furnaces (Khaliq et al., 2014). There are limitations in the application of pyrometallurgical processes on e-waste. These are that integrated smelters cannot recover aluminium and iron as metals form slag. The ceramic components in e-waste increase the amount of slag formed resulting in the loss of PMs and BMs. The presence of halogenated flame retardants (HFR) in the smelter feed leads to the formation of dioxins thus specialized installations and measures are required to prevent environmental pollution. This is heavily dependent on investment. Other limitations are that the pyrometallurgical processing of e-waste only achieves partial separation of metals resulting in limited upgrading of metals (Cui & Zhang, 2008; Luda, 2011). The co-treatment of e-waste by pyrometallurgy due to the high level of investment required, volumes of WEEE needed to allow sufficient economies of scale and its associated environmental impact suggests that it is currently an unviable business in Africa (Lydall et al., 2017).

According to Cui & Zhang (2008), hydrometallurgy processes are more environmentally friendly, exact, predictable and easier to control than pyrometallurgy processes. The main extraction technology in the hydrometallurgy process involves acid or caustic leaching of solid material into solution. This is usually referred to as chemical leaching. Chemical leaching is the process of extracting a soluble constituent from a solid using chemical solvents (Cui & Zhang, 2008). For electronic waste, leaching involves acid treatment with chemical agents such as sulphuric acid and ferric ions. Acid leaching of e-wastes is considered a feasible approach for the complete extraction of BMs to expose the surface of PMs (Luda, 2011). However, hydrometallurgy in the processing of e-waste show limitations in the acidic leaching stage (Menad et al., 1998). These limitations included non-selective metal dissolution which leads to expensive downstream processes, corrosion problems due to high use of corrosive chemical reagents and difficult in the application which sometimes requires closed operations (Young et al., 2008; Radmehr et al., 2012; Xu et al., 2016). Although currently limited to laboratory studies, bioleaching has been noted to be potentially a more environmentally friendlier route in processing e-waste than pyrometallurgical and hydrometallurgical processes. This is due to its low chemical footprint, less

energy intensiveness, no economies of scale, high metal extraction and selectivity (Kavitha, 2014). Bio-leaching involves the exploitive use of some attributes of micro-organism to facilitate the leaching of metals into solution (Watling, 2016). The ability of bioleaching to regenerate the lixiviants such as ferric ions under acidic conditions results in it having a lower chemical footprint, higher metal extraction efficiency and selectivity than hydrometallurgical processes (Pham Van, 2009). Currently, the extraction of PMs with chemical or bioleaching remains limited due to low recovery efficiencies and pyrometallurgy is still the more efficient technology for PM recovery (Cui & Zhang, 2008).

Due to the heterogeneous nature of e-waste, the metal extraction process is expected to involve an integrated flowsheet using at least two of these technologies (pyrometallurgy, hydrometallurgy and bioleaching) (Kavitha, 2014). and will produce a multi-metal leachate solution. Therefore, the choice of downstream metal recovery processes that selectively recover targeted metals from the multi-metal leachates and that is scalable for an SMME operation, is important. In this dissertation. the ability for a metal upgrading/recovery technology to be able to separate metals from a multi-metal leachate solution and the degree of separation is referred to as metal selectivity. Metal selectivity is important in the upgrading or recover of metals in multi-metal leachate solutions. Metal adsorption with natural sorbents is a promising technology and is considered to be potentially more environmentally friendly, effective, and cheaper than the traditional metal recovery technologies such as precipitation, solvent extraction and electrowinning (Dow Chemical Company, 1999; Ayres et al., 2002; Marchioretto et al., 2005; Bergmann, 2015). Natural sorbents are sorbents obtained from biological material such as polymers (cellulose, chitin, chitosan), fungi, algal biomass, yeast, microbial; material such as zeolites, clay and waste products such as fly ash (Babel & Kurniawan, 2003; Renu et al., 2016). Natural sorbents are relatively cheap due to their sourcing from waste (Gupta & Babu, 2008) and use sorption to adsorb metals from a solution. The adsorbed metals can then be recovered via a process called elution. The sorption of metals using natural sorbents has been applied in water purification processes and is a promising technology in the upgrading of metal solutions. Bio sorbent maximum metal adsorption capacities of chitin, chitosan, chitosan derivatives, cross-linked chitosan have been observed to be higher than those in bacteria, fungi, algae, proteins and tannin derivatives (Cui & Zhang, 2008). Chitin is the second most abundant natural polymer after cellulose and chitosan is a deacylated derivative of chitin. Due to its abundance, chitin is easy to source compared to other bio sorbents and it is non-polluting and biodegradable (MacaskieL et al., 2006). Chitin and chitosan have been shown to have relatively high metal maximum adsorption capacities and to be able to preferential adsorb metals particularly iron and copper, respectively (Guibal, 2004).

Most solid waste and food industrial waste contain large biological material (Bourguignon, 2015), these waste streams may serve as a resource for bio sorbents and focus on bio sorbents provides an increased opportunity for creating circular economies in the waste industry. Chitin and chitosan are available from crustacean shell waste (Kaur & Dhillon, 2014) and insect cuticles such as fly larvae shell waste (Gyliene et al., 2003). Black Soldier Fly (BSF) (*Hermetia illucens)* larvae production is a growing industry providing an alternative source of protein for the growing world population (Nyakeri et al., 2017; Wang & Shelomi, 2017). The outer shell of the BSF larvae

consists of fibre (mostly chitin) (Decraene, 2016) which gets left behind as waste in the final pupation stage. The production of Black soldier fly (BSF) larvae results in a large amount of fly larvae shell waste (Waśko et al., 2016; Nyakeri et al., 2017). Chitin extracted from *Hermetia illucens* was shown to have a high degree of deacetylation and low crystallinity. A crystallinity index of 35 % was observed (Waśko et al., 2016). This is the lowest observed amongst insect chitin (Kaya et al., 2015). Low crystallinity in chitin is attributed to having desirable adsorptive properties (Aranaz et al., 2009) indicating great potential as a bio sorbent.. Potential use of waste streams such as BSF larvae shells for the development of metal recovery technology applicable to e-waste provides an opportunity for the creation of circular economies in the waste industry in Africa. Here, biological waste is used to recover value from electronic waste, increasing the value of both waste streams while reducing their environmental impact.

1.2 Problem statement

There is a necessity to develop new and innovative approaches to neutralize the environmental and social impact, of the growing volumes of waste produced, whilst recovering material and energy that can contribute towards the circular economy. E-waste, identified as the fastest growing waste stream in the world (Baldé et al., 2017), is composed of metal concentrations that exceed those in rich-ore mines, making it a valuable waste for sustainable metal resource development through recycling (Yunus & Sengupta, 2016). PCBs contain the largest concentrations of metals in e-waste (Legarth et al., 1995). Thus, they have become a primary focus in metal recovery from secondary sources. Since e-waste processing in Africa remains at a small scale (Schluep, Wasswa, et al., 2008; Amoyaw-Osei et al., 2011; Schluep et al., 2011; Ogungbuyi et al., 2012; Lydall et al., 2017), there is a need for the development of low investment technologies for the processing of low volumes of e-waste in support of SMMEs.

Research into metal recovery from e-waste is mostly focused on metal extraction/upgrading using either one or a combination of pyrometallurgy, hydrometallurgy or biohydrometallurgy, but there is a lack of focus on downstream processing technologies for selective metal recovery (Brandl et al., 2001; Ilyas et al., 2007; Cui & Zhang, 2008; Young et al., 2008; Pham Van, 2009; Wang et al., 2009; World Economic Forum, 2018). In general, studies that focus on the downstream metal recovery from multi-metal leachates produced after metal extraction from e-waste, do not consider circular economies (Sist & Demopoulos, 2003; Panão et al., 2006; Veit et al., 2006; Neale et al., 2009; Kim et al., 2011; Gurung et al., 2013; Willner & Fornalczyk, 2013).

Chemical metal recovery processes such as precipitation, ion exchange, solvent extraction and electrowinning (Dow Chemical Company, 1999; Ayres et al., 2002; Marchioretto et al., 2005; Bergmann, 2015), have high capital and operation costs in the treatment of metals sourced from waste.. Natural absorbents sourced from biological waste streams are regarded as environmentally friendly, effective, highly selective and cost-effective (Guibal, 2004). Furthermore, processes such as precipitation have poor metal selectivity. Metal recovery selectivity is particularly important in e-waste metal recovery due to the heterogeneous nature of this waste (Luda, 2011). The biopolymers, chitin and chitosan found in large quantities in industrial food waste, have received much attention as metal bio sorbents due to their high metal adsorption

capacities, metal selectivity, biodegradability and low cost of production (MacaskieL et al., 2006; Cui & Zhang, 2008; Renu et al., 2016). Previous studies on the adsorption of metals on chitin and chitosan from multi-metal solutions have shown their ability to preferentially adsorb metals, particularly iron and copper, respectively (Gyliene et al., 2002; Rhazi et al., 2002; Zhou et al., 2004; Wang et al., 2019). However, the application of these polymers for metal recovery from e-waste leachate solutions produced from hydrometallurgical and bio hydrometallurgical extraction remains limited.

Further, most chitin is sourced from crustacean waste and there are limited studies on the extraction of chitin from insect cuticles such as those found in BSF larvae shell waste (Kaur & Dhillon, 2014). Studies on adsorption of metals on chitin and chitosan also generally adopt their extraction and production methodology and lack techno-economic feasibility studies on both the extraction and adsorption process for metal recovery (Chu, 2002; Gyliene et al., 2002; Rhazi et al., 2002; Wan et al., 2004; Zhou et al., 2004). Therefore, there is a need to investigate the application of chitin and chitosan extracted from waste streams such as the BSF larvae shell waste to selectively recover metals from multi-metal leachate solutions. The study will focus on understanding the techno and circular economics of this application and the performance of these polymers for selective metal recovery; in consideration for the development of a low-cost investment technology for use by SMMEs in Africa.

1.3 Scope and Overall Objectives

The project in this dissertation falls under a broader research project by the Council for Scientific and Industrial Research (CSIR) titled “Waste Research, Development and Innovation (RD&I) Roadmap”. The Waste RD&I Roadmap project with regards to e-waste was focused on the development of extraction and recovery technology for metal recovery from e-waste streams in South Africa. This dissertation is focused on the downstream metal recovery of base metals from PCBs after metal extraction/upgrading with hydrometallurgy or bio-hydrometallurgy. The base metals of interest are copper, aluminium and iron. This is due to their value, high concentrations in PCBs and their impact on the extraction of more valuable metals such as PMs and REEs. Adsorption of these metals onto chitin and chitosan sourced from BSF larvae will be investigated to determine their adsorption capacities and character. This will be done in single and bimetal adsorption studies. The application of these polymers on e-waste leachate solutions will be investigated using a synthetic multi-metal solution modelled based on the bioleaching of 1 g of PCB and its techno-economic feasibility assessed.

Chapter 2: Literature Review

2.1 General Process for the Recovery of Metal Value from E-Waste

The general process for value recovery from e-waste can be broken down into 3 major stages. These stages are pre-processing, processing and downstream processing (Kokalj & Samec, 2013). Pre-processing involves waste collection which is often followed by sorting/categorisation via inspection. Sorted components that can be used directly are recycled to the market while those that cannot undergo dismantling. Dismantling is usually achieved by mechanical processes such as milling, magnetic separation and vibrators (Luda, 2011). Sorting and dismantling are energy-intensive processes but necessary as most waste streams are heterogenous either in nature such as PCBs or due to poor categorisation during collection (Abdel-Shafy & Mansour, 2018). Electronic components are removed by a combination of heating and application to shear and vibrations forces to open the soldered connections for effective disassembly. PCBs for example, are cut into pieces of about 1 cm^3 to 2 cm^3 using shredders or granulators. Further particle size reduction to 5 mm to 10 mm is carried out by centrifugal mills, cutting mills, or rotary sample dividers. Magnetic separators and low-intensity drum separators are used for the recovery of ferromagnetic metals such as iron from non-ferrous metals and other non-magnetic material. Electro conductivity-based separation such as eddy current separation is used to separate material with different conductivity and inert material (Luda, 2011). PCB metal and non-metal fraction separation are also achieved by density separation using NaCl. This separation is considered to be particularly important for promising upgrading technologies such as bio-hydrometallurgy due to the inhibitory effects of the non-metallic content of PCB in this process. Mechanical processes cannot efficiently recover metals from e-waste and thus further processing is required (Cui & Zhang, 2008). The mechanically processed components form the feedstock for processing. Processing usually involves chemical reactions which are conducted in reactors. Components in the feedstock are converted into separable or valuable products in the reactor. For example, in pyrometallurgy technology, the e-waste feedstock is recovering non-ferrous metals as well as PMs from e-waste in the past two decades. In this process crushed scraps are burned in a furnace or in a molten bath to remove plastic, the refractory oxides form slag with some metal oxides recovering non-ferrous metals and PMs (Cui & Zhang, 2008).. If multiple products are produced in the reactor then separation is required. The separation and refining of products from the reactor is known as downstream processing. This often involves processes such as solvent extraction, precipitation, ion exchange, adsorption, distillation and electrolysis (Kiss et al., 2016). Figure 2. 1 shows the general process for value recovery from waste.

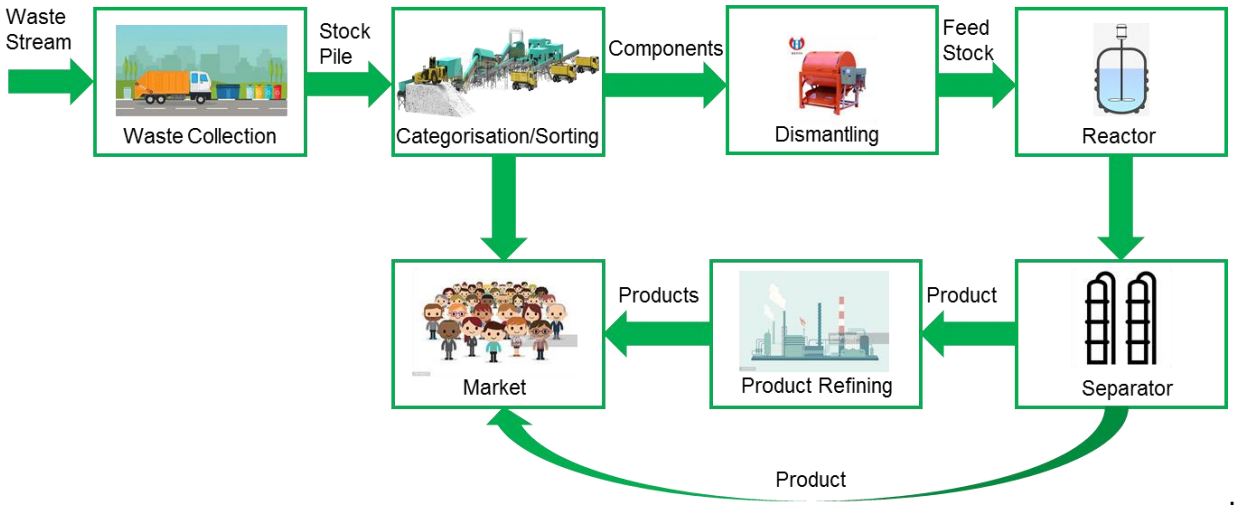

Figure 2. 1: General process for value recovery from e-waste

Consideration of the feedstock is also important as the quantity and quality of products are affected by their composition (Qian et al., 2013). In the case of value recovery from e-waste, the preferred feedstock for metal recovery is printed circuit boards (PCBs) due to their high concentration of metal content. PCBs make up 8 % of the e-waste collected from small appliances and 3 % of the e-waste global mass (Luda, 2011). The high metal concentrations in PCBs makes them a high risk for negative environmental impact, should leachate seepage from landfills occur, but also a valuable source of metals (Legarth et al., 1995). According to Khaliq et al. (2014) the general mass composition of PCBs is 40% metals. 30% of plastics and 30% ceramics. Bizzo et al. (2014), Kavitha (2014) and E-waste guide info (2017) showed the heterogenicity of PCBs, as the composition of metals in the electronic scrap vary. The general metallic mass content in PCBs is 34±12 %. The metals in PCB are in the form of elements and alloys (Szalatkiewicz Jakub, 2014). Base metals such as copper, iron and aluminium make up a large amount of the PCB metal mass content with a composition of 18±8.5 % for copper, 6.2±6.1% for iron, and 7.6±3.2% for aluminium. Other notable base metals are zinc (2.9±2.7%), tin (2.4±1.6%) and nickel (1.7±1.5%) The precious metals which are relatively significant in the composition of PCBs is silver, gold and palladium. Other metals present are REEs such as indium, tantalum and gallium (Bizzo et al., 2014; Kavitha, 2014; E-waste guide info, 2017). For gold, palladium and silver the significant factor in their high metal value in PCB is the high commodity value of these metals at $ 41 700 per kg, $ 25 700 per kg and $ 569 per kg respectively (Indexmundi, 2017). For copper, the significant factor is its high concentration in PCBs. Iron has the lowest metal value in PCB due to a low commodity value of $ 0.0753 per kg (Indexmundi, 2017).

Commercial metal recovery technologies such as precipitation, solvent extraction, electrowinning, adsorption and ion exchange require metals to be in aqueous solutions for application (Cui & Zhang, 2008). Therefore, metal upgrading or extraction of metals into solutions is a necessary step before recovery. Most studies focus on upgrading the PCB stream by extracting base metals and thereby increasing the precious metal concentration (Brandl et al., 2001; Faramarzi et al.,

2004; Ilyas et al., 2007, 2010; Pham Van, 2009; Yang et al., 2014). In pyrometallurgy, these processes occur simultaneously in the integrated smelter recovering both BMs and PMs. However, If bioleaching or chemical leaching is to be further developed to process e-waste metal fractions then selective metal recovery technologies are required to produce concentrated single, metal-rich solutions (Cui & Zhang, 2008), from the resultant leachate solutions of these processes. Laboratory studies show that bioleaching of PCBs/e-waste using acidophiles, ferric and sulfuric acid results in the complete extraction of base metals. The base metals extracted of most significance due to their concentrations and value are copper, iron, aluminium, zinc and nickel. The average concentration of these metals in the resulting leachate solution from leaching 1 g of PCB are shown in Table 2. 1. The average concentrations of metals in Table 2. 1 were developed using the extraction efficiencies from Brandl et al. (2001) and Wang et al. (2009) and the average PCB metal composition stated in this section.

*Table 2. 1: Average concentration of metals in the leachate solution after acidophilic bioleaching of 1g of PCB in 1 litre of medium with acidophilic bacteria. (*Precipitated metals during extraction)*

	Average metal composition in PCB (%)	**Metal extraction efficiency (%) (Brandl et al., 2001)**	**Concentration (mmol/L)**
Cu	18	100	2.79±1.32
Al	7.6	100	2.82±1.19
Fe	6.2	100	1.11±1.09
Ni	1.7	98	0.278±0.245
*Sn	2.4	SnO ppt.	-
*Pb	2.5	PbSO4 ppt.	-
Zn	2.9	100	0.442±0.412

2.2 Downstream processing of metal-rich e-waste

Economic forecasting is important in decision-making processes and the development of strategies to deal with associated costs. It allows for the determination of the economic feasibility of processes and the identification of high-cost stages. Downstream processing has been identified as a high-cost stage in the recovery of value from waste. Downstream processing accounts for 50 to 90 % of the total recovery costs in bioprocesses (Straathof, 2011; Clarke, 2013) and 40 to 60 % in metal recovery processes (Barr et al., 2005). This is due to the heterogeneous nature of feed streams which results in multiple products requiring several separation units to achieve complete recovery. For metal recovery processes, metals are recovered either in solution or solid form to yield products of commercial value. The commercial value of the recovered metal product in comparison with the operating costs for recovery is the heart of the economic feasibility analysis used to select a metal recovery process (Jong et al., 1989). Most metal recovery studies do not consider techno-economics and circular economies (Ayres et al., 2002; Panão et al., 2006;

Blais et al., 2008; Kim et al., 2011; Gurung et al., 2013; Bergmann, 2015; Borja et al., 2016; Renu et al., 2016). Consideration of a circular economy in metal recovery is important to utilise potential waste sources. This gives opportunities for reduction of associated environmental impacts, value recovery in the form of material and energy and by-products which improve the economic feasibility of participating processes (United Nations, 2018).

This review is aimed at identifying base metal recovery techniques to identify that apply to low volumes of e-waste, multi-metal solutions and SMMEs. The base metal recovery techniques must also be low-cost investment, economically feasible, environmentally friendly and circular economy driven. Hydrometallurgical and bio hydrometallurgical routes are the techniques often employed in the recovery of base metals from solutions, with hydrometallurgy being the most dominant. The hydrometallurgical techniques which are used to recover metals from solutions are precipitation, solvent extraction and electrowinning, ion exchange and sorption. For biorefining bio-sorption and sulphide precipitation via biogenic generated sulphide ions, are gaining traction (Blais et al., 2008).

2.2.1 Precipitation by cementation

Cementation is the electrochemical precipitation of metal by another more electropositive metal (Panão et al., 2006). Cementation is simple and easy to control. The major drawback of cementation is the dissolution of the sacrificial metal; this is more critical at low pH values (Demirkiran et al., 2007). Another drawback in the cementation process is the presence of competing reactions which result in large consumption of the sacrificial metal. At low pH, the cementing metal may be lost to reduction reactions of H^+ ions and reaction with oxygen. Zinc and iron are the widely used cementing agents due to their electro positivity. Re-dissolution of cemented metals has been observed for copper with zinc cementation (Panão et al., 2006). Behnamfard et al. (2013) noted that zinc was unsuitable for cementation from acidic solutions considering its high solubility in acid, evoking hydrogen gas leading to high consumption of zinc. Ayres et al. (2002) in their review noted that cemented copper with iron was not pure enough for direct use and had to be further refined. Cementation for the recovery of copper has almost been universally overtaken by solvent extraction (Ayres et al., 2002). Due to the limitations in cementation, its application for metal recovery from multi-metal leachate solutions might not be feasible due to its lack of effectiveness and low metal selectivity.

2.2.2 Precipitation by addition of anions

Metal cations in solution may react with anions to form insoluble compounds/salts. Insoluble metal salts are called precipitates and the reaction is called precipitation. In general, nitrates, halides, sulphates, perchlorate and acetate metal salts are soluble particularly for base metals. Carbonate, phosphate, hydroxide, oxide and sulphides metal salts are generally insoluble therefore metals can be removed by precipitation as these salts (Andrus, 2000). Precipitation of metals remains the most favourable option on an industrial scale due to its cost-effectiveness, performance, and simplicity. Precipitation of metals with phosphates and carbonates are seldomly practised. Of interest are the hydroxide and sulphide salts particularly for base metal recovery. Precipitation of metals with hydroxide anions has been the most utilized precipitation technique in the recovery

of metals from solution. This is due to that hydroxide ions can be sourced from relatively cheap sources such as limestone. Precipitation of metals with sulphides has been garnering interest due to its selectiveness in metal recovery. Cheaper and efficient precipitation technologies often involve biological activities for the recovery of metals from industrial effluents (Blais et al., 2008).

2.2.2.1 Precipitation with hydroxide ions

Precipitation of soluble metals can be achieved by the formation of insoluble hydroxide salts. This is achieved by the addition of alkaline reagents (hydroxide containing/forming) such as (CaO or $Ca(OH)_2$), NaOH, $Mg(OH)_2$, and NH_4OH) (Mirbagheri & Hosseini, 2005; Kurniawan et al., 2006; Meunier et al., 2006; Viadero et al., 2006).. The reaction of base metals with hydroxide ions can be described by Equation 1 where M represents the metal cation.

$$M^{2+} + 2(OH)^{-} \leftrightarrow M(OH)_2 \quad \text{Equation 1}$$

Table 2. 2 shows the hydroxide precipitation pH range and solubility products of the main base metal hydroxide salts of base metals in PCB. Table 2. 2 shows that with regards to the initial pH for hydroxide salt formation, the order of initial precipitation is Fe^{3+}>Al^{3+}>Cu^{2+} >Zn^{2+}>Fe^{2+} >Ni^{2+}. This order is however affected by the precipitation conditions such as hydroxide reagent dosage rate, temperature and initial concentration of the metals in solution. Table 2. 2 also shows that precipitation of metals with hydroxides occurs over pH ranges which overlap thus introducing non-selective metal recovery. Thus, the formation of hydroxides is accompanied by coprecipitation of metal hydroxides which results in a mixed precipitate (Couillard & Mercier, 1992; Marchioretto et al., 2005).

Table 2. 2: Hydroxide precipitation pH range and K_{sp} (Solubility product) of the main base metals hydroxide salts in PCB extracted from (Monhemius, 1977; Abdullah et al., 1999; Marchioretto et al., 2005; Blais et al., 2008; Lewis, 2010; Suponik, 2010)

Metal	Metal Salt	Metal salt precipitation pH range	Log (K_{sp})
Fe^{3+}	$Fe(OH)_3$	1.5-3.5	-37.4
Al^{3+}	$Al(OH)_3$	3.5-12.2	-33.5
Cu^{2+}	$Cu(OH)_2$	5.2-10.0	-18.6
Ni^{2+}	$Ni(OH)_2$	8.0-10.5	-14.7
Fe^{2+}	$Fe(OH)_2$	7.4-10.0	-15.1
Zn^{2+}	$Zn(OH)_2$	7.0-11.2	-16.1

Precipitation of metals with $Ca(OH)_2$ in the presence of acid leachates containing sulphates involves the formation of secondary precipitates such as $CaSO_4$. $2H_2O$. This results in the production of sludges which raise the cost of waste management and disposal (Jüttner et al., 2000), increasing the difficulty in the solid-liquid separation stage (Viadero et al., 2006). It is for this reason that alkaline agents such as NaOH and NH_4OH are the most preferred as they form soluble by-products.

In the study by Balintova & Petrilakova (2011), aluminium was observed to precipitate out at a pH range of 4.0 to 5.5 with a precipitation efficiency of 92.9 % while zinc was observed to precipitate at a pH range of 5.5 to 7.0 with a precipitation efficiency of 84 %. Sist & Demopoulos (2003)

observed that nickel recovery was greater with the use of MgO as a base than NaOH. Similar observations were made by Mubarok & Lieberto (2013).

2.2.2.2 Precipitation with sulphide ions

Precipitation with sulphide can be described by Equation 2 where M represents the metal cation.

$$M^{2+} + S^{2-} \leftrightarrow MS \quad \text{Equation 2}$$

Sulphide precipitation is generally carried out using reagents such as Na_2S, NaHS, H_2S or FeS (Al-Tarazi et al., 2004; Marchioretto et al., 2005). Bio precipitation is a technology that is gaining attention due to its low cost and efficiency in the production of H_2S. The H_2S in bio precipitation is produced by sulphate-reducing (SRB) and sulphur-reducing bacteria such as *Desulfurella Acetrivans* (Mikhailova et al., 2015). These bacteria anaerobically respire using sulphur as an electron acceptor. In acidic effluents, partial neutralization with a base such as NaOH is necessary prior addition of sulphides to prevent the formation of the pollutant gas, H_2S.

Table 2. 3 shows the sulphide precipitation pH range and solubility products of sulphide salts of the base metals in PCB. In general metal, sulphides exhibit lower solubility than hydroxides. They achieve more complete precipitation in a shorter pH range. Table 2. 3 that with regards to the initial pH for sulphide salt formation, the order of initial precipitation is Cu^{2+}>Zn^{2+}>Ni^{2+}>Fe^{2+}. This order is however affected by the precipitation conditions such as sulphide reagent dosage rate, temperature and initial concentration of the metals in solution (Lewis, 2010). Precipitation of ferric ions with sulphide ions results in the reduction of ferric ions with the precipitated metal salt being FeS. (Kiilerich et al, 2018). While for the precipitation of aluminium ions with sulphide ions, Aluminium Sulphide hydrolyses in the presence of moisture to form hydrated Aluminium Oxides/Hydroxides (Lopez et al, 2011).

Table 2. 3: Sulphide precipitation pH range and K_{sp} (Solubility product) of the main base metals hydroxide salts in PCB extracted from (Monhemius, 1977; Marchioretto et al., 2005; Blais et al., 2008; Lewis, 2010; Wang et al., 2014; Prokkola et al., 2020)

Metal	Metal Salt	Metal salt precipitation pH range	Log (K_{sp})
Cu^{2+}	CuS	0.5-2.0	-35.2
Fe^{3+}	FeS	4.2-12	, Reduction of ferrous to form FeS and sulphur
Al^{3+}	$Al(OH)_3$	-	hydrolyses to form oxides/hydroxides
Zn^{2+}	ZnS	1.0-4.1	-23
Ni^{2+}	NiS	1.8-8.6	--21.0
Fe^{2+}	FeS	4.2-12	-18.8

Sulphide precipitation is generally more expensive than precipitation with hydroxide. The production of H_2S during precipitation for acidic conditions or when sulphide ions are in excess is a safety concern (Sist & Demopoulos, 2003; Veeken & Rulkens, 2014). Precipitation with sulphides however has the following advantages over hydroxide precipitation:

- Residual metal concentrations in effluents are lower (high recovery efficiencies).

- Precipitation has better selectivity.
- High reactions rates result in lower hydraulic retention time.
- Sulphide sludges thicken and dry better than hydroxide sludges.

Sulphide precipitation due to its cheapness, high metal selectivity and recovery efficiency seems to be an applicable technique for the recovery of metals from multi-metal leachate solutions (Veeken & Rulkens, 2014). Although Hydroxide precipitation is cheaper with high recovery efficiencies, it, however, has low metal selectivity. This makes its direct application to multi-metal solutions unfeasible.

2.2.3 Solvent Extraction and Electrowinning

Agitation leaching with solvent extraction is used to produce a relatively pure solution of concentrated metals such as copper sulphate for electrowinning. Kerosene (containing 12 % mixture of LIX hydroxy oximes) a proprietary solvent is mixed with the metal solution in an agitating tank. The metal combines with the solvent to form a complex. When the agitation is stopped, the organic solvent with metal (denser) layer and water layer with impurities form. The water layer is drained off and H_2SO_4 is used to break down the complex and to recover the metal. The H_2SO_4 with the metal (for example copper sulphate) is recycled through electrowinning. Electrowinning involves the deposition of metals by reduction on a cathode produced by an electric potential. The need for high voltages during electro winning result in high usage of electricity. The SX-EW process differs from traditional electrolyte refining as it uses inert anodes (PB-Sn-Ca). For example, copper is deposited at the cathode releasing oxygen and regenerating the sulphate ion. The purity of the cathode copper produced can be as high as 99.99 % (Ayres et al., 2002). Electrowinning usually requires a concentrated solution (pregnant solution) thus a pre-concentration step such as solvent extraction is usually required prior.

SX-EW process is a continuous process and suitable for large scale operations and has relatively no economies of scale. The cost per ton of copper for small operations is the same as those for large operations (Ayres et al., 2002). Willner & Fornalczyk (2013) conducted a study on the recovery of copper after bioleaching PCBs with *A. ferrooxidans.* In this study solvent extraction was used to extract copper from the bio leachate solution. Willner & Fornalczyk (2013) used organic solvent, LIX 860N-IC and achieved an extraction of 98.5 % of copper and 3.8 % iron. Neale et al. (2011) also recovered copper by solvent extraction followed by electrowinning. The organic solvent LIX984N-C was used in a mixer-settler unit. Copper extraction between 98.2 % and 98.9 % were achieved using three stages. Veit et al. (2006) concentrated the copper from PCBs by mechanical processes before electrowinning. The electrolytic cell used in Veit et al. (2006) encompassed a copper plate as the cathode and a platinum plate as the anode. There was complete recovery of copper in 90 mins with a purity of 99.5 %. Mecucci & Scott (2002) studied the recovery of copper, lead and tin from a leachate solution of scrap PCB using a rotating cylinder electrode reactor (RCER). The purity of the copper deposit was 99.8 % copper while the deposited lead was pure in the anode (Mecucci & Scott, 2002).

Due to having no economies of scale, the SX-EW is potentially applicable to recover metals from low volumes of e-waste and applicable to SMMEs (Neale et al., 2009). The process is quite

efficient and has become the prominent method of recovering base metals such as copper (Blais et al., 2008). The major drawback of SX-EW is its high environmental impact. SX-EW has a higher environmental impact concerning climate change/global warming indicator (about 25 % more) than furnaces due to high (coaled based) electricity requirements (Ayres et al., 2002). This will be the case if SX-EW is used in South Africa as 92 % of electricity generation is produced by coal-fired plants (Newbery & Eberhard, 2008). SX-EW indirect emissions from the use of coal-based electricity also lead to acidification effects (Ayres et al., 2002). Another drawback to the use of EW is the need for concentrated solutions and expensive anodes making it a high-cost investment (Veit et al., 2006). SX-EW'S potential for application in multi-metal leachate solutions rests on its source of electricity considering its environmental impact and the choice of the anodes used in the electrowinning. If renewables energies such as solar energy are considered to power this technology, then SX-EW will become one of the most efficient environmentally friendly metal recovery technologies (Ayres et al., 2002).

2.2.4 Ion exchange resins

Ion exchange is the exchange of ions between two electrolytes or between an electrolyte solution/complex. Ion exchange for effluent remediation is very cost-effective. It requires a little amount of energy and the regeneration of resins make them economical (Kansara et al., 2016). In a study by Kim et al. (2011), copper was shown to have high adsorption with Amberlite XAD-7HP with an adsorption capacity of 596 mg/L achieving a recovery of 97.7 % from a leachate solution of waste mobile PCB. Elution of copper from the resin was achieved using HCl (Kim et al., 2011). Ion exchange has disadvantages, particularly when considering the application on PCB base metal bio leachate solutions. These are that presence of organic matter and ferric ions in the leachate solution may result in fouling of the resins (Dow Chemical Company, 1999; Kansara et al., 2016). Mabuka et al. (2018) showed that bio sorbents (chitin sourced from Black soldier flies) had cheaper recovery costs when compared to ion exchange resins in the recovery of ferrous ions.

2.2.5 Sorbents and Sorption

Sorption is gaining traction as a more efficient technique for the recovery of metals from the solution. It is a relatively new process providing high quality treated effluents, flexible designs, reversibility which allows for the regeneration of the adsorbents. The limitation in other techniques such as large production of sludge, low efficiencies, sensitive operation conditions and high-cost disposal give adsorption an advantage (Bergmann, 2015).

Sorption is a physio-chemical and metabolic independent process based on mechanisms such as absorption, adsorption, ion exchange, surface complexation and precipitation (Fomina & Gadd, 2014). Adsorption is an interface phenomenon that involves the change in concentration of a given substance at the interface concerning neighbouring phases. For solid-liquid systems, the adsorbent is the solid phase and the adsorbate are the molecules that attach to the adsorbent (Compton & Nguyen, 2010). When adsorbate molecules penetrate the bulk of the solid phase this is then defined as absorption. The process of sorption falls into 4 categories and these are:

1. Transport of the adsorbate from the bulk solution to the film around the adsorbent (This stage is typically fast in agitated systems).
2. Diffusion mass transfer of the adsorbate through the film.
3. Intraparticle diffusion of adsorbate through the pores of the adsorbent.
4. Binding of adsorbate to active sites in the pore of the adsorbent, (This stage is generally faster than the diffusion of the adsorbate and thus it is usually assumed to not limit mass transfer) (Wong et al., 1998)

The sorption process is shown in Figure 2. 2. There are two types of adsorption based on the binding force of the adsorbate to the active sites. These are physical adsorption (physisorption) and chemical adsorption (chemisorption).

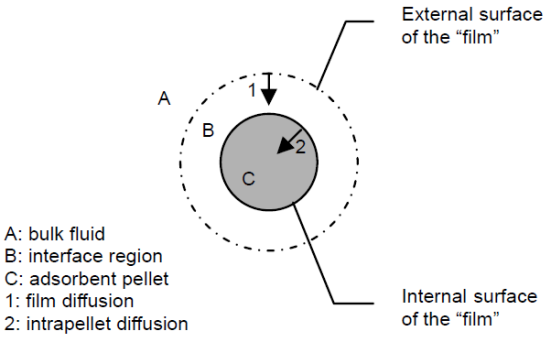

Figure 2. 2: Macroscopic adsorption process of an adsorbent pellet extracted from (Xu et al., 2013)

Physisorption involves relatively week intermolecular forces between the adsorbate and active sites. It is non-specific, with low heat of adsorption, forming a monolayer or multilayer, no dissociation of adsorbent molecules and no electron transfer (although polarization of sorbate may occur). Chemisorption involves the formation of a chemical bond between the adsorbent molecules on the active sites. It is specific with high heat of adsorption, forming a monolayer, involve dissociation and electron transfer leading to bond formation (lijima, 1991). The absorbed metals are recovered by either elution into solution using an eluting agent or the sorbent is combusted leaving the metal behind (Cui & Zhang, 2008). Further metal refining might be required to recover the concentrated metal solutions from desorption.

Sorbents can be divided into two categories which are commercial sorbent and natural bio sorbents. Commercial sorbents are sorbents produced commercially on large scale such as activated carbon, silica gel, magnetic adsorbents and alumina (Renu et al., 2016). Natural sorbents include sorbents obtained from biological material such as natural polymers (chitosan), fungi, algal biomass, yeast, microbial; natural material such as zeolites, clay and waste products such as fly ash (Babel & Kurniawan, 2003; Renu et al., 2016). The cost of the sorption process depends on the cost of the sorbent. Commercial sorbents are characterized by high costs while natural sorbents are relatively cheaper due to their sourcing from waste. For example, the cost of commercial activated carbon was $ 7.07 per kg while the cost of bio-sorbents ranged from $ 0.0777 to $ 0.514 per kg (Gupta & Babu, 2008).

Commercial and natural adsorbents can adsorb for example, between 0.4-260 mg copper /g adsorbent (Findon et al., 1993; Lu & Wilkins, 1996; Ajmal et al., 1998; Pagnanelli et al., 2003; Zhou et al., 2004; Prado Acosta et al., 2005; Tunali et al., 2006; Mukhopadhyay et al., 2007; Bhainsa & D'Souza, 2008; Ren et al., 2008; Yu et al., 2008; Hassan et al., 2009; Herrero et al., 2011; Christoforidis et al., 2015). Table A1. 1 in Appendix: A1 Literature Review Figures and Tables shows the natural sorbents' adsorption capacities, best model fit, process pH, initial copper concentration, contact time and adsorbent dose for bio-sorbents. The maximum adsorption capacity of copper by commercial adsorbents was found to be 71.4 mg/g by Cu(II) ion-imprinted composite adsorbent (Cu(II)-MICA) (Ren et al., 2008) while that of natural sorbents was found to be 260 mg/g by chitosan which was immobilized on sand (Findon et al., 1993; Wan et al., 2004). Bio-sorbents in general seem to have high adsorption capacities because of their stable carbon structures, accessible metal-binding sites such as amine and hydroxyl groups (Renu et al., 2016). Bio sorbent maximum metal adsorption capacities of chitin, chitosan, chitosan derivatives, cross-linked chitosan were observed to be higher than those in bacteria, fungi, algae, proteins and tannin derivatives (Cui & Zhang, 2008). Chitin is the second most abundant natural polymer after cellulose and is easy to source than other bio sorbents. Chitin and chitosan are also non-polluting and biodegradable (MacaskieL et al., 2006). Due to its high metal adsorption capacity and selectivity, environmentally friendliness, availability and cheapness, a great focus has been placed on metal adsorption studies with chitin and chitosan (Cui & Zhang, 2008).

The use of bio sorbents for metal adsorption from PCB/e-waste leachate solutions provides an opportunity for a circular economy in the waste industry in South Africa. Natural waste biomass generated from the production and processing of crustaceans such as shell fish and fish scales is a large waste and poses a serious environmental hazard towards marine ecosystems (Knuckey et al., 2004). Natural waste biomass currently has low economic value (Suchiva et al., 2002). However, the presence of chitosan in this material suggests potential value addition with tremendous applications (Hossain & Iqbal, 2014). Application of chitin and chitosan on PCB/e-waste leachate solutions will mean the creation of a circular economy in the waste industry were bio waste is used to remediate electronic waste concerning metal recover, increasing the value of both wastes while reducing their environmental impact.

2.2.5.1 What is Chitin and Chitosan?

Chitin is a linear basic polysaccharide poly-(1-4)-2-acetamido-2-deoxy-D-glucopyranose (N-acetyl-D-glucosamine) with a molecular formula of $(C_8H_{13}O_5N)_n$, found in fungal cell walls, crustacean shells and insect cuticle. Chitin is the second most abundant natural polymer after cellulose while chitosan is the deacetylated product of chitin (Zhang et al., 2000). Figure 2. 3 shows the chemical structure of chitin and chitosan. Chitin and chitosan all contain glucosamine and acetyl glucosamine units and the only possible differentiation between the two is solubility in acidic solutions which corresponds to a degree of deacetylation greater than 60 %. The degree of deacetylation is defined as the ratio of the number of amino groups in chitosan relative to the summation of amino acid and acetamido groups present in the chitosan (Gyliene et al., 2002). There are three types of chitin which have been identified α-chitin, β-chitin and γ-chitin (Guibal, 2004) in which α-chitin is the most abundant in nature (Zhang et al., 2000). Chitin is brown, hard

(brittle), inelastic, highly hydrophobic, insoluble in water and many solvents (Dutta et al., 2004; Zhou et al., 2004) however is it soluble in hexafluoro isopropanol, hexafluoroacetone, chloro alcohols with aqueous mineral acids, and dimethylacetamide containing 5 % lithium Chloride (Dutta et al., 2004). Chitin is resistant to acid action (Zhou et al., 2004) while chitosan is soluble in most mineral and organic acids. However, chitosan is relatively stable in sulfuric acid (Guibal, 2004).

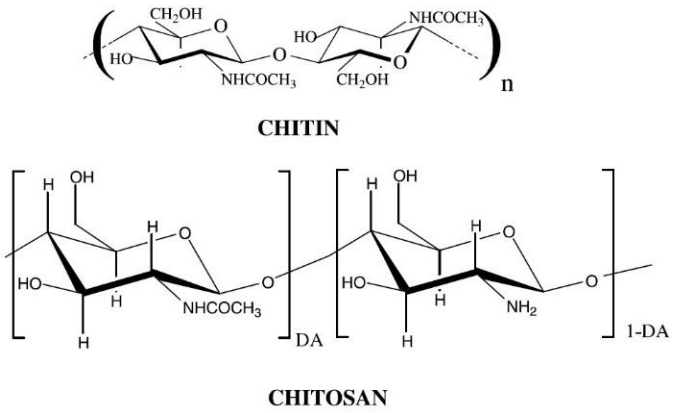

Figure 2. 3: Chemical structure of chitin and chitosan (Rhazi et al., 2002)

The amino group and hydroxyl groups in chitin and chitosan are reactive, chelating many transitional metal ions. They undergo reaction typical for amines such as N-acetylation and Schiff reactions. Chitin and chitosan currently have application in cosmetics, water engineering (flocculant), paper industry, textile industry, food processing, agriculture, photography, chromatographic separation, solid-state batteries, light-emitting diode (LED) applications, tissue engineering and drug delivery systems (Dutta et al., 2004). Due to the versatility of this polymer sourcing, it from waste provides a great opportunity to create circular economics in the bio-industry.

2.2.5.2 Sources of Chitin and chitosan

Chitin is a major component in crustacean shells, insect cuticles, cell walls of fungi and green algae (Kaur & Dhillon, 2014). It is estimated that about 10 Giga tons of chitin are constantly available in the biosphere (Jeuniaux & Voss-Foucart, 1991). On the industrial commercial-scale chitin is sourced from waste residuals of crustacean exoskeletons from the seafood industry. Chitosan is a commercial produced from the deacetylation of chitin. The annual production of chitosan and glucosamine was about 2000 and 4000 tons respectively in 2003 (Kaur & Dhillon, 2014).

Crustacean shells as a source for chitin have the disadvantages of high calcium which is about 30 % to 50 % of the shell mass. Fungal biomass presents potential as a biological source of chitosan. Chitin sourced from fungal biomass has relatively better physiochemical properties such as a higher degree of deacetylation, low molecular weight, low protein content and high bioactivity than crustaceans (Kaur & Dhillon, 2014). Fungal biomass is however currently limited in South Africa (Wood, 2017). Insects have more chitin than crustaceans but are difficult to source due to their sparse distribution (Gyliene et al., 2003). The need for alternative sources of proteins to meet

the growing food demand has led to research into Insect larvae due to their high-quality protein content. The Black solider fly (BSF) larvae (*Hermetia illucens*) particularly have been gaining interest due to their high protein content, high producing ability, high resistance to the environment and ability to feed on a range of organic waste. BSF larvae not only reduce organic waste but also reduce pathogens in waste such as *Escherichia coli* and *Salmonella enteric* (serotype enteritids) (Nyakeri et al., 2017). The BSF larvae belong to the *Stratiomyidae* family (Dortsmans et al., 2017). BSF are native to South America and common in warm temperature climates. They have been reported in nearly 80% of the world including in Africa. In Africa, they have been sighted in Ghana and South Africa.

The outer shell of the BSF larvae consists of fibre (mostly chitin) (Decraene, 2016) which gets left behind as waste in the final pupation stage. The production of Black solider fly (BSF) larvae results in a large number of fly larvae shell waste which has a high content of chitin (Waśko et al., 2016; Nyakeri et al., 2017). Chitin extracted from *Hermetia illucens* was shown to have a high degree of deacetylation and low crystallinity. A crystallinity index of 35 % was observed (Waśko et al., 2016). This is the lowest observed amongst insect chitin (Kaya et al., 2015). Low crystallinity in chitin is attributed to having desirable adsorptive properties (Aranaz et al., 2009) thus indicating great potential as a bio sorbent. Chitin extracted from fly larvae has been shown to have better adsorptive properties that chitin sourced from crustaceans (Gyliene et al., 2002). The use of chitin from BSF fly larvae shell may provide a cheap sorbent with great metal adsorption efficiency for application on PCB/e-waste leachate solutions.

The BSF larvae contain about 35 to 40 % crude protein, 35 % fat content and have higher calcium than other insects. They contain about 9 % (dry mass) chitin. Gyliene et al. (2002) quantified that the amount of chitin recovered from the FLS during their study was 40 % to 45 % of the original weight of the raw FLS. The large amounts of proteins, lipids and minerals in BSF larvae indicate the need for deproteination and demineralization if chitin will be sourced directly from the BSF larvae.

2.2.5.3 Chitin Extraction and Chitosan Production

Sometimes biomass cannot be used directly as a bio sorbent and the adsorptive component must be extracted. This is true for chitin and chitosan considering the source (crustacean shells and insect cuticle) which contain proteins, lipids and minerals. Since the cost of sorption is dependent on the cost of the sorbent, the extraction process must be cheap to reduce the commodity value of the sorbent. Major developments in the methodology of chitin extraction and chitosan production only emerged in the early 1940s (Muzzarelll, 1977). Chitin extraction usually involves demineralization, deproteination and decolourisation Chitosan is then produced by the de-acetylation of the extracted chitin (Muzzarelll, 1977). Shells are usually washed, dried and then ground to a fine powder to particle sizes between 200 mm to 700 mm before these processes (Hackman, 1953; Tetteh, 1991; Rhazi et al., 2000; Gyliene et al., 2002). Particle size reduction is necessary to improve the efficiency of reactions (Tetteh, 1991).

Demineralization is required for the removal of minerals such as calcium carbonate and phosphate from the shells (Gyliene et al., 2002). Calcium, potassium and sodium carbonate is

converted into soluble calcium chloride and CO_2 gas is evolved (Tetteh, 1991). Demineralisation is usually conducted at room temperature and pressure (r.t.p) using HCl with a concentration between 1 M to 2.25 M for 30 minutes to 5 hours at a liquor ratio range between 1 g to 5 mL HCl to 1 g to 25 mL of HCl (Hackman, 1953; Tetteh, 1991; Rhazi et al., 2000; Zhang et al., 2000; Gyliene et al., 2002). Acid treatment of chitin or chitin containing raw material usually results in partial or extended depolymerization and a decrease in viscosity (Madhavan & Ramachandran Nair, 1974; Muzzarelll, 1977; Tetteh, 1991). The demineralization of minerals with HCl undergo the following reaction given in Equation 3, Equation 4 and Equation 5:

$$CaCO_3 + HCl \rightarrow CaCl_2 + CO_2 + H_2O \quad \text{Equation 3}$$

$$K_2CO_3 + 2HCl \rightarrow 2KCl + CO(OH)_2 \quad \text{Equation 4}$$

$$CO(OH)_2 \rightarrow CO_2 + H_2O \quad \text{Equation 5}$$

According to Muzzarelll (1977), the mineral content of chitin has no effect on the adsorption of metals in solution. Therefore, demineralisation might not be a necessary step for the extraction of chitin as a metal bio sorbent.

Deproteination is the removal of lipids and protein from the shells (Gyliene et al., 2002). Deproteination is usually conducted between 55 ^oC to 100 ^oC using caustic soda (NaOH) with a concentration between 1.75 % (W/V) to 2.25 % (W/V) for 1 hour to 5 hours at a liquor ratio range between 1 g to 5 mL HCl to 1 g to 25 mL of HCl (Hackman, 1953; Tetteh, 1991; Rhazi et al., 2000; Zhang et al., 2000; Gyliene et al., 2002). The use of enzymes (proteinase, papain, bacterial proteinase, pepsin, trypisin) for the deproteination process are ineffective (Takeda & Abe, 1962; Broussignac, 1968). Proteins and lipids in the deproteination process with NaOH undergo the following reaction given in Equation 6 and Equation 7 respectively were R' is the carbon chain of the fatty acid:

$$-C(NH_2)(COOH) + NaOH \rightarrow -C(NH_2)(COO^-)Na^+ + H_2O \quad \text{Equation 6}$$

$$R' - (COOH) + NaOH \rightarrow -R' - (COO^-)Na^+ + H_2O \quad \text{Equation 7}$$

The use of harsh conditions concerning temperature, a large amount of reagents with long reaction times results in low yields (Hackman, 1953; Whistler & BeMiller, 1962). Horowitz et al. (1957) proposed mild conditions for deproteination. The deproteination was done with 500 ml of NaOH under a steam bath (100^oC) for 2.5 hours and gave a chitin yield of 60 % to 70 % with a nitrogen content of 6.95 %. The deproteinating conditions in Horowitz et al. (1957) have been generally adopted. Due to the corrosiveness of caustic soda on plastic and steel, deproteination is usually conducted in stainless steel containers (Horowitz et al., 1957). This is also the case with de-acetylation with alkali treatments. Muzzarelll (1977) in their review of chitin extraction proposed that if the endpoint of the raw material is chitosan then the deproteination step must be mild due to the further use of alkali treatment in deacetylation. Although low reactivity of chitin is ascribed to the trans arrangement of acetamido groups with respect to the hydroxyl group (OH-3) (Rhazi et al., 2000), Vijayaraghavan et al. (2005) identified that chitin from crab shell particles had better adsorption for Ni^{2+} than the de-acetylated product (chitosan)and presence of proteins improved the adsorption. Studies on the effects of proteins in the chitin and chitosan on metal adsorption remain limited.

De-acetylation is the removal of the acetyl group in chitin and substituting it with a reactive amine group (NH_2) (Muzzarelll, 1977). The result of the de-acetylation process is chitosan. The de-acetylation process is usually achieved using highly concentrated NaOH. This is because the effect of alkali treatment on the macromolecular length during chitosan production is less pronounced than that of acid treatment. De-acetylation is most effective in inert atmospheres (Muzzarelll, 1977). Rigby (1936) and Peniston & Johnson (1975) hold patents for the use of alkali solutions for the production of chitosan from chitin. The method proposed by Rigby (1936) is the most adopted method for de-acetylating chitin. Rigby (1936) deacetylated 50 g of chitin using 2.4 L of 40 % NaOH at 115^oC for 6 hours under N_2 conditions. This method achieved 82 % removal of acetyl groups. Horowitz et al. (1957) proposed heating chitin with solid potassium hydroxide (KOH) under N_2 conditions for 30 min at 180 ^oC. The method in Horowitz et al. (1957) achieved high removal of acetyl groups (95 %) however the chain length of the chitosan produced was short (only 20 units long). Alkali treatment combines deacetylation and protein removal in one step (Muzzarelll, 1977). Chu (2002) reported a methodology for producing chitosan directly by the partial deacetylation of prawn shells. Due to the high presence of reactive amine groups, chitosan is usually ascribed to have better metal adsorptive properties than chitin (Babel & Kurniawan, 2003).

Chitin contains a brown pigment which is mostly melanin (Yen & Mau, 2006). Decolourisation is conducted to remove the brown pigment. Decolourisation is usually conducted using 95% ethanol, sodium hypochlorite (NaClO) (also known as household bleach), potassium permanganate ($KMnO_4$) with Oxalic Acid, sodium met bisulfate ($Na_2S_2O_5$), ammonium per sulfate $(NH_4)_2S_2O_8$ and H_2O_2 or H_2SO_4. Most of the chitin used in metal adsorption studies are usually not decoloured (Chu, 2002; Gyliene et al., 2002; Rhazi et al., 2002; Wan et al., 2004; Zhou et al., 2004; Wang et al., 2019). Decolourisation seems to be an unnecessary step for extracting chitin and producing chitosan for metal adsorption. However, its effects or the effect of the colour pigment in chitin on metal adsorption is not clear (Muzzarelll, 1977). $KMnO_4$ with oxalic acid and household bleach has been the most preferred decolourising agents due to their availability, cheapness and effectiveness (Madhavan & Ramachandran Nair, 1974; Yen & Mau, 2006). Decolourisation with $KMnO_4$ and Oxalic acid is usually conducted at r.t.p with a concentration between 1 % (W/V) for 1 hour.

The major important character of chitin and chitosan in the adsorption of metals from solutions is the degree of deacetylation (DD), molecular weight and crystallinity (Guibal, 2004). These parameters are affected by the extraction process of chitin and the production of chitosan. There are limited studies on the effects of chitin extraction and chitosan production steps on the character and performance of these polymers in metal adsorption. There are also limited studies on the cost of chitin extraction, chitosan production and cost of metal adsorption. Most metal adsorption studies with chitin and chitosan generally adopt their extraction and production methodology (Chu, 2002; Gyliene et al., 2002; Rhazi et al., 2002; Wan et al., 2004; Zhou et al., 2004; Wang et al., 2019). The minerals, proteins and colour pigments from the chitin extraction have value particularly in the bio-industry (Muzzarelll, 1977).

2.2.5.4 Chitin and Chitosan Metal Adsorption and Desorption

Chitin and chitosan efficiently adsorb heavy metals (Ren et al., 2008). Chitosan generally has higher adsorption capacities than chitin however the two polymers' metal adsorption differ in the order of metal selective adsorption and stability in acid conditions (Babel & Kurniawan, 2003). Chitosan has the disadvantage of being mechanically unstable under acidic conditions and may leach carbohydrates when used in its raw form. An effort has been put to stabilize chitosan either by cross-linking or ion print technology (Cui & Zhang, 2008; Renu et al., 2016).

The application of chitin and chitosan as adsorbent material can be in many physical forms such as powder, nano particles, gel beads, membranes, sponge, honeycomb, solutions and fibre. A study by Rhazi et al. (2002) showed that the physical form of chitin and chitosan does not alter its selectivity of metals in metal adsorption. Chitin and chitosan powder are simple forms with small size particles which improve sorption kinetics. However, the application of powders is limited to batch systems due to clogging in column systems (Guibal, 2004). Batch systems are simple and are the most used system for studying the metal adsorption properties of bio sorbents (Cui & Zhang, 2008). Batch metal adsorption studies with chitin and chitosan are usually conducted at r.t.p, at a pH between 3 to 6, with a liquor ratio of 1 g:100 mL to 1 g: 600 mL of chitin/chitosan to a solution under agitation between 50 to 200 rpm. The particle size of the chitin or chitosan is usually in the range of 300 µm to 1500 µm.

Most metal adsorption studies on chitin and chitosan are conducted in single metal solutions to determine the adsorption capacities of the metals. The adsorption capacity is then used to determine the order of selectivity (Gyliene et al., 2002; Rhazi et al., 2002; Zhou et al., 2004; Wang et al., 2019). There are limited studies that conduct metal adsorption studies on multi-metal solutions. Limiting the study on the effects of metal interaction on the adsorption (Guibal, 2004). Gyliene et al. (2002) observed that the sorption of metal ions onto chitin greatly depended on the pH and that chitin and chitosan were selective with respect to metal ion sorption. Chitin was observed to have the following order of selectivity in terms of free metal ion sorption, $Fe^{3+}>Cu^{2+}>Pb^{2+}>Zn^{2+}>Ni^{2+}>Mn^{2+}$ while chitosan had the following order of selectivity for free metal ions $Cu^{2+}>Mn^{2+}>Ni^{2+}>Zn^{2+}>Pb^{2+}>Fe^{3+}$. Similar observations were made by Rhazi et al. (2002), Zhou et al. (2004) and (Wang et al., 2019). The selective order for chitin correlates with that of the metal hydrolysis constants. Metal ions that form less soluble hydroxides were more easily adsorbed (Gyliene et al., 2002). For chitosan, the order is influenced by the size and charge of the ions. The higher the electronegativity of a metal ion, the greater the attraction of a metal ion for electrons. (Wang et al., 2019). The highest metal adsorptions on chitin and chitosan have been observed at pH between 4 and 5 (Guibal, 2004). At low pH, amine groups protonate with H^+ ions which induces electrostatic repulsion of the metal ions resulting in decreased adsorption of metal ions. At a pH greater than 6, a decrease in metal adsorption is attributed to metal hydrolysis of metal ions due to interaction with OH^- ions (Zhou et al., 2004). The temperature was observed to have a small effect on the equilibrium sorption capacities from the metal ions on chitin and chitosan (Gyliene et al., 2002; Zhou et al., 2004). An inhibitory effect on the adsorption of ferrous ions onto chitin was observed in the presence of chloride ions (Karthikeyan et al., 2005). Presence

of chloride ions results in the formation of soluble chloro-complexes which have less affinity towards chitin than free ferric ions (Anastopoulos et al., 2017).

A large amount of the metal ions (90%) are adsorbed in the first 4 to 5 hours and the sorption ability of chitin does not change after three subsequent sorption-desorption cycles (Gyliene et al., 2002). Complete adsorption is usually achieved with sorption capacities between 0.5 to 4.0 mmol/g for base metals (Chu, 2002; Gyliene et al., 2002; Rhazi et al., 2002; Wan et al., 2004; Zhou et al., 2004). Amino and hydroxyl group (C-3 position) groups are responsible for the uptake of metal cations by chelation mechanism. Amine groups in chitosan are much more reactive than the acetamide group on chitin (Guibal, 2004). Zhou et al. (2004) concluded that the adsorption mechanism of metals was complexation (non-stoichiometric) rather than ion-exchange adsorption. Complexation was at an initial pH between 1 to 5, hydrolysis and surface micro precipitation at initial pH between 6 to 7. A three-step biosorption process was proposed in Zhou et al. (2004), first the formation of a complex of the heavy metal with the amine (nitrogen), then the adsorption of the heavy metal next to the one complexed by the chitin nitrogen and finally the hydrolysis of the complex formed by the first complexation and precipitation of hydrolysis product. Therefore the complexation bond is between the free electron pairs of the coordinate pair in the amino group and the void orbital of the metal (Rhazi et al., 2002; Guibal, 2004). The mechanism of co-ordination implied in the formation of complexes is usually described by two proposed models is the “The bridge model” and “The pendant model”. In the bridge model, the metallic ion is bound by four nitrogen atoms from the same or different chain of chitosan while the pendant model suggests that the metallic ion is bound to the amino group as a pendant. The complexation reaction between metallic ions and chitosan can be described using the Lewis acid-based theory as given by Equation 8 below:

$$Chitosan + M^{n+} \rightarrow (Complex)^{n+}$$ .....Equation 8 (Rhazi et al., 2002)

Adsorption of metals onto chitin and chitosan seems to have metal selectivity, efficiency, effectiveness and are potentially cheap due to the source (Gyliene et al., 2002). It is also applicable and most efficient in acidic conditions which makes it directly applicable to PCB/e-waste leachate solutions. The complexed metal on chitin/chitosan still needs to be recovered and this process is usually conducted via desorption rather than combustion of the polymers. This is usually achieved using eluting agents. The major factors considered when choosing an eluting agent is its effectiveness to elute metals, chemical and physical effect on the bio sorbent (should be non-damaging), environmental impact (should be non-polluting) and cost (Vijayaraghavan et al., 2005). Vijayaraghavan et al. (2005) investigated the use of HCl, H_2SO_4, HNO_3, $CaCl_2$, NaCl, KCl, NH_4Cl, NaOH, EDTA (free acid), EDTA (Na) and NH4OH as eluting reagents for the elution of Ni^{2+} ions adsorbed onto crab shells. Vijayaraghavan et al. (2005) observed complete elution with mineral acids (0.1 M HCl, 0.1M H_2SO_4, 0.1 M HNO_3) and NH_4OH. This was also observed in the study by Wan et al. (2004). Very efficient eluting agents such as mineral acids lead to damage to the macroscopic appearance and weight loss of the bio material (Vijayaraghavan et al., 2005) similar to that observed during demineralization. De-ionized water and boiled water are not capable of eluting metal from chitin and chitosan (Wan et al., 2004; Vijayaraghavan et al., 2005). NaOH, 0.1M solutions of NaCl, KCl, NH_4Cl exhibited low effectiveness in eluting while the use of

EDTA was less effective at high solid to liquid ratios (Vijayaraghavan et al., 2005). The elution efficiency of HCl was found to be independent of the liquor ratio. Most metal adsorption studies on chitin and chitosan conduct desorption using mineral acids. Complete desorption is achieved between 30 minutes to 1 hour (Wan et al., 2004; Zhou et al., 2004; Vijayaraghavan et al., 2005; Wang et al., 2019).

2.3 Characterisation of Sorption

Characterisation of the sorption process is of importance to be able to develop this technology further. This is because the characterisation of sorption processes allow for the development of models which predict and quantify the sorption process (Bergmann, 2015). The characterisation of the application of chitin/chitosan on the PCB/e-waste leachate solution is made complex due to the presence of multi-metals in this solution. This review is conducted to identify possible models that can be applied in the application of chitin and chitosan on the PCB/e-waste leachate solution, particularly for multi-metal adsorption studies.

2.3.1 Adsorption isotherms

At a constant temperature, the relationship between the amount of adsorbate adsorbed by the adsorbent and the concentration remaining in the bulk solution after equilibriums can be described by adsorption isotherms (Bergmann, 2015). Considering that most adsorption processes are run at constant temperatures these are useful correlations to understand the adsorption mechanisms. The most frequently used adsorption isotherms to describe metal sorption onto sorbent are the Langmuir isotherm (Langmuir, 1918; Kim et al., 2009) and Freundlich isotherm (Singh et al., 2011). In general adsorption of metals onto chitin and chitosan seem to fit the Langmuir and Freundlich isotherm models (Bergmann, 2015). Liu isotherm which was developed based on the Hill isotherm has been garnering interest as it is a combination of the Langmuir and Freundlich isotherm (Liu et al., 2014). The adsorbed adsorbate can be calculated based on Equation 9 below:

$$q_{A_t} = \frac{V(C_{A_o} - C_{A_t})}{S} \quad \text{Equation 9}$$

Where A is the adsorbate species such as a metal of interest/target metal being adsorbed; q_A is the amount adsorbate adsorbed onto the adsorbent at a specific time (mol A/ g mass of adsorbate); V is the volume of the bulk solution phase (L); C_{Ao} is the initial concentration of the adsorbate in the bulk solution phase (mol/L): C_{At} is the concentration of the adsorbate in the bulk solution phase at a specific time; S is the amount of adsorbent in equilibrium with the bulk solution (g). This equation assumes that the change in concentration of the bulk solution is due to adsorption and no other processes such as precipitation out of the bulk solution occur during the adsorption process.

2.3.1.1 Langmuir isotherm

The Langmuir isotherm (Langmuir, 1918; Kim et al., 2009) is a theoretic model based on the following assumptions:

- Adsorbates are chemically adsorbed at a fixed number of defined sites.

- A monolayer of the adsorbate is formed over the surface of the adsorbent when it is saturated.
- Active sites can only hold one adsorbate species.
- All active sites are energetically equivalent.
- Interactions between the adsorbate species are non-existent.

The Langmuir isotherm can be described by Equation 10 below:

$$q_{A_t} = \frac{Q_{max}.K_L.C_{A_t}}{1+K_L.C_{A_t}} \quad \text{Equation 10}$$

Where K_L is the Langmuir equilibrium constant (L/mol) and Q_{max} is the maximum adsorption capacity of the adsorbent (mol/g). To determine K_L and Q_{max} the Langmuir isotherm can be put in a linear form such as Equation 11 given below:

$$C_{A_t} = \frac{C_{A_t}}{q_{A_t}}.Q_{max} - K_D \quad \text{Equation 11}$$

Where K_D is the inverse of the Langmuir equilibrium constant (mol/L). Plotting C_{At} (y-axis) against C_{At}/q_{At} (x-axis) yields a linear correlation where the gradient (m)= Q_{max} and y-axis intercept (c)=-K_D. The favourability of adsorption can be determined by the Langmuir separation factor. The Langmuir separation factor is given by Equation 12.

$$R_L = \frac{1}{1+K_L.C_{A,o}} \quad \text{Equation 12}$$

Where R_L is the Langmuir separation factor and $C_{A,o}$ is the initial concentration of component A in the bulk liquid. If R_L is 0 then the adsorption is irreversible as this occurs when K_L is large, if R_L is between 0 and 1 then this is referred to as favourable adsorption, if R_L is 1 then K_L is 0 meaning this is linear adsorption and If R_L>1 then K_L is negative leading to unfavourable adsorption (desorption) (Bergmann, 2015).

When there are two or more adsorbent components present in a system with the possibility of occupying the same adsorption sites, isotherm relations become more complex (Senthilkumar & Murugappan, 2015; Girish, 2017). In cases of effluents containing various components such as in PCB/e-waste leachate solutions, interaction and competition among the adsorbing components may have a critical role or influence in the adsorption. Langmuir isotherm described before are limited to single components systems. Therefore, single component isotherm models are modified for multi-component systems. For the Langmuir isotherm, there are three modified models. These are the Extended Langmuir isotherm. The Non-modified competitive Langmuir isotherm and the Modified competitive Langmuir isotherm (Girish, 2017).

The Extended Langmuir isotherm and the Non-modified competitive Langmuir isotherm can be described by Equation 13.

$$q_{e,i} = \frac{Q_{max,i}.K_{L,i}.C_{e,i}}{1+\Sigma_{j=1}^{N}(K_{L,j}.C_{e,j})} \quad \text{Equation 13}$$

Where $q_{e,i}$ is the equilibrium adsorption capacity for component i (mol/g), $C_{e,i}$ is the equilibrium concentration (mol/L), $K_{L,i}$ is the Langmuir constant for component i (L/mol) for the Non-modified

competitive. This value is calculated from the experimental data of the individual Langmuir isotherms, $Q_{max,i}$ is the monolayer adsorption for component i (mol/g) and N the total number of components in the solution. The Extended Langmuir isotherm is developed with the same assumptions as of the single component system (Leodopoulos et al., 2012). For solutions containing two components for the Extended Langmuir isotherm, the equilibrium adsorption capacity (q_a, q_b) can be calculated using Equation 14 and Equation 15 respectively.

$$q_a = \frac{Q_{max,a}.K_{L,a}.C_a}{1+(K_{L,a}.C_a+K_{L,b}.C_b)} \quad \text{Equation 14}$$

$$q_b = \frac{Q_{max,b}.K_{L,b}.C_b}{1+(K_{L,a}.C_a+K_{L,b}.C_b)} \quad \text{Equation 15}$$

The Modified competitive Langmuir isotherm introduces an interaction term called the interaction factor (N_L). The interaction factor shows the competitive effect of adsorbates in solution and it is dependent on the concentration of the components (Srivastava et al., 2009; Kumar et al., 2011). The Modified competitive Langmuir isotherm can be described by Equation 16:

$$q_{e,i} = \frac{Q_{max,i}.K_{L,i}.\frac{C_{e,i}}{N_{L,i}}}{1+\Sigma_{j=1}^{N}(K_{L,j}.\frac{C_{e,j}}{N_{L,j}})} \quad \text{Equation 16}$$

2.3.1.2 Freundlich isotherm

The Freundlich isotherm (Singh et al., 2011) has been presented as an empirical model however it can be derived theoretically (Skopp, 2009) and the model is based on the following assumptions:

- The concentration of adsorbate on the adsorbent surface increases as the adsorbate concentration is increased
- Adsorption can occur via multiple layers
- An infinite amount of adsorption can occur.

The Freundlich isotherm can be described by Equation 17 below:

$$q_{A_t} = K_F.{C_{A_t}}^{\frac{1}{n_f}} \quad \text{Equation 17}$$

Where K_F is the Freundlich equilibrium constant (mol/g(mol/L)$^{-1/nf}$ and n_f is the Freundlich exponent (dimensionless). To determine K_L and Q_{max} the Freundlich isotherm can be put in a linear form such as Equation 18 given below:

$$lgq_{A_t} = lgK_F + \frac{1}{n_f}.lgC_{A_t} \quad \text{Equation 18}$$

Plotting lgq_{At} (y-axis) against lgC_{At} (x-axis) yields a linear correlation where the gradient (m)=$1/n_f$ and y-axis intercept (c)=lgK_F

The mono-component Freundlich equation can be extended to binary systems. The result is the Extended Freundlich isotherm (Luo et al., 2015). The Extended Freundlich isotherm for a binary system can be described by Equation 19 and Equation 20 below:

$$q_{A_t} = \frac{K_{F,a}.{C_{A_t}}^{\left(\frac{1}{n_{f,a}}\right)+x_a}}{{C_{A_t}}^{x_a}+y_a.{C_{B_t}}^{Z_a}} \quad \text{Equation 19}$$

$$q_{B_t} = \frac{K_{F,b}.C_{B_t}{}^{\left(\frac{1}{n_{f,b}}\right)+x_b}}{C_{B_t}{}^{x_b}+y_b.C_{A_t}{}^{z_b}}$$ ..... Equation 20

The values of the Freundlich constants $K_{F,a}$, $K_{F,b}$ and adsorption intensity $n_{f,a}$ and $n_{f,b}$ are obtained from the individual experiment data. The constants x_a, y_a, z_a and x_b, y_b, z_b are obtained by minimizing the error in non-linear regression analysis when plotting q_a vs C_a and q_b vs C_b.

2.3.1.3 Liu isotherm

The Liu isotherm is a combination of the Langmuir and Freundlich isotherms. It is derived from the Hill isotherm (Liu et al., 2014) and it is based on the following assumptions:

- The monolayer (Langmuir) and infinite adsorption (Freundlich) assumptions are discarded. Therefore, saturation of active sites should occur.
- Actives sites of the adsorbent cannot possess the same energy.

The Liu isotherm can be described by Equation 21 below:

$$q_{A_t} = \frac{Q_{max}.K_L.C_{A_t}{}^{n_L}}{(1+K_L.C_{A_t})^{n_L}}$$ ..... Equation 21

Where n_L is the dimensionless exponent of the Liu equation and it can be any positive value.

2.3.2 Adsorption kinetic models

2.3.2.1 Pseudo first order

Adsorption kinetics are an important tool in the analysis of the adsorption reaction pathway in adsorption processes. The most commonly applied models for adsorption kinetics bases on chemical reaction kinetics are the Pseudo-first order and Pseudo-second-order adsorption kinetic models. Adsorption onto chitin and chitosan has been shown to fit both models (Bergmann, 2015).The exponent of the rate laws of the chemical reaction are usually independent of the coefficient of chemical equations but in some case are related. Theoretically, the order with respect to adsorption represents the number of active sites in the chemical reaction. The simplest model and traditional kinetic model is described using an expression originally developed by Lagergren (Pumera, 2011). This kinetic model is known as the Pseudo-first-order model and is given by Equation 22:

$$\frac{dq_t}{dt} = K_f.(q_e - q_t)$$ ..... Equation 22

Where q_t is the adsorbed sorbate (mol/g), q_e is the equilibrium adsorption capacity (mol/g), K_f is the pseudo-first-order rate constant (h^{-1}) and t is the contact time (h). The integration of Equation 33 with initial conditions q_t=0 at t=0 and q_t=q_t at t=t yields a linearized equation, Equation 23:

$$\ln\left(\frac{q_e-q_t}{q_e}\right) = -K_f.t$$ ..... Equation 23

Plotting $\ln(q_e-q_t/q_e)$ (y-axis) against t (x-axis) yields a linear correlation where the gradient (m)=-K_f. The nonlinear form is given by Equation 24:

$$q_t = q_e.[1 - \exp(-K_f.t)]$$ ..... Equation 24

2.3.2.2 Pseudo second order

The Pseudo-second-order adsorption kinetic model is given by Equation 25 (Bergmann, 2015):

$$\frac{dq_t}{dt} = K_f.(q_e - q_t)^2 \quad \text{Equation 25}$$

The integration of Equation 26 with initial conditions q_t=0 at t=0 and q_t=q_t at t=t yields Equation 26:

$$q_t = \frac{K_s.q_e{}^2.t}{1+q_e.K_s.t} \quad \text{Equation 26}$$

The initial sorption rate (Ho) in mol/g/h is obtained when t approaches zero and is given by Equation 27:

$$h_o = K_s.q_e{}^2 \quad \text{Equation 27}$$

The linearized Pseudo-second-order adsorption kinetic model is given by Equation 28:

$$\frac{\mathrm{t}}{q_t} = \frac{1}{k_s.q_e^2} + \frac{1}{q_e}.t \quad \text{Equation 28}$$

Plotting t/q_t (y-axis) against t (x-axis) yields a linear correlation where the gradient (m)=$1/q_e$ and y-intercept (c)=$1/K_s.q_e{}^2$.

2.3.2.3 Intra particle Diffusion model

The possibility of intra particle diffusion can be explored using the Weber and Morris Intraparticle diffusion model. The Weber and Morris Intra particle diffusion model can be described by Equation 29 (Weber Jr et al., 1963; Hall et al., 1966; Simonin & Boute, 2016):

$$q_t = K_{id}.\sqrt{t} + C \quad \text{Equation 29}$$

Where q_t is the amount of adsorbate adsorbed onto sorbent (mol. g^{-1}. h^{-1}), K_{id} is the intraparticle diffusion rate constant (mol. g^{-1}. $H^{-0.5}$) and C is a constant related to the thickness of the boundary layer (mol/g). Plotting q_t (y-axis) against $t^{1/2}$ (x-axis) yields a linear correlation where the gradient (m)=K_{id} and y-intercept (c)=C. Generally, adsorption has three zones. To illustrates an example in the application of the Intraparticle diffusion model, Figure 2. 4 shows the plot of q_t against $t^{1/2}$ with multi linear for RB-4 dye using SWCNT adsorbent (lijima, 1991). The first linear section (1st Zone) in Figure 2. 4 was assigned to the diffusion of dye onto the adsorbent surface (fastest sorption stage), the second linear section (2nd Zone) is intraparticle diffusion and the third stage is diffusion through smaller pores (lijima, 1991).

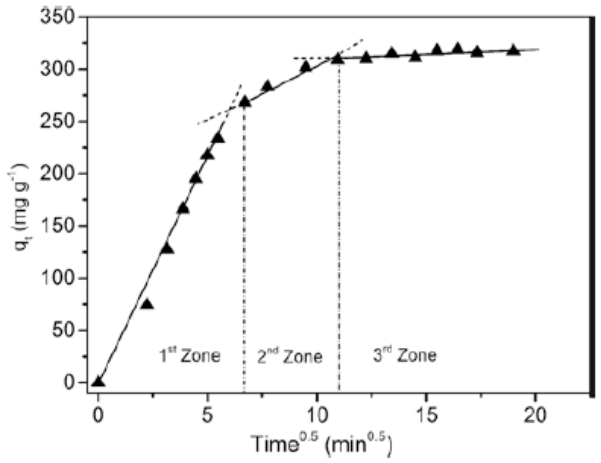

Figure 2. 4: Intraparticle kinetic adsorption curve of RB-4 dye using SWECNT at pH of 2, temperature of 25^{o}C and initial concentration of 800 mg L^{-1} adsorbate.

2.4 Summary of Literature Review

Downstream processing has been identified as a high-cost stage in the recovery of value from waste. Commercial metal recovery technologies such as precipitation, solvent extraction, electrowinning, adsorption and ion exchange require metals in aqueous solutions for application (Cui & Zhang, 2008). Therefore, metal upgrading or extraction of metals into solutions with pyrometallurgy/bioleaching/chemical leaching is a necessary step before recovery. Bioleaching of PCBs/e-waste using acidophiles, ferric and sulfuric acid results in the complete extraction of base metals to form base metal-rich leachates. The hydrometallurgical techniques which are used to recover metals from solutions are precipitation (often via cementation), solvent extraction and electrowinning, ion exchange and sorption. For bio hydrometallurgical, sorption is used extensively while sulphide precipitation is gaining traction (Blais et al., 2008).

Cementation has a drawback in that there is a dissolution of the sacrificial metal and competing reactions (Demirkiran et al., 2007). Precipitation of metals remains the most favourable option on an industrial scale due to its cost-effectiveness, performance, and simplicity. However, precipitation with hydroxides is accompanied by coprecipitation which results in mixed precipitates (Couillard & Mercier, 1992; Marchioretto et al., 2005). Precipitation with sulphides has the advantages of high recovery efficiencies, high metal selectivity, low hydraulic retention time and production of disposable sludges. The solvent extraction-electrowinning (SX-EW) process has the major drawback of higher environmental impact concerning the climate change indicator than pyrometallurgy due to the high use of (coal-based) electricity (Ayres et al., 2002). This will be the case if used in South Africa due to the high use of coal for electricity generation. Another drawback with the use of EW is the need for concentrated solutions and expensive anodes making it a high-cost investment (Veit et al., 2006). Ion exchange has disadvantages in particular when considering the application on PCB base metal bio leachate solutions. These are that presence of organic matter and ferric ions in the leachate solution may result in fouling of the resins (Dow Chemical Company, 1999; Kansara et al., 2016). Mabuka et al. (2018) showed that chitin sourced from Black soldier flies had cheaper recovery costs when compared to ion exchange resins in the recovery of ferrous ions.

Adsorption is gaining traction as a more efficient technique for the recovery of metals from the solution. The limitation in other techniques such as large production of sludge, high capital costs, lack of metal recovery selectivity, low efficiencies, sensitive operation conditions and high cost in disposal give adsorption an advantage (Bergmann, 2015). Bio sorbent maximum metal adsorption capacities of chitin, chitosan, chitosan derivatives, cross-linked chitosan were observed to be higher than those of commercial sorbents, bacteria, fungi, algae, proteins and tannin derivatives (Cui & Zhang, 2008). Chitin has been observed to have the following order of selectivity in terms of free metal ion sorption, $Fe^{3+}>Cu^{2+}>Pb^{2+}>Zn^{2+}>Ni^{2+}>Mn^{2+}$ while chitosan had the following order of selectivity for free metal ions $Cu^{2+}>Mn^{2+}>Ni^{2+}>Zn^{2+}>Pb^{2+}>Fe^{3+}$. The application of chitin and chitosan on metal solutions results in refined solutions. This indicates the need for a secondary metal recovery technology to recover metals as solid products. The BSF larvae contain about 9 % (dry mass) chitin which is mostly located in the FLS. The large amounts of proteins, lipids and minerals in BSF larvae indicate the need for deproteination and demineralization if chitin will be sourced directly from the BSF larvae.

2.5 Dissertation Objectives and Key Questions

2.5.1 Objectives and Scope

The literature review on the metal recovery process for PCBs/e-waste showed the need to focus on investigating metal recovery techniques for downstream metal processing. Therefore, this dissertation will focus on the recovery of three primary base metals in the PCB leachate solution resulting from the acidic leaching of PCBs. The primary base metals are copper, aluminium and iron. Copper, aluminium and iron's high concentrations in PCBs reduce the efficiency in the recovery of precious metals. Therefore, their recovery before precious metal recovery is necessary. Copper has a high metal value in PCBs while the iron is a lixiviant in the leaching process. Therefore, these metals will also be recovered for this rationale. Adsorption onto chitin and chitosan seems to be a promising method for the recovery of metals from solutions. Adsorption onto chitin and chitosan is a metal selective, efficient, cheap, environmentally friendly and circular economy driven due to the sourcing of these sorbents from waste.

The BSF larvae shell waste is of interest due to its high chitin content and low crystallinity. Therefore, chitin and chitosan used in this study will be sourced from the BSF larvae. The cost of the sorption process depends on the cost of the sorbent. This is affected by the extraction and production methodology. This also has effects on the character of chitin and chitosan. There is a need to investigate the effects of the extraction methodology of chitin and chitosan from BSF larvae shells on the cost of producing these bio sorbents and their performance during metal adsorption. The order of metal adsorption selectivity on chitin and chitosan is usually determined from single metal adsorption studies. This limits the investigation of the effects of metal interactions on metal adsorption. Therefore, this study will consider multi-metal adsorption studies. The application of these sorbents on multi-metal solutions results in selective metal recovery in the form of refined/ single metal concentrated solutions. Therefore, further refining is required to recover the metals in solid form. Precipitation with sulphides is also a promising technique due to its low cost, metal selectiveness and high recovery efficiencies. This makes it a potentially applicable technique for the recovery of solid metals from PCB leachate solutions and

desorbed leachate solutions. Techno-economic studies of the combined use of adsorption with chitin and chitosan and precipitation with sulphides for metal recovery are limited. Thus, they will be investigated in the dissertation.

The objectives of this dissertation are therefore the following:

- To develop a cost-effective methodology of extraction of chitin and production of chitosan from BSF fly larvae shell waste for application as a metal sorbent.
- To determine the sorption character, adsorption capacities, order and degree of metal selectivity for the adsorption of copper, iron and aluminium ions onto chitin and chitosan sourced from the BSF larvae shells.
- To investigate the effects of metal interaction in copper, iron and aluminium adsorption onto chitin and chitosan.
- To determine the recovery efficiency, order and degree of metal selectivity for the recovery of copper, from PCB leachate solutions by sulphide precipitation.
- To conduct a techno-economic analysis on the combined application of adsorption with chitin/chitosan and sulphide precipitation in the recovery of copper and iron from PCB leachate solutions.

2.5.2 Hypotheses

This dissertation has 3 proposed hypotheses which are:

- The order of metal adsorption selectivity of copper, iron, aluminium from a PCB leachate solution onto chitin extracted from BSF larvae will be $Fe^{3+}>Al^{3+}>Cu^{2+}>Fe^{2+}$

The order of selectivity of chitin has been identified to be $Fe^{3+}>Cu^{2+}>Pb^{2+}>Zn^{2+}>Ni^{2+}>Mn^{2}$ (Gyliene et al., 2002; Zhou et al., 2004) and this order closely follows the order of hydrolysis constants of the metal hydroxides (Gyliene et al., 2002) were the metals with lower solubility products precipitate first

- The order of metal adsorption selectivity of copper, iron, aluminium from a PCB leachate solution onto chitosan produced from chitin extracted from BSF larvae will be $Cu^{2+}>Fe^{3+}>Al^{3+}$.

The order of metal adsorption selectivity of chitosan has been identified to be $Cu^{2+}>Hg^{2+}>Zn^{2+}>Cd^{2+}>Ni^{2+}>Co^{2+}>Ca^{2+}$ (Rhazi et al., 2002) and $Cu^{2+}>Mn^{2+}>Al^{3+}$ (Wang et al., 2019) this order is influenced by the size and charge of the ions. Electronegativity is directly and inversely proportional to the effective nuclear charge and covalent radius respectively. The higher electronegativity of a metal ion the greater the attraction of metal ion for electrons. (Wang et al., 2019).

- The order of metal selectivity for the precipitation of copper, iron, aluminium from a PCB leachate solution using sulphide precipitation will be $Cu^{2+}>Al^{3+}>Fe^{3+}$ with the metals forming CuS, $Al(OH)_3$and FeS respectively.

The order of initial precipitation of metal sulphide salts is $Cu^{2+}>Zn^{2+}>Ni^{2+}>Fe^{2+}$and this is based on the solubility products of the metal sulphide salts. The lower the solubility product of the metal

sulphide, the more the ease for precipitation (Blais et al., 2008; Lewis, 2010; Wang et al., 2014). Precipitation of ferric ions with sulphide ions results in the reduction of ferric ions with the precipitated metal salt being FeS. (Kiilerich et al, 2018). While for the precipitation of aluminium ions with sulphide ions, Aluminium Sulphide hydrolyses in the presence of moisture to form hydrated Aluminium Oxides/Hydroxides (Lopez et al, 2011).

2.5.3 Key questions

The key questions in this dissertation are as follows:

- What are the necessary steps for chitin extraction and chitosan production from BSF larvae for the use in the adsorption of metals from solutions?
- How much chitin and chitosan can be extracted and produced from the BSF larvae and what is the cost of production?
- What is the order and degree of metal adsorption selectivity (adsorption capacity) of iron, copper and aluminium onto chitin and chitosan?
- What are the active sites on chitin and chitosan involved in the adsorption of iron, copper, and aluminium?
- What is the techno-economic feasibility of using chitin/chitosan and sulphide precipitation for the recovery of iron, copper, and aluminium from PCB leachate solutions?
- How many times can the chitin and chitosan be recycled into the metal adsorption process?
- What is the recovery efficiency of copper by sulphide precipitation and what is its purity?

Chapter 3: Materials and Methods

3.1 Overview of Research Method Approach

The approach to the methodology in this dissertation was broken down into three phases. The initial phase (Phase 1) involved chitin extraction from the fly larvae and chitosan production from the extracted chitin. Both these processes (chitin extraction and chitosan production) were optimized to produce chitin and chitosan that is selective towards the adsorption of free ferrous and copper ions respectively. Metal adsorption selectivity is important when considering applications of these polymers on the PCB metal-rich leachate solutions due to the multi-metals in the solution. The second phase (Phase 2) involved metal adsorption and desorption studies with the produced chitin and chitosan. The third phase (Phase 3) involved selective precipitation of copper with NaHS on the Model leachate solution.

3.1.1 The Development of the Model Leachate Solution

PCBs have various metals (precious and base). In this dissertation, the focus is on base metal recovery after the bio-assisted chemical leaching using a two-step bioleaching process with ferric and sulfuric acid as done in Brandl et al. (2001). The removal of base metals in PCBs results in improved extraction efficiency of gold as demonstrated in Pham Van (2009). Base metal leaching with ferric and sulfuric acid results in the complete dissolution of iron, aluminium, copper, nickel, zinc into solution. Lead and tin are observed to precipitate out in the form of $PbSO_4$ and SnO respectively during the leaching process (Brandl et al., 2001; Ilyas et al., 2007; Wang et al., 2009). A PCB leachate model solution (hereafter called the Model leachate solution) was developed using the extraction efficiencies from Brandl et al. (2001) and Wang et al. (2009) and the average PCB metal composition of the PCB composition range in Section 2.1. The Model leachate solution was based on leaching 1g of PCB with the average PCB metal composition.

The concentration of the metals in the Model leachate solution are shown in Table 2. 1 in Section 2.1. Table 2. 1 in Section 2.1 shows that the concentration of copper, aluminium and iron are in the highest amounts in the model leachate solution at 2.79 mmol/L, 2.82 mmol/L and 1.11 mmol/L respectively. Iron extraction from PCB is generally not quantified in the acidophilic bioleaching studies as iron is the lixiviant in the mechanism. However, according to Choi et al. (2004), almost all the iron in the PCB is leached into solution in the form of ferrous ions. Nickel and zinc are also present in the model leachate solution at 0.278 mmol/L and 0.442 mmol/L respectively. Tin and lead were not considered in the model leachate solution due to their potential of precipitating out of solution during the leaching stage and the potential reduction of lead in PCBs due to the (RoHS) (2002/95/EC) directive. The model leachate solution was then created by dissolution of Copper Sulphate heptahydrate, Aluminium Sulphate octa decahydrate, and anhydrous Ferrous Sulphate salts for the respective metals in an acidic solution with an initial pH of 3.4. At a working pH of 3.4 and the initial concentrations described in Table 2.1, the metal salts were dissolute particularly metal ions with relatively low solubility products (aluminium and ferric ions). Ferrous ions were chosen as the dissolute iron species due to the oxidation of ferric ions during acidic leaching processes particularly in the presence of other base metals. Ferric ions were only investigated for the understanding of their adsorption onto chitin and chitosan in Section 5.3.

3.1.2 Investigation of the Order of Metal Adsorption Selectivity

The order of metal sorption capacity indicates the order of metal adsorption selectivity of the sorbent (Gyliene et al., 2002; Rhazi et al., 2002; Zhou et al., 2004). Adsorption is affected by the initial concentration of free metals in the solution. An increase in the initial concentration of metal results in higher adsorption rates and metal adsorption capacities onto chitin/chitosan (Guibal, 2004; Ren et al., 2008). Therefore, the consideration of the initial concentration of the base metals in the Model leachate solution is important. Only copper, ferrous and aluminium ions were considered for the sorption experiments due to their high concentrations in the model leachate solution. The order of metal adsorption selectivity is difficult to decipher in multi-metal leachate solutions. This is because it is difficult to isolate individual metal influence on the adsorption selectivity of metals in multi-metal solutions (Bergmann, 2015). Therefore, most adsorption studies decipher the order of metal adsorption selectivity using single metal studies (Guibal, 2004; Bergmann, 2015; Wang et al., 2019). However, this approach limits the study on the effects of metal interaction on adsorption (Guibal, 2004).

Therefore, a simplified approach was developed to understand the effect of metal interaction on the order of metal adsorption selectivity for copper, ferrous and aluminium onto chitin and chitosan. This simplified approach involved the use of bimetal solution studies as shown in Figure 3. 1. Bimetal solutions studies allow for metal interaction while remaining simple enough to determine the order of metal selective adsorption. Figure 3. 1 shows that the bimetal study approach in determining the metal adsorption selectivity of copper, aluminium and iron on chitin and chitosan. The bimetal test solution of copper and ferrous ions was chosen as the initial stage for optimizing the extraction and production of chitin and chitosan for two reasons. Firstly, copper and ferrous ions are in high concentration in the Model leachate solution. Lastly and most importantly, iron and copper have been shown to have the highest order of metal adsorption selectivity on chitin and chitosan respectively. They also have been shown to follow each other closely in the order of metal selective adsorption on chitin and chitosan (Gyliene et al., 2002; Rhazi et al., 2002; Zhou et al., 2004; Wang et al., 2019).

The second stage in the approach to decipher the order of metal adsorption selectivity using bimetal test solutions involved sorption studies on an equimolar copper-aluminium bimetal solution. For chitosan, if aluminium is adsorbed more than copper in the equi molar copper-aluminium bimetal solution then that system will have to be optimized to reverse this order. This would be done by either optimizing the degree of acetylation of the chitosan using chitosan production parameters described in Section 2.2.5.3 or the initial adsorption pH. For chitin, if copper is adsorbed more than aluminium in the equi molar copper-aluminium bimetal solution then the order of selectivity can be conclusive however if the sorption is reverse then a further test with an equimolar ferrous-aluminium solution must be conducted. If aluminium is adsorbed more than ferrous in the equimolar ferrous-aluminium solution then that system will have to be optimized to reverse this order. This would be done by either optimizing the degree of acetylation of chitin using the chitin extraction parameters described in Section 2.2.5.3 or adsorption pH.

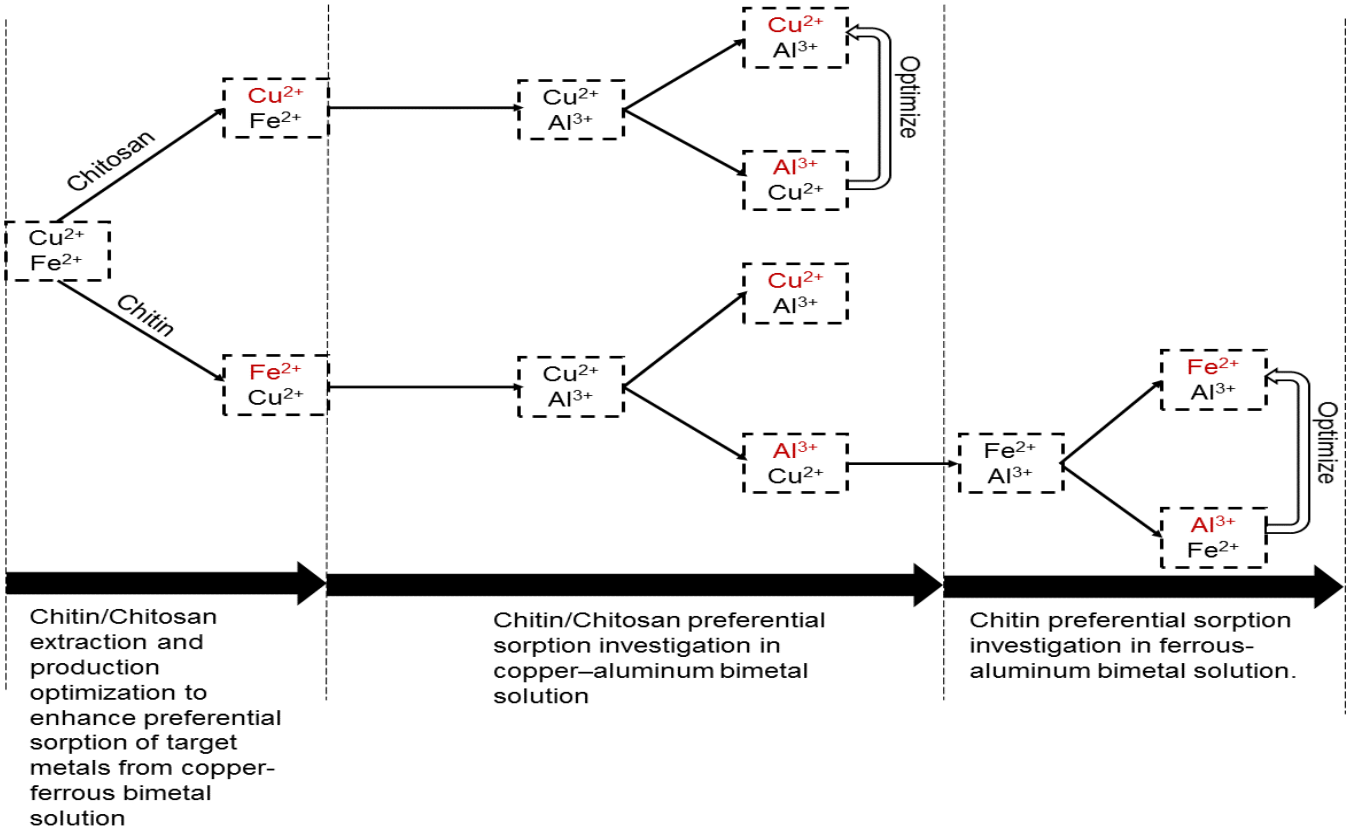

Figure 3. 1: Approach method towards the investigation of the order of metal sorption selectivity on chitin and chitosan using a bimetal test solution approach

Single metal test solutions were also used to investigate the order of metal adsorption selectivity on the chitin and chitosan. The single metal solution study was used to compare the order of metal adsorption selectivity determined by the bimetal test solution approach. The single metal solution study also allows for a better fundamental understanding of the sorption of the individual metals in the Model leachate solution.

3.1.3 Techno-Economic Analysis of Chitin and Chitosan Production and Metal Adsorption

The techno-economic analysis of the metal recovery costs for the combined use of adsorption with chitin and chitosan and sulphide precipitation in the recovery of copper and iron from the Model leachate solution was calculated based on three parameters. These parameters were the cost of production of chitin and chitosan from BSF larvae, the cost of desorption and precipitation.

The cost of production of chitin and chitosan was calculated using Equation 30 and Equation 31:

$$Cost\ of\ process\ production = \frac{Cost\ of\ reagents\ used\ in\ process}{Mass\ yield\ of\ chitin/chitosan} \quad \text{Equation 30}$$

$$Total\ cost\ of\ production = \frac{Cost\ of\ (Demineralization + Deproteination + Decolourization + De-acetylation)}{Overal\ mass\ yield\ of\ chitin/chitosan} \quad \text{Equation 31}$$

Where the cost of reagents used in the process is the cost of used HCl in demineralization, electricity (heating plate), NaOH in deproteination and de-acetylation and NaClO in decolourization. Table 3. 1 shows the cost of the reagents used in the processes for chitin extraction and chitosan production.

Table 3. 1: Cost of reagents used in chitin extraction and chitosan production

Cost of Caustic Soda (NaOH) ($/kg)	0.425	(Alibaba, 2019a)
Cost of Electricity in South Africa ($/kWh)	0.0715	(Eskom, 2018)
Cost of HCl ($/kg)	0.3	(Alibaba, 2019b)
Cost of NaClO ($/kg)	1.3	(Alibaba, 2019c)
Cost of H_2SO_4 ($/kg)	0.3	(Alibaba, 2019d)
Cost of NaHS ($/kg)	0.3	(Alibaba, 2019e)

The cost of desorption was calculated based on 100 mL of 0.1M H_2SO_4. The amount of H_2SO_4 used was 0.01 moles of H_2SO_4 (0.981 g) which costs \$ 2.94×10^{-4}.

The cost of precipitation was calculated based on Equation 32:

$$Cost\ of\ precipitation = \in_i\ (Cost\ of\ NaHS \times Amount\ of\ metal\ (i) recovered) \quad \text{Equation 32}$$

Where metal (i) is either copper, aluminium or iron, $\in_i$ is the extent of the reaction for metal i, the amount of metal (i) recovered in moles per gram of chitin/chitosan and the cost of NaHS is in ($/mole). $\in_i$ is calculated based on Equation 33, Equation 34 and Equation 35, for copper and ferrous ions $\in$=1, for aluminium $\in$=1.5.

$$NaHS_{(aq)} + Cu^{2+}{}_{(aq)} \rightarrow Na^{+}{}_{(aq)} + H^{+}{}_{(aq)} + CuS_{(s)} \quad \text{Equation 33}$$

$$NaHS_{(aq)} + Fe^{2+}{}_{(aq)} \rightarrow Na^{+}{}_{(aq)} + H^{+}{}_{(aq)} + FeS_{(s)} \quad \text{Equation 34}$$

$$3NaHS_{(aq)} + 2Al^{3+}{}_{(aq)} \rightarrow Na^{+}{}_{(aq)} + H^{+}{}_{(aq)} + Al_2S_{3_{(s)}} \quad \text{Equation 35}$$

The potential revenue from the sale of the recovered metal salts was calculated using Equation 36.

$$Revenue\ of\ recovered\ metals = (Cost\ of\ metal\ (i)\ sulfide \times metal\ (i) recovered) \quad \text{Equation 36}$$

Where the cost of metal(i) sulphide is given in Table 3. 2 and in the case of Aluminium Sulphide, Aluminium Hydroxide was used as Aluminium Sulphide hydrolyses to form Aluminium Hydroxide when exposed to moisture or the atmosphere (Jensen, 2002). It was assumed that all desorbed metals could be recovered by precipitation with NaHS. Included in the potential revenue was the revenue from sales of the chitin/chitosan used in the adsorption process. This revenue was calculated based on the market prices of agricultural grade chitin and chitosan in Table 3. 2.

Table 3. 2: Market prices of precipitated metal salts and agricultural grade chitin/chitosan

Cost of CuS (s) ($/kg)	200	(Alibaba, 2019f)
Cost of FeS (s) ($/kg)	300	(Alibaba, 2019g)
Cost of Al(OH)3 (s) ($/mole)	1.03×10^{-5}	(Alibaba, 2019h)
Cost of agricultural grade chitin ($/g)	0.014	(Alibaba, 2019i)
Cost of agricultural grade chitosan ($/g)	0.020	(Alibaba, 2019i)

The potential gross profit of the recovery process was calculated using Equation 37.

$$Gross\ profit = Revenue - Cost\ of\ (production + desorption + precipitation) \quad \text{.....Equation 37}$$

In general, this techno-economic analysis does not include capital costs and only includes operational costs which include reagent costs and energy costs. A basis of 1 kg of metal recovered was used for the techno-economic analysis.

3.2 Preparation of Sorbents

3.2.1 Liberation of Fly Larvae Shells

BSF larvae (*Hermetia illucens*) were obtained from AgriProtein technologies in Philippi, Cape Town and stored at -20 ^{o}C. To extract the fly larvae shells (FLS) from the fly larvae, the inside material was liberated using a washing and milling process. The initial liberation step involved grinding the fly larvae from storage with a pestle and mortar to expose the inside material of the fly larvae, followed by washing the fly larvae with 500 mL of distilled water in 1 L beakers to remove the liberated material. This process was repeated three times with ceramic filters (1 mm diameter) being used to separate the washed FLS from the supernatant material. The FLS were then dried in an iron pan at r.t.p until the mass of the iron pan with the fly larvae shells remained constant. The drying process of the FLS took 48 hours.

3.2.2 Demineralization of Fly Larvae Shells.

Dry FLS were demineralized using 2 M HCL at r.t.p for 2 hours using a liquor ratio of 1 g of FLS to 11.25 mL of 2 M HCl. 200 g of dry FLS were demineralized using 2250 mL of 2 M HCl split into two 1500 mL plastic beakers. The 2 M HCl was prepared by the addition of 442 mL of 32 % HCl into 1808ml of De-ionized water. The demineralization process was run using magnetic stirrers to stir the mixture in an acid fume hood. Figure 3. 2 shows the experimental setup for the demineralization of the FLS. Initially, the bubbling of gases was observed however after 2 hours, there was no visible bubbling of gas. The demineralized FLS were then filtered using (1 mm diameter) ceramic filters and washed with de-ionized water until the pH of the wash water was 7 (neutral). The washed demineralized FLS were then dried on an iron pan at r.t.p until the mass of the iron pan with the demineralized FLS remained constant. The drying process of the demineralized FLS took 24 hours. The mass of the dry demineralized FLS was then measured using a scale to obtain the yield for demineralization.

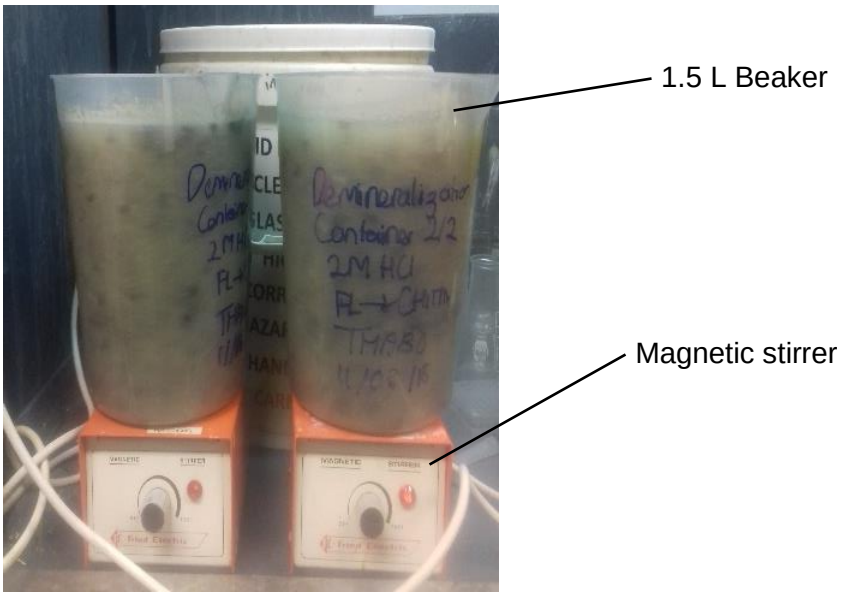

Figure 3. 2: Experimental setup for the demineralization of fly larvae in acid fume hood

3.2.3 Deproteination of Fly Larvae Shells

FLS/demineralized FLS were deproteinated using 4 (wt %) NaOH at 60 ^{o}C for 2 hours using a liquor ratio of 1 g of FLS/demineralized FLS to 25 mL of the 4 wt % NaOH solution. The FLS/demineralized FLS were ground to a seize size between 100 mm and 200 mm using a mortar and pestle. 16 g of 98 % NaOH pellets were placed gradually in 400 mL of de-ionized water in a 500 ml glass Erlenmeyer flask under stirring with a magnetic stirrer. The addition of the 98 % NaOH pellets resulted in the release of heat and the mixture was air-cooled. The prepared 4 wt % NaOH solution was then mixed with 16 g of grounded FLS/demineralized FLS and poured into a 500 ml 316L Stainless steel container using a funnel. The deproteination was done under a reflux system in an organic fume hood with a stainless-steel condenser using mono ethylene glycol coolant which was run at 5 ^{o}C. The refluxing was conducted by connecting the 500 ml Stainless steel reactor containing the FLS/demineralized FLS to the condenser and placing it in a 1 L beaker with water heated by an electric heating plate. Figure 3. 3 shows the experimental setup for the deproteination process of the FLS/demineralized FLS. The temperature of the water was monitored using a digital thermometer. The electric heating plate was adjusted until the temperature of the water was constant at 60 ^{o}C and this was monitored for the duration of the reaction time. The power on the electric heating plate was adjusted accordingly to ensure the temperature remained constant. The deproteinated FLS/demineralized FLS was then washed with de-ionized water until the pH of the wash water was 7 (neutral) and filtered using Whatman filters paper (90mm Diameter and 2.7 Micron). The demineralized and deproteinated FLS were called Chitin 2 while FLS which were only deproteinated were called Chitin 3. Chitin 2 and Chitin 3 were then dried at r.t.p, and their dry weight measured using a scale to obtain the yields from deproteination.

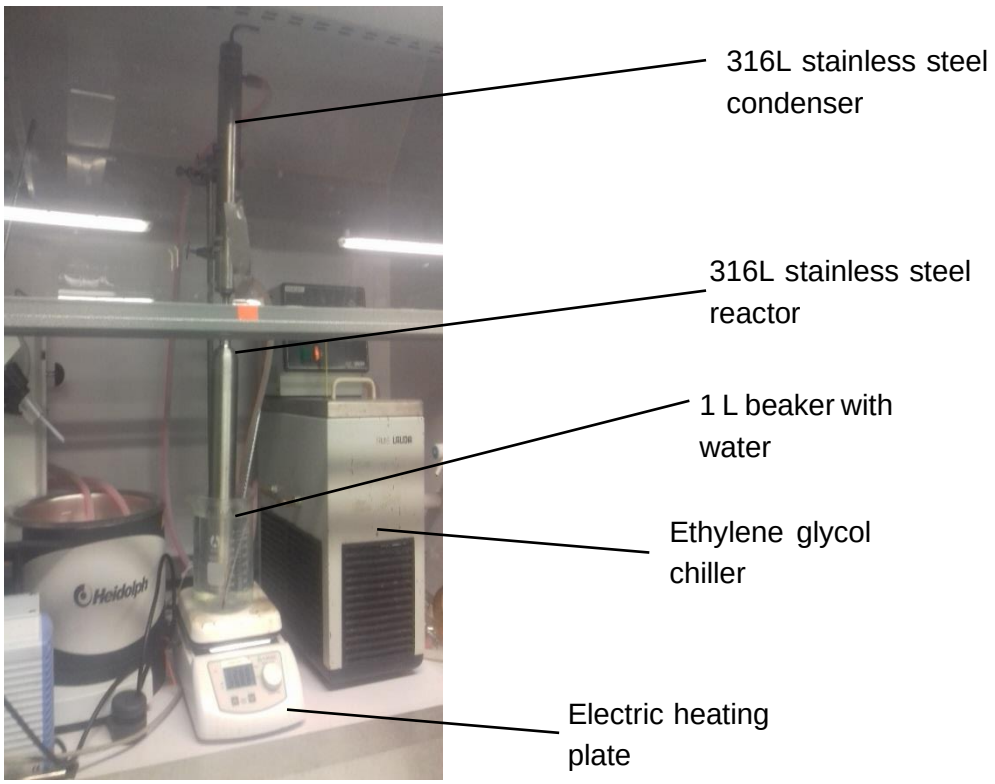

Figure 3. 3: experimental setup for the deproteination and deacetylation of Chitin/ FLS in organic fume hood.

An investigation on the effect of deproteination reaction time on Chitin 3 character and its performance in the adsorption studies was conducted. This was done by keeping the concentration of NaOH at 4 (wt %), the temperature at 60 ^{o}C, the working volume at 400 mL of the reagent, the liquor ratio at 1 g FLS: 25 mL but varying the reaction time at 1 h, 2 h and 4 h in the deproteination process. The Chitin 3 produced were called Chitin 3 (1h Deprot), Chitin 3 (2h Deprot) and Chitin 3 (4h Deprot) respectively.

3.2.4 Decolorization of Chitin

An attempt was made to decolourize Chitin 2 with 1 % KMnO4 for 1 hour thereafter 1 % Oxalic acid for another 1 hour both at a liquor ratio of 1 g to 10 mL reagent. However, after 3 days there was no visible colour change. Decolourization of Chitin 2 was then conducted using 3.5 % NaClO (Bleach) at a liquor ratio of 1 g of Chitin 2 to 10 mL of Bleach for 24 hours at r.t.p. 20 g of Chitin 2 was placed in 200 ml of Bleach in a 500 ml Erlenmeyer flask under stirring for 24 hours at r.t.p. After 24 hours, there was a visible colour change from dark brown to white. The decoloured Chitin 2 were then washed with de-ionized water until the pH of the wash water was 7 (neutral) and filtered using Whatman filter paper (90mm Diameter and 2.7 Micron). The decoloured Chitin 2 was then called Chitin 1. Chitin 1 was then dried at r.t.p, and its dry weight measured using a scale to obtain the yields from decolourization.

3.2.5 Deacetylation of Chitin and FLS

Chitin/FLS were deproteinated using 40 wt % NaOH solution at 90 ^{o}C for 6 hours using a liquor ratio of 1 g of Chitin/FLS to 25 mL of the 40 wt % NaOH solution. 160 g of 98 % NaOH pellets were placed gradually in 400 mL of de-ionized water in a 500 mL glass Erlenmeyer flask under stirring with a magnetic stirrer. The addition of the NaOH resulted in the release of heat and the mixture was then air-cooled. The prepared 40 wt % NaOH solution was then mixed with 16 g of Chitin/grounded FLS and poured into a 500 mL 316L Stainless steel container using a funnel. The deacetylation was done under a reflux system with a stainless-steel condenser using a coolant which was run at 5 ^{o}C in an organic fume hood. The refluxing was conducted by connecting the 500 mL Stainless steel container containing the Chitin/grounded FLS to the condenser and placing it in a 1L beaker with water heated by an electric heating plate. Figure 3. 3 shows the experimental setup for the de-acetylation process of the Chitin/grounded FLS. The temperature of the water was then monitored using a digital thermometer. The power of the electric heating plate was adjusted until the temperature of the water was constant at 90 ^{o}C and this was monitored for the duration of the reaction time to ensure the temperature remained constant. This was done by adjusting the power of the electric heating plate accordingly. The deproteinated Chitin/grounded FLS was then washed with de-ionized water until the pH of the wash water was 7 (neutral) and filtered using Whatman filter paper (90mm Diameter and 2.7 Micron). The de-acetylated Chitin 2, Chitin 3 and grounded FLS were called Chitosan 2, Chitosan 3 and Chitosan 4 respectively. Chitosan 2, Chitosan 3 and Chitosan 4 were then dried at r.t.p, and their dry weight measured using a scale to obtain the yields from deacetylation.

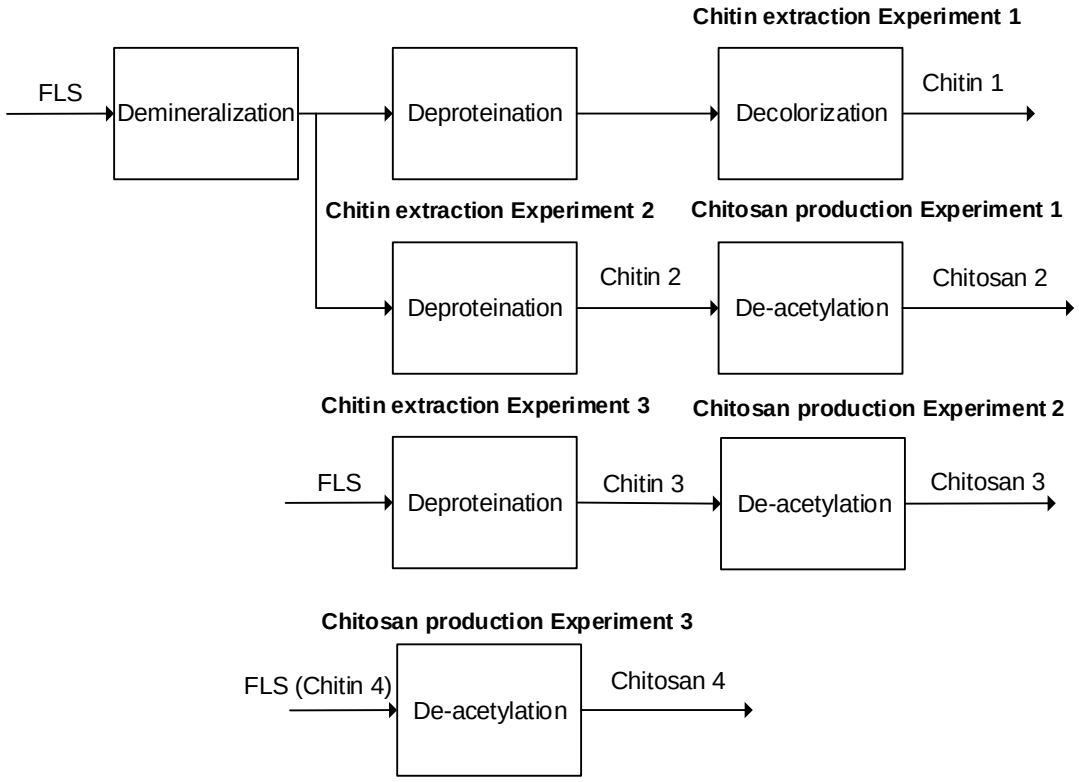

Figure 3. 4: Experimental protocol for the extraction and production of chitin and chitosan from BSF larvae shells.

Figure 3. 4 shows the general experimental protocol for the extraction and production of chitin and chitosan from BSF larvae shells and Table 3. 4 shows the conditions used for demineralization, deproteination, decolourization and deacetylation.

Table 3. 3: Condition in demineralization, deproteination, decolourization and deacetylation of FLS.

	Demineralization	**Deproteination**	**Decolorization**	**Deacetylation**
Concentration of HCl (M)	2			
Concentration of NaOH (%) (W/V)		4		40
Concentration of NaClO (%) (V/V)			3	
Reaction time (h)	2	2	24	6
Temperature (ºC)	r.t.p	60	r.t.p	100
Liquor ratio (g/ml)	1.:11.25	1:25	1:10	1:25
Particle size (µm)	2000 to 5000	100 to 200	100 to 200	100 to 200

3.3 Characterization of Sorbents

The major output variables in chitin extraction and chitosan production are the yield of chitin/chitosan, degree of deacetylation (DD), viscosity and the molecular weight of chitosan. In this study, only yield, structure and DD were determined for the characterisation of chitin extracted and chitosan produced from the BSF FLS.

3.3.1 Yield

The yield of FLS, chitin and chitosan was obtained from the dry mass of the material after each extraction/production step.

3.3.2 Chitin/Chitosan Structure

Infra-Red Spectra of the FLS, chitin and chitosan were performed using a Nicolet iS50 Fourier-transform infrared spectroscopy (FTIR) spectrometer. 5 mg of FLS/chitin/chitosan sample were mixed with 500 mg of potassium bromide (KBr) with a mortar and pestle until a fine granulation and a homogenous consistency was reached. This mixture was then inserted into a stainless-steel matrix to undergo compression at 4 tons in an automatic hydraulic press. Under compression pressure which took 2 minutes with a slow hydraulic release, a compact transparent mass was obtained. This was then inserted into the FTIR spectrometer. Both absorbance and transmission readings of the samples were taken within a frequency (wavenumber) range of 400 cm^{-1} to 4000 cm^{-1}. Table 3. 4 shows the wavenumber of functional groups of chitin and chitosan from various studies. The data obtained from the FTIR spectrometry will be compared with Table 3. 4 to assign functional groups or structures to the analysed spectra of the chitin/chitosan samples.

3.3.3 Degree of De-acetylation

The degree of acetylation (DA) was determined using the FTIR spectroscopy degree of the acetylation calibration curve in Equation 38 from Brugnerotto et al (2001), Czechowska-Biskup et al (2012) and El Knidri et al (2017).

$$A_{1655}/A_{3450} \times 100 = 1.33DA \quad \text{Equation 38}$$

Where A_{1655} and A_{3450} is the intensity of absorption at reference bands 1655cm^{-1} and 3450 cm^{-1} respectively. The degree of de-acetylation (DD) was determined by Equation 39.

$$DD = 100 - DA \quad \text{Equation 39}$$

Table 3. 4: Identification and assignment of functional group/structures of extracted chitin from insects (Black soldier fly larvae shells, Beetle), Crustaceans (Shrimp, Squilla and Crab) and squid pens by various authors using FTIR spectrometry

	(Waśko et al., 2016)	(Liu et al., 2012)	(Liu et al., 2012)	(Kumari & Rath, 2014)	(Prabu & Natarajan, 2012)	(Lavall et al., 2007)	(Lavall et al., 2007)	(Lavall et al., 2007)
Source	BSF chitin	Beetle Chitin	Shrimp Chitin	Shrimp, Squilla, Crab Chitin	Shrimp, Squilla, Crab	Crab shells	Squid pens (L. plei)	Squid pens (L. sanpaulensis)
Polymorph	Alpha-chitin	Alpha-chitin	Alpha-chitin	Alpha-chitin	Alpha-chitin	Alpha chitin	Beta chitin	Beta chitin
Structure	**Wavenumber, cm^{-1}**							
Alpha crystallinity	1650, 1620, and 1550							
C=O secondary amide stretch (Amide I), (v (C=O of N-acetyl group))	1654	1655	1654		1672	1657	1660	1655
N-H bend, v (C-O)	1617	1624	1627		1627	1627		
N-H stretch (Amide II), (δ (N-H of N-acetyl group))	1550	1560	1560		1,560	1560	1556	1557
protein contaminants	1540							
O H stretching (v (O-H)) (v (N-H) in NH2)	3400	3424	3440	3425-3422		3447		
Methyl group in NHCOCH3, Methylene group in CH2OH, asymmetric C-H stretching (v (COCH3))	2920	2934	2932	2921-2879		2929	2931	2933
C-H bend, CH3symmetricdeformation	1377				1,340	1379	1377	1376
C-N vibrations from amides (amide III of C-N,)	1309	1310			1,261	1316	1314	1314
C-O-C asymmetric stretching	1152				1152-1156	1157	1156	1155
C O C symmetric stretching	1152, 1114, 1069					1026	1030	1032
v (N-H) (Amine) (v (N-H) in v (NH2))		3262	3268	3425-2881		3268	3284	3278
v (C-H) asymmetric CH2			2874				2877	2874
v (C-H) asymmetric CH2		2884				2889		
Amno peak, alpha-Chitin					3102			
Amno peak, alpha-Chitin					3265			
Amno peak, alpha-Chitin					3420			
Amno peak, alpha-Chitin					3450			
Glucopyranose (Ring stretching)					890	895	899	899
Carbohydrate back bone					1040-1070			
Acetyl ester bonds					1720-1760			

3.4 Adsorption and Desorption Experiments

The major input parameters for chitin and chitosan metal adsorption in batch systems is the degree of deacetylation, temperature, pH, liquor ratio (adsorbent mass per volume of solution), adsorbent particle size, initial concentration of metals in solution, presence of anions, adsorption time and agitation. While the output variable is the concentration of metals in the solution and on the adsorbent material (Guibal, 2004).

3.4.1 Metal Sorption onto FLS, Chitin, Chitosan in a Binary Copper-Ferrous Test Solution.

The investigation on the sorption of copper and ferrous onto FLS, chitin and chitosan from a binary mixture of copper and ferrous ions was performed under batch conditions in 500 mL Erlenmeyer flasks at 30 ^{o}C in a shaker at 110 rpm in triplicate. 200 mL of the binary mixture of copper and ferrous ions were prepared by the addition of 200 mL of de-ionized water with a 500 mL of measuring cylinder into each Erlenmeyer flask. 3 µm of 99 % H_2SO_4 was then added to each flask using a 20P micropipette to adjust the pH from 7 to 3.4. After that process, 2.79 mmol/L of ferrous and copper ions were added to each flask by the addition of 0.08462 g of anhydrous Ferrous Sulphate and 0.1391 g of Copper Sulphate heptahydrate. This aliquot was then mixed to allow for the dissolution of the metals. Thereafter, in each experiment, a set amount of FLS, chitin, chitosan was loaded into the Erlenmeyer flasks. The amount of FLS/chitin/Chitosan product loaded in each experiment is shown in Table 3. 6. Experiments were grouped for comparative studies and comparative experimental grouping was conducted at the same time. 2 mL solutions were sampled hourly for the first 4 hours and there after scattered within 24 hours. Ferrous and copper ions were measured spectrophotometrically in a HELIOS UV–Visible Spectrophotometer v4.04. This was done using the modified ferric chloride assay developed in Govender et al (2012) and the Copper-2,5-Dimercapto-1,3,4-thiadiazole (DMTD) assay developed in Ahmed et al (2002).

Table 3. 5: Comparative experimental grouping of sorbents for copper-ferrous bimetal adsorption studies

Comparative experimental grouping	**Sorbents used**	**Amount used (g)**
Effect of chitin extraction steps	Chitin 1, Chitin 2, Chitin 3, Chitin 4	0.5
Effect of chitosan production steps	Chitosan 2, Chitosan 3, Chitosan 4	0.5
Effect of deproteination time	Chitin 3 (1h Deprot), Chitin 3 (2h Deprot), Chitin 3 (4h Deprot)	0.5

3.4.2 Metal Sorption onto Chitin and Chitosan in a Binary Copper-Aluminium Test Solution

The investigation on the sorption of copper and aluminium onto chitin and chitosan from a binary mixture of copper and aluminium ions was performed under batch conditions in 500 mL Erlenmeyer flasks at 30 ^{o}C in a shaker at 110 rpm in triplicate. 200 mL of the binary mixture of copper and aluminium ions were prepared by the addition of 200 mL of de-ionized water

with a 500 mL measuring cylinder into each Erlenmeyer flask. 3 μm of 99 % H_2SO_4 was then added to each flask using a 20P micropipette to adjust the pH from 7 to 3.4. After that process, 2.79 mmol/L of copper and aluminium ions were added to each flask by the addition of 0.1391 g of Copper Sulphate pentahydrate and 0.1856 g of Aluminium Sulphate octa decahydrate. This aliquot was then mixed to allow for the dissolution of the metals. Thereafter, in each experiment 0.1 g of CHITIN-CBR-ELN/CHITOSAN-CBR-ELN was loaded into the Erlenmeyer flasks. 2 mL solutions were sampled hourly for the first 4 hours and there after scattered within 24 hours. Aluminium and copper ions were measured spectrophotometrically in a HELIOS UV–Visible Spectrophotometer v4.04. This was done using the aluminium-morin assay developed in Ahmed & Hossan (1995) and the Copper-2,5-Dimercapto-1,3,4-thiadiazole (DMTD) assay developed in Ahmed et al (2002).

3.4.3 Metal Sorption onto Chitin and Chitosan in Copper, Aluminium, Ferric and Ferrous Test Solutions

The investigation on the sorption of copper, aluminium, ferric and ferrous onto chitin and chitosan from single copper, aluminium. ferric and ferrous ion test solutions were performed under batch conditions in 500 mL Erlenmeyer flasks at 30 ^{o}C in a shaker at 110 rpm in triplicate. 200 mL of the copper, aluminium, ferric and ferrous test solutions were prepared by the addition of 200 mL of de-ionized water with a 500 mL measuring cylinder into each Erlenmeyer flask. 3 μM of 99 % H_2SO_4 was then added to each flask using a 20P micropipette to adjust the pH from 7 to 3.4. After that, 2.79 mmol/L of copper aluminium, ferric, ferrous ions were added to each flask by the addition of 0.1391 g of Copper Sulphate heptahydrate, 0.1856 g of Aluminium Sulphate octa decahydrate, 0.15059 g of Ferric Chloride hexahydrate and 0.08462 g of anhydrous Ferrous Sulphate. The aliquot was then mixed to allow for the dissolution of the metals. Thereafter, in each experiment 0.1 g of CHITIN-CBR-ELN/CHITOSAN-CBR-ELN was loaded into the Erlenmeyer flasks. 2 mL solutions were sampled hourly for the first 4 hours and there after scattered within 24 hours. The ferric, ferrous, copper and aluminium ions were measured spectrophotometrically in a HELIOS UV–Visible Spectrophotometer v4.04.

An investigation on the effect of the initial concentration of ferrous ions on the sorption of ferrous ions onto the CHITIN-CBR-ELN was conducted by varying the initial concentration in the 200 ml aliquot solutions from 2.79 mmol/L to 1,39 mmol/L and 0.6963 mmol/L. This was done by addition of 0.08463 g, 0.04231 g and 0.02116 g of anhydrous Ferrous Sulphate respectively into the 200 mL aliquots. An investigation on the effect of the initial concentration of copper ions on the sorption of copper ions onto the CHITOSAN-CBR-ELN was conducted by varying the initial concentration in the 200 ml aliquot solutions from 2.79 mmol/L to 1,39 mmol/L and 0.6963 mmol/L. This was done by addition of 0.1391 g, 0.07913 g and 0.03957 g of Copper Sulphate pentahydrate respectively into the 200 mL aliquots. For the effect of the initial concentration of ferrous and copper ions, 0.05g of CHITIN-CBR-ELN and CHITOSAN-CBR-ELN were used respectively.

3.4.4 Metal Sorption onto Chitin and Chitosan in Model Leachate Solution

The investigation on the sorption of metals from the model leachate solution onto the CHITIN-CBR-ELN and CHITOSAN-CBR-ELN were performed under batch conditions in 500 mL Erlenmeyer flasks at 30 ^{o}C in a shaker at 110 rpm in triplicate. 200 mL of the copper,

aluminium, and ferrous aliquot solutions were prepared by the addition of 200 mL of de-ionized water with a 500 mL measuring cylinder into each Erlenmeyer flask. 3 μM of 99 % H_2SO_4 was then added to each flask using a 20P micropipette to adjust the pH from 7 to 3.4. After that, 2.79 mmol/L of copper, 2.82 mmol/L of aluminium and 1.11 mmol/L of ferrous ions were added to each flask by the addition of 0.1391 g of Copper Sulphate heptahydrate, 0.1879 g of Aluminium Sulphate octa decahydrate and 0.03373 g of anhydrous Ferrous Sulphate. The aliquot was then mixed to allow for the dissolution of the metals. Thereafter, in each experiment 0.4 g of CHITIN-CBR-ELN/CHITOSAN-CBR-ELN was loaded into the Erlenmeyer flasks. 2 mL solutions were sampled hourly for the first 4 hours and there after scattered within 24 hours. The ferrous, copper and aluminium ions were measured spectrophotometrically in a HELIOS UV–Visible Spectrophotometer v4.04. For the measurement of ferrous ions in solution, the modified ferric chloride assay developed in Govender et al (2012) had to be further modified to mask for interference from aluminium. This modification is shown in Appendix A2.3.

3.4.5 Desorption of Chitin and Chitosan

All chitin and chitosan sorbents used in the adsorption studies were desorbed. The desorption was carried out in 200 mL Erlenmeyer flasks at 30 ^{o}C in a shaker at 110 rpm in triplicate for 2 hours with 100 mL of 0.1 M H_2SO_4. The 100 mL of H_2SO_4 was prepared by the addition of 99.4 mL of de-ionized water with a 200 mL measuring cylinder and 555 μm of 98% H_2SO_4 with a 1000P autopipette. The chitin/chitosan saturated sorbents were placed in this solution for 3 hours. The ferrous, ferric, copper and aluminium ions in solution were measured spectrophotometrically in a HELIOS UV–Visible Spectrophotometer v4.04.

3.4.6 Effect of Recycling Chitin/Chitosan

The investigation on the recyclability of the CHITIN-CBR-ELN and CHITOSAN-CBR-ELN were performed under batch conditions in 500 mL Erlenmeyer flasks at 30 ^{o}C in a shaker at 110 rpm in triplicate.1 g of CHITIN-CBR-ELN was placed in 2.79 mmol/L of ferrous ions and 1 g of CHITOSAN-CBR-ELN was placed in 2.79 mmol/L of copper ions. 2 mL solutions were sampled hourly for the first 4 hours and thereafter scattered within 24 hours. The ferrous, copper and aluminium ions were measured spectrophotometrically in a HELIOS UV–Visible Spectrophotometer v4.04. After that, the CHITIN-CBR-ELN and CHITOSAN-CBR-ELN were desorbed. The sorption experiment on ferrous and copper ions was repeated once with the recovered CHITIN-CBR-ELN and CHITOSAN-CBR-ELN after desorption.

3.5 Characterisation of Adsorption

The amount of metal adsorbed onto the chitin and chitosan was calculated based on Equation 9 in Section 2.3.1. Concentrations of metals in solution measured spectrophotometrically were used in Equation 9 with the assumption that the concentration decrease is due to adsorption only unless visible precipitation was observed. The Langmuir and Freundlich Isotherms, Pseudo 1st and 2nd Order adsorption reaction kinetics parameters were calculated using Equation 11 and 12 in Section 2.3.1.1, Equation 18 in Section 2.3.1.2, Equation 24 in Section 2.3.2.1 and Equation 27 and 28 in Section 2.3.2.2 respectively. Intraparticle diffusion was determined using Equation 29 in Section 2.3.2.3.

3.5.1 Linearization of models and statistics

To determine equilibrium and rate constants, linearization of models was required to plot experimental data. Miss use of linearization is the most common error in data analysis of adsorption studies (Marković et al., 2014). The problems that come with the linearization of inherently non-linear equations is the assumption of homoscedasticity when data is heteroscedastic. Linearization is based on the variance of experimental data and assumes the variance for all the range of data is equal. The result is an over-estimation of the goodness of fit usually by the measure of the correlation coefficient (R) which is translated into an error in the coefficient of the determinant (R^2). This is sometimes achieved by the removal of experimental data which reduces the degrees of freedom. Higher R^2 values do not necessarily mean a better fit for experimental data. It is however to note that the model with the best R^2 and lowest standard deviation values should be chosen. Statistical analysis should be viewed as a guide in the choice of a model and it is necessary to check if parameters obtained have physical meaning (Bergmann, 2015). The standard deviation (SD) between the predicted and experimental data was calculated using Equation 40:

$$\mathrm{SD} = \sqrt{\left(\frac{1}{n_p - p}.\Sigma_i^N (qi, exp - qi, model)^2\right)}. \quad \text{Equation 40}$$

Where $q_{i,\,model}$ is the predicted amount adsorbed, $q_{i,exp}$ is the experimentally determined amount adsorbed, n_p is the number of experiments performed and p is the number of parameters of the fitted model.

An adjusted coefficient of the determinant (R_{adj}^2) is often applied. This considers experimental precision and model characters. The adjusted coefficient of the determinant (R_{adj}^2) was calculated using Equation 41:

$$R_{adj}^2 = 1 - (1 - R^2).\left(\frac{n_p - 1}{n_p - p - 1}\right) \quad \text{Equation 41}$$

A residual plot is another assessment that can be used to check the goodness of fit of models to experimental data. The Standard Residual (SR) was calculated using Equation 42:

$$\text{Standard Residual} = \frac{q_{i,experimental} - q_{i,model}}{SD} \quad \text{Equation 42}$$

3.5.2 Adsorption thermodynamics

Thermodynamics can be used to quantify or infer information about the adsorption process. Thermodynamic parameters such as the Gibb's free energy change (ΔG^o ,Kj/mol), enthalpy change (ΔH^o ,Kj/mol) and entropy change (ΔS^o ,Kj/mol) can be utilized to define the magnitude of the adsorption process (Kallay et al., 2011). These thermodynamic parameters were calculated using Equation 43 and Equation 44:

$$\Delta G^o = \Delta H^o - T.\Delta S^o \quad \text{Equation 43}$$

$$\Delta G^o = -R.T.In\,(K) \quad \text{Equation 44}$$

Where R is the universal gas constant (8.314 $J.K^{-1}.mol^{-1}$), T is the absolute temperature (Kelvin) and K is the equilibrium adsorption constants. To calculate ΔH^o and ΔS^o at least two isotherms of the same adsorption conditions is required while for several isotherms a linear plot of In(K) versus (1/T) cab be used.

Physisorption such as Van der Waal forces usually has activation energy lower than 20 KJ mol^{-1} while for electrostatic interactions the activation energy ranges from 20 KJ mol^{-1} to 80 KJ mol^{-1}. Chemisorption bonds are stronger and have activation energies in the range of 80 KJ mol^{-1} to 450 KJ mol^{-1}. Positive values of ΔH^o indicate an endothermic process while the exothermic process yields negative values. Positive values of ΔS^o suggest preference of adsorbate for active sites and possible structural changes. ΔG^o indicate the spontaneity and favourability of the adsorption process. The more negative value of ΔG^o, the greater the driving force of the adsorption process (Bergmann, 2015).

3.6 Precipitation Experiments

The precipitation studies were conducted using dosing of 0.222M NaHS solution into 3 aliquots (mixtures) of copper, ferrous and aluminium ions at r.t.p under stirring in the acid fume hood for an hour. 200 mL of 0.222M NaHS stock solution was created by the addition of 200 mL of deionized water into a 500 ML Erlenmeyer flask and the addition of 2.489 g of 98% NaHS hydrate. The 3 aliquots were created in triplicate by the addition of 400 mL of deionized water using a measuring cylinder into 500 mL Erlenmeyer flasks. 3 μM of 99 % H_2SO_4 was then added to each flask using a 20P micropipette to adjust the pH from 7 to 3.4. Copper, aluminium and ferrous ions were added to each flask by the addition of Copper Sulphate heptahydrate, Aluminium Sulphate octa decahydrate and anhydrous Ferrous Sulphate respectively according to the amount of salt stated in Table 3. 6. The aliquot was then mixed to allow for the dissolution of the metals. Precipitation was conducted by initial dosing Mixture 1, Mixture 2 with 5 ml and Mixture 3 with 10 mL of the NaHS stock solution. After 20 mins, the mixtures were dosed again with 5 mL of the NaHS stock solution. 5 mL solutions were sampled every 10 mins during the 1-hour precipitation studies. The sample solutions were then passed through a vacuum filtration using 0.2 μm membrane filter paper to remove the precipitates and the solutions were analysed for ferrous, copper and aluminium ions. The ferrous, copper and aluminium ions were measured spectrophotometrically in a HELIOS UV–Visible Spectrophotometer v4.04.

Table 3. 6: Amount of copper, ferrous, and aluminium metal ions and metal salts added in 400 mL precipitation study mixtures

	Mixture 1		**Mixture 2**		**Mixture 3**	
Metal ions	**Concentration (mmol/L)**	**Amount of salt added (g)**	**Concentration (mmol/L)**	**Amount of salt added (g)**	**Concentration (mmol/L)**	**Amount of salt added (g)**
Cu2+	2.79	0.2782	2.79	0.2782	5.57	0.5563
Fe2+	2.79	0.1692	5.57	0.3385	2.79	0.1692
Al3+	2.79	0.1856	2.79	0.1856	2.79	0.1856

Chapter 4: Preparation of Bio Sorbents

4.1 Preparation of Chitin

4.1.1 Effect of Chitin Extraction Steps on Chitin Character

Chitin was extracted from BSF larvae in 3 different methodologies/production sequences as described in Section 3.2 to produced four chitins (Chitin 1, Chitin 2, Chitin 3 and Chitin 4). Chitin 1 was produced by liberation, demineralization, deproteination and decolourization. Chitin 2 was produced by liberation, demineralization and deproteination while Chitin 3 was produced by liberation and deproteination. Chitin 4 is the FLS from the liberation step. 2 M HCl was used for demineralization while 4 wt % NaOH was used for deproteination. For decolourization bleach (3 % NaClO) was used.

Figure 4. 1 shows the FTIR spectra of Chitin 1, Chitin 2, Chitin 3 and Chitin 4 in a KBr media taken from wavenumbers of 4000 cm^{-1} to 400 cm^{-1}. Figure 4. 1 shows that Chitin from BSF larvae was characterized by three amide bands corresponding to C=O secondary amide stretch (Amide I), N-H bend and N-H stretch (Amide II) at 1654, 1617 and 1550 cm^{-1} respectively. Chitin exists in three forms which are α, β, γ crystal forms that are distinguishable using FTIR spectroscopy. Chitin with an α crystalline form displays bands near 1650, 1620 and 1550 cm^{-1} attributed to the acetamido groups in chitin (Brugnerotto et al., 2001; Lavall et al., 2007). The presence of these bands in the chitin extracted from BSF larvae suggests that chitin in BSF larvae is in the α form. Most insect chitin has been observed to be of the α crystalline form (Kaya et al., 2015). Major bands were detected in the FITR spectra at: 3433-3443 cm^{-1} (O H stretching), 2921-2928 cm^{-1} (CH_3 group in $NHCOCH_3$), 2853 cm^{-1} (asymmetric CH_2), 1379 cm^{-1} (C-H bend, CH_3 symmetric deformation), 1320 cm^{-1} (C-N from amides (amide III)), 1158cm^{-1} (C-O-C asymmetric stretching), 1073 cm^{-1} (C-O-C symmetric stretching) and 875-895 cm^{-1} (glucopyranose ring stretching). The observation of these bands is consistent with the observations made by Waśko et al. (2016). Waśko et al. (2016) characterized the physicochemical structure of chitin extracted from the BSF. The presence of N-H group in amine was observed at 3289-3287 cm^{-1} for Chitin 1, Chitin 2 and Chitin 4. The presence of the amine group in Chitin 1 and Chitin 2 may be attributed to the partially de-acetylation of the chitin during demineralization and decolourization. The presence of the amine group in Chitin 4 may be attributed to the presence of protein contaminants. This is also consistent with the observation of the 1540 cm^{-1} band in Chitin 4 which is often attributed to protein contaminants. The absence of the N-H group in amine in Chitin 3 suggests effective deproteination with the 4 wt % NaOH.

Table 4. 1 shows the degree of acetylation, relative overall yield and cost of production of Chitin 1, Chitin 2, Chitin 3 and Chitin 4. The degree of acetylation was determined using Equation 38 and Equation 39 as described in Section 3.3.3. Table 4. 1 shows that the degree of acetylation of Chitin 1, Chitin 2, Chitin 3 and Chitin 4 was 63.8 %, 72.3 %, 86.0 % and 75.5 % respectively.

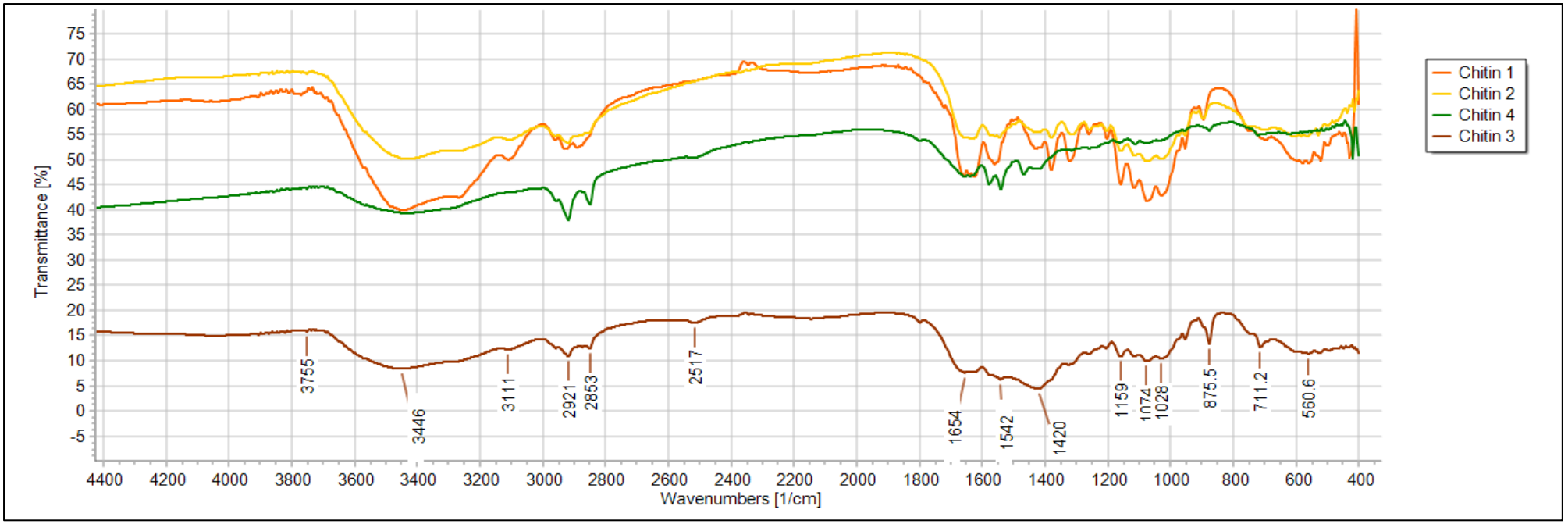

Figure 4. 1: FTIR spectra of Chitin 1, Chitin 2, Chitin 3 and Chitin 4 in KBr.

Table 4. 1: Chitin 1-Chitin 4 Degree of acetylation, relative yield and cost of production

Product	Production sequence	A1655	A3450	Degree of acetylation	Relative Overall Yield (%)	Cost of production ($/kg)
Chitin 1	Liberation, Demineralization, Deproteination, Decolorization	0.3148	0.3712	63.8	4	20.7
Chitin 2	Liberation, Demineralization, Deproteination	0.1749	0.182	72.3	4.75	5.30
Chitin 3	Liberation, Deproteination	1.611	1.409	86.0	25.3	1.75
Chitin 4	Liberation	0.3206	0.3194	75.5	100	-

The values of DA obtained from chitin extracted from BSF larvae are in the range of those obtained from chitin from other insects. Insects have been shown to have a DA in the range of 59.3 % to 71.6 % (Badawy & Mohamed, 2015). The DA is the ratio of acetamido groups to the summation of amino acid and acetamido groups in chitin/chitosan. DA serves to characterize the biopolymer as either chitin or chitosan. Chitosan has a DD greater than 60 % which is attributed to solubility in acids (Gyliene et al., 2003; Guibal, 2004). The observed DA of Chitin 1, Chitin 2, Chitin 3 and Chitin 4 and the FTIR spectra suggest that the polymers may be identified as the chitin polymer.

The impact of demineralizing the FLS from BSF larvae with 2M HCl prior deproteination can be observed by comparing Chitin 2 and Chitin 3. Demineralization resulted in a lower degree of acetylation and lower overall yields. The lower degree of acetylation was observed by comparing the DA of Chitin 2 and Chitin 3. Demineralization resulted in a decrease in acetylation from 86.0 % (Chitin 3) to 72. 3 % (Chitin 2). The overall yield for Chitin 3 and Chitin 2 was 25.7 % and 4.74 % respectively. There was an overall decrease of 21 % in chitin overall yield due to the demineralization step. Hydrochloric acid results in the degradation of the chitin polymer (Muzzarelll, 1977; Tetteh, 1991) which results in loss of yield. The impact of the decolourization step with bleach (3 % NaClO) on chitin from BSF larvae can be observed by comparing Chitin 1 and Chitin 2. Decolourization resulted in a lower degree of acetylation and lower overall yields. The lower degree of acetylation was observed by comparing the DA of Chitin 1 and Chitin 2. Decolorization resulted in the decrease in acetylation from 72.3 % (Chitin 2) to 63.8 % (Chitin 1). The overall yield for Chitin 1 was 4 %. These results show that demineralization with 2 M HCl has a greater impact on the decrease of the overall yield than decolourization with 3% NaClO. Both reagents result in the de-acetylation of chitin. Chitin 4 which is the raw FLS had a DA value of 75.5 % as shown in Table 4. 1. The lower DA of Chitin 4, when compared to Chitin 3, can be attributed to the presence of protein contaminants in the Chitin 4. The results observed in the DA of the chitin are consistent with the observed presence of amine groups in the FITR data. The presence of protein contaminants in Chitin 4 suggests that the liberation step is not efficient in the deproteination of the FLS from BSF larvae.

The cost of production of Chitin 1, Chitin2, Chitin 3 and Chitin 4 was calculated using Equation 31 in Section 3.1.3. Table 4. 1 shows the cost of production of Chitin 1, Chitin 2, Chitin 3 was 20.7 $/kg, 5.30 $/kg, 1.75 $/kg respectively. Figure 4. 2 shows the contribution of demineralization, deproteination and decolourization on the cost of production of chitin from BSF larvae. Demineralization, deproteination and decolourization contribute 8 %, 18 % and 74 % respectively towards the cost of production of chitin from BSF larvae. Decolourization has little impact on the overall yield however it is the most expensive step due to the higher NaClO reagent costs. NaClO costs are at an average of 1.3 $/kg (Alibaba, 2019c) while HCl costs are 0.3 $/kg (Alibaba, 2019b) and NaOH costs are 0.425 $/kg (Alibaba, 2019a). The overall yield of chitin from BSF larvae has a great impact on the cost of production (Mabuka et al., 2018). The increase in the cost of production from Chitin 3 to Chitin 2 due to demineralization of FLS can be attributed to the decrease in overall yield due to the impact of demineralization. Chitin 3 had the lowest cost of production. The cost of production for Chitin 3 was 1.75 $/kg. This is lower than the market value of agricultural grade chitin which costs

14 $/kg (Alibaba, 2019i). The low cost of production of extracting chitin from FLS suggests potential value recovery from the production of chitin from BSF larvae shell waste.

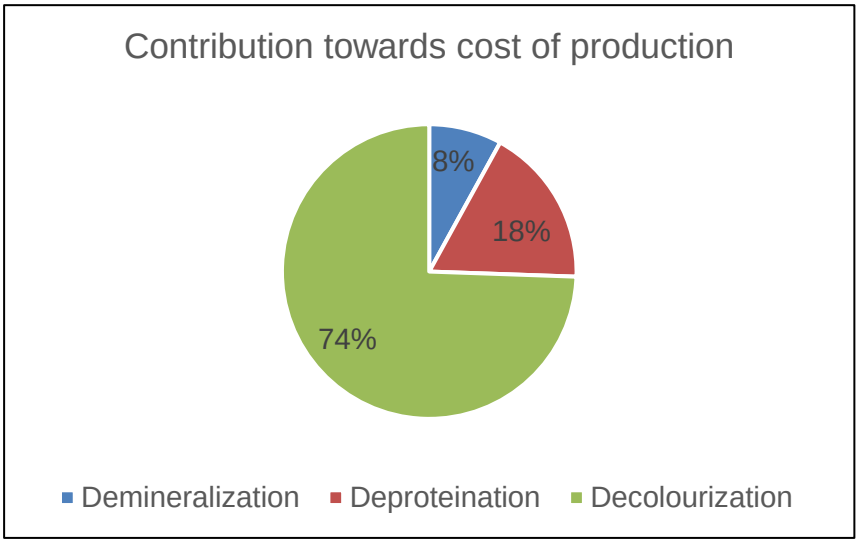

Figure 4. 2: Extraction steps contribution towards the cost of production of chitin from BSF larvae

Bio sorbents range from $ 0.0777 to $ 0.514 per kg (Gupta & Babu, 2008), although the cost of production of Chitin 3 is higher than this range, it is still lower than the cost of commercial activated carbon at $ 7.07 per kg (Gupta & Babu, 2008) indicating competitive production costs as a sorbent. The cost of production of Chitin 1 and Chitin 2 suggests that inclusion of the demineralization and decolourization step in the extraction of chitin from BSF larvae results in chitin which may not be competitive in costs to other bio sorbets and commercial sorbents.

Although the minerals, lipids and proteins removed from the BSF larvae in this study were not characterised. St-Hilaire et al., 2007, Tschirner & Simon, 2015 and Al-Qazzaz et al., 2016 characterised the fatty acid, mineral and amino acid composition in BSF larvae respectively. This is summarised in Table 4. 2. Table 4. 2 shows that BSF larvae contain a variety and a large amount of minerals, lipids and proteins. Therefore, the extraction of chitin directly from the BSF larvae provides an opportunity for the production of these by-products. Minerals, lipids and proteins from BSF larvae have potential uses as protein feed (Wang & Shelomi, 2017; Noor et al., 2018), in manure management (Newton et al., 2005) and for biodiesel production (Wong et al., 2019). The mineral, lipid and protein content in the FLS is much less than that in the larvae however the potential use of these by-products is consistent. The extraction of chitin from the BSF larvae provides an opportunity for the production of these by-products improving the circular economics of sourcing chitin from the BSF larvae or FLS waste.

Table 4. 2: Amino acid composition of BSF larvae (Al-Qazzaz et al., 2016)*, fatty acid composition of BSF prepupae* (St-Hilaire et al., 2007) *and mineral content of young larvae of BSF* (Tschirner & Simon, 2015).

Proteins		Fats		Minerals	
Amino acid	**g//kg**	**Fatty acids**	**BSF prepupae oil (%)**	**Mineral**	**g/kg**
Arginine	93.3	Lauric	49.34	Ca	22.26
Histidine	14.8	Myristic	6.83	P	19.51
Isoleucine	12.2	Palmitic	10.48	Mg	5.73
Leucine	37.3	Palmitoleic	3.45	K	19.51
Lysine	28.6	Stearic	2.78	Na	1.62
Methionine	26.5	Oleic	11.81	Mn	0.25
Phenylalanine	16.3	Linoleic	3.68	Fe	0.34
Threonine	22.4	Linolenic	0.08	Zn	0.23
Valine	21.9	Saturated Fatty Acids	69.9	Cu	0.0236
Tryptophan	0.49	Monounsaturated Fatty Acids	14.9	Co	0.0002
Aspartic acid	48.1	Polyunsaturated Fatty Acids	12.5	Mo	0.0011
Alanine	52.5			Cd	0.0004
Cysteine	89.2			Pb	0.0008
Glutamic acid	65.8			**Total**	**69.5**
Glycine	10.9				
Proline	36.7				
Serine	32.9				
Tyrosine	22.0				
Total	**637**				

4.1.2 Effect of Chitin Extraction Steps on Metal Adsorption Kinetics

0.5 g of Chitin 1, Chitin 2, Chitin 3 and Chitin 4 were placed in a bimetal copper and ferrous test solution with initial concentrations of 2.79 mmol/L respectively. The decrease in the

concentration of the ferrous and copper ions due to adsorption was observed and is shown in Figure A5. 1 and Figure A5. 2 respectively in Appendix A5 Metal concentration and pH-time graphs. Equation 9 in Section 2.3.1 was used to calculate the amount of ferrous and copper ions adsorbed onto the chitin.

Table 4. 3 shows the adsorption initial pH, final pH and the maximum adsorption capacity for ferrous and copper ions for Chitin 1, Chitin 2, Chitin 3 and Chitin 4.

Table 4. 3: Initial and final adsorption pH, maximum adsorption capacity for ferrous and copper ions onto Chitin 1, chitin 2, Chitin 3 and chitin 4

Product	Initial adsorption pH	Final adsorption pH	Fe2+ Q_{max} (Fe^{2+} mmol/g chitin)	Cu 2+ Q_{max} (Cu^{2+} mmol/g chitin)
Chitin 1	3.45	3.56	0.834± 0.003	0.849± 0.006
Chitin 2	3.47	3.61	0.910± 0.003	0.887± 0.007
Chitin 3	3.45	4.05	1.11± 0.003	0.889± 0.005
Chitin 4	3.45	6.71	1.09± 0.005	0.933± 0.008

The maximum adsorption capacities for ferrous ions onto Chitin 1, Chitin 2, Chitin 3 and Chitin 4 were 0.834 ± 0.003 mmol/g, 0.91± 0.003 mmol/g, 1.11± 0.003 mmol/g and 1.09 ± 0.005 mmol/g respectively. While for copper ions the maximum adsorption capacity was 0.849 ± 0.006 mmol/g, 0.887± 0.007 mmol/g, 0.889± 0.005 mmol/g and 0.933 ± 0.008 mmol/g. Of the studied chitin, Chitin 3 and Chitin 4 had the highest maximum adsorption capacity for ferrous and copper ions. Ferrous and copper ions were adsorbed simultaneously. The maximum adsorption capacities for ferrous ions for the studied chitin were higher than that for copper ions except for Chitin 1. This indicates that the chitin extracted from BSF larvae had a metal adsorption selectiveness for ferrous ions over copper ions. However, the degree of metal adsorption selectivity was low. Chitin 3 and Chitin 4 only adsorbed 19.9 % and 14.4 % more ferrous than copper respectively. Gyliene et al. (2002) showed that FLS from house fly (*Musca Domestica*) do not adsorb copper or ferrous ions. However, the FLS (Chitin 4) in this study was able to adsorb both metals. The difference between the adsorption behaviour of the two sources of FLS may be due to chitin from BSF larvae having a low crystalline index. A low crystalline index is associated with high sorption properties (Waśko et al., 2016). Gyliene et al. (2002) obtained a maximum adsorption capacity of 0.6 mmol/ g with chitin extracted from the house fly (*Musca domestica*). The maximum adsorption capacity for ferrous ions on FLS (Chitin 4) from BSF larvae was twice that of the house fly (*Musca domestica*) obtained in Gyliene et al. (2002). The maximum adsorption capacities obtained in this study are in the range of those obtained by other bio sorbents and competitive to commercial sorbents. This can be observed by comparison with the maximum desorption capacities for bio sorbent and commercial sorbents in Table A1. 1 in Appendix A1 Literature Review Figures and Tables. Chitin has been observed to be able to adsorb ferrous and copper ions in the range of 0.023 mmol/g to 1.43 mmol/g. (Zhou et al., 2004; Anastopoulos et al., 2017; Boulaiche et al., 2019). While commercial sorbent such as activated carbon adsorb copper and ferrous ions in the

range from 0.103 mmol/g to 1.50 mmol/g (Kouakou et al., 2013; Fouladgar et al., 2015; Lim et al., 2019)

The presence of protein contaminants in the FLS seemed to improve the adsorption of ferrous and copper ions onto chitin from BSF larvae. This is shown by Chitin 4 having the highest maximum adsorption capacity of ferrous and copper ions. It has been demonstrated that large amounts of salts of lithium, sodium, potassium, caesium, thallium, ammonium, magnesium, calcium, barium, rubidium and strontium do not alter chitin/chitosan significantly and are not adsorbed onto chitin/chitosan. These salts also do not prevent the collection of transition metal ions when simultaneously present (Muzzarelll, 1977). The effect of demineralization and decolourization can be seen by comparing the maximum adsorption capacities for copper and ferrous ions of Chitin 1, Chitin 2 and Chitin 3. The demineralization and decolourization extraction step decrease the maximum adsorption capacity of ferrous and copper ions onto chitin from BSF larvae. The decrease in sorption maybe attributed to the degradation of these polymers due to acid action.

Figure 4. 3 and Figure 4. 4 shows the adsorption of ferrous and copper ions respectively onto the chitin. In general, the adsorption of ferrous and copper ions took 2 to 4 hours to reach maximum adsorption capacity (adsorption equilibrium) with 65 % to 83 % of the adsorption occurring within the first hour. This is in agreement with several authors who conducted metal adsorption studies with chitin (Rhazi et al., 2000; Gyliene et al., 2002; Zhou et al., 2004). The fast adsorption of ferrous and copper ions onto the chitin indicates good adsorptive properties in these polymers as well as efficiency in recovering metals from solution. The pH at adsorption equilibrium for the adsorption of copper and ferrous ions on Chitin 1, Chitin 2, Chitin 3, Chitin 4 was 3.56, 3.61, 4.05 and 6.71 as shown in Table 4.3. The pH at adsorption equilibrium was higher than the initial pH of 3.45. The adsorption pH change may have contributed to the higher maximum adsorption capacities obtained by Chitin 3 and Chitin 4. An increase in pH has been shown to increase the maximum adsorption capacity of metal ions on chitin (Rhazi et al., 2000; Gyliene et al., 2002). At low pH, amine groups on the chitin protonate with H^+ ions which induces electrostatic repulsion of the metal ions resulting in decreased adsorption of metal ions (Zhou et al., 2004). The adsorption equilibrium pH of Chitin 4 was the highest at 6.71. The presence of proteins in this chitin may have resulted in the consumption of the H^+ ions by protonation with amine groups in the proteins. There was visible degradation of proteins in the Chitin 4 in the form of a reddish-brown precipitate in the acidic test solution indicating instability of this polymer. Proteins in insects hydrolyse in the presence of acids (Kasaai et al., 2013; Yi, 2015). The adsorption equilibrium pH of Chitin 4 was within the hydroxide pH range of most base metals (aluminium, nickel, zinc). Therefore, the use of Chitin 4/ FLS extracted from BSF larvae maybe limited in the application on the Model leachate due to the polymer's instability and the potential of co-precipitation of base metals during the adsorption process.

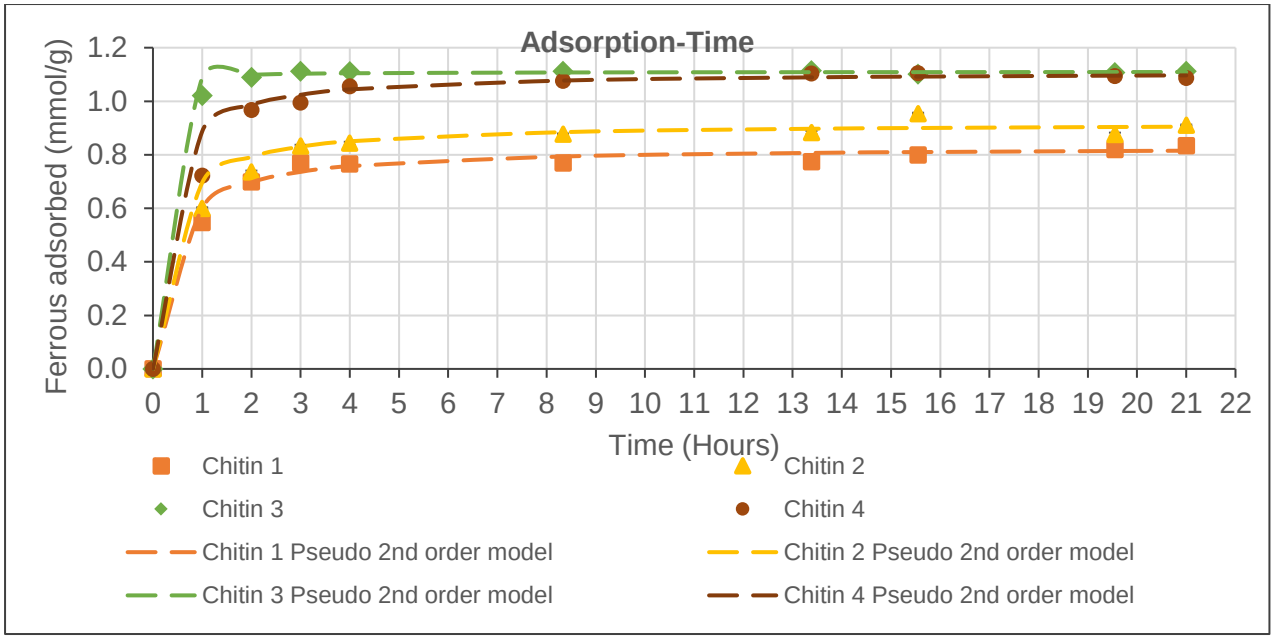

Figure 4. 3: Chitin 1-Chitin 4 ferrous adsorption and pseudo second-order kinetics

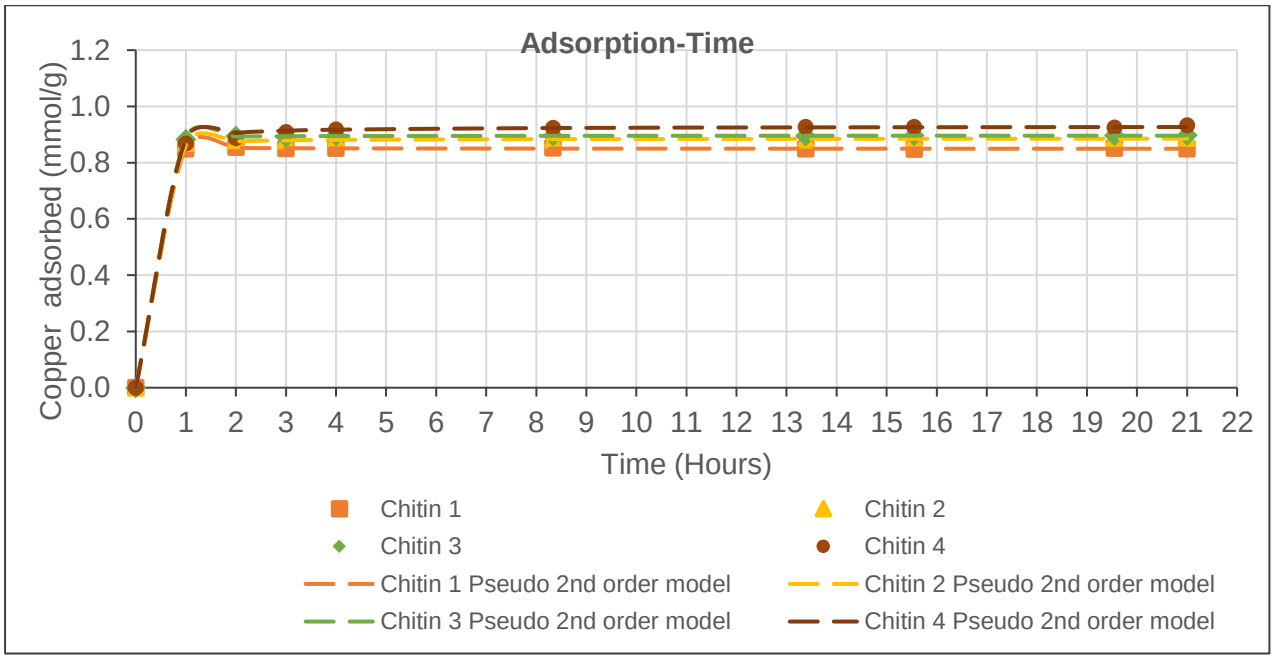

Figure 4. 4: Chitin 1-Chitin 4 copper adsorption and pseudo second-order kinetics

Figure 4. 3 and Figure 4. 4 also shows that ferrous and copper adsorption on Chitin 1, Chitin 2, Chitin 3 and Chitin 4 was well modelled by the Pseudo 2nd order kinetic model. Most bio sorbents are well modelled by the Pseudo 1st and 2nd order as shown in Table A1. 1 in Appendix A1 Literature Review Figures and Tables. Table 4. 4 and Table 4. 5 show the maximum sorption capacity (Q_{max}), pseudo 2nd order adsorption initial rate (h_o) and rate constant (k_f), standard deviation (SD), correlation coefficient (R_2) and the adjusted correlation coefficient ($AdjR_2$) for ferrous and copper adsorption respectively onto Chitin 1, Chitin 2, Chitin 3 and Chitin 4. The Pseudo 2nd order adsorption model linear fit for ferrous and copper

adsorption onto Chitin 1, Chitin 2, Chitin 3 and Chitin 4 is shown in Figure A7. 1 and Figure A7. 2 in Appendix A7 Adsorption reaction kinetics.

Table 4. 4 and Table 4. 5 show that the Pseudo 2nd order adsorption kinetic model linear fit had $AdjR_2$ values between 0.9975 to 1.0000 for both ferrous and copper adsorption onto the chitin. This indicates a good fit with the adsorption experimental data. The SD range between the pseudo 2nd order model predicted adsorption and the experimental adsorption for both ferrous and copper was 0.00260 to 0.0644 mmol/g. The low SD values indicate that the Pseudo 2nd order model can accurately predict the adsorption of ferrous and copper ion onto the chitin studied.

Table 4. 4: Chitin 1-Chitin 4 pseudo second-order kinetics parameters for ferrous adsorption

	Pseudo 2nd order kinetics					
	Ferrous					
Product	**Qmax (mmol/g)**	**k_f (h^{-1})**	**h_o (mmol g^{-1} h^{-1})**	**SD**	**R^2**	**AdjR^2**
Chitin 1	0.830	3.15	2.17	0.0299	0.9984	0.9952
Chitin 2	0.919	3.40	2.86	0.0484	0.9975	0.9925
Chitin 3	1.11	42.9	52.9	0.0261	1.0000	1.0000
Chitin 4	1.11	3.59	4.42	0.0644	0.9995	0.9985

Table 4. 5: Chitin-Chitin 4 pseudo second-order kinetics parameters for copper adsorption

	Pseudo 2nd order kinetics					
Product	**Qmax (mmol/g)**	**k_f (h^{-1})**	**h_o (mmol g^{-1} h^{-1})**	**SD**	**R^2**	**AdjR^2**
Chitin 1	0.849	-154.1	-111.11	0.0032	0.9986	0.9958
Chitin 2	0.886	46.8	36.76	0.00260	0.9989	0.9967
Chitin 3	0.896	146.4	117.65	0.0030	0.9998	0.9994
Chitin 4	0.929	21.22	18.315	0.0099	0.9978	0.9934

The fitting of the Pseudo 2nd order adsorption kinetic model onto the experimental data of ferrous and copper adsorption onto the chitin suggests that the reaction path way of ferrous and copper adsorption was by chemisorption (Ho & McKay, 1998). It also suggests that the reaction path way of adsorption of ferrous and copper ions may be reaction rate-limited as opposed to diffusion-limited with the reaction path being dependent on both the sorbate (ferrous and copper ions) and the sorbent (chitin) (Bergmann, 2015). The use of pseudo 2nd order adsorption kinetic models to conclusively deduce the nature of the adsorption process is often debated. Further examination such as thermodynamic parameters and the intra particle diffusion may be needed to conclude the nature of the adsorption process (Ho & McKay, 1999).

Table 4. 4 shows the adsorption rate constant for ferrous ions onto Chitin 1, Chitin 2, Chitin 3 and Chitin 4 were 3.15 h^{-1}, 3.40 h^{-1}, 42.9 h^{-1} and 3.59 h^{-1} respectively. The higher the reaction rate constant the faster the adsorption rate and as a result the higher the maximum adsorption capacity of the metal (Bergmann, 2015). Chitin 3 had an adsorption rate constant for ferrous ions 14 times higher than that of the other chitin indicating more favourable adsorptive

properties. The order of magnitude of the pseudo 2nd order adsorption rate constants for ferrous and copper correlate with the order of the maximum adsorption capacity as shown in Table 4. 4.

The desorption of ferrous and copper ions from the Chitin 1, Chitin 2, Chitin 3 and Chitin 4 is shown in Figure A5. 3 and Figure A5. 4 respectively in Appendix A5 Metal concentration and pH-time graphs. Complete desorption of the adsorbed ferrous and copper ions onto the chitin was achieved using 0.1 M H_2SO_4. in 2 hours. This desorption time is in agreement with metal desorption studies on chitin in Wan et al. (2004) and Vijayaraghavan et al. (2005). The final concentration of the desorbed solution was higher than the initial concentration of the metals in the bimetal solution due to the lower volume used for desorption. The desorption volume can be used to control the concentration of the desorbed solution. This provides an opportunity to be able to create solutions with specific concentrations of metal. This can be used to create solution by-products or refining solutions for further metal recovery with other technologies such as electrowinning or precipitation.

4.1.3 Effect of Chitin Extraction Steps on Chitin Metal Recovery Techno economics

The recovery costs were calculated based on the cost of adsorption (which includes the cost of production of the chitin), the cost of desorption (which was calculated to be $ 2.94×10^{-4} per desorption cycle) and the cost of precipitation (given by Equation 32 in Section 3.1.3). The revenue from the recovered metal sulphides was calculated by Equation 36 in Section 3.1.3. The chitin used during the adsorption process has potential use as agricultural grade chitin (Sharp, 2013). Therefore, revenue from the sale of chitin after desorption using the market price of agricultural grade chitin which is $ 14/kg (Alibaba, 2019i) was considered. The techno-economic analysis was conducted based on the recovery of 1kg of metal using the chitin and precipitation with NaHS.

Figure 4. 5 shows total recovery costs, the revenue of sales of metal sulphide, the revenue of sale of used chitin, gross profit/loss (excluding chitin revenue) and gross profit/loss (including chitin revenue) for the recovery of copper and ferrous ions using the chitin.

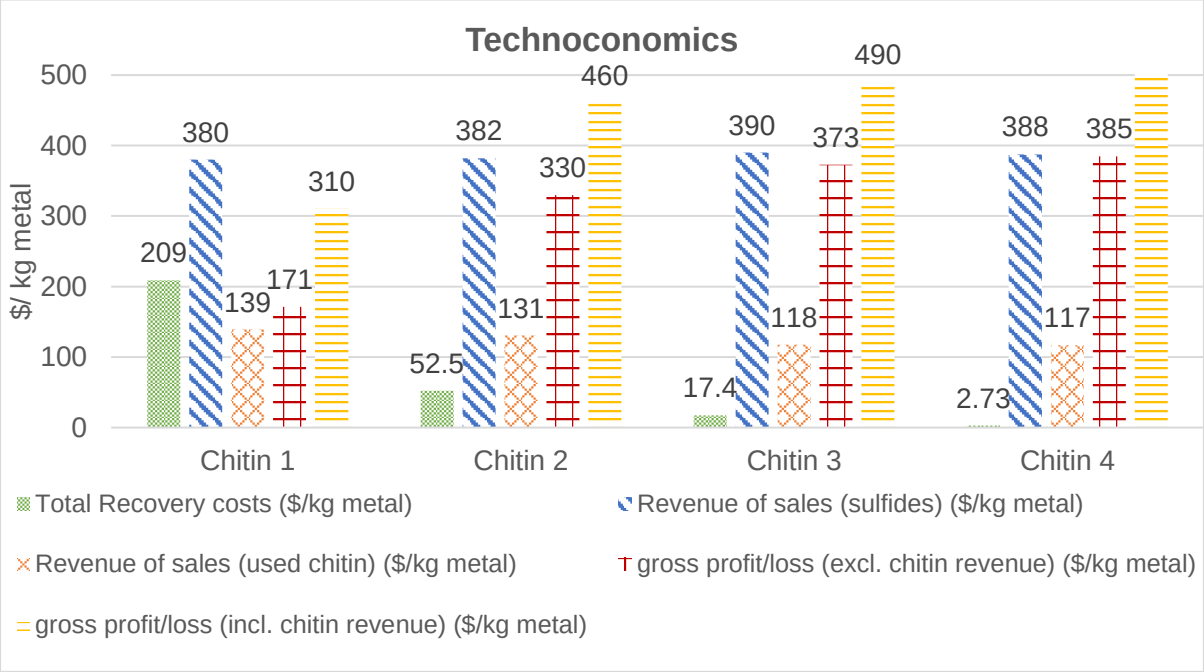

Figure 4. 5; Chitin 1, Chitin 2, Chitin 3 and Chitin 4 total recovery costs, the revenue of sales of metal sulphide, the revenue of sale of used chitin, gross profit/loss (excluding chitin revenue) and gross profit/loss (including chitin revenue)

Figure 4. 5 shows that the metal recovery costs of Chitin 1, Chitin 2, Chitin 3 and Chitin 4 was $ 380/ kg metal, $ 52.5/kg metal, $ 17.4/ kg metal and $ 2.73/kg metal respectively. Chitin 4 had the lowest cost of production followed by Chitin 3. Chitin 1 had the most expensive metal recovery costs. The yield of chitin, ferrous and copper maximum adsorption capacity had the greatest effects on the metal recovery costs. Figure 4. 5 shows the revenue of sales of the recovered sulphides of Chitin 1, Chitin 2, Chitin 3 and Chitin 4 was $ 380/ kg metal, $ 382 /kg, $ 390/ kg and $ 388/kg. The revenue of sales of the recovered metal sulphides after the desorption process is in the range of $ 380/kg to $ 390/kg. The market value of CuS and FeS is at $ 200/kg (Alibaba, 2019f) and $ 300/kg (Alibaba, 2019g) respectively. Although the value of copper is higher than that of iron in PCBs, the reverse is seen when these metals are in the form of metal sulphides. This indicates the importance of considering the form in which metals are recovered when determining metal value in PCBs. Figure 4. 5 shows the gross profit from

the sale of the recovered sulphides of Chitin 1, Chitin 2, Chitin 3 and Chitin 4 was $ 171/ kg metal, $ 330/kg, $ 373/ kg and $ 385/kg. All chitin had a gross profit indicating economic feasibility in the use of chitin extracted from BSF larvae as an adsorbent. Chitin 3 and Chitin 4 had the highest gross profit (excluding chitin revenue). To produce 1 kg of metal (iron and copper) in the PCB leachate solution at least 8.6 kg of PCBs are required. To recover the extracted 1 kg of metal (iron and copper),9.95 kg, 9.33 kg, 8.40 kg and 8.34 kg of Chitin 1, Chitin 2, Chitin 3 and Chitin 4 are required respectively. Using the deproteination liquor ratio of 1 g of chitin to 25 mL of reagent at least a working deproteination reactor volume of 398 L is required. Considering that the deproteination time is 2 hours, the reactor volume can be reduced to less than 50 L by allowing for more reaction runs. This is in consideration of the need to create a low-cost investment recovery technology in South Africa (African Development Bank, 2018). which involves reducing capital costs.

The consideration of generating revenue from the used chitin after desorption resulted in an increased in the gross profit of the metal recovery for Chitin 1, Chitin 2, Chitin 3 and Chitin 4 to $ 310/ kg metal, $ 460/kg, $ 490/ kg and $ 385/kg respectively. Chitin 3 and Chitin 4 had the highest gross profit in the recovery process of copper and ferrous ions. The potential use of chitin for secondary processes after desorption provides potential in further increasing circular economics and improving the economic feasibility of the metal recovery process. The extraction of chitin from BSF larvae shells using the deproteination step only with 4 wt % NaOH creates chitin with the highest metal adsorption capacity for copper and ferrous ions, the highest reaction rate (faster adsorption), relatively cheaper production costs, recovery costs and the highest potential gross profit in the metal recovery with NaHS precipitation.

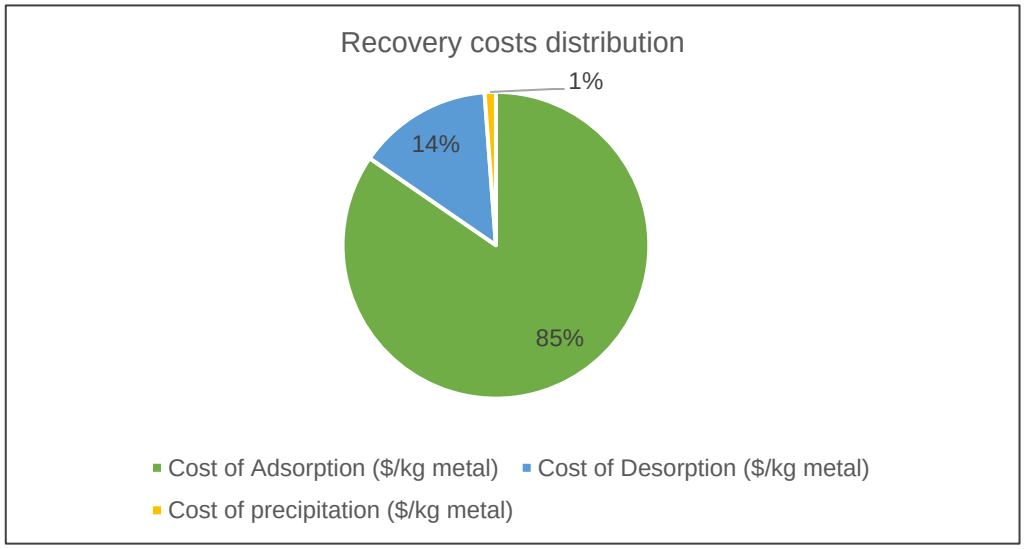

Figure 4. 6: Percentage contribution by recovery steps in the total metal recovery costs for copper and ferrous ions using Chitin 3 and NaHS precipitation.

Figure 4. 6 shows the percentage contribution of the cost of adsorption, cost of desorption and cost of precipitation in the total metal recovery costs for 1 kg of copper and iron using Chitin 3 and NaHS precipitation. Figure 4. 6 shows that the major contributor to the recovery costs is adsorption at 85 % followed by desorption at 14 %. The cost of precipitation only contributed 1 % to the total metal recovery costs. The cost of production of chitin has a significant effect on the adsorption process thus the total recovery costs follow the same order as the cost of

production of the chitin. The cost of the adsorption is highly dependent on the cost of the adsorbent (Anirudhan & Sreekumari, 2011).

4.1.4 Effect of deproteination time on chitin character

The effect of deproteination time on chitin extracted from BSF larvae was investigated by the extraction of chitin from BSF larvae shells using the deproteination step only. The deproteination liquor ratio, NaOH concentration, deproteination reactor working volume, deproteination temperature were kept constant and the deproteination time was varied at 1h, 2h and 4 h to produce three chitins. The chitin produced was Chitin 3 (1 h Deprot), Chitin 3 (2 h Deprot) and Chitin 3 (4 h Deprot) respectively.

Figure 4. 7 shows the FTIR spectra of Chitin 3 (1 h Deprot), Chitin 3 (2 h Deprot) and Chitin 3 (4 h Deprot) in a KBr media taken from wavenumbers of 4000 cm^{-1} to 400 cm^{-1}. Amide bands corresponding to C=O secondary amide stretch (Amide I), N-H bend and N-H stretch (Amide II) at 1654, 1617 and 1550 cm^{-1} respectively were observed. Major bands were detected in the FITR spectra at: 3415-3446 cm^{-1} (O H stretching), 2921 cm^{-1} (CH_3 group in $NHCOCH_3$), 2853 cm^{-1} (asymmetric CH_2), 1320 cm^{-1} (C-N from amides (amide III)), 1158cm^{-1} (C-O-C asymmetric stretching), 1073 cm^{-1} (C-O-C symmetric stretching) and 875-895 cm^{-1} (glucopyranose ring stretching). The presence of N-H group in amine was observed at 3274 cm^{-1} for Chitin 3 (1 h Deprot). The presence of the amine group in Chitin 3 (1 h Deprot) may be attributed to the presence of protein contaminants. This is also consistent with the observation of the 1540 cm^{-1} band in Chitin 3 (1 h Deprot) which is often attributed to protein contaminants. The absence of the N-H group in amine in Chitin 3 (2 h Deprot) and Chitin 3 (4 h Deprot) suggests effective deproteination with the 4 wt % NaOH in 2 hours.

Table 4. 6 shows the degree of acetylation, relative overall yield and cost of production of Chitin 3 (1 h Deprot), Chitin 3 (2 h Deprot) and Chitin 3 (4 h Deprot). The degree of acetylation was determined using Equation 38 and Equation 39 as described in Section 3.3.3. Table 4. 6 shows that the degree of acetylation of Chitin 3 (1 h Deprot), Chitin 3 (2 h Deprot) and Chitin 3 (4 h Deprot) was 54.4 %, 86.0 % and 75.5 % respectively. The low DA obtained for Chitin 3 (1 h Deprot) can be attributed to the presence of protein contaminates indicating that 1 h of deproteination with 4 wt % NaOH does not effectively remove proteins from the liberated BSF larvae shells. This is consistent with the observed results from the FTIR spectra. The DA of Chitin 3 (4 h Deprot) was lower than that of Chitin 3 (2 h Deprot) indicating that deproteination of BSF larvae shells in 4 wt % NaOH for 4 hours results in partial deacetylation of the FLS. Table 4. 6 shows that the yield of Chitin 3 (1 h Deprot), Chitin 3 (2 h Deprot) and Chitin 3 (4 h Deprot) was 50.6 %, 35 % and 31.3 % respectively. An increase in deproteination time from 1 hour to 2 hours resulted in a decrease in the yield of 15.6 %. This can be attributed to the loss of protein mass during the deproteination stage. Increasing the deproteination time from 2 hours to 4 hours only resulted in a decrease in the yield of 3.7 % suggesting that the major deproteination of chitin in 4 wt % NaOH occurs within 2 hours. The results of the yield are consistent with that obtained from the FTIR spectra and the DA values of the chitin. Table 4. 6 shows the cost of production of Chitin 3 (1 h Deprot), Chitin 3 (2 h Deprot) and Chitin 3 (4 h Deprot). was 0.91 $/kg, 1.36 $/kg, 1.64 $/kg respectively. The decrease in yield due to increased deproteination time results in a higher cost of production.

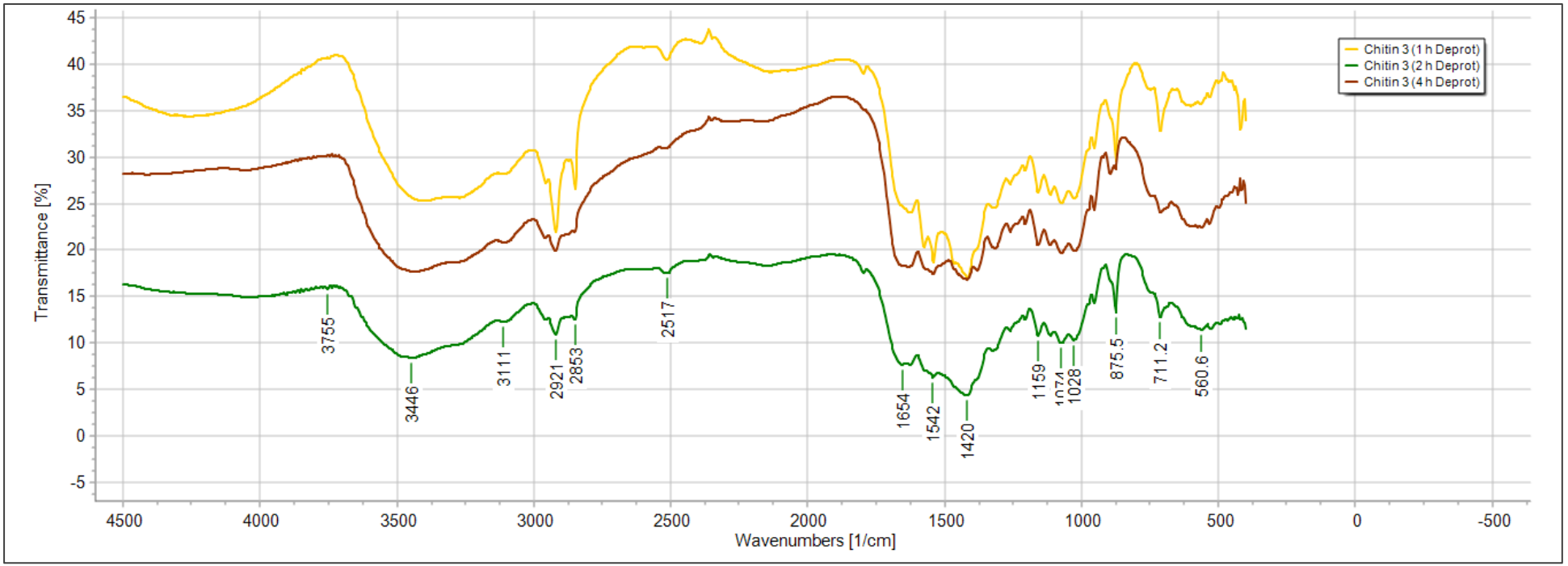

Figure 4. 7: FTIR spectra of Chitin 3 (1 h Deprot), Chitin 2 (2 h Deprot) and Chitin 3 (4 h Deprot) in KBr.

Table 4. 6: Chitin 3 (1 h Deprot), Chitin 2 (2 h Deprot) and Chitin 3 (4 h Deprot) Degree of acetylation, relative yield and cost of production

Product	Production sequence	A1655	A3450	Degree of acetylation	Relative Yield (%)	Cost of production ($/kg)
Chitin 3 (I h Deprot)	(Deproteinated)	0.2933	0.4056	54.4	50.6	0.91
Chitin 3 (2 h Deprot)	(Deproteinated)	1.611	1.409	86.0	35	1.36
Chitin 3 (4 h Deprot)	(Deproteinated)	0.8318	0.9996	62.6	31.3	1.64

4.1.5 Effect of deproteination time on chitin adsorption reaction kinetics

0.5 g of Chitin 3 (1 h Deprot), Chitin 3 (2 h Deprot) and Chitin 3 (4 h Deprot) were placed in a bimetal solution of copper and ferrous ions with initial concentrations of 2.79 mmol/L respectively. Chitin 3 (1 h Deprot) was also placed in the leachate bimetal solution of ferrous and copper ions (Cu/Fe leachate) with an initial concentration of 1.07 mmol/L and 2.79 mmol/L respectively. The decrease in the concentration of the ferrous and copper ions due to adsorption was observed and shown in Figure A5. 5 and Figure A5. 6 respectively in Appendix A5 Metal concentration and pH-time graphs. Equation 9 in Section 2.3.1 was used to calculate the amount of ferrous and copper ions adsorbed onto the chitin. Table 4. 7 shows the adsorption initial pH, final pH and the maximum adsorption capacity for ferrous and copper ions for Chitin 3 (1 h Deprot)-(Cu/Fe leachate), Chitin 3 (1 h Deprot), Chitin 3 (2 h Deprot) and Chitin 3 (4 h Deprot).

Table 4. 7: Initial and final adsorption pH, maximum adsorption capacity for ferrous and copper ions onto Chitin 3 (1 h Deprot)-(Cu/Fe leachate), Chitin 3 (1 h Deprot), Chitin 3 (2 h Deprot) and Chitin 3 (4 h Deprot)

Product	Production sequence	Initial adsorption pH	Final adsorption pH	Fe2+ Q_{max} (Fe^{2+} mmol/g chitin)	Cu 2+ Q_{max} (Cu^{2+} mmol/g chitin)
Chitin 3 (I h Deprot)-(Cu/Fe leachate)	(Deproteinated for 1 hour)	3.47	5.68	0.409±0.002	1.115±0.001
Chitin 3 (I h Deprot)	(Deproteinated for 1 hour)	3.45	5.68	1.053±0.006	1.076±0.001
Chitin 3 (2 h Deprot)	(Deproteinated for 2 hours)	3.46	4.05	1.11±0.002	0.915±0.009
Chitin 3 (4 h Deprot)	(Deproteinated for 4 hours)	3.45	3.71	1.11±0.002	0.883±0.004

The maximum adsorption capacity for ferrous ions onto Chitin 3 (1 h Deprot)-(Cu/Fe leachate), Chitin 3 (1 h Deprot), Chitin 3 (2 h Deprot) and Chitin 3 (4 h Deprot) was 0.409 ± 0.002 mmol/g, 1.053± 0.006 mmol/g, 1.11± 0.002 mmol/g and 1.11 ± 0.002 mmol/g respectively. While for copper, the maximum adsorption capacity was 1.115 ± 0.006 mmol/g, 1.076± 0.007 mmol/g, 0.915± 0.005 mmol/g and 0.883 ± 0.008 mmol/g respectively. Chitin 3 (2 h Deprot) and Chitin 3 (4 h Deprot) had the highest adsorption capacity for ferrous ions. A decrease in DA from 86.0 % (Chitin 3 (2 h Deprot) to 62.6 % (Chitin 3 (4 h Deprot)) did not change the maximum adsorption capacity for ferrous ions onto these polymers. This suggests that low DA is associated with high ferrous adsorption indicating that the adsorption sites of ferrous ions onto chitin maybe on acetamido groups. Adsorption of metals onto chitin is largely attributed to the amine and hydroxyl groups on the chitin (Guibal, 2004). Chitin 3 (1 h Deprot)-(Cu/Fe leachate) had the highest adsorption for copper ions and the lowest adsorption for ferrous ions. This is due to the high initial copper to ferrous mole ratio in the solution. Chitin 3 (1 h Deprot) in the Cu/Fe leachate was able to completely adsorb all ferrous ions even in the presence of a high initial copper to ferrous mole ratio in the solution. This indicates the high metal adsorption selectivity for ferrous ions over copper ions by the chitin from BSF larvae. This is consistent with observations in Section 4.1.2 Increase in deproteination time resulted in lower adsorption of copper ions onto chitin extracted from BSF larvae. This is observed by the order of

maximum copper adsorption capacity of Chitin 3 (1h Deprot), Chitin 3 (2 h Deprot) and Chitin 3 (4 h Deprot) respectively. The decrease in copper adsorption as deproteination time is increased suggests that the amine groups from proteins may be have been involved as active sites for copper adsorption. The pH at adsorption equilibrium for Chitin 3 (1 h Deprot), Chitin 3 (2 h Deprot) and Chitin 3 (4 h Deprot) was 5.68. 4.05 and 3.71 respectively The pH at adsorption equilibrium was higher than that of the initial pH. An increase in deproteination time resulted in a decrease in the adsorption equilibrium pH during ferrous and copper adsorption. Deproteination results in less available amines (from proteins) on the sorbet. The result is less protonation (acid consumption) thus a reduced pH change during adsorption. The pH at adsorption equilibrium obtained for Chitin 3 (1 h Deprot) was within the pH range for hydrolysis of some of the base metals (iron, aluminium and copper) in PCB. Therefore, the application of Chitin 3 (1 h Deprot) on a PCB leachate solution would result in co-precipitation of these metals during adsorption. This suggests that 1-hour deproteination time is not enough to produce chitin from BSF larvae applicable to PCB leachate solutions. Chitin 3 (4 h Deprot) had the highest degree of metal adsorption selectivity for ferrous ion. Adsorbing 20.5 % more ferrous ions than copper ions.

Figure 4. 8 and Figure 4. 9 shows the adsorption of ferrous and copper ions respectively onto the chitin. Figure 4. 8 and Figure 4. 9 shows that ferrous adsorption on Chitin 3 (1 h Deprot)-(Cu/Fe leachate), Chitin 3 (1 h Deprot), Chitin 3 (2 h Deprot) and Chitin 3 (4 h Deprot) was well modelled by the Pseudo 2nd order kinetic model. For ferrous adsorption, adsorption equilibrium was reached within the first 4 hours of adsorption while for copper adsorption the chitin took 22 hours to reach adsorption equilibrium. This indicates a higher adsorption rate for ferrous ions over copper ions by Chitin 3 (1 h Deprot), Chitin 3 (2 h Deprot) and Chitin 3 (4 h Deprot).

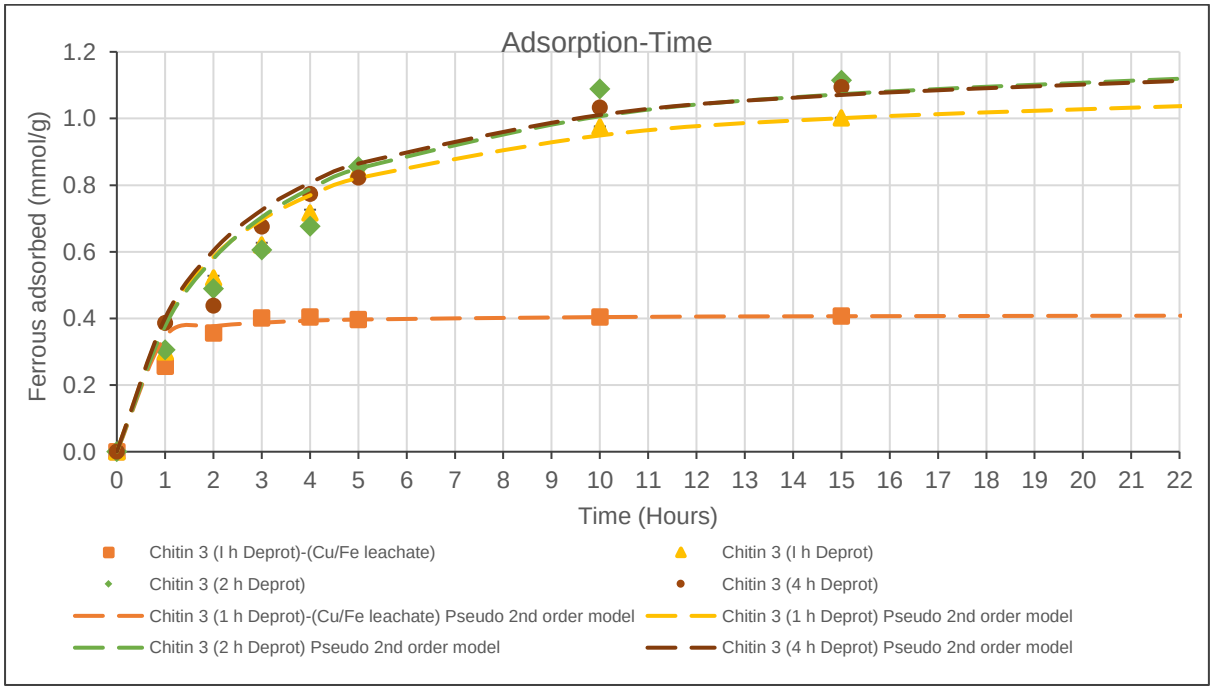

Figure 4. 8: Chitin 3 (1 h Deprot)-(Cu/Fe leachate), Chitin 3 (1 h Deprot), Chitin 3 (2 h Deprot) and Chitin 3 (4 h Deprot) ferrous adsorption and pseudo second order kinetics

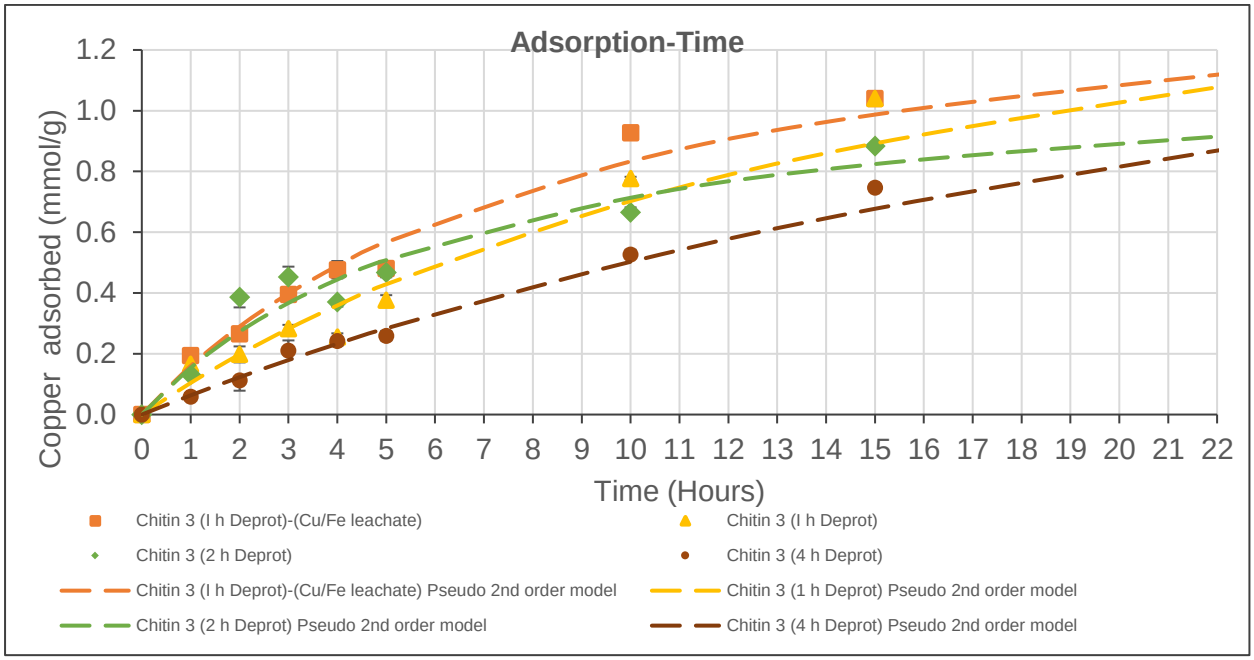

Figure 4. 9: Chitin 3 (1 h Deprot)-(Cu/Fe leachate), Chitin 3 (1 h Deprot), Chitin 3 (2 h Deprot) and Chitin 3 (4 h Deprot) copper adsorption and pseudo second order kinetics

Table 4. 8 and Table 4. 9 show the maximum sorption capacity (Q_{max}), pseudo 2nd order adsorption initial rate (h_o), rate constant (k_f), standard deviation (SD), correlation coefficient (R_2) and the adjusted correlation coefficient ($AdjR_2$) for ferrous and copper adsorption respectively onto Chitin 3 (1 h Deprot)-(Cu/Fe leachate), Chitin 3 (1 h Deprot), Chitin 3 (2 h Deprot) and Chitin 3 (4 h Deprot). The Pseudo 2nd order adsorption model linear fit for ferrous and copper adsorption onto Chitin 3 (1 h Deprot)-(Cu/Fe leachate), Chitin 3 (1 h Deprot), Chitin 3 (2 h Deprot) and Chitin 3 (4 h Deprot) is shown in Figure A7. 3 and Figure A7. 4 in Appendix A7 Adsorption reaction kinetics.

Table 4. 8 and Table 4. 9 show that the Pseudo 2nd order adsorption kinetic model linear fit had $AdjR_2$ values between 0.428 to 0.999 for both ferrous and copper adsorption onto the chitin. This indicates a good fit with the adsorption experimental data. Low SD were observed between 0.0352 to 0.0815 mmol/g between the pseudo 2nd order model predicted adsorption and the experimental adsorption for both ferrous and copper onto the chitin.

Table 4. 8: Chitin 3 (1 h Deprot)-(Cu/Fe leachate), Chitin 3 (1 h Deprot), Chitin 3 (2 h Deprot) and Chitin 3 (4 h Deprot) pseudo second order kinetics parameters for ferrous adsorption

	Pseudo 2nd order kinetics					
	Ferrous					
Product	**Qmax (mmol/g)**	**k_f (h^{-1})**	**h_o (mmol g^{-1} h^{-1})**	**SD**	**R^2**	**$AdjR^2$**
Chitin 3 (I h Deprot)-(Cu/Fe leachate)	0.412	12.78	2.17	0.0355	0.9996	0.9988
Chitin 3 (I h Deprot)	1.124	0.48	0.61	0.0573	0.9926	0.9779
Chitin 3 (2 h Deprot)	1.23	0.4	0.5	0.0794	0.9865	0.9598
Chitin 3 (4 h Deprot)	1.22	0.41	0.60	0.0694	0.9901	0.9704

Table 4. 9: Chitin 3 (1 h Deprot)-(Cu/Fe leachate), Chitin 3 (1 h Deprot), Chitin 3 (2 h Deprot) and Chitin 3 (4 h Deprot) pseudo second order kinetics parameters for ferrous adsorption

	Pseudo 2nd order kinetics					
	Copper					
Product	**Qmax (mmol/g)**	**k_f (h^{-1})**	**h_o (mmol g^{-1} h^{-1})**	**SD**	**R^2**	**AdjR^2**
Chitin 3 (I h Deprot)-(Cu/Fe leachate)	1.567	0.0724	0.18	0.0561	0.9743	0.9239
Chitin 3 (I h Deprot)	1.941	0.0292	0.11	0.0815	0.7864	0.4276
Chitin 3 (2 h Deprot)	1.197	0.1232	0.18	0.0696	0.9663	0.9006
Chitin 3 (4 h Deprot)	2.213	0.0133	0.065	0.0352	0.8645	0.6210

Table 4. 8 shows the pseudo 2nd order adsorption rate constant for ferrous ions onto Chitin 3 (1 h Deprot)-(Cu/Fe leachate), Chitin 3 (1 h Deprot), Chitin 3 (2 h Deprot) and Chitin 3 (4 h Deprot) was 12.78 h^{-1}, 0.48 h^{-1}, 0.4 h^{-1} and 0.41 h^{-1}. While for copper ions, the pseudo 2nd order adsorption rate constant onto Chitin 3 (1 h Deprot)-(Cu/Fe leachate), Chitin 3 (1 h Deprot), Chitin 3 (2 h Deprot) and Chitin 3 (4 h Deprot) was 0.0724 h^{-1}, 0.0292 h^{-1}, 0.123 h^{-1} and 0.0133 h^{-1}. The ferrous ion adsorption rate constants were 3 to 5 times higher than those for copper ion adsorption. Hence, the faster adsorption of ferrous ions over copper ions. The desorption of ferrous and copper ions from the Chitin 3 (1 h Deprot)-(Cu/Fe leachate), Chitin 3 (1 h Deprot), Chitin 3 (2 h Deprot) and Chitin 3 (4 h Deprot) is shown in Figure A5. 7 and Figure A5. 8 respectively in Appendix A5 Metal concentration and pH-time graphs Complete desorption of the adsorbed ferrous and copper ions onto the chitin was achieved using 0.1 M H_2SO_4.

4.1.6 Effect of deproteination time on chitin metal recovery techno-economic

Figure 4. 10 shows total recovery costs, the revenue of sales of metal sulphide, the revenue of sale of used chitin, gross profit/loss (excluding chitin revenue) and gross profit/loss (including chitin revenue) for the recovery of copper and ferrous ions using Chitin 3 (1 h Deprot)-(Cu/Fe leachate), Chitin 3 (1 h Deprot), Chitin 3 (2 h Deprot) and Chitin 3 (4 h Deprot).

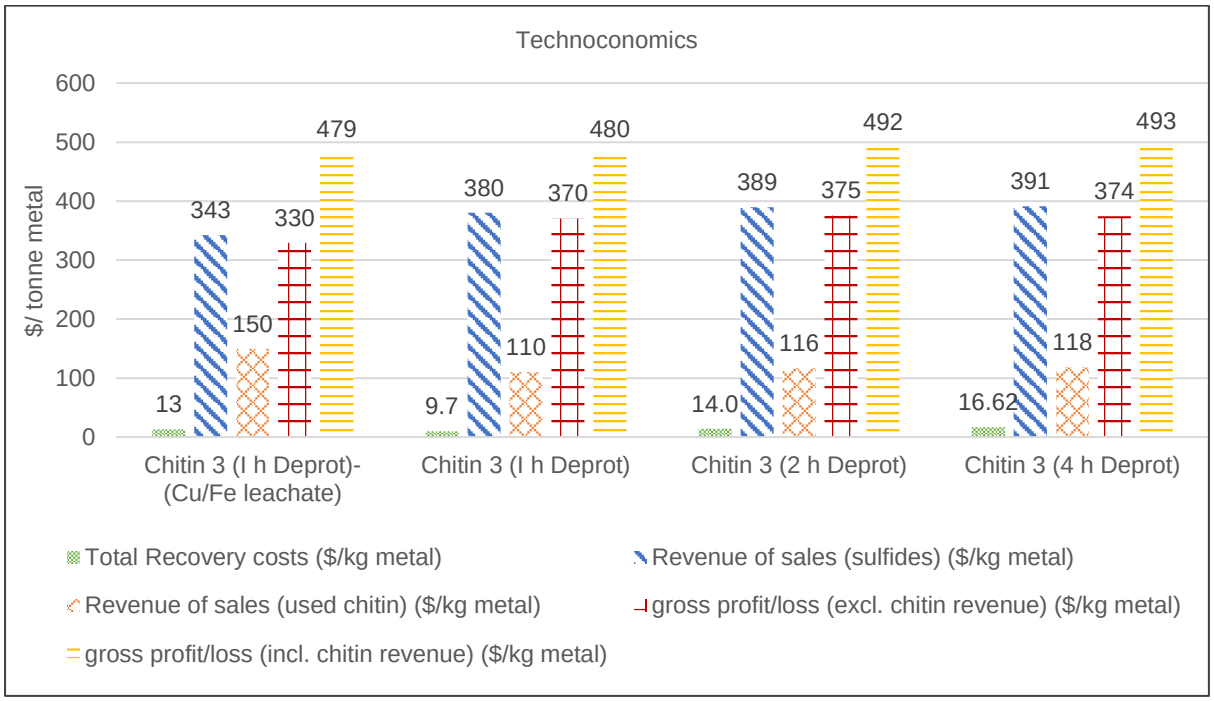

Figure 4. 10: Chitin 3 (1 h Deprot)-(Cu/Fe leachate), Chitin 3 (1 h Deprot), Chitin 3 (2 h Deprot) and Chitin 3 (4 h Deprot) total recovery costs, the revenue of sales of metal sulfide, the revenue of sale of used chitin, gross profit/loss (excluding chitin revenue) and gross profit/loss (including chitin revenue)

Figure 4. 10 shows the gross profit from the sale of the recovered sulphides of Chitin 3 (1 h Deprot)-(Cu/Fe leachate), Chitin 3 (1 h Deprot), Chitin 3 (2 h Deprot) and Chitin 3 (4 h Deprot) was $ 330/ kg metal, $ 370/kg, $ 375/ kg and $ 374/kg. Chitin 3 (2h Deprot) and Chitin 3 (4 h Deprot) had the highest gross profits due to the high adsorption of ferrous ions. Chitin 3 (4 h deprot) of the extracted chitin from the BSF larvae was the optimum chitin sorbent for ferrous and copper adsorption. This is because Chitin 3 (4 h deprot) had a high metal adsorption selectivity for ferrous ions over copper ions, high adsorption capacity for both metals, low cost of production and recovery costs, relatively higher gross profit in metal recovery and relatively low pH at adsorption equilibrium. Chitin 3 (Deprot 4 h) had an adsorption equilibrium pH of 3.71. This pH is below the hydrolysis pH range for base metals (copper, aluminium, nickel, zinc) in the Model Leachate solution. Therefore Chitin 3 (Deprot 4 h) maybe used in the adsorption of ferrous and copper ions in e-waste leachate solutions without co-precipitation of the metals. Chitin 3 (Deprot 4 h) was extracted from the BSF larvae using the liberation and deproteination steps, deproteinating with 4 % (W/V) NaOH for 4 hours. Therefore, this methodology for extracting chitin is the optimum method for producing chitin from BSF larvae for metal adsorption in PCB leachate solutions. The cost of production of Chitin 3 (Deprot 4 h) was $ 1.64 per kg which is competitive to other commercial and bio sorbents. Chitin 3 (Deprot 4 h) was given a product name of CHITIN-CBR-ELN

4.2 Preparation of Chitosan

4.2.1 Effect of chitin extraction steps on chitosan character

The effect of chitin extraction steps on chitosan production from chitin extracted from BSF larvae was investigated by the de-acetylation of Chitin 2, Chitin 3, Chitin 4 using 40 wt % NaOH for 6 hours as described in Section 3.2.5. The chitosan produced was Chitosan 2, Chitosan 3 and Chitosan 4.

Figure 4. 11 shows the FTIR spectra of Chitosan 2, Chitosan 3 and Chitosan 4 in a KBr media taken from wavenumbers of 4000 cm^{-1} to 400 cm^{-1}. Amide bands corresponding to C=O secondary amide stretch (Amide I), the N-H stretch (Amide II) were observed at 1657 and 1559 cm^{-1} respectively. Major bands were detected in the FITR spectra at: 3445-3481 cm^{-1} (O H stretching), 2925 cm^{-1} (CH_3 group in $NHCOCH_3$), 2852 cm^{-1} (asymmetric CH_2), 1315 cm^{-1} (C-N from amides (amide III)), 1159cm^{-1} (C-O-C asymmetric stretching), 1075 cm^{-1} (C-O-C symmetric stretching) and 875-895 cm^{-1} (glucopyranose ring stretching). The presence of the N-H group in amine was observed at 3258- 3274 cm^{-1} for all chitosan. The presence of the amine group in the chitosan is attributed to the de-acetylation of the acetamido groups in the chitin (Rigby, 1936).

Table 4. 10 shows the degree of de-acetylation, relative overall yield and cost of production of Chitosan 2, Chitosan 3 and Chitosan 4. The degree of de-acetylation was determined using Equation 38 and Equation 39 as described in Section 3.3.3. Table 4. 10 shows that the degree of de-acetylation (DD) of Chitosan 2, Chitosan 3 and Chitosan 4 was 33.2 %, 40.9 % and 37.1 % respectively. The DD of the chitosan obtained from the de-acetylation of Chitin 2, Chitin 3, and Chitin 4 was less than that ascribed to chitosan. Chitosan has a DD value of greater than 60 % (Gyliene et al., 2003; Guibal, 2004). However, when Chitosan 2, Chitosan 3 and Chitosan 4 were placed in 1 % HCl they dissolved in the acid solution within 1 hour. Chitosan is soluble in most mineral acids (Guibal, 2004) and has been shown to dissolve in 1 % HCl (Van Toan & Hanh, 2013). The solubility of Chitosan 2, Chitosan 3 and Chitosan 4 in 1 % HCl suggest the extracted polymers can be identified as chitosan regardless of their low DD values. The DD of Chitosan 3 is greater than that of Chitosan 4. This indicates that deproteination of the FLS prior to de-acetylation results in an increase in de-acetylation. This can be attributed to the use of NaOH for both deproteination and de-acetylation. The difference between the DD of Chitosan 3 and Chitosan 4 was only 3.8 % indicating that direct de-acetylation of the FLS is effective in the de-acetylation of the FLS. Muzzarelll (1977) in their review of chitin extraction proposed that if the endpoint of the raw material is chitosan then the deproteination step must be mild as the deacetylation process involves the use of alkalis at high temperatures which also removes remaining lipids and proteins. Table 4. 10 shows that the yield of Chitosan 2, Chitosan 3 and Chitosan 4 was 1.01 %,7.87 % and 17.5 % respectively.

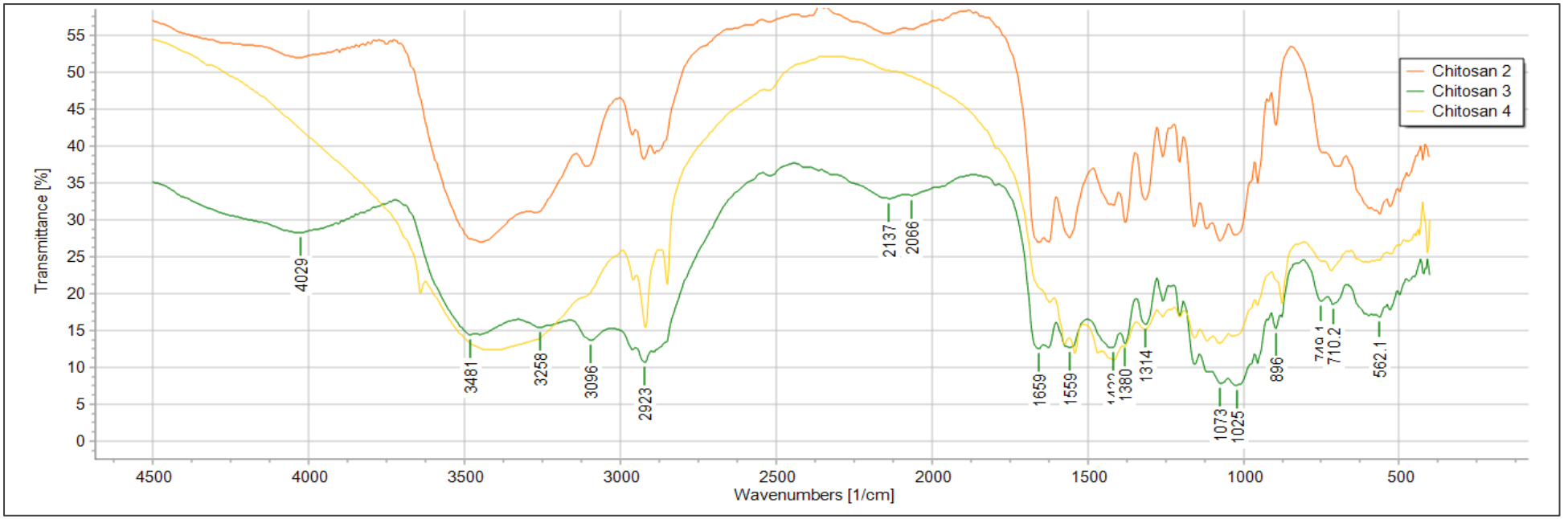

Figure 4. 11: FTIR spectra of Chitosan 2, Chitosan 3 and Chitosan 4 in KBr.

Table 4. 10: Chitosan 2, Chitosan 3 and Chitosan 4 Degree of acetylation, relative yield and cost of production

Product	Production sequence	A1655	A3450	Degree of De-acetylation	Relative Yield (%)	Cost of production ($/kg)
Chitosan 2	Demineralization, Deproteination, De-acetylation	0.5698	0.6409	33.2	1.01	26.0
Chitosan 3	Deproteination, De-acetylation	1.063	1.353	40.9	7.87	16.1
Chitosan 4	De-acetylation	0.6281	0.7503	37.1	17.5	24.8

Table 4. 10 shows the cost of production of Chitosan 2, Chitosan 3 and Chitosan 4 was 26.0 $/kg, 16.1 $/kg, 24.8 $/kg respectively. The cost of production of chitosan extracted from BSF larvae is higher than that of other bio-sorbents which range from $ 0.0777 to $ 0.514 per kg (Gupta & Babu, 2008) and commercial activated carbon at $ 7.07 per kg (Gupta & Babu, 2008). Chitosan 3 had the lowest cost of production due to having the highest yield during de-acetylation of 31.1 % as shown in Table A4. 3 in Appendix A4 Chitin and chitosan cost of production. Figure 4. 12 shows that demineralization, deproteination and de-acetylation contribute to 4 %, 16 % and 80 % of the total cost of production of the chitosan extracted from the BSF larvae. De-acetylation is the most expensive step in the production of chitosan due to the use of highly concentrated alkali (40 % NaOH).

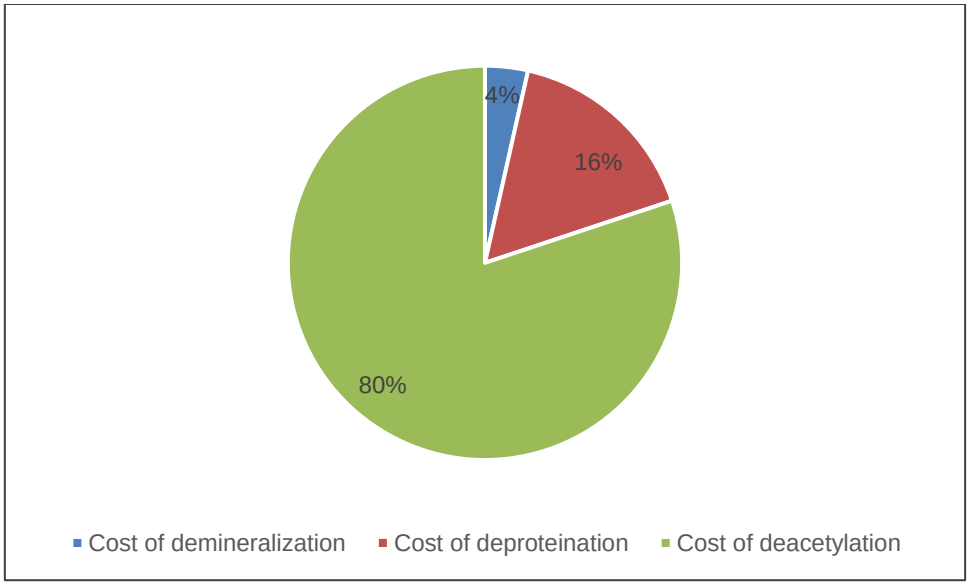

Figure 4. 12: Extraction steps contribution towards the cost of production of chitosan from BSF larvae

4.2.2 Effect of chitin extraction steps on chitosan adsorption kinetics

0.5 g of Chitosan 2, Chitosan 3 and Chitosan 4 were placed in a bimetal copper and ferrous test solution with initial concentrations of 2.79 mmol/L respectively. The decrease in the concentration of the ferrous and copper ions due to adsorption was observed and is shown in Figure A5. 9 and Figure A5. 10 respectively in Appendix A5 Metal concentration and pH-time graphs. Equation 9 in Section 2.3.1 was used to calculate the amount of ferrous and copper ions adsorbed onto the chitosan. Table 4. 11 shows the adsorption initial pH, final pH and the maximum adsorption capacity for ferrous and copper ions for Chitosan 2, Chitosan 3 and Chitosan 4.

Table 4. 11: Initial and final adsorption pH, maximum adsorption capacity for ferrous and copper ions onto Chitosan 2, Chitosan 3 and Chitosan 4

Product	Initial adsorption pH	Final adsorption pH	Fe2+ Q_{max} (Fe^{2+} mmol/g chitin)	Cu 2+ Q_{max} (Cu^{2+} mmol/g chitin)
Chitosan 2	3.45	4.18	0.278± 0.04	0.245± 0.01
Chitosan 3	3.46	4.94	1.086± 0.001	1.091± 0.01
Chitosan 4	3.45	7.34		0.530± 0.01

The maximum adsorption capacity for ferrous ions onto Chitosan 2 and Chitosan 3 was 0.278 ± 0.04 mmol/g and 1.086± 0.003 mmol/g respectively. While, the maximum adsorption capacity for copper ions onto Chitosan 2, Chitosan 3 and Chitosan 4 was 0.245 ± 0.01 mmol/g, 1.09± 0.01 mmol/g and 0.530±0.01 mmol/g respectively. Chitosan 4 did not adsorb ferrous ions due to the precipitation of the ferrous ions out of solution during the adsorption. Visible brown precipitates attributed to ferric hydroxide were observed at the start of the adsorption study with Chitosan 4. There was a rapid adsorption pH change during adsorption of ferrous and copper onto Chitosan 4 as shown in Figure A5. 11 in Appendix A5 Metal concentration and pH-time graphs. The adsorption pH increased from 3.46 to 5.2 within the first hour and a final adsorption pH of 7.34 was observed after 21 hours. The pH precipitation range of ferric and ferrous ions in the presence of hydroxide ions is between 1.5-3.5 and 6.6 to 10 respectively according to Blais et al*. (*2008*)*. The observed brown precipitates indicate that the ferrous ions were oxidized to ferric ions prior/during precipitation in the adsorption study. The oxidation of ferrous to ferric ion was attributed to the antioxidant properties of Chitosan 4 and the increase in the adsorption pH. Chitosan has antioxidant properties(Cho et al., 1998; Ngo & Kim, 2014; Trung & Bao, 2015) and can scavenge free radicals through the action of the nitrogen in the C-2 position (Ngo & Kim, 2014). The nitrogen in the amino groups has a lone pair of electrons in which protonation can occur with H+ ions to form ammonium groups (NH_3^+). The free radicals can react with the hydrogen ion in the ammonium groups (NH_3^+) to form a stable molecule. The higher final adsorption pH in Chitosan 4 suggests that this Chitosan 4 had an increased antioxidant property relative to the other chitosan in this study. The protonation of the amine groups in Chitosan 4 resulted in the increased pH (Cho et al., 1998). Ferrous ions oxidize to the ferric state in atmospheric conditions when exposed to air (Lamb & Jacques, 1938; Stumm & Lee, 1961). However, this oxidative process is slow at pH

lower than 2.1 with half-life lives of more than 21 days (Hem & Cropper, 1962). At pH above 2.1, ferric hydroxide precipitation from ferrous solutions becomes more rapid (Lamb & Jacques, 1938; Lu et al., 2008). Also, the presence of copper ions acts as a catalyst in the oxidation of ferrous ions(Stumm & Lee, 1961). The free radical scavenging activity of Chitosan 4 could have accelerated the oxidation of ferrous ions to ferric with the electrons in the process reacting with the ammonium groups (NH_3^+). .The impact of demineralization can be seen by comparing the adsorption of copper and ferrous ions onto Chitosan 2 and Chitosan 3. Chitosan 2 had a 78 % lower maximum adsorption capacity for copper and ferrous ions than Chitosan 3. This was due to a decrease in Chitosan 2 during the adsorption. There was visible solubilisation of Chitosan 2 during the adsorption study. This indicates that demineralization has negative impacts on the solubility stability of chitosan extracted from BSF larvae in acid solutions. Chitosan 3 had the highest adsorption of ferrous and copper ions.

Chitosan 3 had similar maximum adsorption capacities for ferrous ions to that observed of the studied chitin and the highest maximum adsorption capacity for copper ions. Chitosan 3 adsorbed 20 % more copper ions than CHITIN-CBR-ELN. Chitosan has been noted to have higher copper maximum adsorption capacities than chitin. This is due to a higher presence of amine groups in chitosan (Guibal, 2004; Anastopoulos et al., 2017). The results suggest that an increase in DA results in increased copper adsorption. This indicates that the active adsorption site for copper ions maybe occurring on the amine group in the de-acetylated acetamido group of the chitin and chitosan. Chitosan 3 adsorbed 0.458 % more copper ions more than ferrous ions. This degree of metal adsorption selectivity is lower than that obtained for chitin. This indicates that chitin has a higher degree of metal adsorption selectivity for ferrous ion than chitosan has for copper ions. Chitosan had higher adsorption equilibrium pH than chitin. They can also be attributed to a higher presence of amine groups in the chitosan. At low pH protonation on both chitin and chitosan occurs however this effect is more pronounced on chitosan due to higher DD (ie more amine groups) and solubility in acid. Chitosan is soluble in most mineral acids and it is relatively stable in sulfuric acid (Guibal, 2004).The solubilization of chitosan results in the protonation of the chitosan in solution which is more rapid than the protonation observed in the chitin. The maximum adsorption capacities obtained in this study are in the range of those obtained by other bio sorbents and higher than that of most commercial sorbents. This can be observed by comparison with the maximum adsorption capacities for bio sorbent and commercial sorbents in Table A1. 1 in Appendix A1 Literature Review Figures and Tables. Chitosan has been observed to be able to adsorb ferrous and copper ions in the range of 0.952 mmol/g to 3.52 mmol/g. (Findon et al., 1993; Rhazi et al., 2000; Babel & Kurniawan, 2003; Wan et al., 2004; Wang et al., 2019).

Figure 4. 13 and Figure 4. 14 shows the adsorption of ferrous and copper ions respectively onto the chitosan. In general, the adsorption of ferrous and copper ions took 5 hours to reach maximum adsorption capacity (adsorption equilibrium) with 63 % to 90 % of the adsorption occurring within the first hour. This is in agreement with several authors who have conducted metal adsorption studies with chitosan (Chu, 2002; Rhazi et al., 2002; Wang et al., 2019). Figure 4. 13 and Figure 4. 14 also shows that ferrous and copper adsorption on Chitosan 2, Chitosan 3 and Chitosan 4 was well modelled by the Pseudo 2nd order kinetic model.

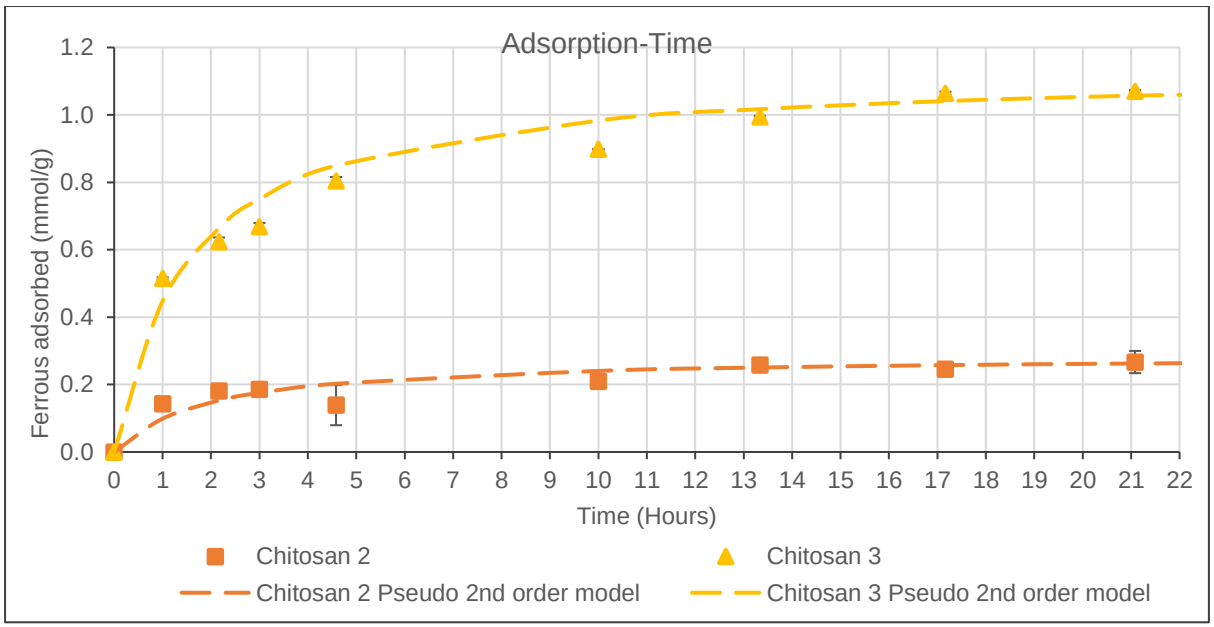

Figure 4. 13: Chitosan 2, Chitosan 3, Chitosan 4 ferrous adsorption and pseudo second order kinetics

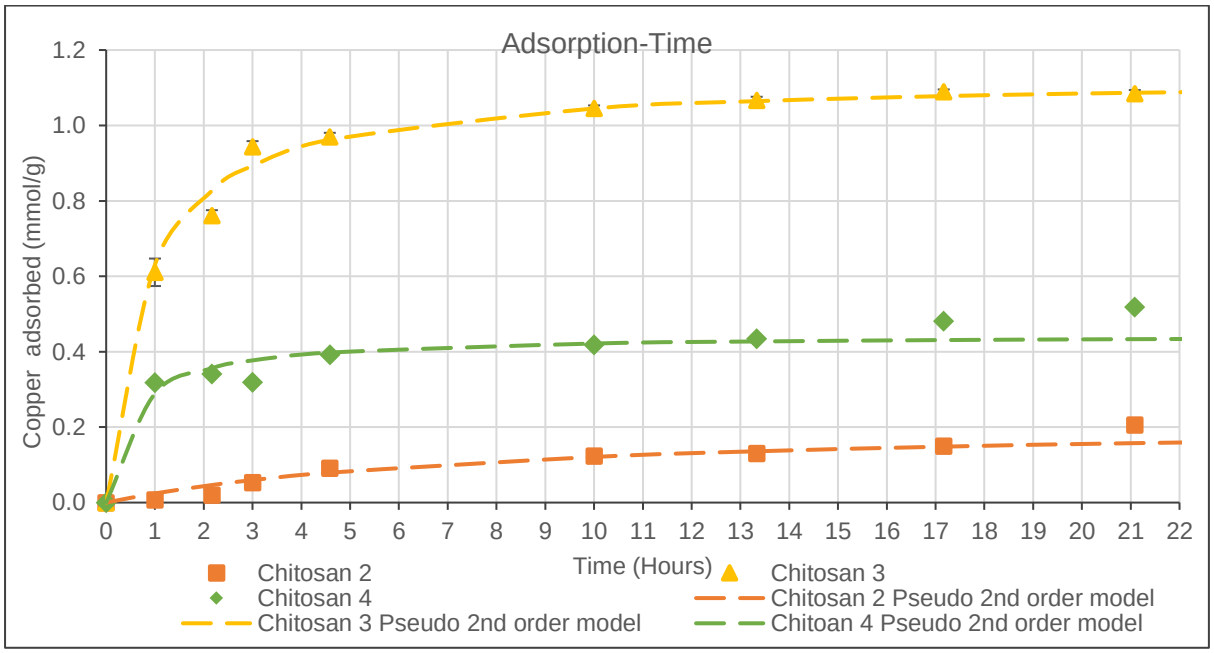

Figure 4. 14: Chitosan 2, Chitosan 3, Chitosan 4 copper adsorption and pseudo second-order kinetics

Table 4. 12 and Table 4. 13 show the maximum sorption capacity (Q_{max}), pseudo 2nd order adsorption initial rate (h_o) and rate constant (k_f), standard deviation (SD), correlation coefficient (R_2) and the adjusted correlation coefficient ($AdjR_2$) for ferrous and copper adsorption respectively onto Chitosan 2, Chitosan 3 and Chitosan 4. The Pseudo 2nd order adsorption model linear fit for ferrous and copper adsorption onto Chitosan 2, Chitosan 3 and Chitosan 4 is shown in Figure A7. 5 and Figure A7. 7 in Appendix A7 Adsorption reaction kinetics.

Table 4. 12 and Table 4. 13 show that the Pseudo 2nd order adsorption kinetic model linear fit has $AdjR_2$ values were between 0.9620 to 0.9998 for ferrous and copper adsorption onto the chitosan. Indicating a good fit with the adsorption experimental data. The result was low SD

between 0.0342 to 0.0582 mmol/g between the pseudo 2nd order model predicted adsorption and the experimental adsorption for both ferrous and copper onto the chitosan. The low SD values indicate that the Pseudo 2nd order model can accurately predict the adsorption of ferrous and copper ion onto the chitosan studied. Similar results were observed for the studied chitin.

Table 4. 12: Chitosan 2, Chitosan 3 and Chitosan 4 pseudo-second-order kinetics parameters for ferrous adsorption

	Pseudo 2nd order kinetics					
	Ferrous					
Product	**Qmax (mmol/g)**	**k_f (h^{-1})**	**h_o (mmol g^{-1} h^{-1})**	**SD**	**R^2**	**AdjR^2**
Chitosan 2	0.286	1.84	0.15	0.0342	0.9766	0.9306
Chitosan 3	1.134	0.57	0.74	0.0582	0.9942	0.9827

Table 4. 13: Chitosan 2, Chitosan 3 and Chitosan 4 pseudo-second-order kinetics parameters for copper adsorption

	Pseudo 2nd order kinetics					
	Copper					
Product	**Qmax (mmol/g)**	**k_f (h^{-1})**	**h_o (mmol g^{-1} h^{-1})**	**SD**	**R^2**	**AdjR^2**
Chitosan 2	0.217	0.6	0.03	0.0369	0.9620	0.8882
Chitosan 3	1.127	1.1	1.43	0.03294	0.9998	0.9994
Chitosan 4	0.444	4.2	0.83	0.0577	0.9946	0.9838

Table 4. 12 shows the pseudo 2nd order adsorption rate constant for ferrous ions onto Chitosan 3 and Chitosan 4 was 0.286 h^{-1} and 1.134 h^{-1}. While the pseudo 2nd order adsorption rate constant for copper ions onto Chitosan 2, Chitosan 3 and Chitosan 4 were 0.6 h^{-1}, 1.1 $h^{-1}$and 4.2 h^{-1}. The copper ion pseudo 2nd order adsorption rate constant for the chitosan was higher that of CHITIN-CBR-ELN indicating faster adsorption reaction rates with copper ions. This observation is consistent with the observed maximum adsorption capacity of copper ions onto chitin and chitosan. The desorption of ferrous and copper ions from Chitosan 2, Chitosan 3 and Chitosan 4 are shown in Figure A5. 12 and Figure A5. 13 respectively in Appendix A5 Metal concentration and pH-time graphs. Complete desorption of the adsorbed ferrous and copper ions onto the chitosan was achieved using 0.1 M H_2SO_4.

4.2.3 Effect of chitin extraction steps on chitosan metal recovery techno-economic

Chitosan used during the adsorption process has potential use as agricultural grade chitosan (Orzali et al., 2018). Therefore, revenue from the sale of chitosan after desorption using the market price of agricultural grade chitosan which is $ 20/kg (Alibaba, 2019i) was used also in the calculation of the potential gross profit/loss of the metal recovery process. The techno economics was conducted based on the recovery of 1kg of metal using the chitosan and precipitation with NaHS. Figure 4. 15 shows total recovery costs, the revenue of sales of metal sulphide, the revenue of sale of used chitosan, gross profit/loss (excluding chitosan revenue) and gross profit/loss (including chitosan revenue) for the recovery of copper and ferrous ions using Chitosan 2, Chitosan 3 and Chitosan 4.

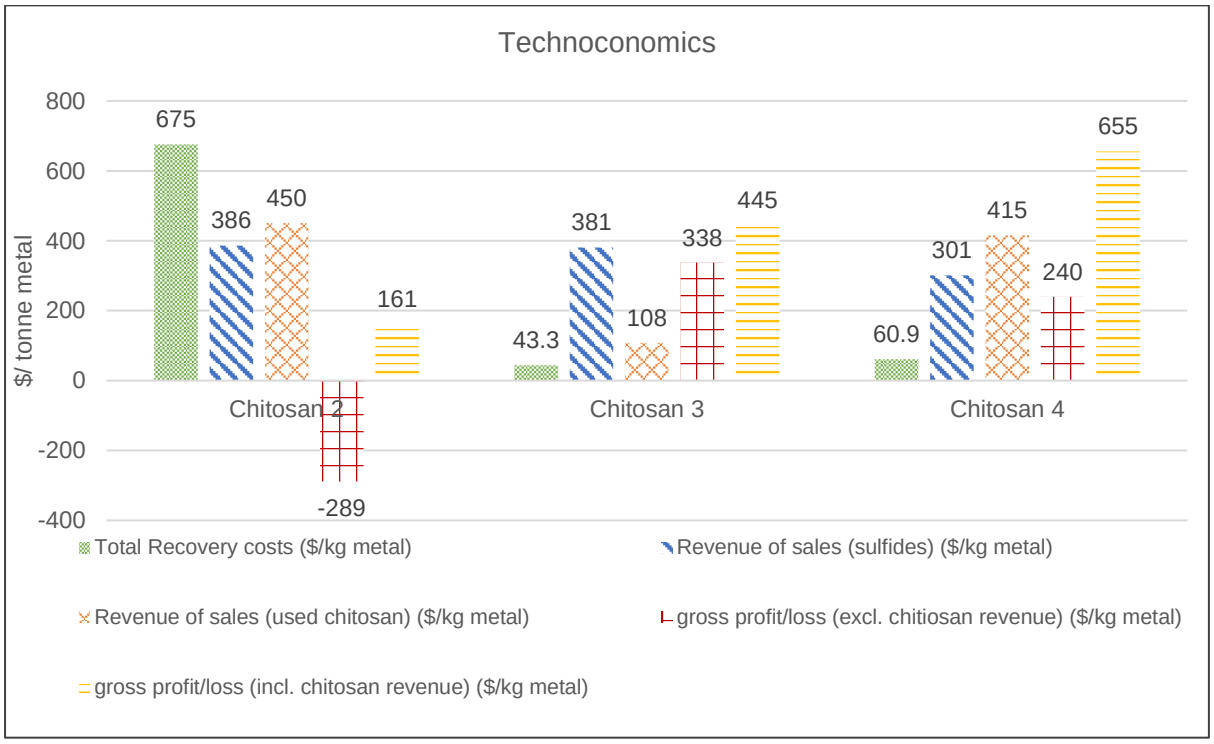

Figure 4. 15: Chitosan 2, Chitosan 3, Chitosan 4 total recovery costs, revenue of sales of metal sulphide, revenue of sale of used chitin, gross profit/loss (excluding chitin revenue) and gross profit/loss (including chitin revenue))

Figure 4. 15 shows that the total recovery costs for Chitosan 2, Chitosan 3 and Chitosan 4 were 675 $/kg metal, 43.3 $/kg metal and 60.9 $/kg metal respectively. The recovery costs of chitosan extracted from BSF larvae were twice that of the chitin due to the high cost of de-acetylation. The revenue for the sale of sulphides was 386 $/kg metal, 381 $/kg metal and 301 $/kg metal respectively This was lower than that of chitin due to the adsorption of more copper ions than ferrous ions. Copper sulphide is cheaper than ferrous sulphide. The gross profit/loss of the recovery process excluding chitosan revenue was -289 $/kg metal, 338 $/kg metal and 240 $/kg metal respectively. Chitosan 2 made a gross loss due to the high costs of production. Chitosan 3 and Chitosan 4 made a profit with Chitosan 3 having a higher profit due to cheaper production costs. The gross profit of chitosan excluding the revenue of sale of chitosan was less than that of the chitin. This was due to higher recovery costs of chitosan because of the higher cost of production of the chitosan. The gross profit/loss of the recovery process including chitosan revenue was 161 $/kg metal, 445 $/kg metal and 655 $/kg metal respectively. The inclusion of sales of the chitosan resulted in Chitosan 2 having a profit in the

metal recovery process. The revenue of sales of the chitosan for Chitosan 2, Chitosan 3 and Chitosan 4 was 450 $/kg metal,108 $/kg metal and 415 $/kg metal respectively. Agricultural grade chitosan has a higher market value than agricultural grade chitin. The amount of mass of Chitosan 2, Chitosan 3 and Chitosan 4 used to recovery 1 kg of copper and ferrous metal was 32.2 kg, 7.7 kg and 29.7 kg respectively.

Chitosan 4 resulted in the precipitation of ferrous ions due to the increase in the adsorption pH. While Chitosan 2 had low metal adsorption capacities due to solubility instability. Therefore, the application of these polymers to PCB leachate solutions is limited. Chitosan 3 is proposed as the optimum chitosan produced from BSF larvae for application as a metal bio sorbent. This is because Chitosan 3 had a metal adsorption selectivity for copper ions over ferrous ions, the high adsorption capacity of both metals, low cost of production and recovery costs, relatively higher gross profit in metal recovery and relatively low final adsorption pH. Chitosan 3 was produced from the BSF larvae using the liberation, deproteination and de-acetylation steps. Therefore, this methodology is the optimum method for producing chitosan for metal adsorption in PCB leachate solutions. The cost of production of Chitosan 3 was $ 16.1 per kg. Although not competitive with other sorbents, the potential of generating revenue from the secondary application of this polymer improves its economic outlook. Chitosan 3 was given the product name of CHITOSAN-CBR-ELN.

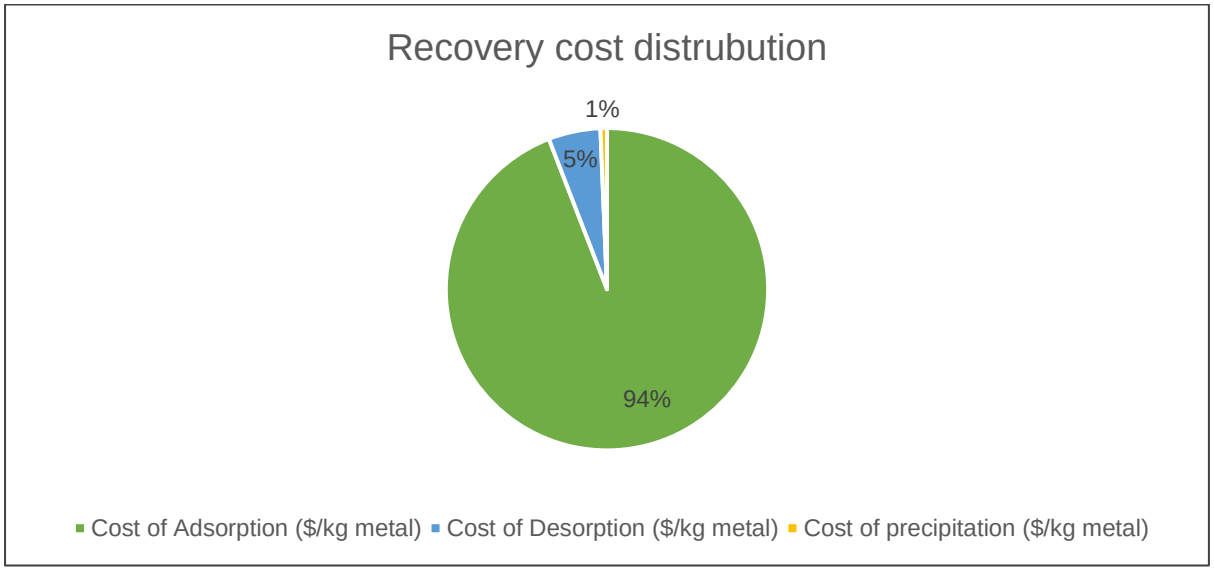

Figure 4. 16: Percentage contribution by recovery steps in the total metal recovery costs for copper and ferrous ions using Chitin 3 and NaHS precipitation.

Figure 4. 16 shows that adsorption, desorption and precipitation account for 94 %, 5 % and 1 % of the total recovery costs. As observed in the techno-economics of chitin, adsorption is the most expensive recovery step. The adsorption step percentage contribution to the total recovery costs for chitosan was higher than that of chitin due to the higher cost of production of the chitosan.

Chapter 5: Evaluation of optimum bio sorbents

5.1 Adsorption of Copper and Aluminium from a Bimetal Solution onto CHITIN-CBR-ELN and CHITOSAN-CBR-ELN

0.1 g of CHITIN-CBR-ELN and CHITOSAN-CBR-ELN were placed in a bimetal aluminium and copper test solution with initial concentrations of 2.79 mmol/L respectively. The decrease in the concentration of the aluminium and copper ions due to adsorption was observed and is shown in Figure A5. 14 and Figure A5. 15 respectively in Appendix A5 Metal concentration and pH-time graphs. Equation 9 in Section 2.3.1 was used to calculate the amount of aluminium and copper ions adsorbed onto CHITIN-CBR-ELN and CHITOSAN-CBR-ELN. Table 5. 1 shows the adsorption initial pH, final pH, maximum adsorption capacity for aluminium and copper ions for CHITIN-CBR-ELN and CHITOSAN-CBR-ELN.

Table 5. 1: Initial and final adsorption pH, maximum adsorption capacity for aluminium and copper ions onto CHITIN-CBR-ELN and CHITOSAN-CBR-ELN

Product	Production sequence	Initial adsorption pH	Final adsorption pH	Al3+ Q_{max} (Al^{3+} mmol/g chitin)	Cu 2+ Q_{max} (Cu^{2+} mmol/g chitin)
CHITIN-CBR-ELN-	(Deproteinated)	3.46	3.76	0.927± 0.001	0.843± 0.005
CHITOSAN-CBR-ELN-	(Deproteinated, Deacetylated)	3.44	4.56	0.762± 0.001	1.00± 0.003

Table 5. 1 shows the maximum adsorption capacity for aluminium ions onto CHITIN-CBR-ELN and CHITOSAN-CBR-ELN was 0.927± 0.001 mmol/g and 1.52± 0.001 mmol/g respectively. While for copper ions, the maximum adsorption capacity was 0.843± 0.005 mmol/g and 1.00± 0.003 mmol/g respectively. For CHITIN-CBR-ELN, the maximum adsorption capacity for aluminium was higher than that of copper. This indicates that chitin from BSF larvae has a higher metal adsorption selectivity for aluminium ions over copper ions. CHITIN-CBR-ELN adsorbed 9.06 % more aluminium than copper. This degree of metal adsorption selectivity was however lower than that observed for adsorption with ferrous and copper ions. The maximum adsorption capacity for aluminium observed for CHITIN-CBR-ELN was lower than that obtained for ferrous ions in Section 4.1.5. CHITIN-CBR-ELN had a maximum adsorption capacity for ferrous ions of 1.11 ± 0.002 mmol/g. The order of maximum adsorption capacity of ferrous, copper, aluminium ions onto chitin from BSF larvae suggests that the order of metal adsorption selectivity of these metals is Fe^{2+}>Al^{3+}>Cu^{2+}. This order of metal adsorption selectivity is similar to that observed by Gyliene et al. (2002) and Zhou et al. (2004). The order of metal adsorption selectivity onto chitin has been shown to closely follows the order of hydrolysis constants of the metal hydroxides (Zhou et al., 2004). Ferrous oxidation to ferric ions was observed in the adsorption of ferrous ions onto chitin and chitosan in Section 4. Ferrous ions are maybe oxidising during the adsorption process due to the increase in the adsorption pH and antioxidant properties of chitin and chitosan. The result is that the adsorption of ferrous ions onto chitin and chitosan can be characterised by ferric ion precipitation. Therefore the order of metal adsorption selectivity of ferrous, aluminium and copper ions onto chitin from BSF larvae indicates that the metal adsorption onto the chitin involves surface precipitation whereby the metal hydroxides that precipitates at the lower pH

being adsorbed preferentially (Gyliene et al., 2002). The observed order of metal adsorption selectivity of ferrous, aluminium and copper ion adsorption onto CHITIN-CBR-ELN supports the first hypothesis proposed in Section 2.5.2.

CHITOSAN-CBR-ELN adsorbed 23.8 % more copper ions than aluminium ions. This observation indicates that chitosan from BSF larvae has a higher metal adsorption selectivity for copper ions over aluminium ions. The maximum adsorption capacity for aluminium observed for CHITOSAN-CBR-ELN was lower than that obtained for ferrous ions in Section 4.1.5. CHITOSAN-CBR-ELN had a maximum adsorption capacity for ferrous ions of 1.11 $\pm$ 0.002 mmol/g. The order of maximum adsorption capacity of ferrous, copper, aluminium ions onto chitosan from BSF larvae suggests that the order of metal adsorption selectivity of these metals is Cu^{2+}>Fe^{2+}>Al^{3+}. This order of metal adsorption selectivity is similar to that observed by Wang et al. (2019)**.** The order of metal adsorption selectivity onto chitosan has been shown to closely follows the order of electronegativity of the metal ions. The order is influenced by the size and charge of the ions. Oversize and undersize metal ions hinder the co-ordinate binding between metal ions and active sites. Therefore, the higher the electronegativity of a metal ion, the greater the attraction of metal ion for electrons (Wang et al., 2019). Electronegativity is directly and inversely proportional to the effective nuclear charge and covalent radius. The values of Paulin's electronegativity index for copper, iron and aluminium ions are 1.90, 1.83, 1.61 respectively (Haynes, 2010). The order of metal adsorption selectivity of ferrous, aluminium and copper ions onto chitosan from BSF larvae indicates that the metal adsorption has correlations with the electronegativity of the metals. The observed order of metal adsorption selectivity of ferrous, aluminium and copper ion adsorption onto CHITOSAN-CBR-ELN supports the second hypothesis proposed in Section 2.5.2.

Figure 5. 1 and Figure 5. 2 shows the adsorption of aluminium and copper ions respectively onto CHITIN-CBR-ELN and CHITOSAN-CBR-ELN. In general, the adsorption of aluminium and copper ions took 5 hours and 16 hours respectively to reach maximum adsorption capacity (adsorption equilibrium) with 73 % to 95 % of the adsorption occurring within the first 4 hours. The adsorption of copper onto CHITOSAN-CBR-ELN took a longer time to reach adsorption equilibrium in the Copper-Aluminium bimetal solution than the Copper-Iron bimetal solution. In the Copper-Aluminium bimetal solution, maximum adsorption capacity on the CHITOSAN-CBR-ELN was reached in 18 hours whereas in the Copper-Iron bimetal solution it took 10 hours. Figure 5. 1 and Figure 5. 2 shows that aluminium and copper adsorption onto CHITIN-CBR-ELN and CHITOSAN-CBR-ELN was well modelled by the Pseudo 2^{nd} order kinetic model. Similar observations were made with the adsorption of iron and copper in Section 4.1. The pseudo 2^{nd} order adsorption rate constant for copper ions onto CHITOSAN-CBR-ELN in the Copper-Aluminium bimetal solution was 0.271 h^{-1} while for the Copper-Iron bimetal solution it was 1.10 h^{-1}. These results indicate that there was a reduced adsorption rate of copper onto CHITOSAN-CBR-ELN in the Copper-Aluminium bimetal solution. This may be due to the metal interaction between copper and aluminium. Copper and aluminium in acidic solutions may react to form copper-aluminium co-ordinate bonds. This reaction is noted to be galvanic (Idrac et al., 2007; Musa et al., 2012). The metal interaction reaction between aluminium and copper in the Copper-Aluminium bimetal solution may have resulted in reduced adsorption reactions of these metals with CHITOSAN-CBR-ELN therefore resulting in a slower adsorption rate for copper.

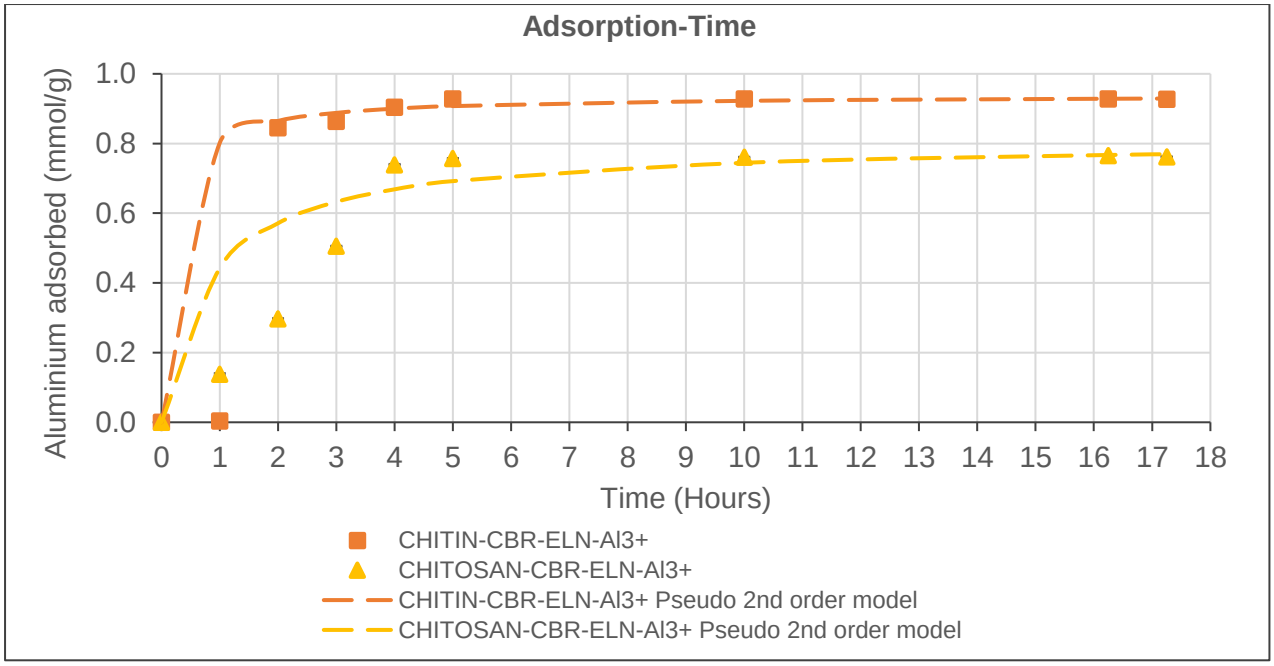

Figure 5. 1: CHITIN-CBR-ELN and CHITOSAN-CBR-ELN aluminium adsorption and pseudo-second-order kinetics

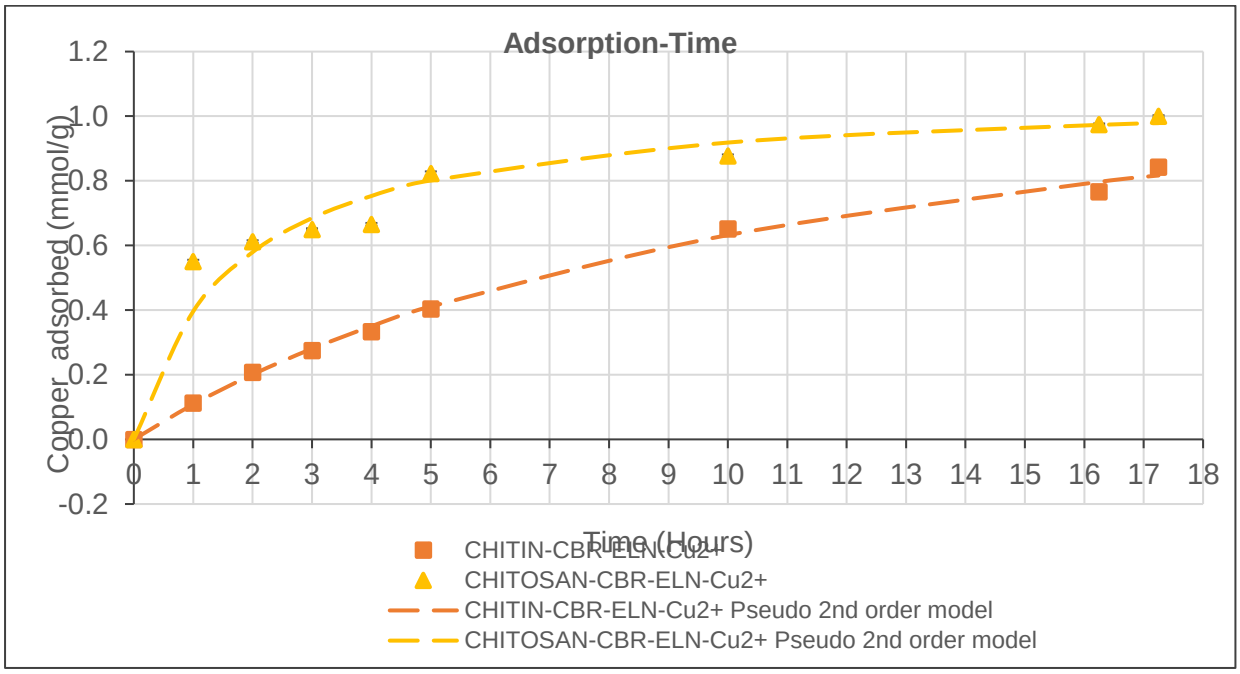

Figure 5. 2: CHITIN-CBR-ELN and CHITOSAN-CBR-ELN copper adsorption and pseudo-second-order kinetics

5.2 Adsorption of Ferrous, Ferric, Aluminium and Copper onto CHITIN-CBR-ELN

0.05 g of CHITIN-CBR-ELN were placed in single metal test solutions of ferrous, ferric, copper and aluminium with initial concentrations of 2.79 mmol/L respectively as described in Section 3.4.3. The decrease in the concentration of the ferrous, ferric, copper and aluminium ions due to adsorption was observed and is shown in Figure A5. 16 in Appendix A5 Metal concentration and pH-time graphs. Equation 9 in Section 2.3.1 was used to calculate the ferrous, ferric, copper and aluminium ions adsorbed onto CHITIN-CBR-ELN.

5.2.1 Active Sites in the Adsorption of Ferrous, Ferric, Aluminium and Copper onto Chitin

An FTIR analysis was conducted on CHITIN-CBR-ELN and the CHITIN-CBR-ELN with adsorbed ferrous, ferric, copper and aluminium ions respectively. Figure 5. 3, Figure 5. 4, Figure 5. 5 and Figure 5. 6 shows the FTIR spectra of CHITIN-CBR-ELN with adsorbed ferrous, ferric, copper and aluminium ions respectively in a KBr media taken from wavenumbers of 4000 cm^{-1} to 400 cm^{-1}.Adsorption of metals onto chitin and chitosan result in bond formation/chelation between the polymer and the metals (Cui & Zhang, 2008; Renu et al., 2016). The result is a reduction in FITR transmittance due to increased bond strength on the active sites or scattering by the metal chelate bond formed (Jaafarzadeh et al., 2014).

Figure 5. 3 that the transmittance of CHITIN-CBR-ELN with adsorbed ferrous ions was lower than that of CHITIN-CBR-ELN at wavenumbers: 3439cm^{-1} (O H stretching), 2921 cm^{-1} (CH_3 group in $NHCOCH_3$), 1654 cm^{-1} (C=O secondary amide stretch (Amide I)), 1550 cm^{-1} (N-H stretch (Amide II)) 1379 cm^{-1} (C-H bend, CH_3 symmetric deformation), 1320 cm^{-1} (C-N from amides (amide III)), 1158cm^{-1} (C-O-C asymmetric stretching) and 1073 cm^{-1} (C-O-C symmetric stretching). These results suggest that the active sites in ferrous adsorption onto CHITIN-CBR-ELN are the hydroxyl, ester and amide functional groups in the chitin. Similar results were observed with the transmittance in the CHITIN-CBR-ELN with adsorbed copper ions in Figure 5. 5 and adsorbed aluminium ions in Figure 5. 6. Indicating that copper and aluminium ion share the same active sites as ferrous ions.

For CHITIN-CBR-ELN with adsorbed ferric ions in Figure 5. 4, the transmittance in the amide bands (1654 cm^{-1}, 1550 cm^{-1}) remained relatively constant when compared to CHITIN-CBR-ELN. This indicates that the amide functional groups did not take part in the adsorption of ferric ions onto CHITIN-CBR-ELN. Suggesting that the active sites for ferric ions were the hydroxyl and ester groups. These results indicate that ferrous ions and ferric ions have different active adsorption sites onto the chitin extracted from BSF larvae and potentially different adsorption pathways. The FITR results of the ferrous actives sites on the chitin from BSF larvae are consistent with the observation in Section 4.1 that low DA is associated with high ferrous adsorption. Adsorption of metals onto chitin is largely attributed to the amine and hydroxyl groups on the chitin (Guibal, 2004; Jaafarzadeh et al., 2014).

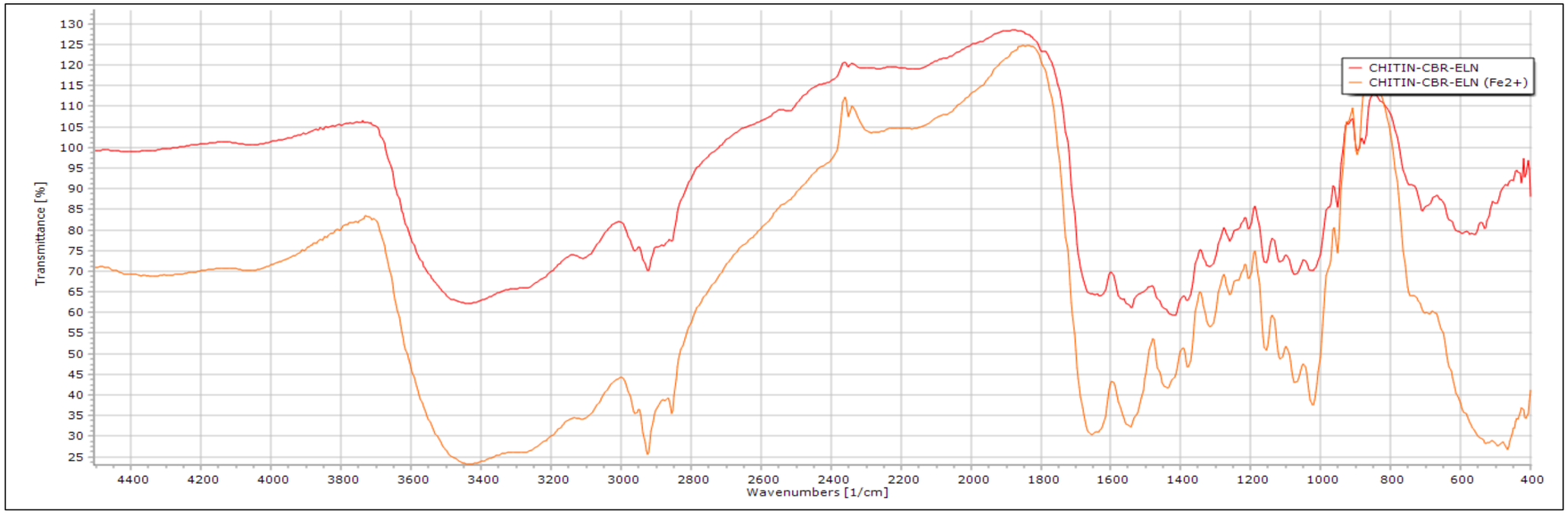

Figure 5. 3: FTIR spectra of CHITIN-CBR-ELN with adsorbed ferrous ions

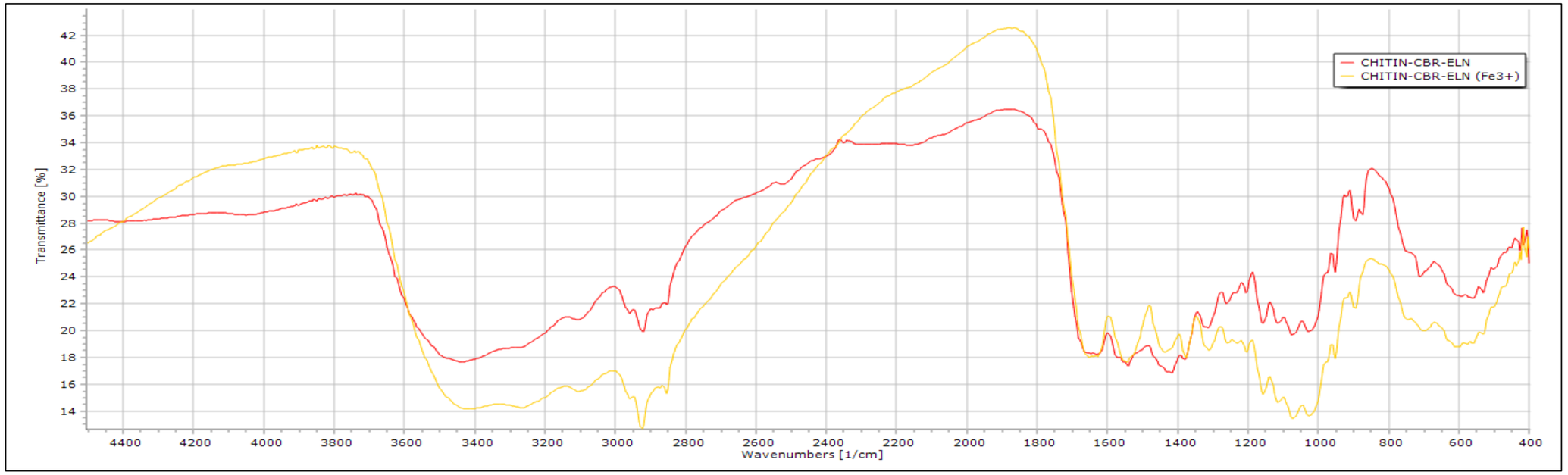

Figure 5. 4: FTIR spectra of CHITIN-CBR-ELN with adsorbed ferric ions

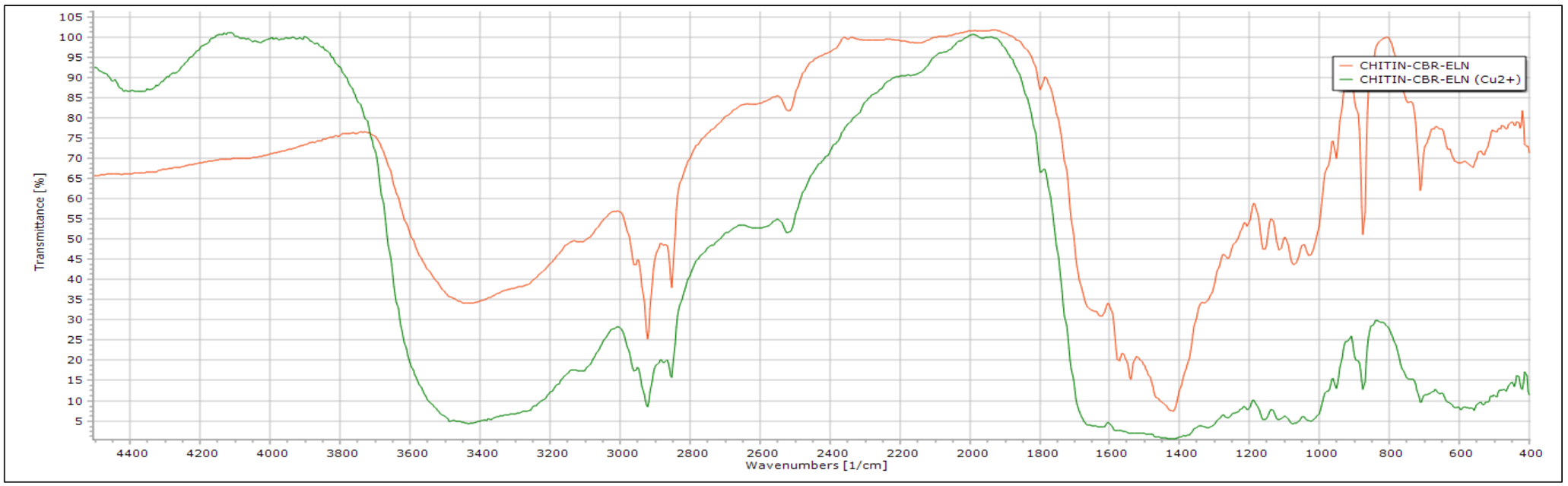

Figure 5. 5: FTIR spectra of CHITIN-CBR-ELN with adsorbed copper ions

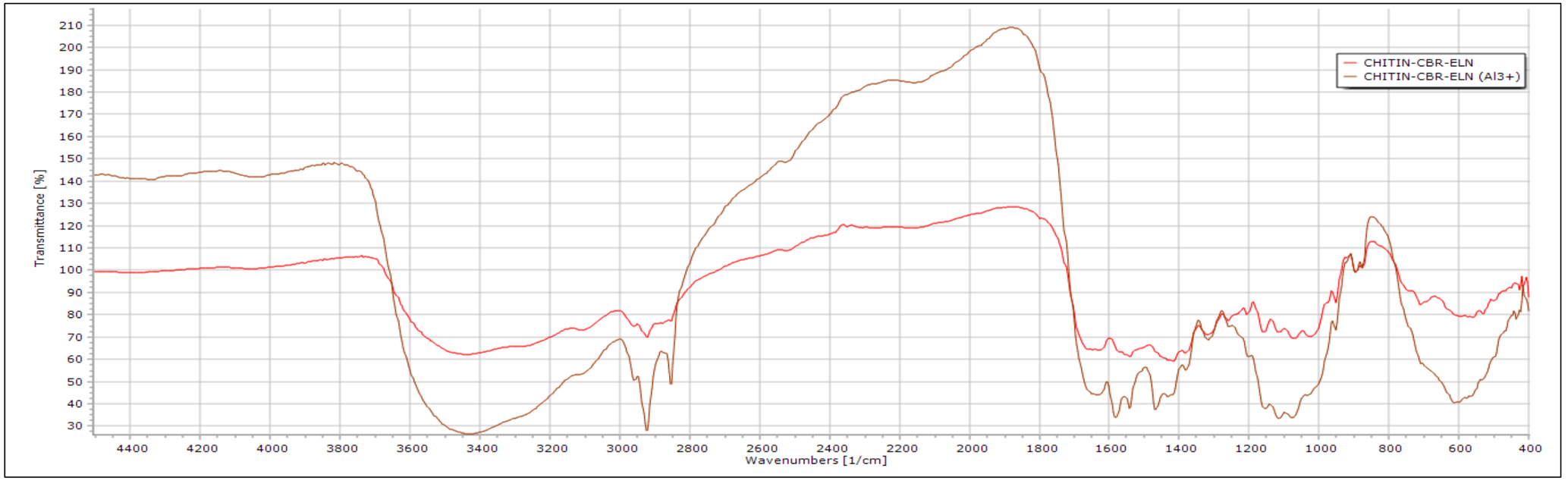

Figure 5. 6: FTIR spectra of CHITIN-CBR-ELN with adsorbed aluminium ions

5.2.2 Adsorption Isotherms of Ferrous, Ferric, Aluminium and Copper onto Chitin

Table 5. 2 shows the Langmuir maximum adsorption capacity (Q_{max}), Langmuir constant (K_L), Langmuir separation factor (R_L), change in Gibb's free energy (ΔG), standard deviation(SD), correlation coefficient (R^2) and adjusted correlation coefficient ($AdjR^2$) for the adsorption of ferrous, ferric, copper and aluminium onto CHITIN-CBR-ELN. Table 5. 2 shows that the adjusted correlation coefficient for the adsorption of ferrous, ferric, copper and aluminium onto CHITIN-CBR-ELN for the Langmuir isotherm lies between 0.9400 to 0.9964 while the standard deviation was between 0.089 to 0.739. The correlation coefficient suggests a good fit to the experimental data however the SD suggests that there is a significant deviation between the modelled and experimental data. According to Marković et al. (2014) and Bergmann (2015), a correlation coefficient close to 1 does not necessarily mean a good fit and further statistics are required to analyse the goodness of fit of a model. In this case, the SD suggests that the Langmuir isotherm does not adequately describe the adsorption of ferrous, ferric, copper and aluminium onto chitin extracted from BSF larvae.

The Langmuir isotherm is derived from the assumption of mono layer adsorption, equivalent active sites, non-existent interaction between adsorbate species and active sites only holding one adsorbate species (Langmuir, 1918). The inadequacy of the Langmuir isotherm to describe the experimental data accurately suggest that the adsorption of ferric, ferrous, copper and aluminium onto chitin is not monolayer adsorption, active sites do not have equivalent energies, there is an interaction between adsorbate species and active sties may hold more than one adsorbate species. The presence of interaction between adsorbate species in the adsorption of metal onto chitin and chitosan can be seen by the influence of the presence of ferrous and aluminium on the adsorption of copper onto chitosan. The active sites for the adsorption of ferrous, ferric, copper and aluminium onto chitin from BSF larvae were identified to be he hydroxyl, ester and amide functional groups. The decrease in transmission in the FTIR analysis observed at the wavenumber of these functional groups were different indicating different energies. Table 5. 2 shows the change in Gibb's free energy for the adsorption of ferrous, ferric, copper and aluminium onto CHITIN-CBR-ELN was -5.15 J/mol, -3.92 J/mol, -4.43 J/mol and -4.73 J/mol respectively. The change in Gibb's free energy observed is negative indicating that the adsorption of the metals onto chitin is spontaneous. Table 5. 2 also shows the Langmuir separation factor for the adsorption of ferrous, ferric, copper and aluminium onto CHITIN-CBR-ELN was 0.410, 0.299, 0.341 and 0.369 respectively. The Langmuir separation factors were between 0 and 1 indicating favourable adsorption.

Table 5. 2: Langmuir isotherm parameters for ferrous, ferric, copper, aluminium adsorption onto optimized Chitin

	Langmuir isotherm						
Product	**Q_{max} (mmol/g)**	**K_L (L/mmol)**	**R_L**	**ΔG (J/mol)**	**SD**	**R^2**	**$AdjR^2$**
CHITIN-CBR-ELN-Fe2+	0.270	0.518	0.410	-5.15	0.721	0.9798	0.9400
CHITIN-CBR-ELN-Fe3+	0.664	0.845	0.299	-3.92	0.089	0.9988	0.9964
CHITIN-CBR-ELN-Cu2+	0.439	0.690	0.341	-4.43	0.739	0.9986	0.9955
CHITIN-CBR-ELN-Al3+	0.285	0.612	0.369	-4.73	0.150	0.9799	0.9403

Table 5. 3 shows the Freundlich exponent (n_f), Freundlich equilibrium constant (K_f), standard deviation (SD), correlation coefficient (R_2), adjusted correlation coefficient ($AdjR_2$) for the adsorption of ferrous, ferric, copper and aluminium onto CHITIN-CBR-ELN. Table 5. 3 shows that the adjusted correlation coefficient for the adsorption of ferrous, ferric, copper and aluminium onto CHITIN-CBR-ELN for the Freundlich isotherm lies between 0.9900 to 0.9993 while the standard deviation was between 0.00671 to 0.115. The Freundlich isotherm has adjusted correlation coefficients closer to 1 and lower standard deviation to the experimental data than the Langmuir isotherm. These results suggest that the adsorption experimental data for the adsorption of ferrous, ferric, copper and aluminium onto CHITIN-CBR-ELN is better described by the Freundlich model than the Langmuir model. The Freundlich model is derived based on the assumptions of multilayer adsorption and an increase in the concentration of the adsorbate in solution results in an increase in the adsorption of the adsorbate (Skopp, 2009). This suggests that the adsorption of ferrous, ferric, copper and aluminium onto CHITIN-CBR-ELN from BSF larvae occurs on multilayers and is affected by the concentration of these metals. The multi-active sites of the CHITIN-CBR-ELN observed in the FTIR analysis are consistent with the Freundlich model's interpretation of the adsorption layer being multi-layered.

Table 5. 3: Freundlich isotherm parameters for ferrous, ferric, copper, aluminium adsorption onto optimized Chitin

	Freundlich isotherm				
Product	**n_f**	**k_f (mmol/g.(mmol/L)$^{-1/nf}$**	**SD**	**R^2**	**$AdjR^2$**
CHITIN-CBR-ELN-Fe2+	-0.201	119	0.115	0.9931	0.9794
CHITIN-CBR-ELN-Fe3+	-0.512	6.12	0.0473	0.9982	0.9946
CHITIN-CBR-ELN-Cu2+	-0.390	9.47	0.00671	0.9993	0.9979
CHITIN-CBR-ELN-Al3+	-0.306	15.1	0.0642	0.9900	0.9702

5.2.3:Weber-Morris Intraparticle Diffusion of Ferrous, Ferric, Aluminium and Copper onto Chitin

Figure 5. 7 shows the Weber-Morris intraparticle diffusion model liner fit plots for ferrous, ferric, copper and aluminium adsorption onto CHITIN-CBR-ELN. Weber Jr et al. (1963) developed an intraparticle diffusion model on adsorption onto carbon polymers. Intraparticle diffusion models are fundamental for the determination of the rate-limiting step(s) in the adsorption process (Bergmann, 2015). The steps involved in the adsorption of an adsorbate involve diffusion of the adsorbate through the film around the adsorbent, adsorbent pores (if absorption) and reaction at the active sites of the adsorbent (Wong et al., 1998). Adsorption can either be diffusion or reaction rate-limited or limited by both in which the limiting steps are the rate-controlling step (Bergmann, 2015). Weber Jr et al. (1963) suggested that if the plot of the equilibrium adsorbed sorbate on the adsorbent (Q) plotted against the square root of the time ($t^{1/2}$) is linear then particle diffusion is involved in the adsorption. If the linear fit passes through the origin, then intra particle diffusion is rate-controlling. However, if there is an intercept obtained in the linear fit then intra particle diffusion is not the only rate-limiting step and there is a degree of boundary layer control (Yakout & Elsherif, 2010). Figure 5. 7 shows that the diffusion of ferrous, ferric and copper onto CHITIN-CBR-ELN can be described by two linear fit lines while that of aluminium is described by one. The initial linear fit line observed in the diffusion of these metals is relatively steep (higher gradient values) followed by a relatively less steep (lower gradient values). This observation suggests that intraparticle diffusion is involved in the adsorption of ferric, ferrous, copper and aluminium onto chitin from BSF larvae.

Figure 5. 7 shows that the linear fits obtained had intercepts indicating that diffusion is not the only rate-limiting step in the adsorption of ferric, ferrous, copper and aluminium onto chitin from BSF larvae. The initial linear fit lines observed in Figure 5. 7 can be described as the 1st zone of diffusion and the second linear fit line as the 2nd zone of diffusion. The 1st zone of diffusion is ascribed to the adsorbate diffusing through the film layer around the adsorbent. The 2nd zone is ascribed to intra particle diffusion of the adsorbate into the pores of the adsorbent (Iijima, 1991). 32 % to 83 % of the adsorption of ferrous, ferric, copper and aluminium onto CHITIN-CBR-ELN occurred within the first hour with adsorption equilibrium being reached after 5 hours. This correlates to $t^{1/2}$ values of 7.75 $min^{1/2}$ and 17.3 $min^{1/2}$ respectively. This indicates that the adsorption of ferrous, ferric, copper and aluminium onto the chitin from BSF larvae largely occurs in the 1st zone indicating surface complexation.

Surface precipitation of the ferric, ferrous, aluminium and copper on the CHITIN-CBR-ELN during adsorption was observed as shown in Figure 5. 8, Figure 5. 9, Figure 5. 10 and Figure 5. 11 respectively. The imaging was taken by a 10 Megapixel camera at a resolution of 640 by 480 pixels; therefore, the precipitates are in the visible spectrum. Figure 5. 8, Figure 5. 9, Figure 5. 10 and Figure 5. 11 show that the observed precipitates of adsorbed ferric, ferrous, aluminium and copper ion onto CHITIN-CBR-ELN were brown, brown, blue and white respectively.

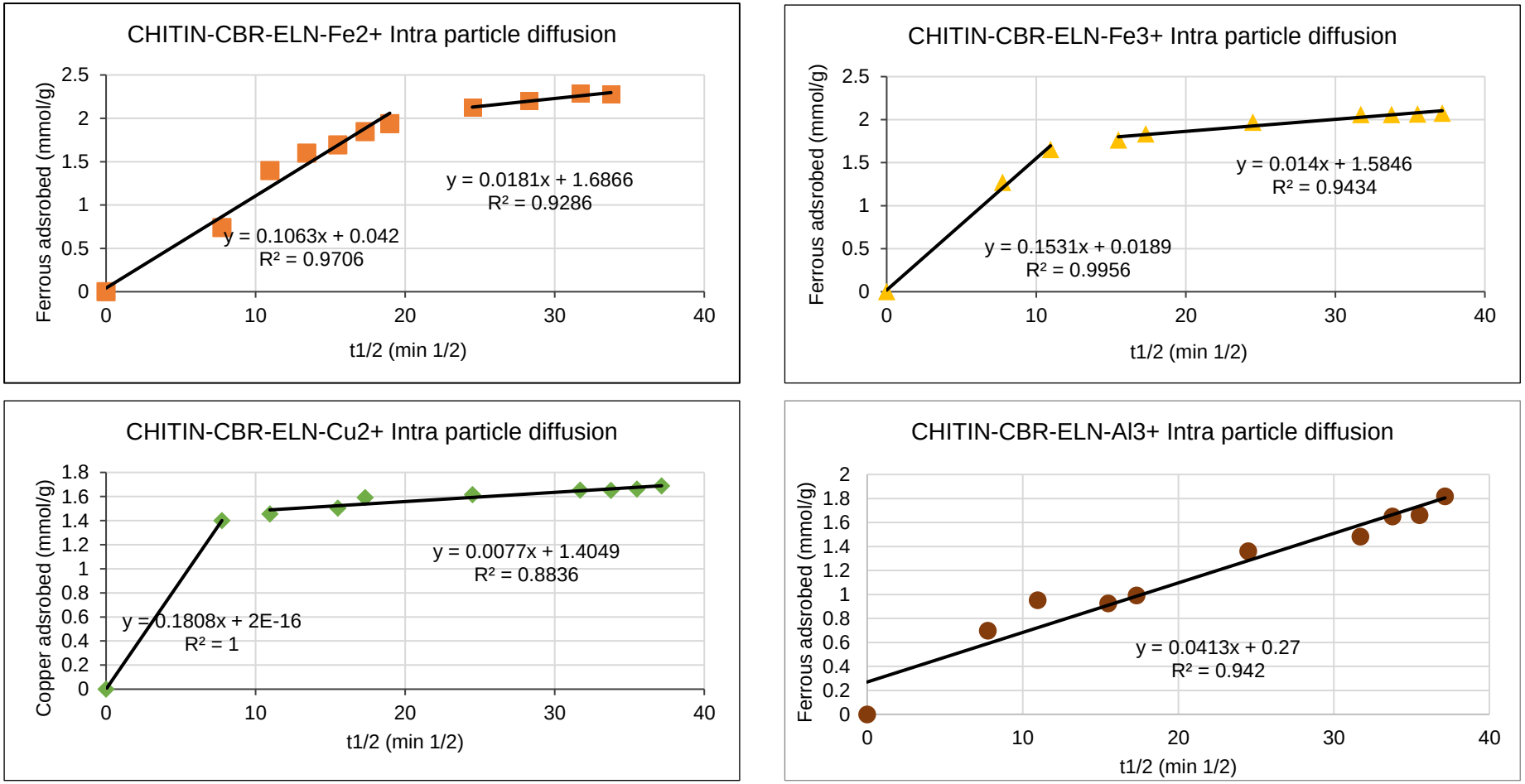

Figure 5. 7: Weber-Morris intraparticle diffusion model liner fit plots for ferrous, ferric, copper and aluminium adsorption onto CHITIN-CBR-ELN

Figure 5. 9: Imaging of CHITIN-CBR-ELN with adsorbed ferrous ions

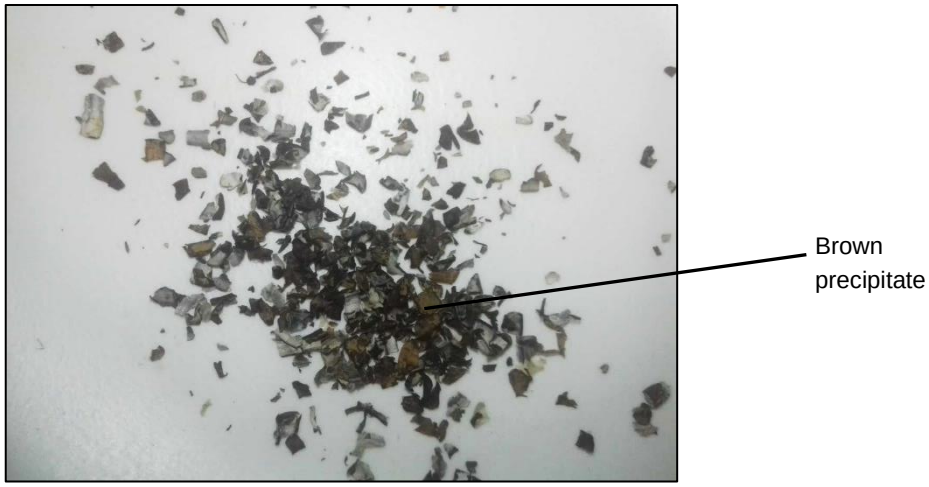

Figure 5. 8: Imaging of CHITIN-CBR-ELN with adsorbed ferric ions

Figure 5. 11: Imaging of CHITIN-CBR-ELN with adsorbed copper ions

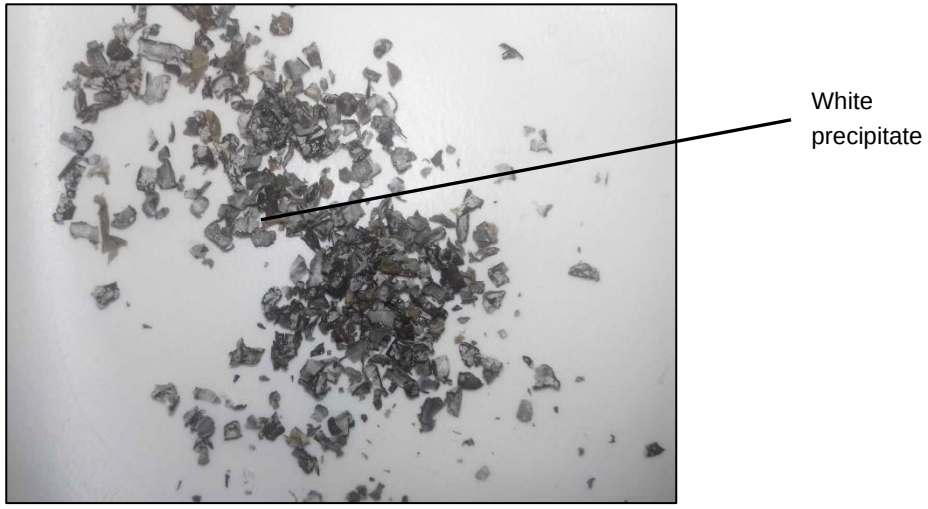

Figure 5. 10: Imaging of CHITIN-CBR-ELN with adsorbed aluminium ions

These colours correspond to the metal hydroxides of these metals except for the initial ferrous ion solution. Ferrous ions adsorbed onto the chitin were observed to be brown. Ferrous hydroxide and Ferric hydroxide are green and brown precipitates respectively (Blais et al., 2008). The observation of a brown precipitate on the ferrous ion adsorbed chitin suggests that there is the oxidation of the ferrous ions to ferric ions during the adsorption of ferrous ions onto chitin from BSF larvae. This formation of a brown ppt in the adsorption of ferrous ion onto chitin was also observed in the precipitation of ferrous ions in the adsorption studies with Chitosan 4 in Section 4.2.2.

5.2.4 Adsorption Reaction Kinetics of Ferrous, Ferric, Aluminium and Copper onto Chitin

Table 5. 4 shows the adsorption initial pH, final pH and the maximum adsorption capacity for ferrous, ferric, copper and aluminium ions onto CHITIN-CBR-ELN.

Table 5. 4:: Initial and final adsorption pH, maximum adsorption capacity for ferrous, ferric, aluminium and copper ions onto CHITIN-CBR-ELN

Product	Production sequence	Initial adsorption pH	Final adsorption pH	Metal Q_{max} (Metal mmol/g chitin)
CHITIN-CBR-ELN-Fe2+	(Deproteinated)	3.45	6.17	2.29 $\pm$ 0.0023
CHITIN-CBR-ELN-Fe3+	(Deproteinated)	3.46	3.41	2.07$\pm$ 0.0025
CHITIN-CBR-ELN-Cu2+	(Deproteinated)	3.47	4.94	1.69$\pm$ 0.0032
CHITIN-CBR-ELN-Al3+	(Deproteinated)	3.45	4.93	1.82$\pm$ 0.0021

Table 5. 4 shows the maximum adsorption capacity for ferrous, ferric, copper and aluminium ions onto optimized Chitin was 2.29 $\pm$ 0.0001 mmol/g, 2.07 $\pm$ 0.0001 mmol/g, 1.69 $\pm$ 0.0001 mmol/g and 1.82$\pm$ 0.0001 mmol/g respectively. The order of the maximum adsorption capacity of the metals from highest to lowest was Fe^{2+}>Fe^{3+}>Al^{3+}>Cu^{2+}The same order was observed from the bimetal test studies. The single metal study agrees with the bimetal studies that the order of metal adsorption selectivity of ferrous, ferric, copper and aluminium of chitin from BSF larvae is Fe^{2+}>Fe^{3+}>Al^{3+}>Cu^{2+}. This order is the same as observed in the metal hydrolysis of these metals except for ferrous ions. Ferrous ions have the lowest hydrolysis constant however they had the highest maximum adsorption capacity. This could have been achieved due to the oxidation of ferrous ions to ferric ions therefore increasing the hydrolysis constant of the system. The final adsorption pH of ferrous, ferric, copper and aluminium onto optimized Chitin was 6.17, 3.41, 4.93 and 4.93. The difference in the final adsorption pH indicates different extents of protonation of the CHITIN-CBR-ELN in the presence of the metals. The maximum adsorption capacity of iron, copper and aluminium obtained for chitin in this study shows the competitiveness of chitin from BSF larvae with other sorbents in adsorbing metals from solutions. Chitin has been observed to be able to adsorb ferrous and copper ions in the range of 0.023 mmol/g to 1.43 mmol/g. (Zhou et al., 2004; Anastopoulos et al., 2017; Boulaiche et al., 2019). While commercial sorbents such as activated carbon adsorb copper and ferrous ions in the range from 0.103 mmol/g to 1.50 mmol/g (Kouakou et al., 2013; Fouladgar et al., 2015; Lim et al., 2019). The maximum adsorption capacity of iron, copper and aluminium obtained in this study were above this range.

Figure 5. 12 shows the adsorption of ferrous, ferric, copper and aluminium ions respectively onto the CHITIN-CBR-ELN. Figure 5. 12 shows that ferrous, ferric, copper and aluminium adsorption onto CHITIN-CBR-ELN was well modelled by the Pseudo 2nd order kinetic model. Table 5. 5 show the maximum sorption capacity (Q_{max}), pseudo 2nd order adsorption initial rate (h_o) and rate constant (k_f), standard deviation (SD), correlation coefficient (R_2) and the adjusted correlation coefficient ($AdjR_2$) for ferrous, ferric, copper and aluminium respectively onto CHITIN-CBR-ELN. The Pseudo 2nd order adsorption model linear fit for ferrous, ferric,

copper and aluminium adsorption onto CHITIN-CBR-ELN is shown in Figure A7. 8 in Appendix A7 Adsorption reaction kinetics.

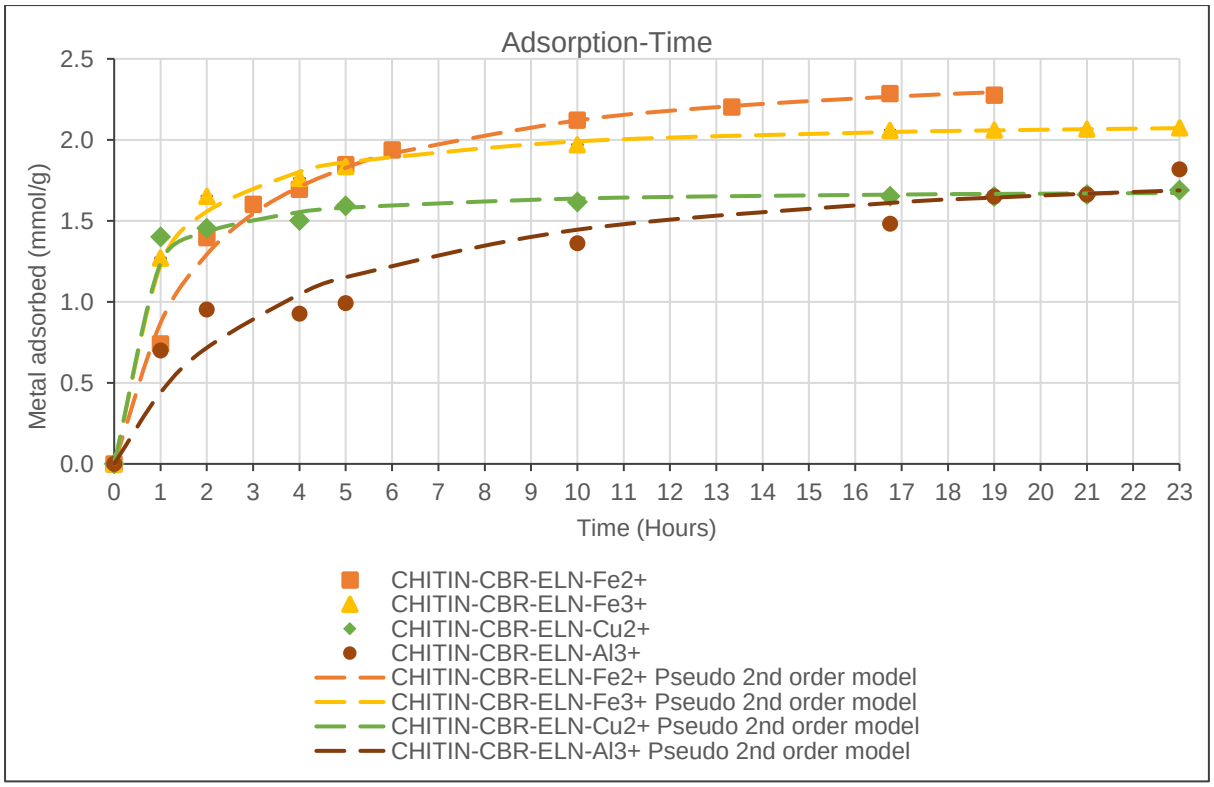

Figure 5. 12: CHITIN-CBR-ELN ferrous, ferric, copper and aluminium adsorption and pseudo-second-order kinetics

Table 5. 5: optimized Chitin pseudo-second-order kinetics parameters for ferrous, ferric, copper and aluminium adsorption

	Pseudo 2nd order kinetics					
Product	**Qmax (mmol/g)**	**k_f (h^{-1})**	**h_o (mmol g^{-1} h^{-1})**	**SD**	**R^2**	**AdjR^2**
CHITIN-CBR-ELN-Fe2+	2.52	0.208	1.33	0.0638	0.9988	0.9964
CHITIN-CBR-ELN-Fe3+	2.14	0.625	2.86	0.0442	0.9999	0.9997
CHITIN-CBR-ELN-Cu2+	1.70	1.58	4.56	0.0665	0.9997	0.9991
CHITIN-CBR-ELN-Al3+	1.94	0.151	0.569	0.171	0.9766	0.9306

Table 5. 5 show that the Pseudo 2nd order adsorption kinetic model linear fit had AdjR_2 values between 0.9306 to 0.9997 for ferrous, ferric, copper and aluminium adsorption onto CHITIN-CBR-ELN. This indicates a good fit with the adsorption experimental data. The result was SD between 0.0442 to 0.171 mmol/g between the Pseudo 2nd order model predicated adsorption and the adsorption experimental data. An attempt to model the experimental data with the Pseudo 1st order kinetic model resulted in lower AdjR values of 0.557 to 0.794 and higher SD of 0.166 to 0.399. Indicating that the Pseudo 2nd order kinetic model is a better fit for the adsorption experimental data than the Pseudo 1st order kinetic model. The fitting of the Pseudo 2nd order kinetic model to the adsorption experimental data indicates that the adsorption of ferrous, ferric, copper and aluminium adsorption onto CHITIN-CBR-ELN was by chemisorption with the chelation reaction being the dominating limiting adsorption step.

Table 5. 5 shows that the pseudo 2nd order adsorption rate constant for ferrous, ferric, copper and aluminium onto CHITIN-CBR-ELN was 0.208 h^{-1}, 0.625 h^{-1}, 1.58 h^{-1}, and 0.151 h^{-1} respectively. The order of pseudo 2nd order adsorption rate constant from highest to lowest was Cu^{2+}>Fe^{3+}>Fe^{2+}>Al^{3+}. Copper ions had the lowest maximum adsorption capacity but the highest pseudo 2nd order adsorption rate constant while adsorption of ferric had a lower pseudo 2nd order adsorption rate constant but higher maximum adsorption capacity than copper. This suggests that the reaction rate is not the only determining factor in the maximum adsorption capacity of the ferrous, ferric, copper and aluminium onto CHITIN-CBR-ELN. Indicating that the available active sites for the respective metals are the major limiting factor of the maximum adsorption capacity.

The desorbed total iron and ferric ions from adsorbed ferrous ions on CHITIN-CBR-ELN. are shown in Figure 5. 13. Figure 5. 13 shows that the total iron desorbed was the same as the ferric ions desorbed. This indicates that during the adsorption or desorption process the ferrous ions were oxidized to ferric ions. The observation of brown precipitates on the CHITIN-CBR-ELN after adsorption suggests that the oxidation of ferrous ions to ferric ions occurred during adsorption.

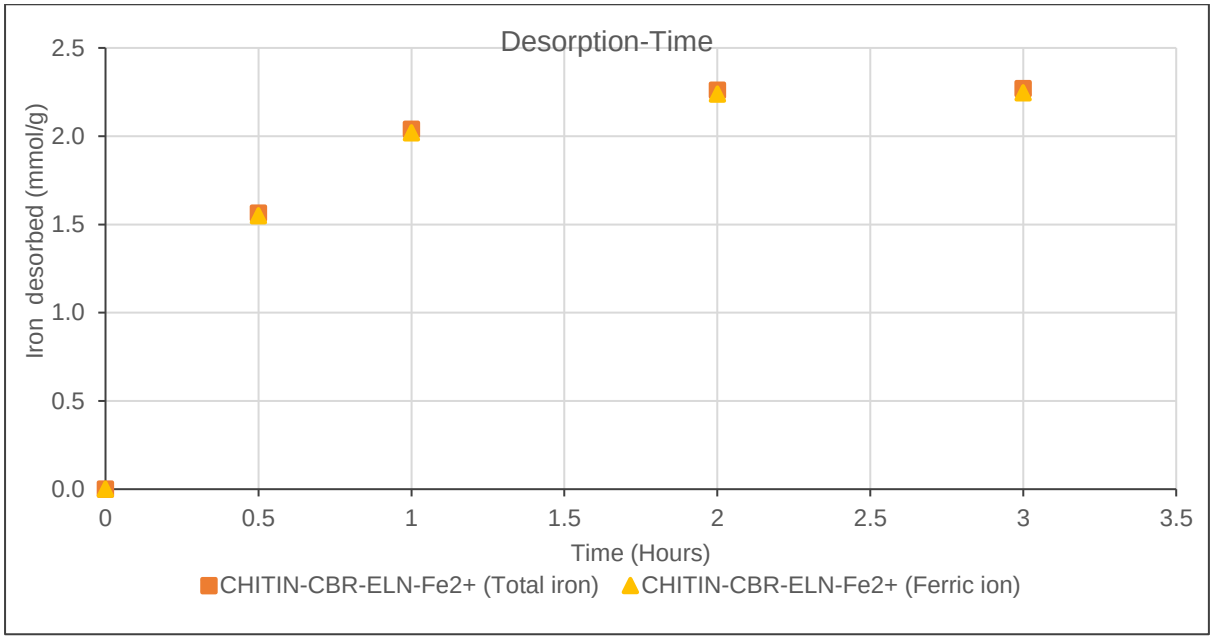

Figure 5. 13: Desorbed total iron and ferrous ion from adsorbed ferrous ion on CHITIN-CBR-ELN

5.3 Adsorption of Ferric, Aluminium and Copper on CHITOSAN-CBR-ELN

0.05 g of CHITOSAN-CBR-ELN were placed in single metal test solutions of ferrous, ferric, copper and aluminium with initial concentrations of 2.79 mmol/L respectively as described in Section 3.4.3. The decrease in the concentration of the ferrous, ferric, copper and aluminium ions due to adsorption was observed and is shown in Figure A5. 18 in Appendix A5 Metal concentration and pH-time graphs. Equation 9 in Section 2.3.1 was used to calculate the ferrous, ferric, copper and aluminium ions adsorbed onto CHITOSAN-CBR-ELN.

5.3.1 Active Sites in the Adsorption of Ferric, Aluminium and Copper onto Chitosan

Figure 5. 14, Figure 5. 15 and Figure 5. 16 show the FTIR spectra of CHITOSAN-CBR-ELN and CHITOSAN-CBR-ELN with adsorbed ferrous, ferric, copper and aluminium ions respectively in a KBr media taken from wavenumbers of 4000 cm^{-1} to 400 cm^{-1}.

Figure 5. 14 shows that the transmittance of CHITOSAN-CBR-ELN with adsorbed ferric ions was lower than that of CHITOSAN-CBR-ELN at wavenumbers: 3445 cm^{-1} (O H stretching), 3272 cm^{-1} (N-H group in amine), 2921 cm^{-1} (CH_3 group in $NHCOCH_3$), 1654 cm^{-1} (C=O secondary amide stretch (Amide I)). These results suggest that the active sites for ferric ion in chitosan are the hydroxyl, amine, methyl group in the acetamido and amide I functional groups.

Figure 5. 15 shows that the transmittance of CHITOSAN-CBR-ELN with adsorbed copper ions was lower than that of CHITOSAN-CBR-ELN at wavenumbers: 3445cm^{-1} (O H stretching), 3272 cm^{-1} (N-H group in amine), 2921 cm^{-1} (CH_3 group in $NHCOCH_3$), 1654 cm^{-1} (C=O secondary amide stretch (Amide I)), 1550 cm^{-1} (N-H stretch (Amide II)) 1379 cm^{-1} (C-H bend, CH_3 symmetric deformation), 1320 cm^{-1} (C-N from amides (amide III)), 1158cm^{-1} (C-O-C asymmetric stretching), 1073 cm^{-1} (C-O-C symmetric stretching).). These results suggest that the active sites of copper adsorption are the hydroxyl, amine, ester and all amide functional groups in the chitosan.

Figure 5. 16 shows that the transmittance of CHITOSAN-CBR-ELN with adsorbed aluminium ions was lower than that of CHITOSAN-CBR-ELN at wavenumbers: 3445cm^{-} (O H stretching), 3272 cm^{-1} (N-H group in amine), 1379 cm^{-1} (C-H bend, CH_3 symmetric deformation), 1315 cm^{-1} (C-N from amides (amide III)), 1159 cm^{-1} (C-O-C asymmetric stretching), 1075 cm^{-1} (C-O-C symmetric stretching). These results suggest that the active sites in aluminium adsorption are the hydroxyl, amine, ester and amide III functional groups in the chitosan. From this analysis, copper seems to have more active sites than ferrous and aluminium ions. The increase in copper adsorption due to an increase in DA as seen in Chapter 4: Preparation of Bio Sorbents suggests that the N-H group in the amine functional group maybe the most active adsorption site for copper ions on chitosan. This is consistent with the high adsorption capacity for copper in chitosan observed in this study. Ferric ions seem to also adsorb onto the amine groups however the relatively constant maximum adsorption capacity for ferrous ions onto chitin and chitosan even with increased DA suggests that the hydroxyl and amide groups maybe the most active adsorption sites for iron.

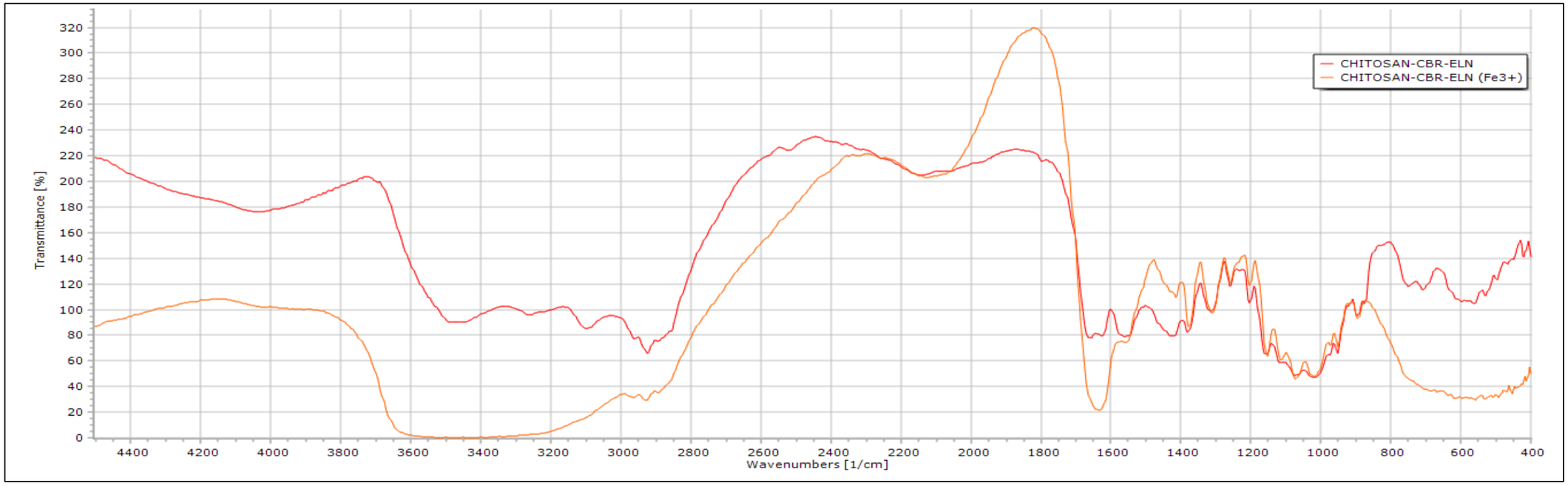

Figure 5. 14: FTIR spectra of CHITOSAN-CBR-ELN with adsorbed ferric ions

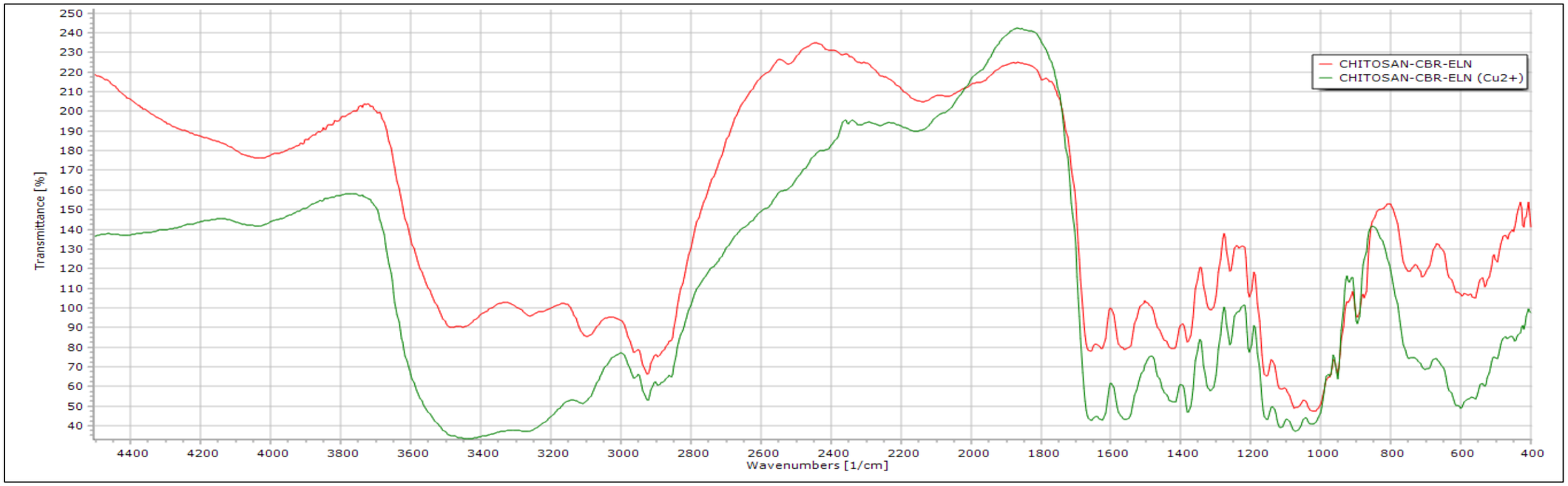

Figure 5. 15: FTIR spectra of CHITOSAN-CBR-ELN with adsorbed copper ions

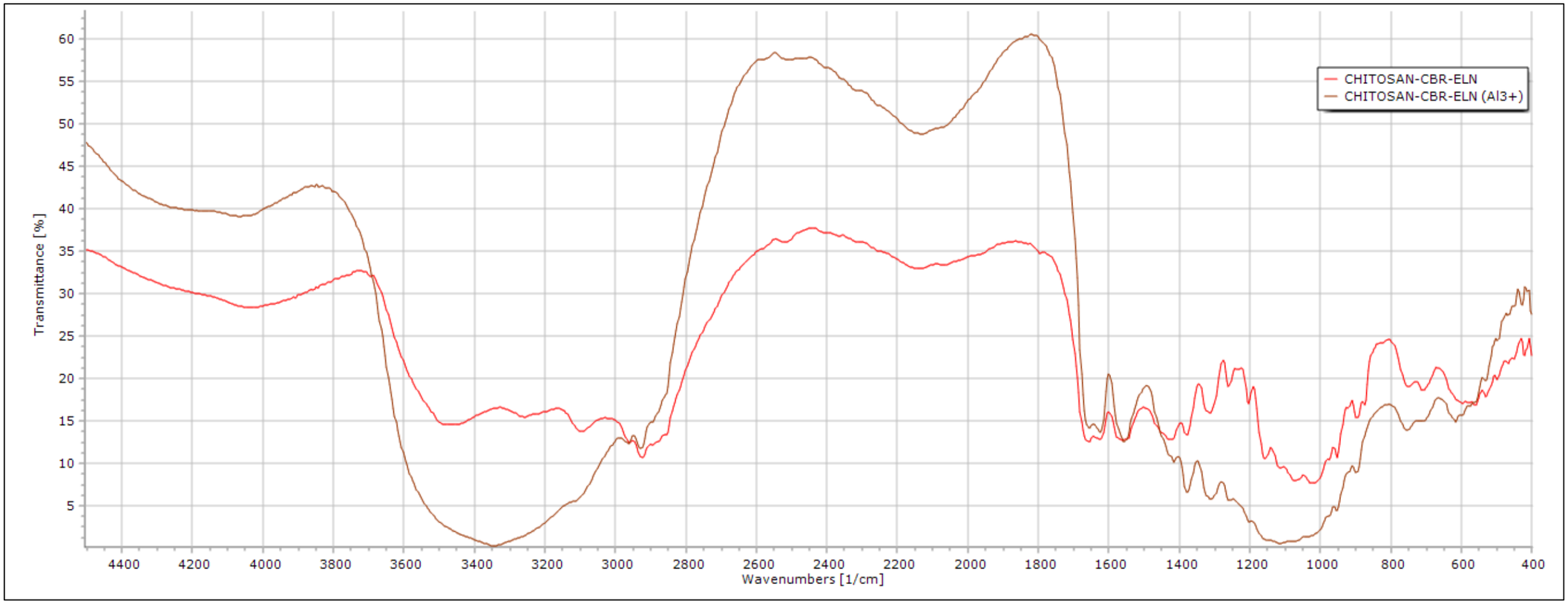

Figure 5. 16: FTIR spectra of CHITOSAN-CBR-ELN with adsorbed aluminium ions

5.3.2 Adsorption Isotherms of Ferrous, Ferric, Aluminium and Copper onto Chitosan

Table 5. 6 shows the Langmuir maximum adsorption capacity (Q_{max}), Langmuir constant (K_L), Langmuir separation factor (R_L), change in Gibb's free energy (ΔG), standard deviation(SD), correlation coefficient (R^2) and adjusted correlation coefficient ($AdjR^2$) for the adsorption of ferrous, ferric, copper and aluminium onto optimized Chitosan. Table 5. 6 shows that the adjusted correlation coefficient for the adsorption of ferric, copper and aluminium onto CHITOSAN-CBR-ELN for the Langmuir isotherm lies between 0.9163 to 0.9979 while the standard deviation was between 0.00269 to 0.126. The correlation coefficient suggests a good fit to the experimental data however the SD suggests that there is a significant deviation between the modelled and experimental data. The SD suggests that the Langmuir isotherm does not adequately describe the adsorption of ferrous, ferric, copper and aluminium onto chitosan extracted from BSF larvae. Similar observations were made for chitin in this study.

Table 5. 6 shows the change in Gibb's free energy for the adsorption of ferric, copper and aluminium onto CHITOSAN-CBR-ELN was -3.60 J/mol, -3.80 J/mol and -3.69 J/mol respectively. The change in Gibb's free energy observed is negative indicating that the adsorption of the metals onto chitin is spontaneous. Table 5. 6 shows the Langmuir separation factor for the adsorption of ferric, copper and aluminium onto CHITOSAN-CBR-ELN was 0.429, 0.447 and 0.436 respectively. The Langmuir separation factors were between 0 and 1 indicating favourable adsorption.

Table 5. 6: Langmuir isotherm parameters for ferric, copper, aluminium adsorption onto CHITOSAN-CBR-ELN

	Langmuir isotherm						
Product	**Q_{max} (mmol/g)**	**K_L (L/mmol)**	**R_L**	**ΔG (J/mol)**	**SD**	**R^2**	**$AdjR^2$**
CHITOSAN-CBR-ELN-Fe3+	0.0949	-0.479	0.429	-3.60	0.0397	0.9758	0.9163
CHITOSAN-CBR-ELN-Cu2+	0.112	-0.442	0.447	-3.80	0.00269	0.9994	0.9979
CHITOSAN-CBR-ELN-Al3+	0.0722	-0.463	0.436	-3.69	0.126	0.9880	0.9583

Table 5. 7 shows the Freundlich exponent (n_f), Freundlich equilibrium constant (K_f), standard deviation (SD), correlation coefficient (R_2), adjusted correlation coefficient ($AdjR_2$) for the adsorption of ferric, copper and aluminium onto CHITOSAN-CBR-ELN. Table 5. 7 shows that the adjusted correlation coefficient for the adsorption of ferric, copper and aluminium onto CHITOSAN-CBR-ELN for the Freundlich isotherm lay between 0.9855 to 0.9998 while the standard deviation was between 0.00145 to 0.0650. The Freundlich isotherm had adjusted correlation coefficients closer to 1 and lower standard deviation to the experimental data than the Langmuir isotherm. These results suggest that the adsorption experimental data for the adsorption of ferric, copper and aluminium onto CHITOSAN-CBR-ELN is better described by the Freundlich model than the Langmuir model. This suggests that the adsorption of ferric, copper and aluminium onto optimized Chitosan from BSF larvae occurs on multilayers and is affected by the concentration of these metals. The multi-active sites of the CHITOSAN-CBR-ELN observed in the FTIR analysis are consistent with the Freundlich model's interpretation

of the adsorption layer being multi-layered. A similar conclusion was drawn for chitin in this study.

Table 5. 7: Freundlich isotherm parameters for ferric, copper, aluminium adsorption onto CHITOSAN-CBR-ELN

	Freundlich isotherm				
Product	**n_f**	**k_f (mmol/g.(mmol/L)$^{-1/nf}$**	**SD**	**R^2**	**AdjR^2**
CHITOSAN-CBR-ELN -Fe3+	-0.155	210	0.0194	0.9926	0.9742
CHITOSAN-CBR-ELN -Cu2+	0	4357	0.00145	0.9998	0.9993
CHITOSAN-CBR-ELN -Al3+	-0.137	447	0.0650	0.9855	0.9496

5.3.3 Weber-Morris Intraparticle Diffusion of Ferric, Aluminium and Copper onto Chitosan

Figure 5. 17 shows the Weber-Morris intraparticle diffusion model liner fit plots for ferric, copper and aluminium adsorption onto CHITOSAN-CBR-ELN. Figure 5. 17 shows that the diffusion of ferric, copper and aluminium can be described by two linear fit lines. The initial linear fit line observed in the diffusion of these metals is relatively steep (higher gradient values) followed by a relatively less steep (lower gradient values). This observation suggests that intraparticle diffusion is involved in the adsorption of ferric, copper and aluminium onto chitin from BSF larvae. Figure 5. 17shows that the linear fits obtained had intercepts indicating that diffusion is not the only rate-limiting step in the adsorption of ferric, copper and aluminium onto chitosan produced from BSF larvae.

The initial linear fit line observed in Figure 5. 17 can be described as the 1^{st} zone of diffusion and the second linear fit line as the 2^{nd} zone of diffusion. The 1^{st} zone of diffusion is ascribed to the adsorbate diffusing through the film layer around the adsorbent. The 2^{nd} zone is ascribed to intra particle diffusion of the adsorbate into the pores of the adsorbent (lijima, 1991). 22 % to 90 % of the adsorption of ferrous, ferric, copper and aluminium occurred within the first hour with adsorption equilibrium being reached after 5 hours. This correlates to $t^{1/2}$ values of 7.75 $min^{1/2}$ and 17.3 $min^{1/2}$ respectively. This indicates that the adsorption of ferrous, ferric, copper and aluminium onto the chitosan from BSF larvae largely occurs in the 1^{st} zone indicating surface complexation.

Surface precipitation of, copper, ferric and aluminium on the CHITOSAN-CBR-ELN during adsorption was observed as shown in Figure 5. 18, Figure 5. 19 and Figure 5. 20 respectively. Figure 5. 18, Figure 5. 19 and Figure 5. 20 show that the observed precipitates of adsorbed copper, ferric and aluminium ion onto the CHITOSAN-CBR-ELN were blue, brown and white respectively. These colours correspond to the metal hydroxides of these metals. A similar observation was made with the adsorbed metals onto the chitin extracted from BSF larvae in Section 5.2.3.

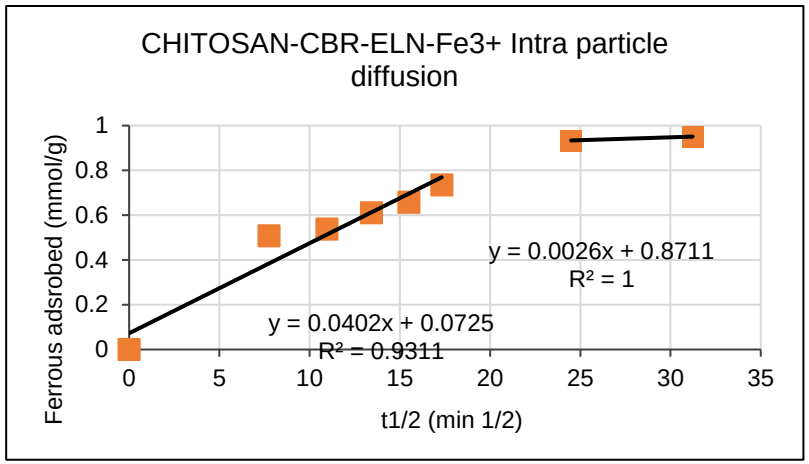

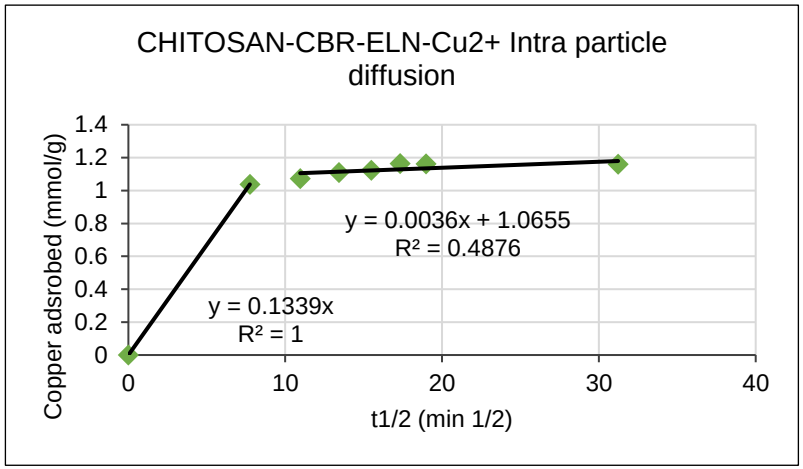

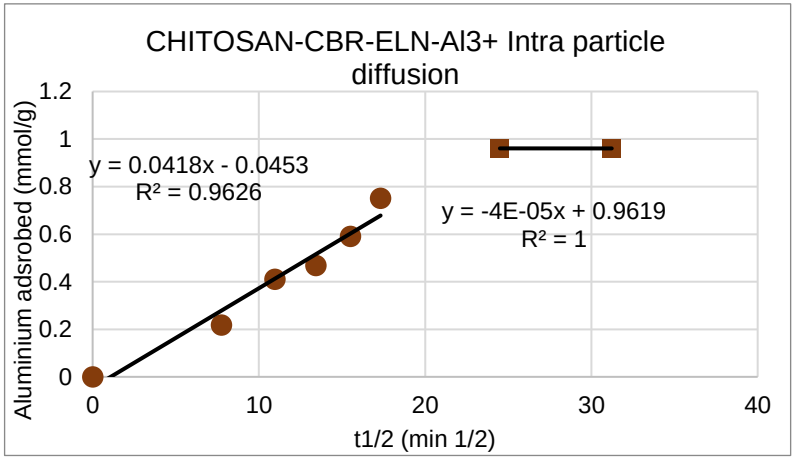

Figure 5. 17: Weber-Morris intraparticle diffusion model liner fit plots for ferric, copper and aluminium adsorption onto CHITOSAN-CBR-ELN

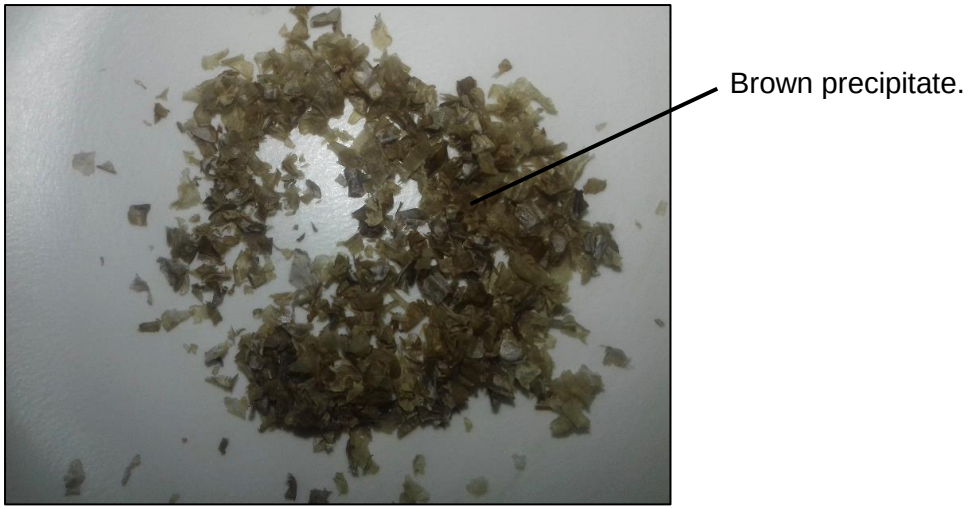

Figure 5. 19: Imaging of CHITOSAN-CBR-ELN with adsorbed ferric ions

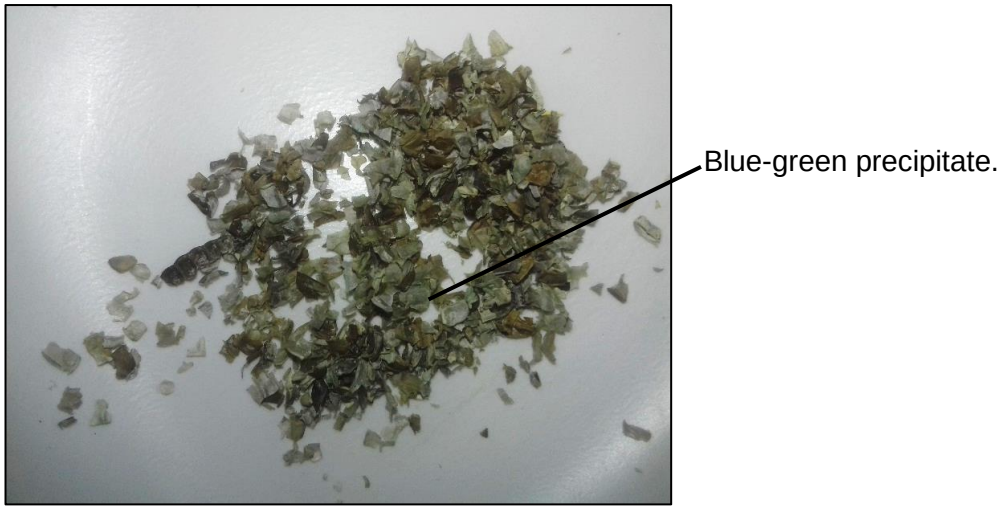

Figure 5. 18: Imaging of CHITOSAN-CBR-ELN with adsorbed copper ions

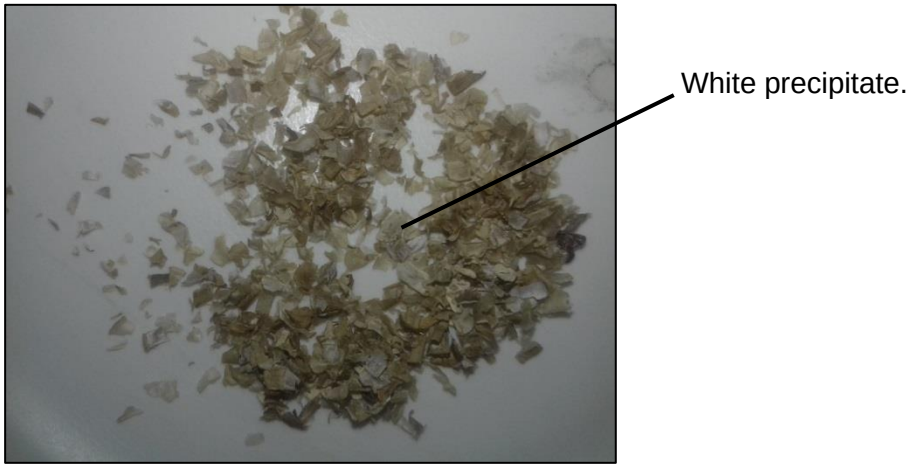

Figure 5. 20: Imaging of CHITOSAN-CBR-ELN with adsorbed aluminium ions

5.3.4 Adsorption Reaction Kinetics of Ferric, Aluminium and Copper onto Chitosan

Table 5. 8 shows the adsorption initial pH, final pH and the maximum adsorption capacity for ferric, copper and aluminium ions onto CHITOSAN-CBR-ELN.

Table 5. 8: Initial and final adsorption pH, maximum adsorption capacity for ferric, aluminium and copper ions onto CHITOSAN-CBR-ELN

Product	Production sequence	Initial adsorption pH	Final adsorption pH	Metal Q_{max} (Metal mmol/g chitin)
CHITOSAN-CBR-ELN-Fe3+	(Deproteinated)	3.43	2.40	0.951± 0.0012
CHITOSAN-CBR-ELN-Cu2+	(Deproteinated)	3.46	4.28	1.16± 0.0016
CHITOSAN-CBR-ELN-Al3+	(Deproteinated)	3.45	3.97	0.961± 0.0013

Table 5.8 shows that the final adsorption pH of ferric, copper, and aluminium adsorption onto CHITOSAN-CBR_ELN was 2.4o, 4.28 and 3.97 respectively. The difference in the final adsorption pH can be attributed to different extents of protonation of the CHITOSAN-CBR-ELN in the presence of these metals. Table 5. 8 shows the maximum adsorption capacity for ferric, copper and aluminium ions onto CHITOSAN-CBR-ELN was 0.951 ± 0.0012 mmol/g, 1.16 ± 0.0016 mmol/g and 0.961± 0.0013 mmol/g respectively. The order of the maximum adsorption capacity of the metals from highest to lowest was Cu^{2+}>Al^{3+}>Fe^{3+}. This suggests that the order of metal adsorption selectivity for ferric, copper and aluminium onto chitosan from BSF larvae is Cu^{2+}>Al^{3+}>Fe^{3+} The order observed from the bimetal test studies in Section 4.2 and Section 5.1 was Cu^{2+}>Fe^{2+}>Al^{3+}. The switch in the order by ferric and ferrous ions suggests that these two metal ions behave differently during adsorption onto Chitosan. The difference between ferric and ferrous ion adsorption can also be attributed to the adsorption pH change. The final adsorption pH for ferric ions adsorbing onto CHITOSAN-CBR-ELN was 2.4. This was lower than the initial pH of 3.43. At low pH, amine groups on the chitosan protonate with H^+ ions which induces electrostatic repulsion of the metal ions resulting in decreased adsorption of metal ions (Zhou et al., 2004). The maximum adsorption capacity for ferric, copper and aluminium obtained for CHITOSAN-CBR-ELN were lower than those of CHITIN-CBR-ELN. The difference in the maximum adsorption capacity might be due to the solubility instability of CHITOSAN-CBR-ELN in acid solutions. Due to being mechanically unstable under acidic conditions effort has been put to stabilize chitosan either by cross-linking or ion print technology. Cross-linking of chitosan sometimes results in lower adsorption capacities (Babel & Kurniawan, 2003). For example, the highest maximum adsorption capacity of copper by commercial adsorbents was found to be 2.13 mmol/g by Cu(II) ion-imprinted composite adsorbent (Cu(II)-MICA). This was a magnetic adsorbent developed by binding of chitosan and industrial waste fungal mycelium on iron oxide nanoparticles (Ren et al., 2008). While, the highest maximum adsorption capacity of copper by natural sorbents was found to be 4.13 mmol/g by chitosan which was immobilized on sand (Wan et al., 2004). The results

of this study suggest that CHITOSAN-CBR-ELN might require stabilisation by either cross-linking or ion print technology.

Figure 5. 21 shows the adsorption of ferric, copper and aluminium ions respectively onto the CHITOSAN-CBR-ELN. Figure 5. 21 shows that ferric, copper and aluminium adsorption CHITOSAN-CBR-ELN was well modelled by the Pseudo 2nd order kinetic model indicating that the adsorption of these metals was by chemisorption with the chelation reaction being the dominating limiting adsorption step. Table 5. 9 shows the maximum sorption capacity (Q_{max}), pseudo 2nd order adsorption initial rate (h_o) and rate constant (k_f), standard deviation (SD), correlation coefficient (R_2) and the adjusted correlation coefficient ($AdjR_2$) for ferrous, ferric, copper and aluminium respectively onto CHITOSAN-CBR-ELN. The Pseudo 2nd order adsorption model linear fit for ferrous, ferric, copper and aluminium adsorption onto optimized Chitin is shown in Figure A7. 9 in Appendix A7 Adsorption reaction kinetics.

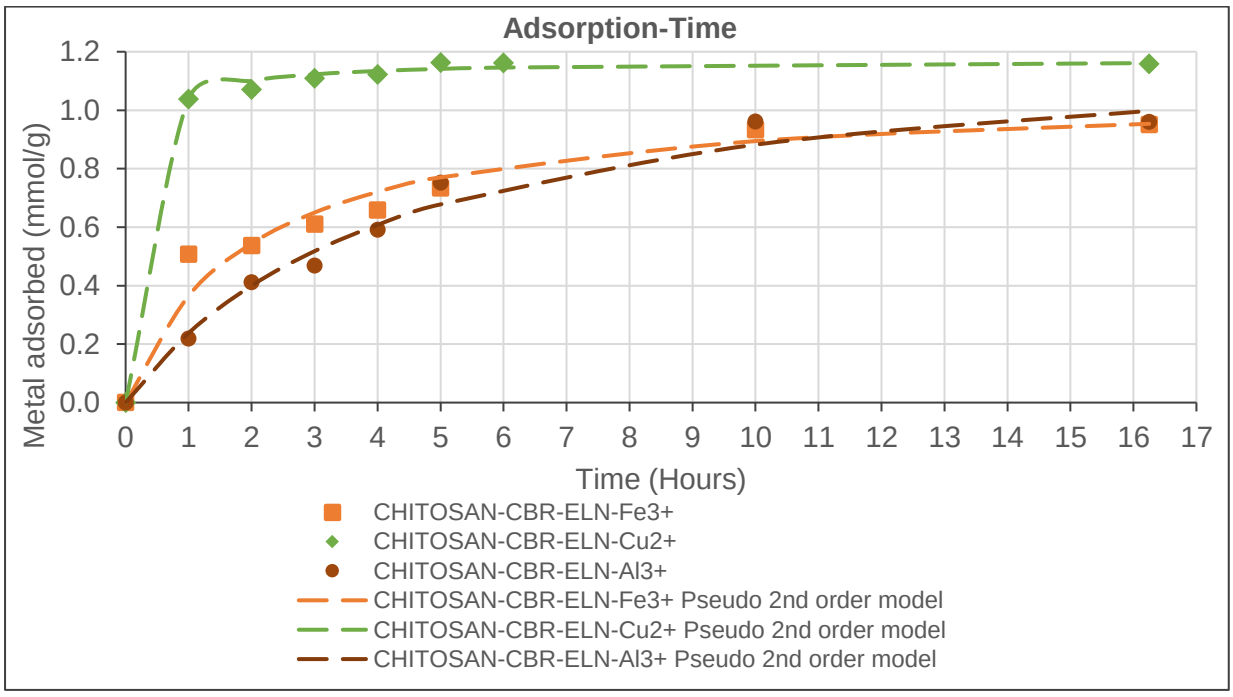

Figure 5. 21: CHITOSAN-CBR-ELN ferric, copper and aluminium adsorption and pseudo-second-order kinetics

Table 5. 9: CHITOSAN-CBR-ELN pseudo-second-order kinetics parameters for ferric, copper and aluminium adsorption

	Pseudo 2nd order kinetics					
Product	**Qmax (mmol/g)**	**k_f (h^{-1})**	**h_o (mmol g^{-1} h^{-1})**	**SD**	**R^2**	**$AdjR^2$**
CHITOSAN-CBR-ELN-Fe3+	1.07	0.488	0.555	0.0755	0.9918	0.9755
CHITOSAN-CBR-ELN-Cu2+	1.17	6.72	9.20	0.0196	0.9998	0.9994
CHITOSAN-CBR-ELN-Al3+	1.26	0.184	0.293	0.0571	0.9791	0.9380

Table 5. 9 shows that the Pseudo 2nd order adsorption kinetic model linear fit has $AdjR_2$ values were between 0.9380 to 0.9994 for ferric, copper and aluminium adsorption onto CHITOSAN-CBR-ELN indicating a good fit with the adsorption experimental data. The result was SD between 0.0196 to 0.0755 mmol/g between the pseudo 2nd order model predicated adsorption and the adsorption experimental data. Table 5. 9 shows that the pseudo 2nd order adsorption

rate constant for ferric, copper and aluminium onto CHITOSAN-CBR-ELN was 0.488 h^{-1}, 6.72 h^{-1} and 0.184 h^{-1} respectively. The order of pseudo 2nd order adsorption rate constant from highest to lowest is Cu^{2+}>Fe^{3+}>Al^{3+}. This corresponds to the order of metal adsorption selectivity for CHITOSAN-CBR-ELN obtained in the bimetal test solution studies.

5.4 Recyclability of Chitin and Chitosan in Metal Adsorption

1 g of CHITIN-CBR-ELN and CHITOSAN-CBR-ELN were placed in a single metal solution of ferrous and copper test solution with initial concentrations of 2.79 mmol/L respectively. After adsorption, the CHITIN-CBR-ELN and CHITOSAN-CBR-ELN were desorbed. The desorbed CHITIN-CBR-ELN and CHITOSAN-CBR-ELN were then placed again in a single metal solution of ferrous and copper test solution with initial concentrations of 2.79 mmol/L respectively and desorbed again.

5.4.1 Effects of recycling chitin and chitosan in metal adsorption on chitin and chitosan character

Figure 5. 22 and Figure 5. 23 shows the FTIR spectra of CHITIN-CBR-ELN and CHITOSAN-CBR-ELN after the second ferrous and copper desorption cycle in a KBr media taken from wavenumbers of 4000 cm^{-1} to 400 cm^{-1}. Amide bands corresponding to C=O secondary amide stretch (Amide I), N-H bend and N-H stretch (Amide II) at 1654, 1617 and 1550 cm^{-1} respectively were observed. Major bands were detected in the FITR spectra at: 3415-3446 cm^{-1} (O H stretching), 2921 cm^{-1} (CH_3 group in $NHCOCH_3$), 2853 cm^{-1} (asymmetric CH_2), 1320 cm^{-1} (C-N from amides (amide III)), 1158cm^{-1} (C-O-C asymmetric stretching), 1073 cm^{-1} (C-O-C symmetric stretching) and 875-895 cm^{-1} (glucopyranose ring stretching). For chitosan, the presence of N-H group in amine was observed at 3258 cm^{-1} The transmission in all bands for CHITIN-CBR-ELN and CHITOSAN-CBR-ELN after the second ferrous and copper desorption cycle respectively were lower than that of the CHITIN-CBR-ELN and CHITOSAN-CBR-ELN before the adsorption-desorption study. Desorption is conducted in 0.1M H_2SO_4. Acid action results in the degradation of the chitin and chitosan polymer (Guibal, 2004; Zhou et al., 2004; Cui & Zhang, 2008). The degradation of the chitin and chitosan in the desorption stage could be seen by the decrease in yield after each desorption cycle.

Table 5. 10 shows that the yield of the CHITIN-CBR-ELN after the first and second desorption cycle was 80 % and 50 % respectively. While for CHITOSAN-CBR-ELN the yield was 72 % and 69 % respectively. The decrease in yield during the adsorption-desorption cycles can also be attributed to mass losses during the filtration stages (after adsorption and desorption).

The CHITIN-CBR-ELN after the second desorption cycle had a lower DA than that before the adsorption-desorption study while the CHITOSAN-CBR-ELN had a higher DA than that before the adsorption-desorption study. This suggests a change in the polymer's structure due to the acidic conditions used in the adsorption and desorption processes.

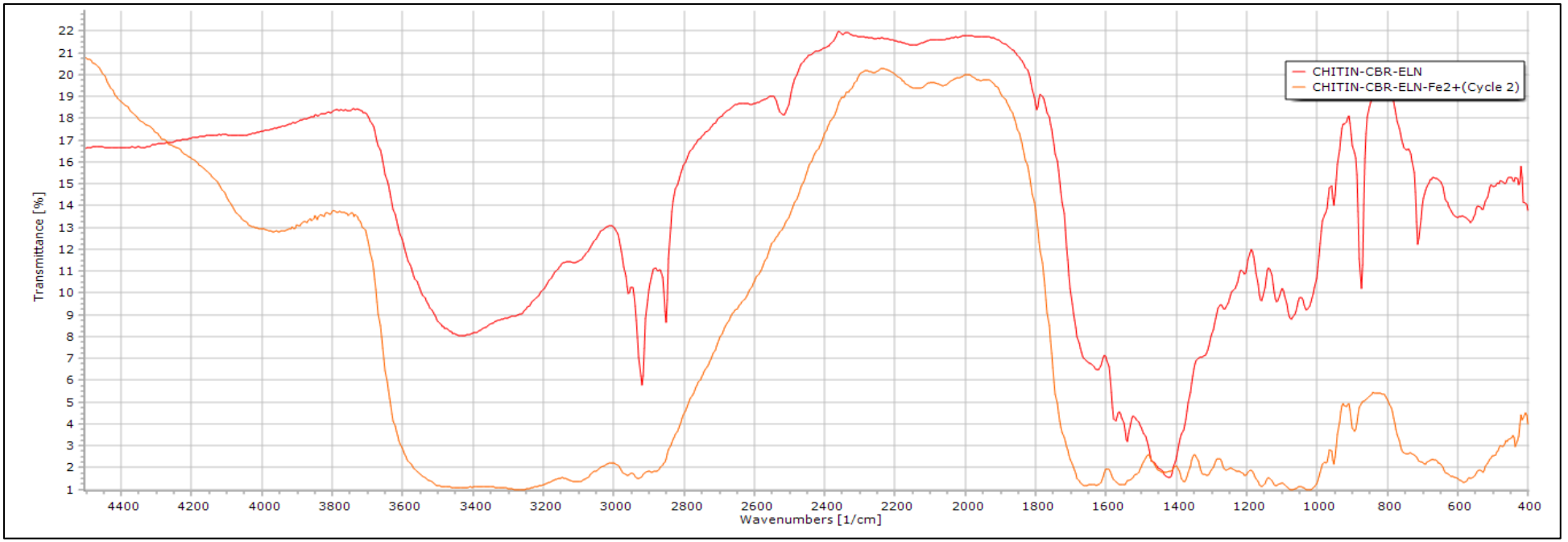

Figure 5. 22: FTIR of CHITIN-CBR-ELN before ferrous adsorption and after 2 ferrous adsorption-desorption cycles.

Table 5. 10: CHITOSAN-CBR-ELN Degree of acetylation and yield after 2 ferrous adsorption-desorption cycles

Product	Production sequence	A1655	A3450	Degree of acetylation	Yield after desorption cycle (%)
CHITIN-CBR-ELN -Fe2+-Cycle 1	(Deproteinated)	0.8318	0.9996	62.6	80
CHITIN-CBR-ELN -Fe2+-Cycle 2	(Deproteinated)	1.711	1.712	75.1	58

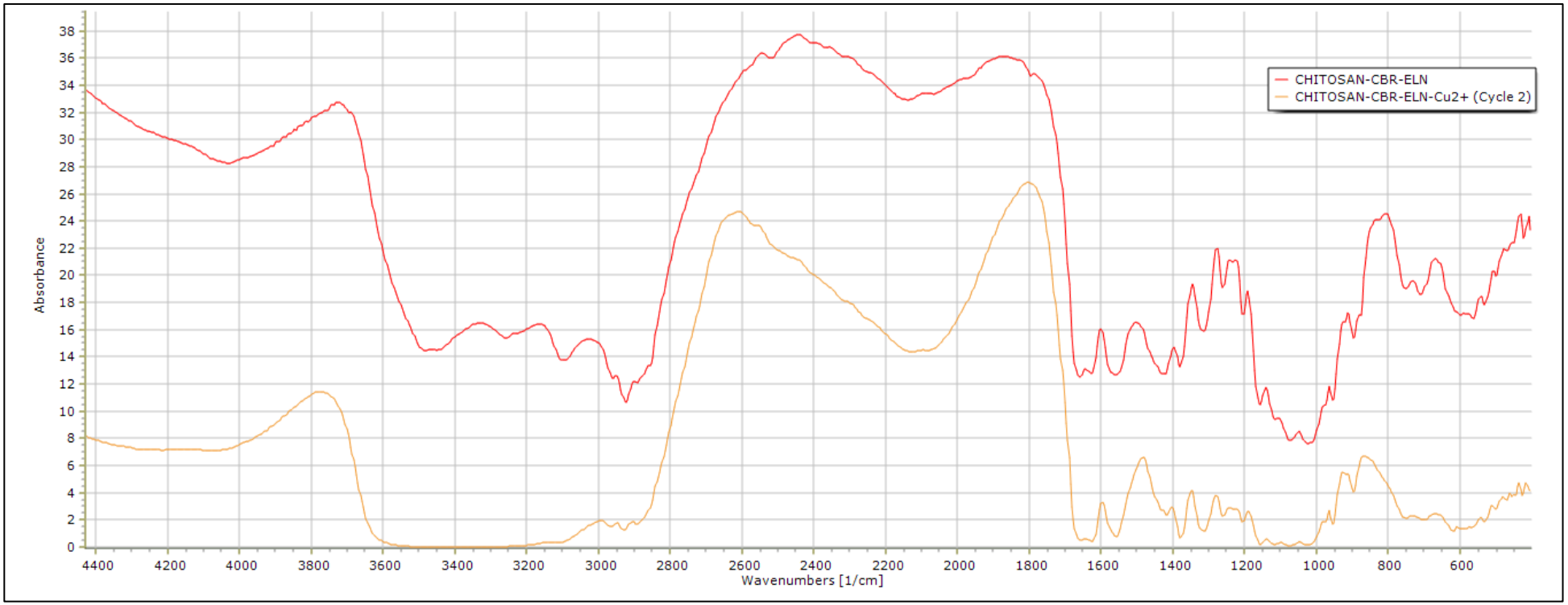

Figure 5. 23: FTIR of CHITOSAN-CBR-ELN Degree of acetylation and yield after 2 copper adsorption-desorption cycles

Table 5. 11: optimized Chitosan Degree of acetylation and yield after 2 copper adsorption-desorption cycles

Product	Production sequence	A1655	A3450	Degree of acetylation	Relative Yield (%)
CHITOSAN-CBR-ELN -Cu2+ Cycle 1	(Deproteinated, Deacetylated)	1.063	1.353	59.1	72
CHITOSAN-CBR-ELN -Cu2+ Cycle 2	(Deproteinated, Deacetylated)	1.301	3.293	29.7	69

5.4.2 Effects of recycling chitin and chitosan on ferrous and copper adsorption

The decrease in the concentration of the ferrous and copper ions due to adsorption onto CHITIN-CBR-ELN and CHITOSAN-CBR-ELN was observed and is shown in Figure A5. 20 and Figure A5. 21 respectively in Appendix A5 Metal concentration and pH-time graphs. Equation 9 in Section 2.3.1 was used to calculate the amount of ferrous and copper ions adsorbed onto the CHITIN-CBR-ELN and CHITOSAN-CBR-ELN. Table 5. 12 and Table 5. 13 shows the adsorption initial pH, final pH and the maximum adsorption capacity for ferrous and copper ions onto CHITIN-CBR-ELN and CHITOSAN-CBR-ELN.

Table 5. 12: Initial and final adsorption pH, maximum adsorption capacity for ferrous ions onto CHITIN-CBR-ELN

Product	Production sequence	Initial adsorption pH	Final adsorption pH	Fe2+ Q_{max} (Fe^{2+} mmol/g chitin)
CHITIN-CBR-ELN -Fe2+-Cycle 1	(Deproteinated)	3.35	4.46	0.558± 0.002
CHITIN-CBR-ELN -Fe2+-Cycle 2	(Deproteinated)	3.35	4.36	0.0188± 0.002

Table 5. 13: Initial and final adsorption pH, maximum adsorption capacity for ferrous ions onto CHITOSAN-CBR-ELN

Product	Production sequence	Initial adsorption pH	Final adsorption pH	Cu 2+ Q_{max} (Cu^{2+} mmol/g chitin)
CHITOSAN-CBR-ELN -Cu2+ Cycle 1	(Deproteinated, Deacetylated)	3.35	4.53	0.683± 0.0003
CHITOSAN-CBR-ELN -Cu2+ Cycle 2	(Deproteinated, Deacetylated)	3.43	4.23	0.026± 0.0008

Table 5. 12 shows that the maximum adsorption capacity for ferrous ions onto CHITIN-CBR-ELN decreased from 0.558± 0.002 mmol/g to 0.0188± 0.002 mmol/g. While for CHITOSAN-CBR-ELN the decrease was from 0.683± 0.0003 mmol/g to 0.026± 0.0008 mmol/g for copper. This represented a decrease of 99.6 % and 96.1 in ferrous and copper maximum adsorption capacity respectively. The results of the effect of the adsorption-desorption cycle on CHITIN-CBR-ELN and CHITOSAN-CBR-ELN show the negative impact of acid conditions on the polymer's metal adsorption performance. This effect was also seen from the effect of demineralization of the chitin and chitosan extracted from BSF larvae. This suggests that under the acidic conditions required in e-waste base metal leaching, the CHITIN-CBR-ELN and CHITOSAN-CBR-ELN. can only be used for only one adsorption-desorption cycle. After which the chitin and chitosan must be used for secondary applications such as manures in agriculture. Consideration of secondary applications of CHITIN-CBR-ELN and CHITOSAN-CBR-ELN. will improve the circular economics of using these sorbents in recovering metals from PCB leachate solutions. This result of improved economics was observed by the improved gross profits due to the revenue of selling agricultural grade chitin and chitosan in the Techno-economic analysis in Section 4.1.3 and 4.2.3.

Chapter 6: Application of Chitin and Chitosan in e-waste leachates

6.1 Adsorption of Model leachate solution Metals onto CHITIN-CBR-ELN

0.1 g of CHITIN-CBR-ELN were placed in the model leachate solution. The Model leachate solution contained 1.11 mmol/l, 2.79 mmol/l, 2.82 mol/l of ferrous, copper and aluminium respectively. The leachate solution was modelled based on the acidic leaching of base metals from 1 g of PCBs as described in Section 3.1.1. The decrease in the concentration of the ferrous, copper and aluminium ions due to adsorption was observed and is shown in Figure A5. 22 in Appendix A5 Metal concentration and pH-time graphs. Equation 9 in Section 2.3.1 was used to calculate the amount of ferrous, copper and aluminium ions adsorbed onto the CHITIN-CBR-ELN. Table 6. 1 shows the maximum adsorption capacity, the adsorbed molar ratio for ferrous, copper and aluminium ions onto CHITIN-CBR-ELN. The basis of the molar ratio was the adsorption of 1 mmol/g of ferrous ions.

Table 6. 1: Maximum adsorption capacity, the adsorbed molar ratio for ferrous, copper and aluminium ions onto CHITIN-CBR-ELN

Product	**Metal Q_{max} (Metal mmol/g chitin)**	**Molar ratio of metals adsorbed (mmol /g chitin**
CHITIN-CBR-ELN **-Fe2+**	0.453± 0.02	1.00
CHITIN-CBR-ELN **-Cu2+**	0.758± 0.02	1.67
CHITIN-CBR-ELN **-Al3+**	1.23± 0.01	2.71

Table 6. 1 shows that the maximum adsorption capacity of ferrous, copper and aluminium ions onto CHITIN-CBR-ELN was 0.453± 0.02 mmol/g, 0.758± 0.02 mmol/g and1.23± 0.01 mmol/g respectively. CHITIN-CBR-ELN adsorbed 18.6 %, 31.1 % and 50.4 % ferrous, copper and aluminium respectively. The relative initial concentration of these metals in the Model leachate solution was 16.5 %, 41.5 %, 42.0 % respectively. These results show that the metal with the highest initial concentration in the Model leachate solution was adsorbed the most onto CHITIN-CBR-ELN. This observation is consistent with the adsorption of chitin metal adsorption being well modelled by the Freundlich Model. This model includes the assumptions that an increase in the concentration of the adsorbate in solution increases the adsorption of the adsorbate (Skopp, 2009). The maximum adsorption capacities observed were lower than those obtained in the single metal test solution study in Section 5.2.4. This suggests that there is a limitation of adsorption active sites in the chitin and that there is a competition of active sites. This observation is consistent with the results in Section 5.2.1 which showed that ferrous, copper and aluminium ions share the same adsorption active sites in chitin. The influence of the degree of metal adsorption selectivity can be seen by comparing the adsorbed copper and aluminium on CHITIN-CBR-ELN. Although aluminium and copper had a difference of 0.5 % in the Model leachate solution, 19.3 % more aluminium was adsorbed over copper. This can be explained by the order of metal adsorption selectivity of chitin observed in Section 5.1 and Section 5.2.4. Aluminium was observed to have a higher metal adsorption selectivity on chitin than copper. This is due to aluminium hydrolysing at lower pH than copper. Ferrous

ions also were adsorbed 2.1 % more than their relative initial concentration in the Model leachate solution indicating a positive degree of metal adsorption selectivity. This degree of metal adsorption selectivity was however lower that observed for aluminium due to ferrous ions having a lower initial concentration than aluminium ions in the Model leachate solution.

Table 6. 2. shows the temperature, pH, concentration of ferrous, copper and aluminium in the Model leachate solution, Model leachate solution after adsorption and the desorbed solution after 1 cycle with CHITIN-CBR-ELN. The desorption was conducted with 1 L of 0.01 M H_2SO_4. The adsorption of 0.453± 0.02 mmol/g, 0.758± 0.02 mmol/g and1.23± 0.01 mmol/g ferrous, copper and aluminium respectively onto CHITIN-CBR-ELN from the Model leachate solution resulted in increased relative copper concentration in Model leachate solution after adsorption. The relative initial concentration of ferrous, copper and aluminium in the Model leachate solution after adsorption was 16.1 %, 44.0 % and 39.9 % respectively. The relative initial concentration after adsorption of copper ions increased by 2.5 % while for ferrous and aluminium ions it decreased by -0.4 % and -2.1 % respectively in the Model leachate solution. These results suggest that the application of CHITIN-CBR-ELN on the Model leachate solution increases the concentration of copper ions and decreases the concentration of ferrous and aluminium ions in the Model leachate solution. This can be explained by the higher order of metal adsorption selectivity of ferrous and aluminium ions over copper ions in chitin. These results also show that 1 adsorption-desorption cycle with CHITIN-CBR-ELN is not enough for the separation of ferrous, copper and aluminium in the Model leachate solution.

Table 6. 2: Model leachate solution after adsorption with CHITIN-CBR-ELN and desorbed solution.

	Stream name	Model leachate solution	Model leachate solution after adsorption	Desorbed solution
	Temperature	30	30	30
	pH	3.45	3.8	1
Component	**Unit**			
Fe2+	mmol/L	1.11	0.882	0.453
Cu2+	mmol/L	2.78	2.41	0.758
Al3+	mmol/L	2.81	2.19	1.23

Figure 6. 1 shows the effect of the initial concentration of ferrous ion on the maximum adsorption capacity of ferrous ions onto CHITIN-CBR-ELN. This study was conducted as described in Section 3.4.3. Figure 6. 1 shows that an increase in the initial ferrous concentration in the test solutions resulted in an increase in the maximum adsorption capacity for ferrous ions onto the CHITIN-CBR-ELN. The maximum adsorption capacity for ferrous ions increased from 0.224 mmol/g (at an initial ferrous concentration of 0.696 mmol/g) to 2.24 mmol/g (at an initial ferrous concentration of 2.77mmol/g). This is consistent with observations made in the adsorption of ferrous, copper and aluminium ion onto CHITIN-CBR-ELN from the Model leachate solution. This result also collaborates with the results from Section 5.2.2. That show that chitin from BSF larvae is best described by the Freundlich model as the concentration of the adsorbate affects the extent of adsorption. The increase in the maximum adsorption capacity for ferrous ions onto the CHITIN-CBR-ELN against initial concentration in

the test solution showed a positive linear correlation with a gradient of 0.792 L/g and an R^2 value of 0.964. For a given amount of sorbet, it must be noted that there is a maximum of the equilibrium adsorption capacity which is a result of the limitation in available active sites on the sorbet for adsorption. (Guibal, 2004). For CHITIN-CBR-ELN this maximum of the equilibrium adsorption capacity for ferrous ions was 2.29 ± 0.0023 mmol/g.

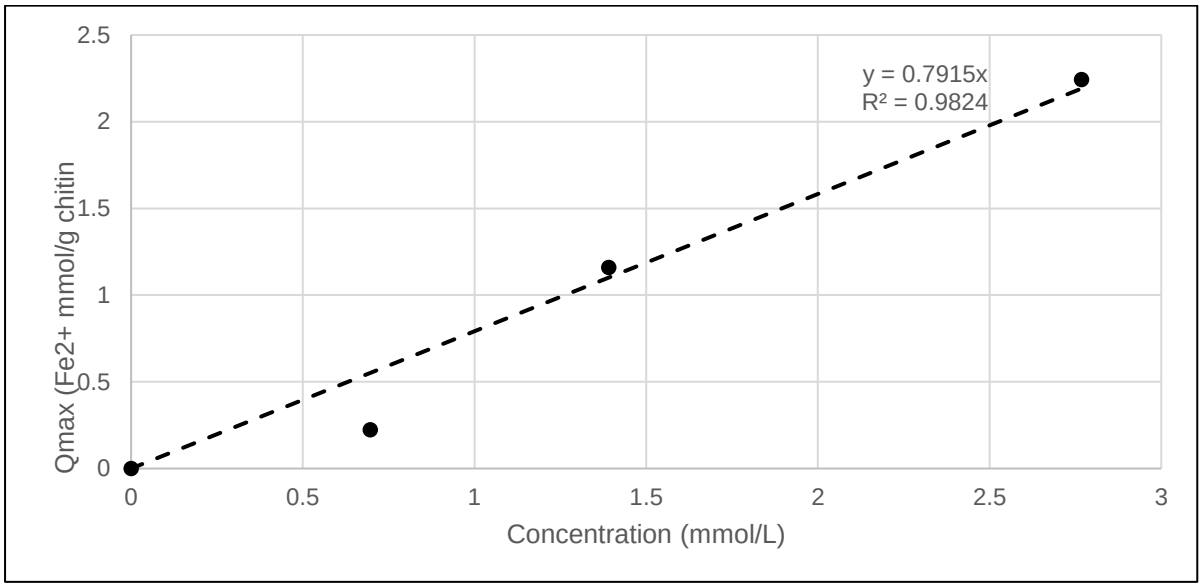

Figure 6. 1: Effect of initial concentration of ferrous ion on the ferrous ion maximum adsorption capacity onto CHITIN-CBR-ELN

6.2 Adsorption of Model leachate solution Metals onto CHITOSAN-CBR-ELN

0.1 g of CHITOSAN-CBR-ELN were placed in the model leachate solution. The decrease in the concentration of the ferrous, copper and aluminium ions due to adsorption was observed and is shown in Figure A5. 23 in Appendix A5 Metal concentration and pH-time graphs. Equation 9 in Section 2.3.1 was used to calculate the amount of ferrous, copper and aluminium ions adsorbed onto the CHITIN-CBR-ELN. Table 6. 3 shows the maximum adsorption capacity, the adsorbed molar ratio for ferrous, copper and aluminium ions onto CHITOSAN-CBR-ELN. The basis of the molar ratio was the adsorption of 1 mmol/g of copper ions.

Table 6. 3: Maximum adsorption capacity, the adsorbed molar ratio for ferrous, copper and aluminium ions onto CHITOSAN-CBR-ELN

Product	Metal Q_{max} (Metal mmol/g chitin)	Molar ratio of metals adsorbed /g chitosan
CHITOSAN-CBR-ELN-Fe2+	0.248± 0.001	0.195
CHITOSAN-CBR-ELN-Cu2+	1.27± 0.001	1.000
CHITOSAN-CBR-ELN-Al3+	1.03± 0.001	0.808

Table 6. 3 shows that the maximum adsorption capacity of ferrous, copper and aluminium ions onto CHITOSAN-CBR-ELN was 0.248± 0.001 mmol/g, 1.27± 0.001 mmol/g and1.03± 0.001 mmol/g respectively. CHITOSAN-CBR-ELN adsorbed 9.73 %, 49.8 % and 40.4 % ferrous, copper and aluminium respectively. The relative initial concentration of these metals in the Model leachate solution was 16.5 %, 41.5 %, 42.0 % respectively. These results show that the metal with the high concentration in the Model leachate solution was adsorbed the most onto CHITOSAN-CBR-ELN. This observation is consistent with the adsorption of chitosan metal adsorption being well modelled by the Freundlich Model. The maximum adsorption capacities observed were lower than those obtained in the single metal test solution study in Section 5.3.4. This suggests that there is a limitation of adsorption active sites in the chitosan and that there is competition for active sites. This observation is consistent with the results in Section 5.3.1 which showed that ferrous, copper and aluminium ions share the same adsorption active sites in chitosan. The influence of the degree of metal adsorption selectivity can be seen by comparing the adsorbed copper and aluminium on CHITOSAN-CBR-ELN. Although aluminium and copper had a difference of 0.5 % with the concentration of copper being lower in the Model leachate solution. 9.4 % more copper was adsorbed over aluminium. This can be explained by the order of metal adsorption selectivity of chitosan observed in Section 5.1 and Section 5.3.4. Copper was observed to have a higher metal adsorption selectivity on chitosan than aluminium. This is attributed to copper having a higher electronegativity than aluminium.

Table 6. 4 shows the temperature, pH, concentration of ferrous, copper and aluminium in the Model leachate solution after adsorption and the desorbed solution after 1 cycle with CHITOSAN-CBR-ELN. The desorption was conducted with 1 L of 0.01 M H_2SO_4. Adsorption of 0.248± 0.001 mmol/g, 1.27± 0.001 mmol/g and1.03± 0.001 mmol/g ferrous, copper and

aluminium respectively onto CHITOSAN-CBR-ELN from the Model leachate solution was observed. This resulted in increased relative copper concentration in the desorbed solution compared to the Model leachate solution. The relative initial concentration of ferrous, copper and aluminium in the Model leachate solution after adsorption was 18.8 %, 41.2 % and 42.2 % respectively. While the relative initial concentration of ferrous, copper and aluminium in the Desorbed solution was 9.73 %, 49.8 % and 40.4 % respectively. The relative initial concentration after adsorption of copper ions increased by 8.3 % while for ferrous and aluminium ions it decreased by -6.77 % and -1.6 % respectively in the Model leachate solution. These results suggest that the application of CHITOSAN-CBR-ELN on the Model leachate solution results in the recovery of copper ions in the desorbed solution. This can be explained by the higher order of metal adsorption selectivity of copper ions over ferrous and aluminium ions in chitosan. These results also show that 1 adsorption-desorption cycle with CHITOSAN-CBR-ELN is not enough for the separation of ferrous, copper and aluminium in the Model leachate solution.

Table 6. 4: Model leachate solution after adsorption with CHITOSAN-CBR-ELN and desorbed solution.

	Stream name	Model leachate solution	Model leachate solution after adsorption	Desorbed solution
	Temperature	30	30	30
	pH	3.45	3.8	1
Component	**Unit**			
Fe2+	mmol/L	1.11	0.989	0.248
Cu2+	mmol/L	2.78	2.16	1.27
Al3+	mmol/L	2.81	2.28	1.03

Figure 6. 2 shows the effect of the initial concentration of copper ion on the maximum adsorption capacity of copper ions onto CHITOSAN-CBR-ELN. This study was conducted as described in Section 3.4.3. Figure 6. 2 shows that an increase in the initial copper concentration in the test solutions resulted in an increase in the maximum adsorption capacity for copper ions onto the CHITOSAN-CBR-ELN. The maximum adsorption capacity for copper ions increased from 0.745 mmol/g (at an initial ferrous concentration of 0.687 mmol/g) to 1.16 mmol/g (at an initial ferrous concentration of 2.77mmol/g). This result collaborates with the results from Section 5.3.2 that chitosan from BSF larvae is best described by the Freundlich model as the concentration of the adsorbate affects the extent of adsorption. The increase in the maximum adsorption capacity for copper ions onto the CHITOSAN-CBR-ELN against initial concentration in the test solution showed a positive linear correlation with a gradient of 0.4785 L/g and an R^2 value of 0.681 L/g. It must be noted for an increase in initial concentration with a given adsorbent this correlation has a maximum of the equilibrium adsorption capacity due to the limitation in the adsorption active sites (Guibal, 2004). For CHITOSAN-CBR-ELN this maximum of the equilibrium adsorption capacity for ferrous ions was 1.27± 0.001.

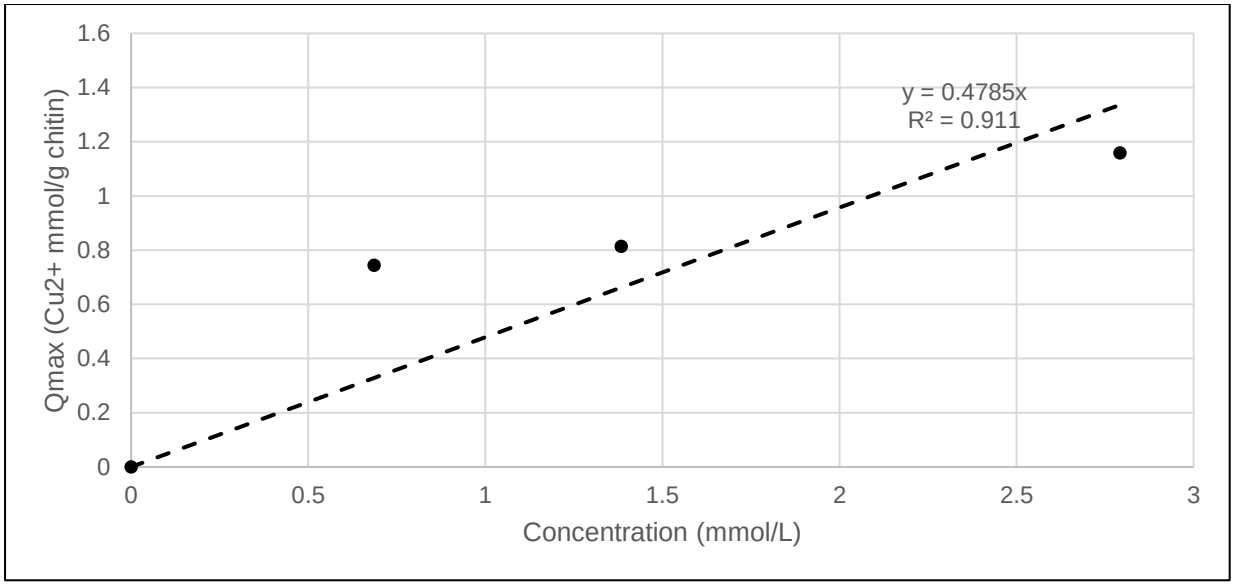

Figure 6. 2: Effect of initial concentration of copper ion on the maximum copper adsorption capacity of CHITOSAN-CBR-ELN

6.3 Application of CHITIN-CBR-ELN and CHITOSAN-CBR-ELN on PCB leachate solutions

The application of CHITIN-CBR-ELN and CHITOSAN-CBR-ELN was modelled on a basis of complete adsorption of ferrous and copper ions respectively in the adsorption cycles. This basis was chosen due to the high degree of metal adsorption selectivity for these metals by the respective polymers. The application was conducted on the Model leachate solution. For the development of the model the following assumptions were taken:

- The maximum adsorption capacity of each metal in each adsorption-desorption cycle is dependent on the initial concentration of the metals in the solution involved in the adsorption. This is affirmed by results observed in Section 5.2.2 and Section 5.3.2 that the nature of adsorption on these polymers is best described by the Freundlich Model. A positive linear correlation with gradient factors of 0.792 and 0.681 L/g was used for CHITIN-CBR-ELN and CHITOSAN-CBR-ELN respectively. This was adopted from the gradients of the maximum adsorption capacity versus initial concentrations graphs obtained in Section 6.1 and Section 6.2 respectively.
- Ferrous ions are oxidised to ferric ions after the first adsorption-desorption cycle. This was based on the observed oxidation of ferrous to ferric ions during the adsorption of ferrous ions onto these polymers in Section 5.2.4.
- CHITIN-CBR-ELN and CHITOSAN-CBR-ELN yield after each adsorption-desorption cycle is 80 % and 72 % respectively. This was based on yields obtained in the recyclability study in Section 5.4.
- Fresh CHITIN-CBR-ELN and CHITOSAN-CBR-ELN can only be used for 1 adsorption-desorption cycle. This was based on the observed negative effects of acid action from one metal adsorption-desorption cycle with CHITIN-CBR-ELN and CHITOSAN-CBR-ELN in Section 5.4.
- Complete desorption with 0.01 M H2SO4 of adsorbed metal metals.
- No material loss during adsorption, desorption and filtration.

Figure 6. 3 and Figure 6. 4 shows the process flow diagram of the application of CHITIN-CBR-ELN and CHITOSAN-CBR-ELN on the Model leachate solution. Figure 6. 3 and Figure 6. 4shows that 7 adsorption-desorption cycles were required for the complete target separation of metals for the Model leachate solution. In each adsorption-desorption cycle, fresh CHITIN-CBR-ELN and CHITOSAN-CBR-ELN are mixed with the desorbed solution from the previous adsorption-desorption cycle. After adsorption, the CHITIN-CBR-ELN and CHITOSAN-CBR-ELN are then filtered and placed into a desorption column were the adsorbed metal desorb into 0.01 M H_2SO_4. The desorbed CHITIN-CBR-ELN and CHITOSAN-CBR-ELN are then filtered and recovered.

Table 6. 5 and Table 6. 6 shows the concentration of ferrous, copper, aluminium and ferric ions in each stream, fresh CHITIN-CBR-ELN and CHITOSAN-CBR-ELN used and recovered. Table 6. 5 and Table 6. 6 also shows the maximum adsorption capacity and the molar ratio of metals adsorbed on the CHITIN-CBR-ELN and CHITOSAN-CBR-ELN in each adsorption-desorption cycle for ferrous, copper, aluminium and ferric ions. Table 6. 5 shows that the application of CHITIN-CBR-ELN on the Model leachate solution results in the complete separation of copper ions from ferrous and aluminium ions. Copper ions remain in streams

2,4,6,8,10,12 after the adsorption-desorption cycles. The driving force of this separation is the higher degree of metal adsorption selectivity for ferrous, ferric and aluminium ions by CHITIN-CBR-ELN over copper ions. This was observed in Section 6.1 and is consistent with the order of metal adsorption selectivity of chitin from BSF larvae observed in Section 5.2.4. Copper recovery efficiency in the adsorption-desorption trains improved as the concentration of copper decreased in the desorbed solutions. The copper recovery efficiency increased from 33.4 % to 83.6 % after 7 adsorption-desorption cycles. 85.3 % of the copper ions were recovered after 3 adsorption-desorption cycles and complete recovery after 7 adsorption-desorption cycles. The result of the application of CHITIN-CBR-ELN on the Model leachate solution were streams that contain copper ions only and a stream with ferric and aluminium ions (Stream 15). Table 6. 5 shows that the application of CHITOSAN-CBR-ELN on the Model leachate solution results in the separation of copper ions from ferrous ions. The general results are streams that contain ferric-aluminium ions and copper-aluminium ions (Stream 15). The driving force of this separation is the higher degree of metal adsorption selectivity for copper and aluminium ions by CHITOSAN-CBR-ELN over ferric ions. This was observed in Section 6.2 and is consistent with the order of metal adsorption selectivity of chitin from BSF larvae observed in Section 5.3.4. Further processing is therefore required to recover the metals in these refined solutions in the solid form

The amount of CHITIN-CBR-ELN and CHITOSAN-CBR-ELN used in the application of these polymers on the Model leachate solution was 29.6 g of Chitin/ g of PCB and 14.6 g of Chitosan/g of PCB respectively. The recovered CHITIN-CBR-ELN and CHITOSAN-CBR-ELN was 23.7g of Chitin/ g of PCB and 10.5 g of Chitosan/g of PCB respectively. Recovered chitin and chitosan provided a revenue potential and improved the profitability of the recovery process as shown in Section 4.1.6 and Section 4.2.3. The oxidation of ferrous ions to ferric ions during adsorption of ferrous ions onto chitin and chitosan from BSF larvae provides an opportunity for use of the ferric ions in refined streams. Ferric ions are a lixiviant in the acidic leaching of the PCB base metals into solution. Therefore, refined streams containing ferric ions could be recycled into the acidic leaching stage of the PCB base metal recovery process. The importance of a multidisciplinary approach in the recovery of metals from e-waste is highlighted by the requirement for further recovery processes after refining the Model leachate solution using CHITIN-CBR-ELN and CHITOSAN-CBR-ELN. A combined application of chitin/ chitosan followed by precipitation with NaHS in recovering copper and iron from the model leachate solution showed a positive economic outlook in Section 4.1.6 and Section 4.2.3. The potential of using NaHS precipitation for metal recovery was made more lucrative due to the low cost associated with this process. NaHS precipitation only contributed 1 % of the total metal recovery process while adsorption and desorption contributed 99 %.

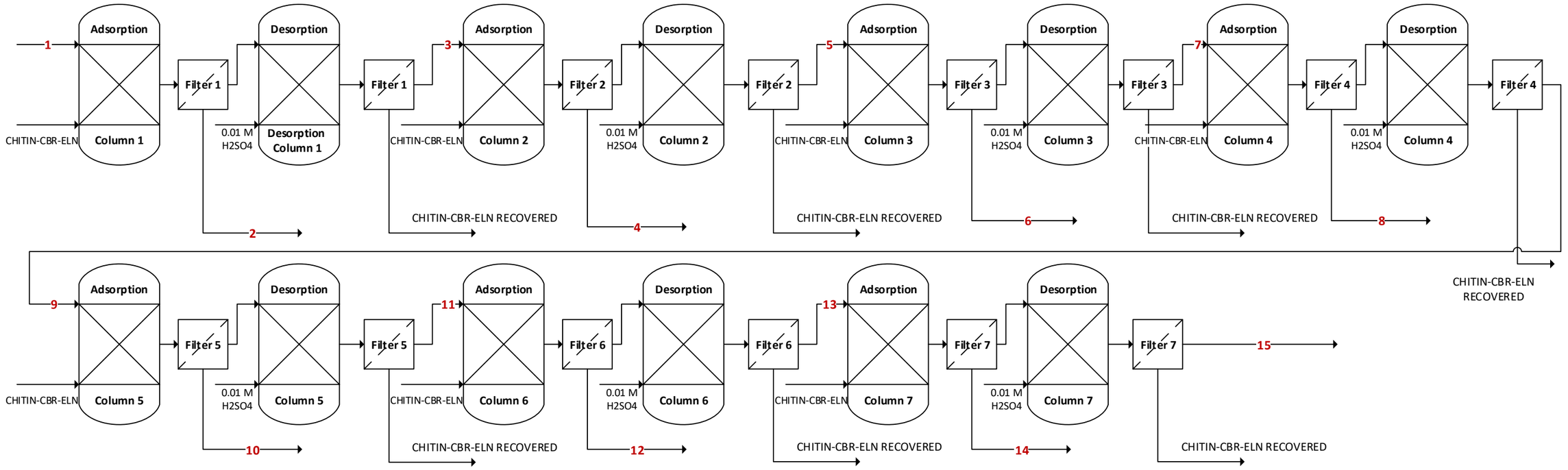

Figure 6. 3: Process flow diagram (PFD) of the application of CHITIN-CBR-ELN on the Model leachate solution

Table 6. 5:: Stream Table for the PFD of the application of CHITIN-CBR-ELN on the Model leachate solution

			Adsorption-Desorption Cycle 1		Adsorption-Desorption Cycle 2		Adsorption-Desorption Cycle 3		Adsorption-Desorption Cycle 4		Adsorption-Desorption Cycle 5		Adsorption-Desorption Cycle 6		Adsorption-Desorption Cycle 7		
		Stream Number	1	2	3	4	5	6	7	8	9	10	11	12	13	14	15
Concentration of Metals	Component	Unit	Model leachate solution	Model leachate solution after Adsorption 1	Desorbed solution 1	Desorbed solution 1 after Adsorption 2	Desorbed solution 2	Desorbed solution 2 after Adsorption 3	Desorbed solution 3	Desorbed solution 3 after Adsorption 4	Desorbed solution 4	Desorbed solution 4 after Adsorption 5	Desorbed solution 5	Desorbed solution 5 after Adsorption 6	Desorbed solution 6	Desorbed solution 6 after Adsorption 7	Desorbed solution 7
	Fe2+	mmol/L	1.11	0.00	0												
	Cu2+	mmol/L	2.78	0.93	1.85	0.88	0.98	0.57	0.41	0.27	0.13	0.10	0.04	0.03	0.01	0.01	0.00
	Al3+	mmol/L	2.81	0.00	2.81	0.00	2.81	0.00	2.81	0.00	2.81	0.00	2.81	0.00	2.81	0.00	2.81
	Fe3+	mmol/L	0	0	1.11	0.00	1.11	0	1.11	0	1.11	0	1.11	0	1.11	0	1.11
	CHITIN-CBR-ELN	g	5.36	4.29	4.35	3.48	4.02	3.22	3.96	3.17	3.96	3.17	3.96	3.17	3.96	3.17	
Maximum Adsorption Capacity	Component	Unit															
	Fe2+	(mmol/g)	0.453														
	Cu2+	(mmol/g)	0.758		0.40		0.17		0.06		0.01		0.00		0.00		
	Al3+	(mmol/g)	1.23		1.23		1.23		1.23		1.23		1.23		1.23		
	Fe3+	(mmol/g)			0.453		0.453		0.453		0.453		0.453		0.453		
Molar ratio of metals adsorbed	Component	Unit															
	Fe2+	(mmol/g)	1.00														
	Cu2+	(mmol/g)	1.67		0.88		0.37		0.12		0.03		0.01		0.00		
	Al3+	(mmol/g)	2.72		2.72		2.72		2.72		2.72		2.72		2.72		
	Fe3+	(mmol/g)			1.00		1.00		1.00		1.00		1.00		1.00		
Recovery Performance	Copper recovery efficiency	%	33.4		47.3		58.3		67.0		73.9		79.3		83.6		
	Copper recovered	%	33.4		64.9		85.3		95.2		98.7		99.7		100.0		

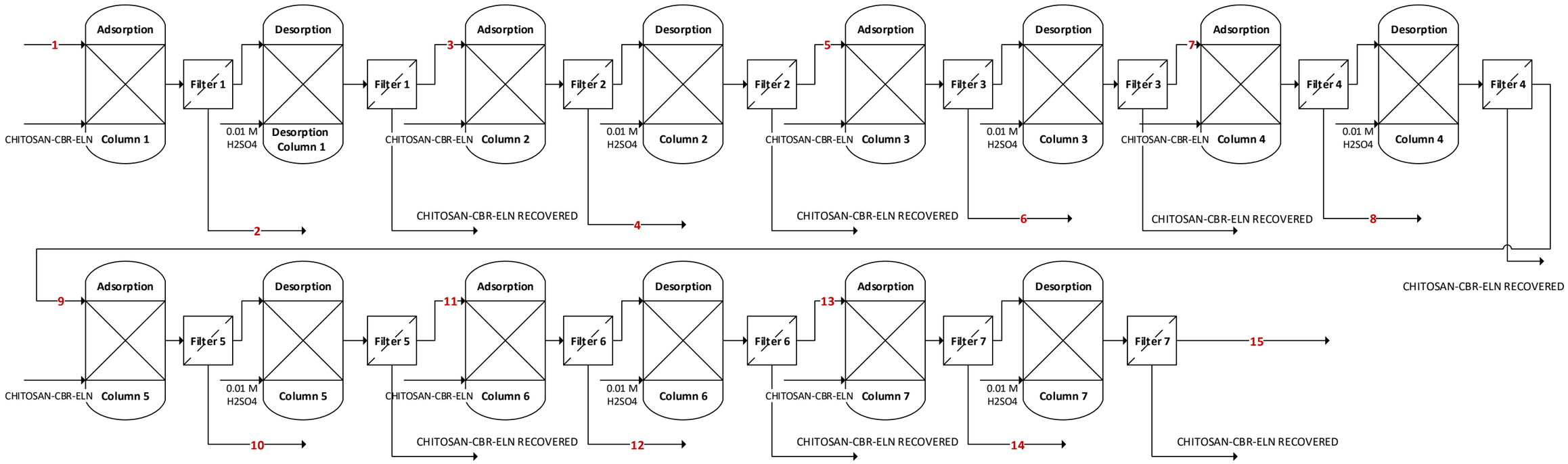

Figure 6. 4: Process flow diagram (PFD) of the application of CHITOSAN-CBR-ELN on the Model leachate solution

Table 6. 6: Stream Table for the PFD of the application of CHITOSAN-CBR-ELN on the Model leachate solution

			Adsorption-Desorption Cycle 1		Adsorption-Desorption Cycle 2		Adsorption-Desorption Cycle 3		Adsorption-Desorption Cycle 4		Adsorption-Desorption Cycle 5		Adsorption-Desorption Cycle 6		Adsorption-Desorption Cycle 7		
		Stream Number	**1**	**2**	**3**	**4**	**5**	**6**	**7**	**8**	**9**	**10**	**11**	**12**	**13**	**14**	**15**
Concentration of Metals	**Component**	**Unit**	**Model leachate solution**	**Model leachate solution after Adsorption 1**	**Desorbed solution 1**	**Desorbed solution 1 after Adsorption 2**	**Desorbed solution 2**	**Desorbed solution 2 after Adsorption 3**	**Desorbed solution 3**	**Desorbed solution 3 after Adsorption 4**	**Desorbed solution 4**	**Desorbed solution 4 after Adsorption 5**	**Desorbed solution 5**	**Desorbed solution 5 after Adsorption 6**	**Desorbed solution 6**	**Desorbed solution 6 after Adsorption 7**	**Desorbed solution 7**
	Fe2+	mmol/L	1.11	0.56	0												
	Cu2+	mmol/L	2.78	0.00	2.78	0.00	2.78	0.00	2.78	0.00	2.78	0.00	2.78	0.00	2.78	0.00	2.78
	Al3+	mmol/L	2.81	0.55	2.26	0.44	1.82	0.36	1.46	0.29	1.17	0.23	0.94	0.18	0.76	0.15	0.61
	Fe3+	mmol/L	0	0	0.54	0.28	0.27	0.14	0.13	0.07	0.06	0.03	0.03	0.02	0.02	0.01	0.01
	CHITOSAN-CBR-ELN	g	6.00	4.32	3.45	2.49	2.09	1.51	1.31	0.95	0.85	0.61	0.56	0.40	0.37	0.27	
Maximum Adsorption Capacity	**Component**	**Unit**															
	Fe2+	(mmol/g)	0.248														
	Cu2+	(mmol/g)	1.27		0.86		0.59		0.40		0.27		0.19		0.13		
	Al3+	(mmol/g)	1.03		0.56		0.31		0.17		0.09		0.05		0.03		
	Fe3+	(mmol/g)			0.08		0.03		0.01		0.00		0.00		0.00		
Molar ratio of metals adsorbed	**Component**	**Unit**															
	Fe2+	(mmol/g)	0.20														
	Cu2+	(mmol/g)	1.00		1.00		1.00		1.00		1.00		1.00		1.00		
	Al3+	(mmol/g)	0.81		0.65		0.52		0.42		0.34		0.27		0.22		
	Fe3+	(mmol/g)			0.10		0.05		0.02		0.01		0.01		0.00		

6.4 Selective Precipitation of Copper with NaHS

Precipitation studies were conducted as described in Section 3.6. A mixture of ferrous, copper and aluminium test solutions was created with a copper to ferrous to the aluminium initial molar ratio of 1:1:1 (equimolar), 1:2:1 (high ferrous solution) and 2:1:1 (high copper solution) ratio. The test solutions were dosed with 5 mL of 0.222M NaHS (this is equivalent to the number of moles of copper in the test solutions). The dosage was done at the start of the precipitation studies and after 20 mins.

Figure 6. 5 shows the concentration-time graph of the NaHS precipitation study on the equimolar copper, ferrous, aluminium test solution. Figure 6. 5 shows that the concentration of copper and aluminium decreased while that of ferrous ions remained constant after the initial dosage. Black precipitates were observed after the initial dosage. The concentration of copper dropped by 67 % after 20 mins while the concentration of aluminium dropped by 29 %. This indicates that the copper co-precipitated with the aluminium ions however the precipitation was more selective towards the copper ions. After the second dosage, the concentration of copper continued to decrease while that of ferrous and aluminium remained constant. The concentration of copper further decreased by 76 %. This study shows that sulphide precipitation with NaHS is selective towards copper precipitation however co-precipitation occurs in the presence of aluminium. Ferrous ions did not precipitate under these pH conditions (pH=3.45). There was a pungent smell during the precipitation suggesting the presence of a gas which is potential H_2S. In acidic effluents, partial neutralization with a base such as NaOH is necessary prior addition of sulphides to prevent the formation of pollutant gas, H_2S (Mikhailova et al., 2015). In the sulphide precipitation of ferrous, copper and aluminium solution neutralisation with NaOH would not be practical as this would result in precipitation of the metals.

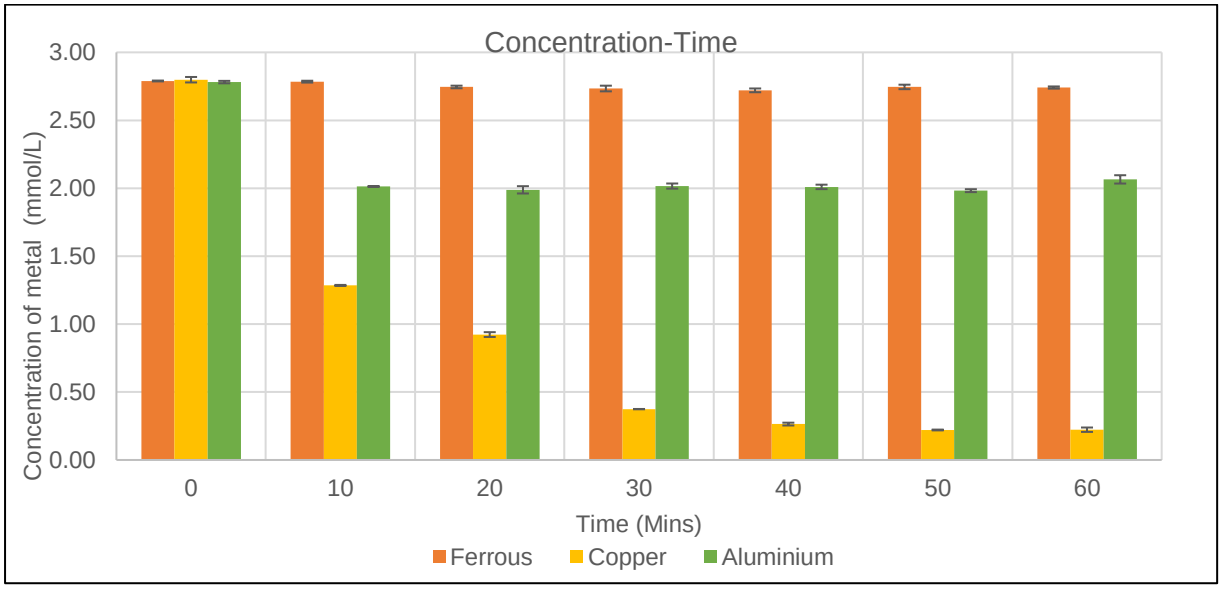

Figure 6. 5: Concentration-time graph of NaHS precipitation studies on equimolar (copper, ferrous, aluminium) test solution

Figure 6. 6 shows the concentration-time graph of the NaHS precipitation study on the high ferrous (copper, ferrous, aluminium) test solution. Figure 6. 6 shows that the concentration of

copper and aluminium decreased while that of ferrous ions remained constant after the initial dosage. Black precipitates were observed after the initial dosage. The concentration of copper dropped by 74 % while the concentration of aluminium dropped by 29 %. After the second dosage, the concentration of copper and aluminium continued to decrease while that of ferrous remained relatively constant. The concentration of copper further decreased by 76 % while aluminium decreased by 31 %. This study shows that sulphide precipitation with NaHS is selective towards copper precipitation even in the presence of relatively high ferrous ions.

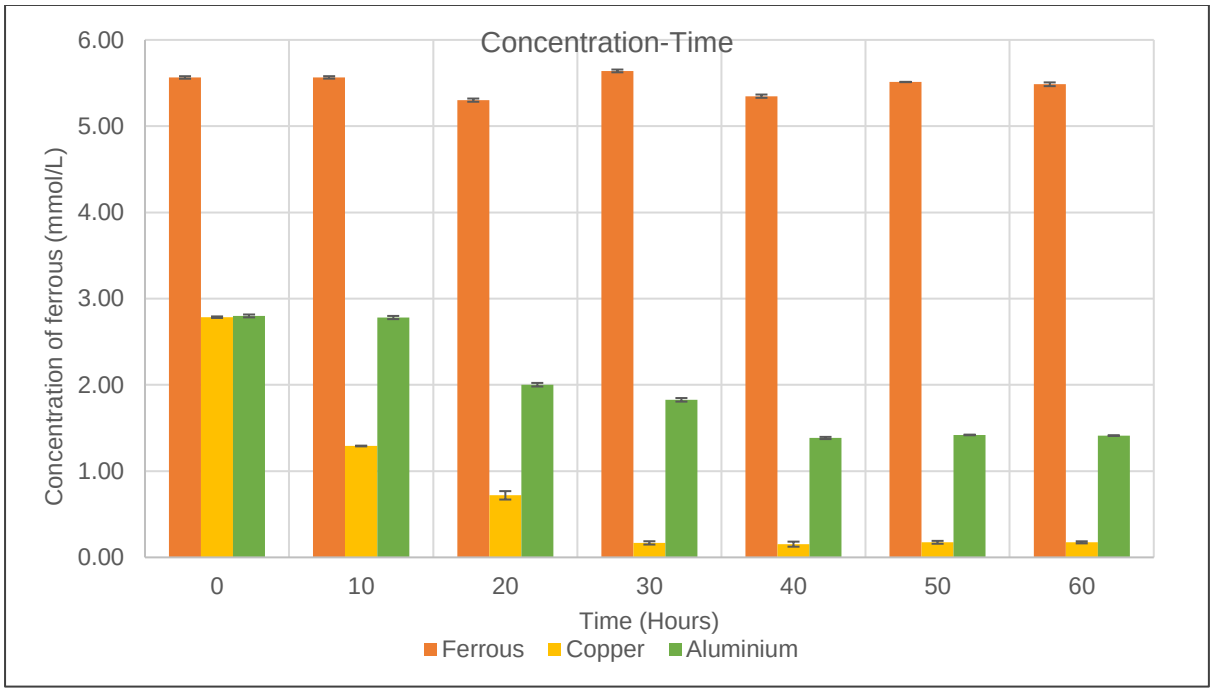

Figure 6. 6: Concentration-time graph of NaHS precipitation studies on high ferrous (copper, ferrous, aluminium) test solution

Figure 6. 7 shows the concentration-time graph of the NaHS precipitation study on the high copper (copper, ferrous, aluminium) test solution. Figure 6. 7 shows that the concentration of copper and aluminium decreased while that of ferrous ions remained constant after the initial dosage. Black precipitates were observed after the initial dosage. The concentration of copper dropped by 97 % after 20 mins while the concentration of aluminium dropped by 53 %. After the second dosage, the concentration of copper and aluminium continued to decrease while that of ferrous remained relatively constant. The concentration of copper further decreased by 100 % while aluminium decreased by 13 %. This study shows that relatively higher initial copper concertation than ferrous and aluminium improves the efficiency of the selective precipitation of copper using sulphide precipitation with NaHS. Although there was an improvement in the selective precipitation of copper there was still co-precipitation of aluminium observed. The precipitation studies with NaHS on the model leachate solution suggest that copper and aluminium must be separated to improve the purity of the two metals in the recovery with sulphides as they co-precipitate. Therefore, the proposed hypothesis stated in Section 2.5.2 with regards to sulphide precipitation is proven to be true. However, the degree of selective precipitation of copper from aluminium ions is low and high for ferrous ions.

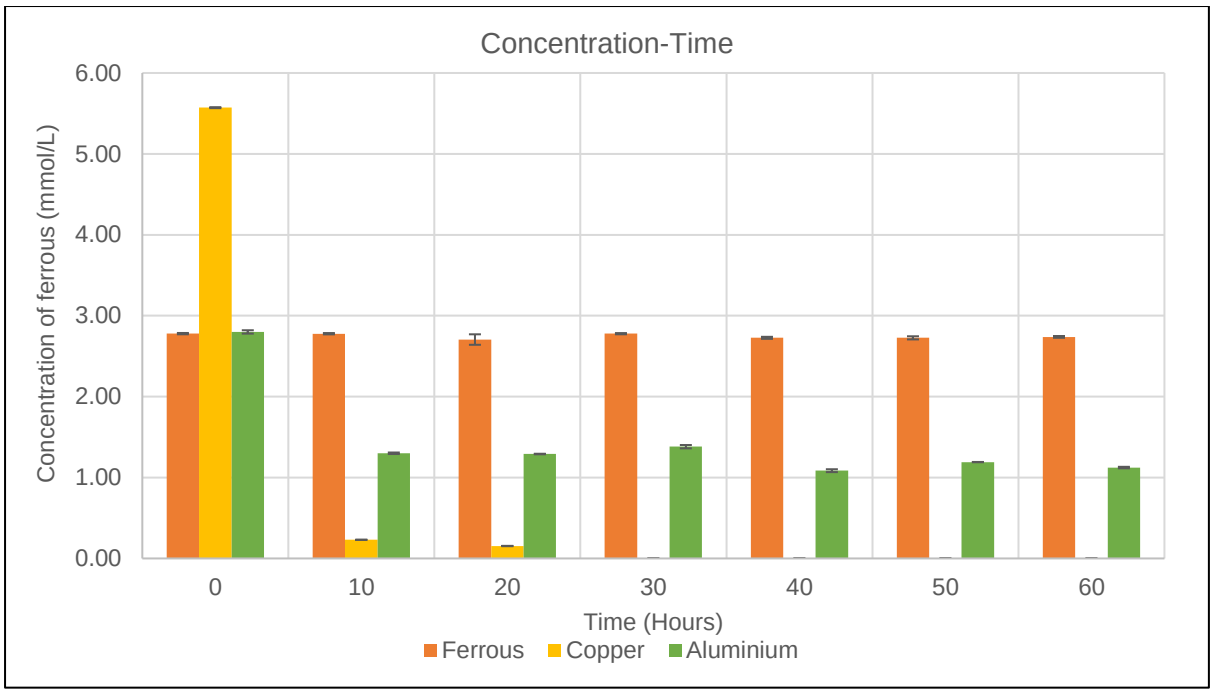

Figure 6. 7: Concentration-time graph of NaHS precipitation studies on high copper (copper, ferrous, aluminium) test solution

Figure 6. 8 show the X-ray diffraction (XRD) of the initial black precipitate obtained from the precipitate study with NaHS. Figure 6. 8 shows that the initial black precipitate observed was copper sulphide (covellite).

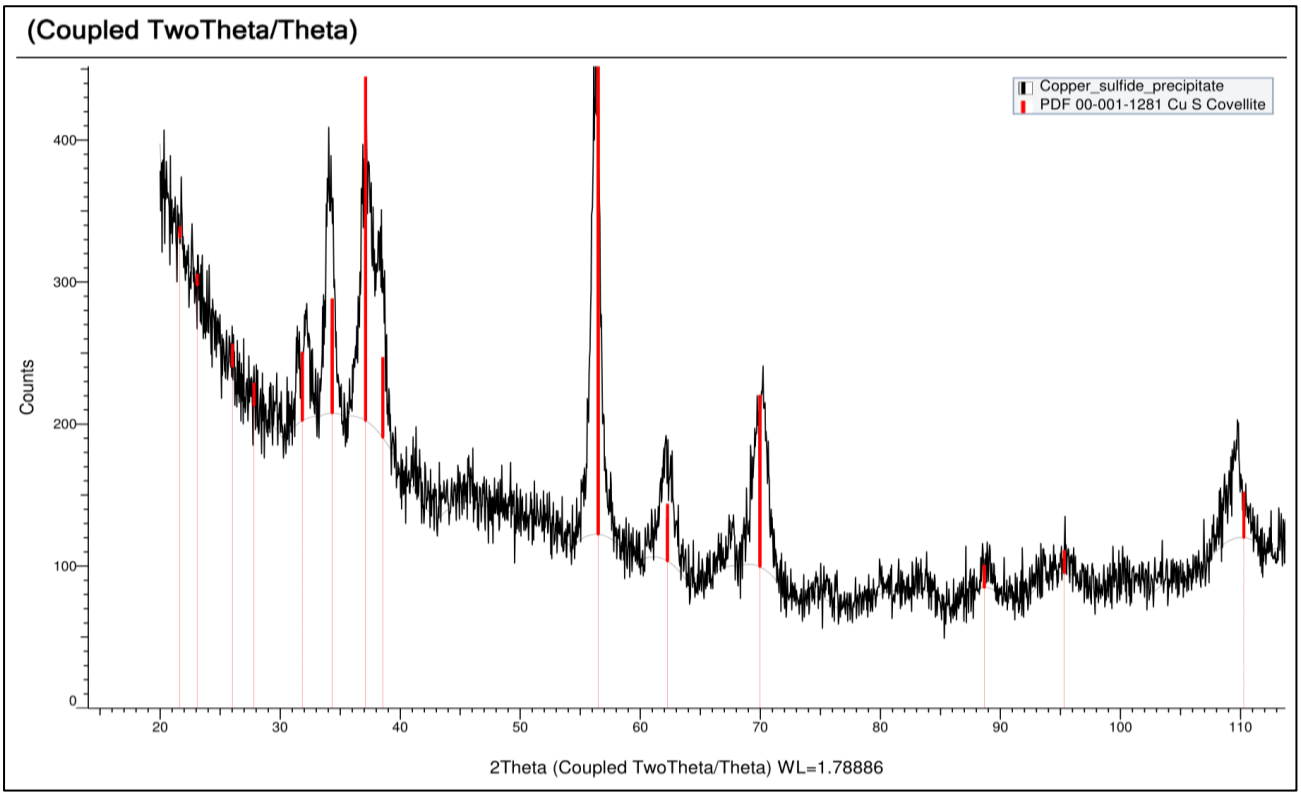

Figure 6. 8: XRD of the initial black precipitate from the precipitation studies with NaHS

6.5 Combined Application of Chitin/Chitosan and NaHS Precipitation on PCB leachates

The application of CHITIN-CBR-ELN on the Model leachate solution resulted in the production of two refined streams as shown in Section 6.3. A stream with copper ions only and another stream with a mixture of ferric and aluminium ions. The application of CHITOSAN-CBR-ELN on the Model leachate solution also resulted in the production of two refined streams. A stream with a mixture of copper and aluminium ions and a secondary stream with a mixture of ferric and aluminium ions. The co-precipitation of copper and aluminium observed in Section 6.4 with NaHS suggests that application of NaHS precipitation to recover separate copper and aluminium ions from the refined copper-aluminium stream produced by CHITOSAN-CBR-ELN will not be feasible. Therefore, the combined application of CHITOSAN-CBR-ELN and NaHS precipitation on PCB leachate solutions is limited. Other recovery technologies such as electrowinning will have to be explored in consideration of a combined recovery process with CHITOSAN-CBR-ELN on PCB leachate solution.

The oxidation of ferrous to ferric ions during the adsorption with CHITIN-CBR-ELN and CHITOSAN-CBR-ELN provides an opportunity for recycling ferric ions into the acidic leaching stage of the PCB metal recovery process. However, the refined streams produced by CHITIN-CBR-ELN and CHITOSAN-CBR-ELN also contain aluminium. If the ferric and aluminium refined streams are to be recycled into the acidic leaching stage of the PCB metal recovery process, a purge will be required to prevent the build-up of these metals in that recovery unit. A limitation then arises in recovering the ferric and aluminium ions in purge streams due to their close solubility products both in hydroxide and sulphide precipitation. Section 6.4 showed that aluminium has a higher degree of precipitation with NaHS than ferrous ions. Therefore, the complete recovery of aluminium from aluminium and ferrous ion mixture can be achieved with NaHS. To apply NaHS precipitation on aluminium and ferric ion mixture, the ferric ions must be reduced first to ferrous ions. Reduction of ferrous ions to ferric ions can be achieved by using enzymes, proteins, bacteria, chemicals such as Sodium Boron Hydrazine, Sodium Thiosulphate, Sodium Formaldehyde Bisulphate and electrolysis (Kojima & Bates, 1979; Johnson & McGinness, 1991; Gallup, 1993; Petrat et al., 2003; Karimi et al., 2017). Therefore, these reducing agents can be considered for the reduction of ferric ions in a ferric and aluminium mixture before NaHS precipitation. Figure 6. 9 shows a proposed process for the combined application of CHITIN-CBR-ELN and NaHS precipitation in a PCB metal recovery process. Nickel and zinc are expected to stay in the solution due to a low degree of adsorption selectivity by CHITIN-CBR-ELN. This is expected due to their low concentrations in the PCB model leachate solutions and their lower position in the order of metal adsorption selectivity on chitin. Nickel will be recovered from a zinc and nickel mixture using hydroxide precipitation due to the large difference in the product constant. The use of seven adsorption-desorption cycles will result in metal recovery costs of $ 116/ kg metal recovered, revenue from sales of sulphide of $ 389/ kg metal recovered, revenue from sales of CHITIN-CBR-ELN of 649.6/ kg metal recovered and overall gross profit of $ 933/ kg metal recovered. These results show the positive economic outlook of using CHITIN-CBR-ELN in e-waste metal recovery. The secondary use of recovered CHITIN-CBR-ELN improves the economic feasibility of the combined application of CHITIN-CBR-ELN with NaHS in base metal recovery from PCB leachate solutions.

The use of chitin and chitosan sourced from BSF larvae in the e-waste metal recovery processes provides the potential for the development of a large circular economy in the waste industry. Figure 6. 10 shows the potential circular economy developed using chitin and chitosan from BSF larvae for e-waste metal recovery. The circular economy developed involves the use of two major waste streams, solid waste and e-waste. The products from this circular economy are chitin/chitosan, proteins, lipids, plastics and metals. Proteins, lipids and metals are particularly in high demand due to population increase (Kaza et al., 2018).

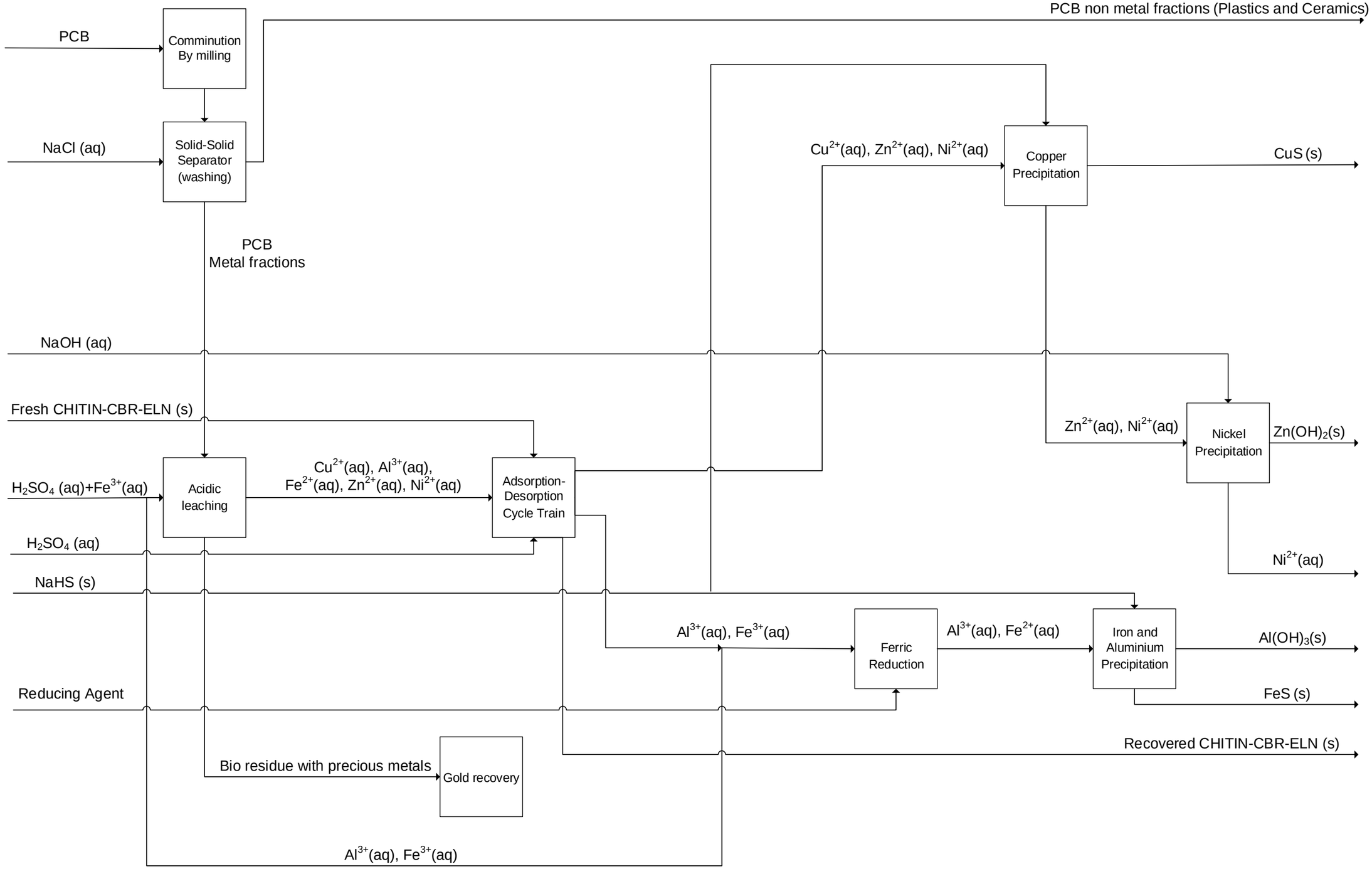

Figure 6. 9: Proposed flow sheet for the recovery of copper, aluminium, iron, nickel and zinc from a PCB leachate solution using CHITIN-CBR-ELN extracted from BSF larvae and sulphide precipitation with NaHS

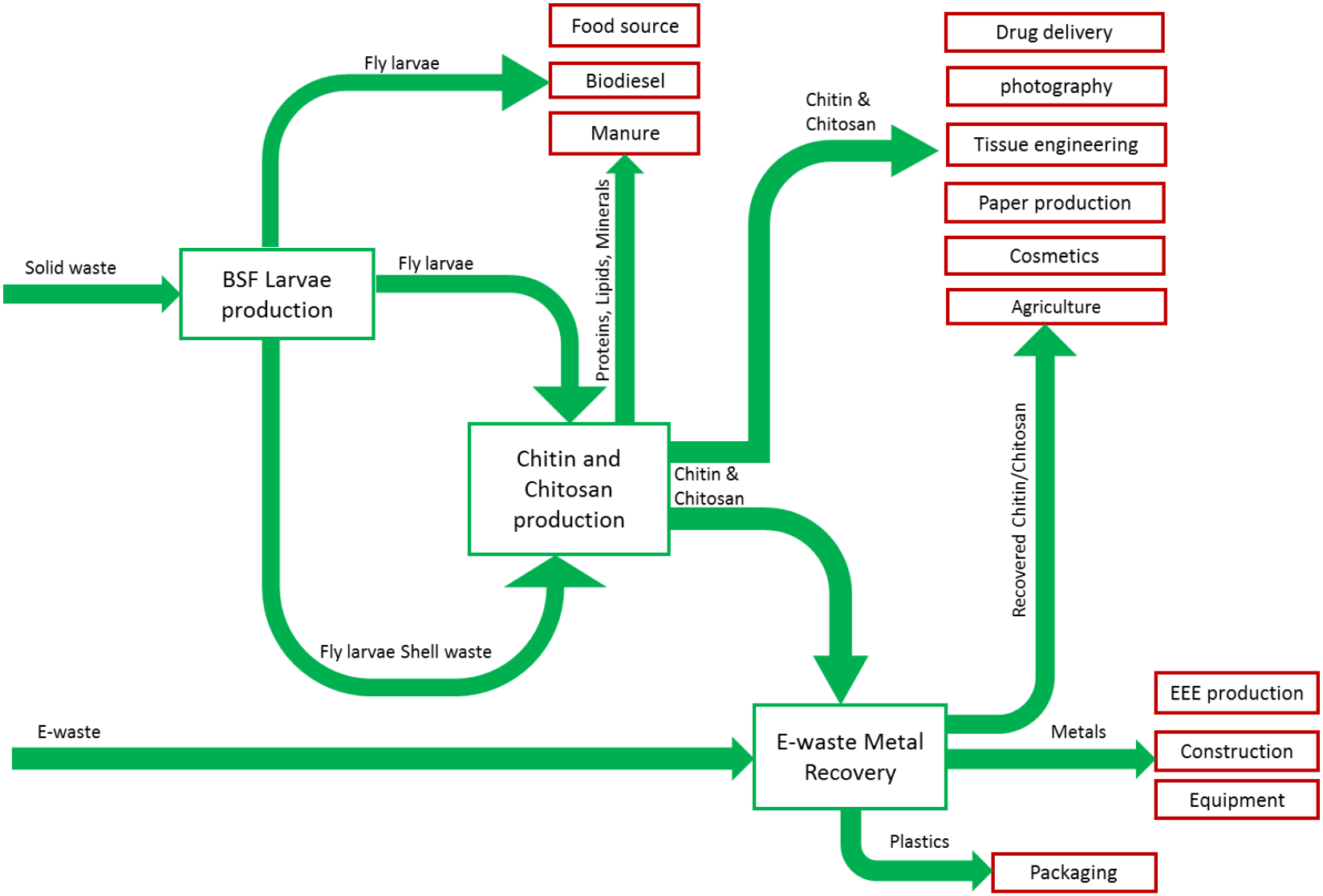

Figure 6. 10: Circular economy in the application of chitin and chitosan from BSF larvae in e-waste metal recovery

Chapter 7: Conclusions and Recommendations

Extracted chitin from BSF larvae was found to be in the alpha form. Inclusion of the de-acetylation and demineralisation steps in the extraction of chitin from BSF larvae resulted in lower overall yields, a lower degree of acetylation, higher cost of production and a decrease in the maximum adsorption capacities of ferrous, copper, and aluminium ions. 4-hour Deproteination of the BSF larvae after liberation with 4 wt % NaOH and de-acetylation of the deproteinated chitin was found to produce chitin and chitosan with the highest metal sorption capacities and lowest cost of production respectively. The chitin and chitosan cost of production was lower than the market value of agricultural grade chitin and chitosan and competitive to commercial sorbents indicating high-value addition to the BSF larvae shell waste. The maximum adsorption capacity for ferrous, ferric, copper and aluminium ions onto chitin from BSF larvae was 2.29 ± 0.0001 mmol/g, 2.07 ± 0.0001 mmol/g, 1.69 ± 0.0001 mmol/g and 1.82± 0.0001 mmol/g respectively. While for chitosan, the maximum adsorption capacity for ferric, copper and aluminium ions was 0.951 $\pm$ 0.0012 mmol/g, 1.16 $\pm$ 0.0016 mmol/g and 0.961$\pm$ 0.0013 mmol/g respectively.

The order of metal adsorption selectivity for ferrous, ferric, copper and aluminium on chitin from BSF larvae was determined to be Fe^{2+}>Fe^{3++}>Al^{3+}>Cu^{2+}. While for chitosan it was determined to be Cu^{2+} >Fe^{3+}>Al^{3+} and at a low pH (below pH of 2) it was observed to be Cu^{2+}>Al^{3+}>Fe^{3+}. These orders were observed in both the bimetal and single test solutions. The order of metal adsorption selectivity for chitin seems to follow the order of hydrolysis constants of the metals while chitosan follows the order of metal electronegativity. There was evidence of ferrous ion oxidation to ferric ions during chitin and chitosan adsorption. This was attributed to the increase in the adsorption pH and the antioxidant properties of chitin and chitosan. The results of the order of metal adsorption selectivity suggest that adsorption of metals onto chitin and chitosan from BSF larvae can be hypothesised according to the hypotheses stated in Section 2.5.2. Adsorption of the metals onto chitin and chitosan were best modelled by the Freundlich isotherm and Pseudo 2^{nd} order kinetic model. Adsorption on both polymers was found to be spontaneous, favourable, chemisorption and predominantly surface complexation occurring mostly in the first zone of diffusion (film layer). Metal adsorption active sites on the chitin and chitosan were found to be the acetamido and amine groups in the polymers. The change in pH during adsorption due to the chitin and chitosan and their antioxidant properties resulted in the oxidation of the ferrous ions into ferric ions during the adsorption process. The driver of the mechanism in the oxidation of ferrous to ferric ions during chitin and chitosan adsorption is thought to be due to the free radical scavenging through the action of the nitrogen in the C-2 position of chitin and chitosan. This is achieved via the protonation of this nitrogen to ammonium ions. The ammonium ions then can accept electrons from the oxidising ferrous ions to form a stable compound. Complete desorption of the metal ions from chitin and chitosan was achieved using 0.1 M H_2SO_4.

Fresh chitin and chitosan were only effective for one metal adsorption-desorption cycle and could not be recycled into this unit because of the effect of acid action on these polymers. 7 adsorption-desorption cycles with chitin/chitosan were required for the complete target separation of metals in the Model leachate solution. The application of chitin and chitosan on

the Model leachate solution resulted in the production of two refined streams, respectively. Further processing is required to recover metals in solid form. Sulphide precipitation with NaHS was observed to be selective towards copper precipitation however co-precipitation with aluminium occurred. The selective NaHS precipitation of copper was improved by an increase in the initial copper concentration in the solution. The order of metal precipitation selectivity was observed to be that hypothesised in Section 2.5.2 were the metals with the lower solubility products precipitate out of solution first. The application of NaHS precipitation seemed to be more feasible for the refined streams produced by the application of chitin on the Model leachate solution. For the combined application of NaHS and chitin/chitosan from BSF larvae on the Model leachate solution, NaHS precipitation only contributed 1 % of the total metal recovery process costs while adsorption and desorption contributed 99 %. The techno-economic analysis of this application showed economic feasibility. The recovery costs were $ 116 per kg metal recovered and an overall gross profit of $ 933/ kg metal recovered was achieved. Further economic studies which include consideration of capital costs need to be conducted to conclusively determine the economic feasibility of this downstream metal recovery process.

The potential use of chitin/chitosan for secondary processes after desorption improves the circular economy and economic feasibility of the metal recovery process. Application of chitin/chitosan from BSF larvae in e-waste metal recovery results in a circular economy where solid waste is utilized to produce BSF larvae and BSF larvae shell waste is used to remediate electronic waste recovering value from these waste streams while reducing their environmental impact. The developed downstream metal recovery process in this dissertation seems to be a promising technology for the recovery of base metals from e-waste leachate solutions. This study recommends the use of chitin from BSF larvae for the upgrading of PCB leachate solutions to produce refined streams of copper, aluminium and ferrous ions for further downstream processing. The study recommends further work in understanding the metal adsorption of zinc and nickel ions onto CHITIN-CBR-ELN and CHITOSAN-CBR-ELN. This is due to that these base metals were not covered in the scope of this study however present in relatively significant concentrations in PCB leachate solutions. Understanding their order of metal adsorption selectivity relative to copper, aluminium and iron covered in this study can assist in the further developments of the chitin adsorption technology recommended in this study. The effect of chitin and chitosan degradation and de-activation in metal adsorption after the use of 0.1 M H_2SO_4 in the desorbing metals in this study suggests the need for alternative desorption reagents. A desorption reagent that is non-degrading will improve the recovery costs of this technology as it allows for the recycling of the chitin and chitosan in the metal adsorption step. To improve the circular economy in the developed technology in this study an investigation on the potential use of the hydrolysed proteins and lipids from the deproteination process would improve value recovery and waste reduction in the extraction and production process of the bio sorbents in this study. The investigation on the potential application of the used chitin and chitosan after the adsorption-desorption cycles is important particularly in improving the circular economy and economic feasibility of the adsorption process recommended in this study. Revenue can potentially be generated if the used chitin and chitosan has further applications. One potential application for consideration is the use of chitin and chitosan in the agriculture industry. This study only considered the use of BSF larvae as the source of chitin and chitosan however investigation of using other sources of chitin and

chitosan such as crustaceans for the application of base metal recovery in e-waste solutions can improve the feasibility of the process by increasing raw material access. This study only considered a techno-economic analysis of the recovery technologies investigated in this study. Further techno-economic analysis of this recovery technology which includes capital costs and consideration of other operational expenses such as labour need to be conducted to ascertain the scalability of the proposed recovery technology.

References

Abdel-Shafy, H.I. & Mansour, M.S.M. 2018. Solid waste issue: Sources, composition, disposal, recycling, and valorization. *Egyptian Journal of Petroleum*. 27(4):1275–1290. DOI: 10.1016/j.ejpe.2018.07.003.

Abdullah, S.R.S., Rahman, R.A., Mohammad, A.B., Mustafa, M.M. & Khadum, A.A.H. 1999. Removal of Mixed Heavy Metals by Hydroxide Precipitation. *Jurnal Kejuruteraan*. 11(2):85–101.

African Development Bank. 2018. *African Economic Outlook*. Abidjan: African Development Bank. DOI: 10.1373/clinchem.2007.093781.

Ahmed, M.J. & Hossan, J. 1995. Spectrophotometric determination of aluminium by morin. *Talanta*. 42(8):1135–1142. DOI: 10.1016/0039-9140(95)01554-O.

Ahmed, J.M., Jahan, I. & Banoo, A. 2002. A simple spectrophotometric method for the determination of copper in industrial, environmental, biological and soil samples using 2,5-Dimercapto-1,3,4-thiadiazole. *Analytical Sciences*. 18:805–810. DOI: 10.1039/c3ay42113a.

Ahmed, M.J., Jahan, I. & Banoo, S. 2004. A simple spectrophotometric method for the determination of cadmium in industrial, environmental, biological and soil samples using 5,7-dibromo-8-hydroxyquinoline. *Analytical sciences : the international journal of the Japan Society for Analytical Chemistry*. 20(6):987–90. DOI: 10.1039/c3ay42113a.

Ajmal, M., Hussain Khan, A., Ahmad, S. & Ahmad, A. 1998. Role of sawdust in the removal of copper(II) from industrial wastes. *Water Research*. 32(10):3085–3091. DOI: 10.1016/S0043-1354(98)00067-0.

Al-Qazzaz, M.F.A., Ismail, D., Akit, H. & Idris, L.H. 2016. Effect of using insect larvae meal as a complete protein source on quality and productivity characteristics of laying hens. *Revista Brasileira de Zootecnia*. 45(9):518–523. DOI: 10.1590/S1806-92902016000900003.

Al-Tarazi, M., Heesink, A.B.M. & Versteeg, G.F. 2004. Precipitation of metal sulphides using gaseous hydrogen sulphide: Mathematical modelling. *Chemical Engineering Science*. 59(3):567–579. DOI: 10.1016/j.ces.2003.11.006.

Alibaba. 2019a. *Cost of NaOH*. Available: https://www.alibaba.com/trade/search?fsb=y&IndexArea=product_en&CatId=&SearchText=NaOH [2019, January 14].

Alibaba. 2019b. *Cost of HCl*. Available: https://www.alibaba.com/trade/search?fsb=y&IndexArea=product_en&CatId=&SearchText=HCL&viewtype= [2019, January 14].

Alibaba. 2019c. *Cost of NaClO*. Available: https://www.alibaba.com/trade/search?fsb=y&IndexArea=product_en&CatId=&SearchText=NaClO&viewtype= [2019, January 14].

Alibaba. 2019d. *Cost of Sulfuric acid*. Available: https://www.alibaba.com/trade/search?fsb=y&IndexArea=product_en&CatId=&SearchText=sulfuric+acid&viewtype= [2019, January 14].

Alibaba. 2019e. *Cost of NaHS*. Available: https://www.alibaba.com/trade/search?fsb=y&IndexArea=product_en&CatId=&SearchText=NaHS&viewtype= [2019, January 14].

Alibaba. 2019f. *Cost of Copper Sulfide*. Available: https://www.alibaba.com/trade/search?fsb=y&IndexArea=product_en&CatId=&SearchText=Copper+sulfide&viewtype= [2019, January 14].

Alibaba. 2019g. *Cost of ferrous sulfide*. Available: https://www.alibaba.com/trade/search?IndexArea=product_en&CatId=&fsb=y&SearchText=ferrous+sulfide [2019, January 14].

Alibaba. 2019h. *Cost of aluminium hydroxide*. Available: https://www.alibaba.com/trade/search?IndexArea=product_en&CatId=&fsb=y&SearchText=aluminium+hydroxide [2019, January 14].

Alibaba. 2019i. *Cost of Agricultural grade Chitin/Chitosan*. Available: https://www.alibaba.com/trade/search?fsb=y&IndexArea=product_en&CatId=&SearchText=chitin+agriculture&viewtype= [2019, January 21].

de Almeida Neto, A.F., Vieira, M.G.A. & da Silva, M.G.C. 2014. Adsorption and desorption processes for copper removal from water using different eluents and calcined clay as adsorbent. *Journal of Water Process Engineering*. 3:90–97. DOI: 10.1016/j.jwpe.2014.05.014.

Amoyaw-Osei, Agyekum Opuku, O., Pwamang, J.A., Mueller, E., Fasko, R. & Schluep, M. 2011. *Ghana e-waste country assessment*. Dubendorf. Available: http://www.ewasteguide.info/files/Amoyaw-Osei_2011_GreenAd-Empa.pdf%5Cnhttp://scholar.google.com/scholar?hl=en&btnG=Search&q=intitle:Ghana+e-Waste+Country+Assessment#0.

Anastopoulos, I., Bhatnagar, A., Bikiaris, D.N. & Kyzas, G.Z. 2017. Chitin adsorbents for toxic metals: A review. *International Journal of Molecular Sciences*. 18(1):1–11. DOI: 10.3390/ijms18010114.

Andrus, M.E. 2000. A review of metal precipitation chemicals for metal-finishing applications. *Metal Finishing*. 98(11):20–23. DOI: 10.1016/S0026-0576(00)83532-1.

Anirudhan, T.S. & Sreekumari, S.S. 2011. Adsorptive removal of heavy metal ions from industrial effluents using activated carbon derived from waste coconut buttons. *Journal of Environmental Sciences*. 23(12):1989–1998. DOI: 10.1016/S1001-0742(10)60515-3.

Aranaz, I., Mengibar, M., Harris, R., Panos, I., Miralles, B., Acosta, N., Galed, G. & Heras, A. 2009. Functional Characterization of Chitin and Chitosan. *Current Chemical Biology*. 3(2):203–230. DOI: 10.2174/187231309788166415.

Arushanyan, Y., Bjorklund, A., Eriksson, O., Finnveden, G., Soderman, M.L., Sundqvist, J.-O. & Stenmarck, A. 2017. Environmental Assessment of Possible Future Waste Management Scenarios. *Energies*. 10(247):1–27. DOI: 10.3390/en10020247.

Ayres, R.U., Ayres, L.W. & Rade, I. 2002. The Life Cycle of Copper, its Co-Products and By-Products. *Journal of Industrial Ecology*. (24). DOI: 10.1162/108819899569458.

Babel, S. & Kurniawan, T.A. 2003. Low-cost adsorbents for heavy metals uptake from contaminated water: A review. *Journal of Hazardous Materials*. B97:219–243. DOI: 10.1016/S0304-3894(02)00263-7.

Babić, B.M., Milonjić, S.K., Polovina, M.J., Čupić, S. & Kaludjerović, B. V. 2002. Adsorption of zinc, cadmium and mercury ions from aqueous solutions on an activated carbon cloth. *Carbon*. 40(7):1109–1115. DOI: 10.1016/S0008-6223(01)00256-1.

Badawy, R.M. & Mohamed, H.I. 2015. Chitin extration, Composition of Different Six Insect Species and Their Comparable Characteristics with That of the Shrimp. *Journal of American Science*. 11(6):127–134.

Baldé, C.P., Forti, V., Kuehr, R. & Stegmann, P. 2017. *The Global E-waste Monitor 2017: Quantities, Flows, and Resources*. Bonn: UNU-VIE SCYCLE. DOI: ISBN 978-92-808-4556-3.

Balintova, M. & Petrilakova, A. 2011. Study of pH influence on selective precipitation of heavy metals from acid mine drainage. *Chemical Engineering Transactions*. 25:345–350. DOI: 10.3303/CET1125058.

Barr, G., Defreyne, J., Jones, D. & Mean, R. 2005. *On-Site Processing Vs. Sale of Copper Concentrates*. Perth. Available: http://www.teck.com/media/CESL-Publication-Copper-On-Site-vs-Cu-Con-Sales-Alta-2005.pdf.

Baxter, R. 2016. *MINING IN SOUTH AFRICA : This is the Mining Industry " Long Cold winters and Short beautiful summers "*. Johannesburg.

Behnamfard, A., Salarirad, M.M. & Veglio, F. 2013. Process development for recovery of copper and precious metals from waste printed circuit boards with emphasize on palladium and gold leaching and precipitation. *Waste Management*. 33(11):2354–2363. DOI: 10.1016/j.wasman.2013.07.017.

Beolchini, F., Pagnanelli, F., Toro, L. & Vegliò, F. 2006. Ionic strength effect on copper biosorption by Sphaerotilus natans: Equilibrium study and dynamic modelling in membrane reactor. *Water Research*. 40(1):144–152. DOI: 10.1016/j.watres.2005.10.031.

Bergmann, C.P. 2015. *Carbon Nanomaterials as Adsorbents for Environmental and Biological Applications*. F.M. Machado, Ed. Pelotas: Springer. DOI: 10.1007/978-3-319-18875-1.

Bertagnolli, C., Kleinübing, S.J. & da Silva, M.G.C. 2011. Preparation and characterization of a Brazilian bentonite clay for removal of copper in porous beds. *Applied Clay Science*. 53(1):73–79. DOI: 10.1016/j.clay.2011.05.002.

Bhainsa, K.C. & D'Souza, S.F. 2008. Removal of copper ions by the filamentous fungus, Rhizopus oryzae from aqueous solution. *Bioresource Technology*. 99(9):3829–3835. DOI: 10.1016/j.biortech.2007.07.032.

Bizzo, W.A., Figueiredo, R.A. & De Andrade, V.F. 2014. Characterization of printed circuit boards for metal and energy recovery after milling and mechanical separation. *Materials*. 7(6):4555–4566. DOI: 10.3390/ma7064555.

Blais, J.F., Djedidi, Z., Cheikh, R. Ben, Tyagi, R.D. & Mercier, G. 2008. Metals Precipitation from Effluents: Review. *Practice Periodical of Hazardous, Toxic, and Radioactive Waste Management*. 12(3):135–149. DOI: 10.1061/(ASCE)1090-025X(2008)12:3(135).

Borja, D., Nguyen, K.A., Park, J.H., Gupta, V., Lee, Y. & Kim, H. 2016. Experiences and Future Challenges of Bioleaching Research in South Korea. *Minerals*. 6(128):1–21. DOI: 10.3390/min6040128.

Boulaiche, W., Hamdi, B. & Trari, M. 2019. Removal of heavy metals by chitin: equilibrium, kinetic and thermodynamic studies. *Applied Water Science*. 9(2):1–10. DOI: 10.1007/s13201-019-0926-8.

Bourguignon, D. 2015. *Understanding waste streams Treatment of specific waste*.

Brandl, H., Bosshard, R. & Wegmann, M. 2001. Computer-munching microbes: Metal leaching from electronic scrap by bacteria and fungi. *Process Metallurgy*. 9(C):569–576. DOI: 10.1016/S1572-4409(99)80146-1.

Broussignac, P. 1968. Chitosan, a natural polymer not well known by the industry. *Chim. Ind. Genie Chim*. 99:1241–1247.

Brugnerotto, J., Lizardi, J., Goycoolea, F.M., Arguelles-Monal, W., Desbrières, J. & Rinaudo, M. 2001. An infrared investigation in relation with chitin and chitosan characterization. *Polymer*. 42:3569–3580.

Chen, X.H., Gosset, T. & Thévenot, D.R. 1990. Batch copper ion binding and exchange properties of peat. *Water Research*. 24(12):1463–1471. DOI: 10.1016/0043-1354(90)90080-P.

Cho, Y.I., No, H.K. & Meyers, S.P. 1998. Physicochemical Characteristics and Functional Properties of Various Commercial Chitin and Chitosan Products. *Journal of Agricultural and Food Chemistry*. 46(9):3839–3843. DOI: 10.1021/jf971047f.

Choi, M.-S., Cho, K.-S., Kim, D.-J.D.-S. & Kim, D.-J.D.-S. 2004. Microbial Recovery of Copper from Printed Circuit Boards of Waste Computer by Acidithiobacillus ferrooxidans. *Journal of Environmental Science and Health, Part A- Toxic/Hazardous Substances & Environmental Engineering*. A 39(11–12):2973–2982. DOI: 10.1081/lesa-200034763.

Christoforidis, A.K., Orfanidis, S., Papageorgiou, S.K., Lazaridou, A.N., Favvas, E.P. & Mitropoulos, A.C. 2015. Study of Cu(II) removal by Cystoseira crinitophylla biomass in batch and continuous flow biosorption. *Chemical Engineering Journal*. 277:334–340. DOI: 10.1016/j.cej.2015.04.138.

Chu, K.H. 2002. Removal of copper from aqueous solution by chitosan in prawn shell: Adsorption equilibrium and kinetics. *Journal of Hazardous Materials*. 90(1):77–95. DOI: 10.1016/S0304-3894(01)00332-6.

Clarke, K.G. 2013. Downstream processing. *Bioprocess Engineering*. 209–234. DOI: 10.1533/9781782421689.209.

Cojocaru, C., Diaconu, M., Cretescu, I., Savić, J. & Vasić, V. 2009. Biosorption of copper(II) ions from aqua solutions using dried yeast biomass. *Colloids and Surfaces A: Physicochemical and Engineering Aspects*. 335(1–3):181–188. DOI: 10.1016/j.colsurfa.2008.11.003.

Compton, O.C. & Nguyen, S.T. 2010. Graphene oxide, highly reduced graphene oxide, and graphene: Versatile building blocks for carbon-based materials. *Small*. 6(6):711–723. DOI: 10.1002/smll.200901934.

Couillard, D. & Mercier, G. 1992. Précipitations sélectives des métaux solubilisés biologiquement de boues aérobies d'épuration. *The Canadian Journal of Chemical Engineering*. 70(5):1021–1029. DOI: 10.1002/cjce.5450700526.

Cui, J. & Zhang, L. 2008. Metallurgical recovery of metals from electronic waste: A review. *Journal of Hazardous Materials*. 158:228–256. DOI: 10.1016/j.jhazmat.2008.02.001.

Czechowska-Biskup, R., Jarosińska, D., Rokita, B., Ulański, P. & Rosiak, J.M. 2012. Determination of Degree of Deacetylation of Chitosan. *Progress on Chemistry and Application of Chitin and Its derviatives*. 17:5–20.

Dahroug, S.M. 2004. *General Assessment of E-waste Problem In Egypt*. Cairo, Egypt.

Decraene, L. 2016. Inclusion of Black Soldier Fly (Hermetia Illucens) Larvae Meal in the Diet for Laying Quails: Effect on Live Performances and Eggs Quality. Ghent University. Available:

https://lib.ugent.be/fulltxt/RUG01/002/352/162/RUG01-002352162_2017_0001_AC.pdf.

Demirkiran, N., Ekmekyapar, A., Künkül, A. & Baysar, A. 2007. A kinetic study of copper cementation with zinc in aqueous solutions. *International Journal of Mineral Processing*. 82(2):80–85. DOI: 10.1016/j.minpro.2006.10.005.

Dortsmans, B., Diener, S., Verstappen, B. & Zurbrugg, C. 2017. *Black Soldier Fly Biowaste Processing A Step-by-Step Guide*. Dubendorf. DOI: 10.1117/12.464354.

Dow Chemical Company. 1999. Ion exchange resins. *Metal Finishing*. 97(12):69–70. DOI: 10.1016/S0026-0576(00)81191-5.

Dutta, P.K., Dutta, J. & Tripathi, V.S. 2004. Chitin and chitosan : Chemistry , properties and applications. *Journal of Scientific & Industrisl Research*. 63(January):20–31.

E-waste guide info. 2017. *Material Composition _ ewasteguide*. Available: http://ewasteguide.info/node/4074 [2017, May 14].

Ejaz, N., Akhtar, N., Nisar, H. & Ali Naeem, U. 2010. Environmental impacts of improper solid waste management in developing countries: A case study of Rawalpindi City. *WIT Transactions on Ecology and the Environment*. 142:379–387. DOI: 10.2495/SW100351.

Eskom. 2018. *SCHEDULE OF STANDARD PRICES FOR ESKOM TARIFFS 1 APRIL 2017 TO 31 MARCH 2018 FOR NON-LOCAL AUTHORITY SUPPLIES, AND 1 JULY 2017 TO 30 JUNE 2018 FOR LOCAL AUTHORITY SUPPLIES 1. Standard prices*. Johannesburg.

Faramarzi, M.A., Stagars, M., Pensini, E., Krebs, W. & Brandl, H. 2004. Metal solubilization from metal-containing solid materials by cyanogenic Chromobacterium violaceum. *Journal of Biotechnology*. 113(1–3):321–326. DOI: 10.1016/j.jbiotec.2004.03.031.

Findon, A., McKay, G. & Blair, H.S. 1993. Transport Studies for the Sorption of Copper Ions by Chitosan. *Journal of Environmental Science and Health. Part A: Environmental Science and Engineering and Toxicology*. 28(1):173–185. DOI: 10.1080/10934529309375870.

Fomina, M. & Gadd, G.M. 2014. Biosorption: Current perspectives on concept, definition and application. *Bioresource Technology*. 160:3–14. DOI: 10.1016/j.biortech.2013.12.102.

Fouladgar, M., Beheshti, M. & Sabzyan, H. 2015. Single and binary adsorption of nickel and copper from aqueous solutions by γ-alumina nanoparticles: Equilibrium and kinetic modeling. *Journal of Molecular Liquids*. 211:1060–1073. DOI: 10.1016/j.molliq.2015.08.029.

Gallup, D.L. 1993. THE USE OF REDUCING AGENTS FOR CONTROL OF FERRIC SILICATE SCALE DEPOSITION. *Geothermics*. 22(1):39–48.

Girish, C.R. 2017. Various Isotherm Models for Multicomponent Adsorption : a Review. *International Journal of Civil Engineering and Technology*. 8(10):80–86.

Gong, J.L., Wang, X.Y., Zeng, G.M., Chen, L., Deng, J.H., Zhang, X.R. & Niu, Q.Y. 2012. Copper (II) removal by pectin-iron oxide magnetic nanocomposite adsorbent. *Chemical Engineering Journal*. 185–186:100–107. DOI: 10.1016/j.cej.2012.01.050.

Gosset, T., Trancart, J.-L. & Thevenot, D.R. 1986. BATCH METAL REMOVAL BY PEAT KINETICS AND THERMODYNAMICS. *Water Research*. 20(1):21–26.

Govender, E., Harrison, S.T.L. & Bryan, C.G. 2012. Modification of the ferric chloride assay for the spectrophotometric determination of ferric and total iron in acidic solutions containing high concentrations of copper. *Minerals Engineering*. 35:46–48. DOI: 10.1016/j.mineng.2012.05.006.

Guibal, E. 2004. Interactions of metal ions with chitosan-based sorbents: A review. *Separation*

and Purification Technology. 38(1):43–74. DOI: 10.1016/j.seppur.2003.10.004.

Gupta, S. & Babu, B.. 2008. Economic Feasibility Analysis of Low cost Adsorbents for the Removal of Cr (VI) from Wastewater. *Birla Institute of Technology and Science (BITS)*. (Vi):1–7.

Gurung, M., Adhikari, B.B., Kawakita, H., Ohto, K., Inoue, K. & Alam, S. 2013. Recovery of gold and silver from spent mobile phones by means of acidothiourea leaching followed by adsorption using biosorbent prepared from persimmon tannin. *Hydrometallurgy*. 133:84–93. DOI: 10.1016/j.hydromet.2012.12.003.

Gyliene, O., Rekertas, R. & Šalkauskas, M. 2002. Removal of free and complexed heavy-metal ions by sorbents produced from fly (Musca domestica) larva shells. *Water Research*. 36(16):4128–4136. DOI: 10.1016/S0043-1354(02)00105-7.

Gyliene, O., Razmute, I., Tarozaite, R. & Nivinskiene, O. 2003. Chemical composition nd sorption properties of chitosan produced from fly larva shells. *Chemija (Vilnius)*. 14(3):121–127.

Hackman, R.H. 1953. ENZYMIC DEGRADATION OF CHITIN AND CHITIN ESTERS. *Division of entimology*. 168–178.

Hall, K.R., Eagleton, L.C., Acrivos, A. & Vermeulen, T. 1966. PORE- AND SOLID-DIFFUSION KINETICS IN FIXED-BED ADSORPTION UNDER CONSTANT- PATTE RN CONDITI0NS. *I&EC FUNDAMENTALS*. 5(2).

Hassan, S., Kim, S. & Jung, A. 2009. Biosorptive capacity of Cd (II) and Cu (II) by lyophilized cells of Pseudomonas stutzeri. *J. Gen. Appl. Microbiol*. 55:27–34. DOI: 10.1163/156853276X00016.

Haynes, W.M. 2010. *CRC Handbook of Chemistry and Physics, 91th Edition*. 91st ed. W.M. Haynes, Ed. CRC Press. DOI: 10.1136/oem.53.7.504.

Hem, J.D. & Cropper, W.H. 1962. Chemistry of Iron in Natural Water. *U.S. Geological Survey*. 1–31. DOI: 10.1063/1.3035572.

Herrero, R., Lodeiro, P., García-Casal, L.J., Vilariño, T., Rey-Castro, C., David, C. & Rodríguez, P. 2011. Full description of copper uptake by algal biomass combining an equilibrium NICA model with a kinetic intraparticle diffusion driving force approach. *Bioresource Technology*. 102(3):2990–2997. DOI: 10.1016/j.biortech.2010.10.007.

Ho, Y.S. & McKay, G. 1998. A COMPARISON OF CHEMISORPTION KINETIC MODELS APPLIED TO POLLUTANT REMOVAL ON VARIOUS SORBENTS. *Trans IChemE*. 76(November):332–340.

Ho, Y.S. & McKay, G. 1999. Pseudo-second order model for sorption processes. *Process Biochemistry*. 34(5):451–465. DOI: 10.1016/S0032-9592(98)00112-5.

Horowitz, T., Roseman, S. & Blumenthal, J. 1957. The Preparation of Glucosamine Oligosaccharides . I . Separation1s2. *J. am. Chem. Soc*. 79:5046–5049.

Hossain, M.S. & Iqbal, A. 2014. Production and characterization of chitosan from shrimp waste. *J. Bangladesh Agril. Univ*. 12(1):153–160.

Ibrahim, K.M., NasserEd-Deen, T. & Khoury, H. 2002. Use of natural chabazite-phillipsite tuff in wastewater treatment from electroplating factories in Jordan. *Environmental Geology*. 41(5):547–551. DOI: 10.1007/s002540100430.

Idrac, J., Mankowski, G., Thompson, G., Skeldon, P., Kihn, Y. & Blanc, C. 2007. Galvanic corrosion of aluminium-copper model alloys. *Electrochimica Acta*. 52(27 SPEC. ISS.):7626–

7633. DOI: 10.1016/j.electacta.2007.05.056.

Ilyas, S., Anwar, M.A., Niazi, S.B. & Afzal Ghauri, M. 2007. Bioleaching of metals from electronic scrap by moderately thermophilic acidophilic bacteria. *Hydrometallurgy*. 88(1–4):180–188. DOI: 10.1016/j.hydromet.2007.04.007.

Ilyas, S., Ruan, C., Bhatti, H.N., Ghauri, M.A. & Anwar, M.A. 2010. Column bioleaching of metals from electronic scrap. *Hydrometallurgy*. 101(3–4):135–140. DOI: 10.1016/j.hydromet.2009.12.007.

Indexmundi. 2017. *Commodity Prices - Price Charts, Data, and News - IndexMundi*. Available: http://www.indexmundi.com/commodities/ [2017, May 20].

Jaafarzadeh, N., Mengelizadeh, N. & Takdastan, A. 2014. Adsorption of Zn (II) from aqueous solution by using chitin extraction from crustaceous shell. *J Health Res*. 5(3).

Jacinto, M.L.J.A.J., David, C.P.C., Perez, T.R. & De Jesus, B.R. 2009. Comparative efficiency of algal biofilters in the removal of chromium and copper from wastewater. *Ecological Engineering*. 35(5):856–860. DOI: 10.1016/j.ecoleng.2008.12.023.

Jensen, W.B. 2002. Holleman-Wiberg's Inorganic Chemistry (edited by Wiberg, Nils). *Journal of Chemical Education*. 79(8):944. DOI: 10.1021/ed079p944.

Jeuniaux, C. & Voss-Foucart, M.F. 1991. Chitin biomass and production in the marine environment. *Biochemical Systematics and Ecology*. 19(5):347–356. DOI: 10.1016/0305-1978(91)90051-Z.

Johnson, D.B. & McGinness, S. 1991. Ferric iron reduction by acidophilic heterotrophic bacteria. *Applied and Environmental Microbiology*. 57(1):207–211.

Jong, B.W., Rhoads, S.C., Stubbs, A.M. & Stoelting, T.R. 1989. Recovery of principal metal values from waste hydroprocessing catalysts. *Report of Investigations - United States, Bureau of Mines*. (9252).

Jüttner, K., Galla, U. & Schmieder, H. 2000. Electrochemical approaches to environmental problems in the process industry. *Electrochimica Acta*. 45(15–16):2575–2594. DOI: 10.1016/S0013-4686(00)00339-X.

K.K.Panday, GurPrasad & V.N.Singh. 1985. Copper removal from aqueous solution by fly ash. *Water Research*. 19(7):869–873.

Kaewsarn P. 2002. Biosorption of copper(II) from aqueous solutions by pre-treated biomass of marine algae Padina sp. *Chemosphere*. 47:1081–1085.

Kallay, N., Preočanin, T., Kovačević, D., Lützenkirchen, J. & Villalobos, M. 2011. Thermodynamics of the Reactions at Solid/Liquid Interfaces. *Croatica Chemica Acta*. 84(1):1–10. DOI: 10.5562/cca1864.

Kansara, N., Bhati, L., Narang, M. & Vaishnavi, R. 2016. Wastewater treatment by ion exchange method: a review of past and recent researches. *Environmental Science - An Indian Journal*. 12(4):143–150. DOI: 10.1039/c2ee22769j.

Karimi, S., Ghahreman, A., Rashchi, F. & Moghaddam, J. 2017. Electrochemical kinetics of ferric-ferrous reduction-oxidation on sphalerite. *the Conference of Metallurgists*. (August).

Karthikeyan, G., Andal, N.M. & Anbalagan, K. 2005. Adsorption studies of iron (III) on chitin. *J. Chem. Sci*. 117(6):663–672.

Kasaai, M.R., Arul, J. & Charlet, G. 2013. Fragmentation of chitosan by acids. *The Scientific World Journal*. 2013. DOI: 10.1155/2013/508540.

Kaur, S. & Dhillon, G.S. 2014. The versatile biopolymer chitosan: Potential sources, evaluation of extraction methods and applications. *Critical Reviews in Microbiology*. 40(2):155–175. DOI: 10.3109/1040841X.2013.770385.

Kavitha, A.V. 2014. Extraction of precious metals from ores thereof. *Journal of Chemical and Pharmaceutical Sciences*. (3):147–149.

Kaya, M., Erdogan, S., Mol, A. & Baran, T. 2015. Comparison of chitin structures isolated from seven Orthoptera species. *International Journal of Biological Macromolecules*. 72:797–805. DOI: 10.1016/j.ijbiomac.2014.09.034.

Kaza, S., Yao, L., Bhada-Tata, P. & Van Woerden, F. 2018. *A Global Snapshot of Solid Waste Management to 2050*. Washington DC. DOI: 10.1596/978-1-4648-1329-0.

Kerroum, D., Mossaab, B.-L. & Abdesslam, M. 2012. Production of Biogas from Sludge Waste and Organic Fraction of Municipal Solid Waste. *Biogas*. (March). DOI: 10.5772/32718.

Khaliq, A., Rhamdhani, M.A., Brooks, G. & Masood, S. 2014. Metal Extraction Processes for Electronic Waste and Existing Industrial Routes: A Review and Australian Perspective. *Resources*. 3:152–179. DOI: 10.1016/j.wasman.2013.01.003.

Kim, E.Y., Kim, M.S., Lee, J.C. & Pandey, B.D. 2011. Selective recovery of gold from waste mobile phone PCBs by hydrometallurgical process. *Journal of Hazardous Materials*. 198:206–215. DOI: 10.1016/j.jhazmat.2011.10.034.

Kim, K.S., Zhao, Y., Jang, H., Lee, S.Y., Kim, J.M., Kim, K.S., Ahn, J.H., Kim, P., et al. 2009. Large-scale pattern growth of graphene films for stretchable transparent electrodes. *Nature*. 457(7230):706–710. DOI: 10.1038/nature07719.

Kiss, A.A., Lange, J.P., Schuur, B., Brilman, D.W.F., van der Ham, A.G.J. & Kersten, S.R.A. 2016. Separation technology–Making a difference in biorefineries. *Biomass and Bioenergy*. 95(January 2019):296–309. DOI: 10.1016/j.biombioe.2016.05.021.

El Knidri, H., Belaabed, R., El Khalfaouy, R., Laajeb, A., Addaou, A. & Lahsini, A. 2017. Physicochemical characterization of chitin and chitosan producted from Parapenaeus Longirostris shrimp shell wastes. *Journal of Materials and Environmental Science*. 8(10):3648–3653.

Knuckey, I., Sinclair, C., Surapaneni, A. & Ashcroft, W. 2004. Utilisation of seafood processing waste – challenges and opportunities . In *3rd Australian New Zealand Soils Conference*. 1–6.

Kojima, N. & Bates, G.W. 1979. The reduction and release of iron from Fe3+ ·Transferrin·CO32-. *Journal of Biological Chemistry*. 254(18):8847–8854.

Kokalj, F. & Samec, N. 2013. Combustion of Municipal Solid Waste for Power Production. *Advances in Internal Combustion Engines and Fuel Technologies*. DOI: 10.5772/55497.

Kouakou, U., Ello, A.S., Yapo, J.A. & Trokourey, A. 2013. Adsorption of iron and zinc on commercial activated carbon. *Journal of Environmental Chemistry and Ecotoxicology*. 5(6):168–171. DOI: 10.5897/JECE2013.0264.

Kumar, S., Zafar, M., Prajapati, J.K., Kumar, S. & Kannepalli, S. 2011. Modeling studies on simultaneous adsorption of phenol and resorcinol onto granular activated carbon from simulated aqueous solution. *Journal of Hazardous Materials*. 185(1):287–294. DOI: 10.1016/j.jhazmat.2010.09.032.

Kumari, S. & Rath, P.K. 2014. Extraction and Characterization of Chitin and Chitosan from (Labeo rohit) Fish Scales. *Procedia Materials Science*. 6(Icmpc):482–489. DOI: 10.1016/j.mspro.2014.07.062.

Kuper, J. & Hojsik, M. 2008. Poisoning the poor Electronic waste in Ghana. *Greenpeace International*. (August):0–20. Available: http://www.greenpeace.de/fileadmin/gpd/user_upload/themen/chemie/GhanaEWaste_FINAL.pdf.

Kurniawan, T.A., Chan, G.Y.S., Lo, W. hung & Babel, S. 2006. Comparisons of low-cost adsorbents for treating wastewaters laden with heavy metals. *Science of the Total Environment*. 366(2–3):409–426. DOI: 10.1016/j.scitotenv.2005.10.001.

Lamb, A.B. & Jacques, A.G. 1938. The Slow Hydrolysis of Ferric Chloride in Dilute Solution. 11. The Change in Hydrogen Ion Concentration. *J. am. Chem. Soc*. 60(5):1212–1225.

Lan, S., Wu, X., Li, L., Li, M., Guo, F. & Gan, S. 2013. Synthesis and characterization of hyaluronic acid-supported magnetic microspheres for copper ions removal. *Colloids and Surfaces A: Physicochemical and Engineering Aspects*. 425:42–50. DOI: 10.1016/j.colsurfa.2013.02.059.

Langmuir, I. 1918. The Adsorption of Gases on Plane Surfaces of Glass, Mica and Platinum. *J. Am. Chem. Soc.* 40(9):1361–1403. DOI: 10.1021/ja02242a004.

Lavall, R.L., Assis, O.B.G. & Campana-Filho, S.P. 2007. β-Chitin from the pens of Loligo sp.: Extraction and characterization. *Bioresource Technology*. 98(13):2465–2472. DOI: 10.1016/j.biortech.2006.09.002.

Lee, S.M. & Davis, A.P. 2001. REMOVAL OF CU (II) AND CD (II) FROM AQUEOUS SOLUTION BY SEAFOOD PROCESSING WASTE SLUDGE. *Water Research*. 35(2):534–540.

Legarth, J.B., Althing, L. & Baldo, G.L. 1995. Sustainability issues in circuit board recycling. *Proceedings of the 1995 IEEE International Symposium on Electronics and the Environment ISEE (Cat. No.95CH35718)*. 126–131. DOI: 10.1109/ISEE.1995.514963.

Lehohla, P. 2015. *Environmental Economics Accounts Compendium*. Pretoria.

Leodopoulos, C., Doulia, D., Gimouhopoulos, K. & Triantis, T.M. 2012. Single and simultaneous adsorption of methyl orange and humic acid onto bentonite. *Applied Clay Science*. 70:84–90. DOI: 10.1016/j.clay.2012.08.005.

Lewis, A.E. 2010. Review of metal sulphide precipitation. *Hydrometallurgy*. 104(2):222–234. DOI: 10.1016/j.hydromet.2010.06.010.

Li, A. & Khraisheh, M. 2007. Municipal solid waste used as bioethanol sources and its related environmental impacts. *Association for Environmental Health and Sciences - 23rd Annual International Conference on Soils, Sediments and Water 2007*. 13(1):167–171.

lijima, S. 1991. Helical microtubules of graphitic carbon. *Nature*. 354:56–58.

Lim, W.R., Kim, S.W., Lee, C.H., Choi, E.K., Oh, M.H., Seo, S.N., Park, H.J. & Hamm, S.Y. 2019. Performance of composite mineral adsorbents for removing Cu, Cd, and Pb ions from polluted water. *Scientific Reports*. 9(1):1–10. DOI: 10.1038/s41598-019-49857-9.

Liu, S., Sun, J., Yu, L., Zhang, C., Bi, J., Zhu, F., Qu, M., Jiang, C., et al. 2012. Extraction and characterization of chitin from the beetle Holotrichia parallela motschulsky. *Molecules*. 17(4):4604–4611. DOI: 10.3390/molecules17044604.

Liu, W. Te, Bien, M.Y., Chuang, K.J., Chang, T.Y., Jones, T., BéruBé, K., Lalev, G., Tsai, D.H., et al. 2014. Physicochemical and biological characterization of single-walled and double-walled carbon nanotubes in biological media. *Journal of Hazardous Materials*. 280:216–225. DOI: 10.1016/j.jhazmat.2014.07.069.

Loutseti, S., Danielidis, D.B., Economou-Amilli, A., Katsaros, C., Santas, R. & Santas, P. 2009. The application of a micro-algal/bacterial biofilter for the detoxification of copper and cadmium metal wastes. *Bioresource Technology*. 100(7):2099–2105. DOI: 10.1016/j.biortech.2008.11.019.

Lu, Y. & Wilkins, E. 1996. Heavy Metal Removal By Yeast Immobilized in Alginate. *J Hazardous Materials*. 49:165–179.

Lu, Y.W., Huang, C.P., Huang, Y.H., Lin, C.P. & Chen, H.T. 2008. Effect of pH on the oxidation of ferrous ion and immobilization technology of iron hydr(oxide) in fluidized bed reactor. *Separation Science and Technology*. 43(7):1632–1641. DOI: 10.1080/01496390801973656.

Luda, M.P. 2011. Recycling of Printed Circuit Boards. *Integrated Waste Management - Volume II*. 285–299. DOI: 10.5772/17220.

Luo, X., Zhang, Z., Zhou, P., Liu, Y., Ma, G. & Lei, Z. 2015. Synergic adsorption of acid blue 80 and heavy metal ions (Cu^{2+}/Ni^{2+}) onto activated carbon and its mechanisms. *Journal of Industrial and Engineering Chemistry*. 27:164–174. DOI: 10.1016/j.jiec.2014.12.031.

Lydall, M., Nyanjowa, W. & James, Y. 2017. *Mapping South Africa ' s Waste Electrical and Electronic Equipment (WEEE) Dismantling , Pre-Processing and Processing Technology Landscape Waste Research Development and Mapping South Africa ' s Waste Electrical and Electronic Equipment (WEEE) Dismant*. Randburg.

Mabuka, T., Harrison, S.T.L. & Govender-opitz, E. 2018. Recovery of Value from an Electronic Waste Stream using a Biological Matrix. *11th iCard IMWA MWD Conference -"Risk to Opportunity"*. 1087–1092.

MacaskieL, L.., Creamer, N.J., Essa, A.M.. & Brown, N.L. 2006. A New Approach for the Recovery of Precious Metals from Solution and From Leachates Derived From Electronic Scrap. *Biotechnology and Bioengineering*. 96(4):631–639. DOI: 10.1002/bit.

Madhavan, P. & Ramachandran Nair, G. 1974. Utilization of prwn waste-isolation of chtin and its conversion to chitosan. *Fishery technology*. 6(1):50–53.

Mahmoud, M.E., Osman, M.M., Hafez, O.F. & Elmelegy, E. 2010. Removal and preconcentration of lead (II), copper (II), chromium (III) and iron (III) from wastewaters by surface developed alumina adsorbents with immobilized 1-nitroso-2-naphthol. *Journal of Hazardous Materials*. 173(1–3):349–357. DOI: 10.1016/j.jhazmat.2009.08.089.

Majumdar, S.S., Das, S.K., Saha, T., Panda, G.C., Bandyopadhyoy, T. & Guha, A.K. 2008. Adsorption behavior of copper ions on Mucor rouxii biomass through microscopic and FTIR analysis. *Colloids and Surfaces B: Biointerfaces*. 63(1):138–145. DOI: 10.1016/j.colsurfb.2007.11.022.

Marchioretto, M.M., Bruning, H. & Rulkens, W. 2005. Heavy metals precipitation in sewage sludge. *Separation Science and Technology*. 40(16):3393–3405. DOI: 10.1080/01496390500423748.

Marković, D.D., Lekić, B.M., Rajaković-Ognjanović, V.N., Onjia, A.E. & Rajaković, L. V. 2014. A new approach in regression analysis for modeling adsorption isotherms. *The Scientific World Journal*. 2014. DOI: 10.1155/2014/930879.

Mecucci, A. & Scott, K. 2002. Electrochemical recovery of copper lead and tin from a nitrate and chloride leaching solutions of scrap printed circuit boards. *Chemical Technology and Biotechnology*. (77):449–457.

Menad, N., Bjorkman, B. & Allain, E.G. 1998. Combustion of plastics contained in electric and electronic scrap. *Resources, Conservation and Recycling*. 24(1):65–85. DOI: 10.1016/S0921-3449(98)00040-8.

Meunier, N., Drogui, P., Montané, C., Hausler, R., Mercier, G. & Blais, J.F. 2006. Comparison between electrocoagulation and chemical precipitation for metals removal from acidic soil leachate. *Journal of Hazardous Materials*. 137(1):581–590. DOI: 10.1016/j.jhazmat.2006.02.050.

Mikhailova, A.N., Faiberg, A.A., Gudkov, S.S. & Dementev, V.Y. 2015. New Technology of Base Metals Precipitation by Hydrogen Sulfide Obtained using Desulfurella Acetivorans and Desulfurella Kamchatkenis. *Advanced Materials Research*. 1130:477–481. DOI: 10.4028/www.scientific.net/AMR.1130.477.

Mirbagheri, S.A. & Hosseini, S.N. 2005. Pilot plant investigation on petrochemical wastewater treatment for the removal of copper and chromium with the objective of reuse. *Desalination*. 171(1):85–93. DOI: 10.1016/j.desal.2004.03.022.

Monhemius, A.J. 1977. Precipitation Diagrams for Metal Hydroxides, Sulphides, Arsenates and Phosphates. *Transactions of the Institution of Mining and Metallurgy, Section C: Mineral Processing and Extractive Metallurgy*. 86(December 1977).

Monser, L. & Adhoum, N. 2002. Modified activated carbon for the removal of copper, zinc, chromium and cyanide from wastewater. *Separation and Purification Technology*. 26(2–3):137–146. DOI: 10.1016/S1383-5866(01)00155-1.

Mubarok, M.Z. & Lieberto, J. 2013. Precipitation of Nickel Hydroxide from Simulated and Atmospheric-Leach Solution of Nickel Laterite Ore. *Procedia Earth and Planetary Science*. 6:457–464. DOI: 10.1016/j.proeps.2013.01.060.

Mukhopadhyay, M. 2008. Role of surface properties during biosorption of copper by pretreated Aspergillus niger biomass. *Colloids and Surfaces A: Physicochemical and Engineering Aspects*. 329(1–2):95–99. DOI: 10.1016/j.colsurfa.2008.06.052.

Mukhopadhyay, M., Noronha, S.B. & Suraishkumar, G.K. 2007. Kinetic modeling for the biosorption of copper by pretreated Aspergillus niger biomass. *Bioresource Technology*. 98(9):1781–1787. DOI: 10.1016/j.biortech.2006.06.025.

Musa, A.Y., Mohamad, A.B., Al-Amiery, A.A. & Tien, L.T. 2012. Galvanic corrosion of aluminum alloy (Al2024) and copper in 1.0M hydrochloric acid solution. *Korean Journal of Chemical Engineering*. 29(6):818–822. DOI: 10.1007/s11814-011-0233-z.

Muzzarelll, R.A.A. 1977. *Chitin*. Ancona: Pergamon press.

Nayyar, D. 2009. *Developing Countries in the World Economy: The Future in the Past?* Helsinki: UNU World Institute for Development Economics Research (UNU-WIDER).

Neale, J.W., Robertson, S.W., Muller, H.H. & Gericke, M. 2009. Integrated piloting of a thermophilic bioleaching process for the treatment of a low-grade nickel-copper sulphide concentrate. *Journal of the Southern African Institute of Mining and Metallurgy*. 109(5):273–293.

Neale, J.W., Gericke, M. & Ramcharan, K. 2011. The Application of Bioleaching To Base Metal Sulfides in Southern Africa : Prospects and Opportunities. *The Southern African Institute of Mining and Metallurgy*. 367–388.

Newbery, D. & Eberhard, A. 2008. *South African Network Infrastructure Review: Electricity*. Pretoria. DOI: 10.1016/j.enpol.2005.10.011.

Newton, L., Sheppard, C., Waston Wes, D., Burtle, G. & Dove, R. 2005. *USING THE BLACK SOLDIER FLY, Hermetia illucens, AS A VALUE-ADDED TOOL FOR THE MANAGEMENT OF SWINE MANURE*. RALEIGH.

Ngo, D.H. & Kim, S.K. 2014. *Antioxidant effects of chitin, chitosan, and their derivatives*. 1st

ed. V. 73. Elsevier Inc. DOI: 10.1016/B978-0-12-800268-1.00002-0.

Noor, S.N.M., Lim, J.W., Lam, M.K., Uemura, Y., Chew, T.L., Ho, Y.C. & Mohamad, M. 2018. Lipid and protein from black soldier fly larvae fed with self- fermented coconut waste medium. *Journal of Advanced Research in Fluid Mechanics and Thermal Sciences*. 46(1):88–95.

Nyakeri, E.M., Ogola, H.J., Ayieko, M.A. & Amimo, F.A. 2017. An open system for farming black soldier fly larvae as a source of proteins for smallscale poultry and fish production. *Journal of Insects as Food and Feed*. 3(1):51–56. DOI: 10.3920/JIFF2016.0030.

Ogungbuyi, O., Nnorom, I.C., Osibanjo, O. & Schluep, M. 2012. *e-Waste Country Assessment Nigeria*. e-Waste Africa project of the Secretariat of the Basel Convention. Available: http://www.ewasteguide.info/files/Ogungbuyi_2012_BCCC-Empa.pdf.

Orzali, L., Corsi, B., Cinzia, F. & Riccioni, L. 2018. Chitosan in Agriculture: A New Challenge for Managing Plant Disease. *Intech open*. 2:64. DOI: 10.5772/32009.

Ouki, S.K. & Kavannagh, M. 1997. Performance of Natural Zeolites for the Treatment of Mixed Metal-Contaminated Effluents. *Waste Management & Research*. 15:383–394.

Pagnanelli, F., Esposito, A., Toro, L. & Vegliò, F. 2003. Metal speciation and pH effect on Pb, Cu, Zn and Cd biosorption onto Sphaerotilus natans: Langmuir-type empirical model. *Water Research*. 37(3):627–633. DOI: 10.1016/S0043-1354(02)00358-5.

Panão, A.S.I., Carvalho, J.M.R. De & Correia, M.J.N. 2006. Copper Removal from Sulphuric Leaching Solutions by Cementation. Technical University of Lisbon. Available: https://fenix.tecnico.ulisboa.pt/downloadFile/395137462214/Artigo_Cementacao.pdf.

Panday, K.K., Prasad, G. & Singh, V.N. 1986. USE OF WOLLASTONITE FOR THE TREATMENT OF Cu(II) RICH EFFLUENTS. *Water, Air, and Soil Pollution*. 27(Ii):287–296.

Peniston, Q.P. & Johnson, E.L. 1975. *Patent No. US 3922260 A*. USA.

Petrat, F., Paluch, S., Dogruöz, E., Dörfler, P., Kirsch, M., Korth, H.G., Sustmann, R. & De Groot, H. 2003. Reduction of Fe(III) ions complexed to physiological ligands by lipoyl dehydrogenase and other flavoenzymes in vitro: Implications for an enzymatic reduction of Fe(III) ions of the labile iron pool. *Journal of Biological Chemistry*. 278(47):46403–46413. DOI: 10.1074/jbc.M305291200.

Pham Van, A. 2009. GOLD BIOLEACHING OF ELECTRONIC SCRAP MATERIAL BY CYANOGENIC BACTERIA AND ITS ENHANCEMENT WITH BIOOXIDATION. National university of singapore.

Prabu, K. & Natarajan, E. 2012. Isolation and FTIR spectroscopy characterization of chitin from local sources. *Advances in Applied Science Research*. 3(2):1870–1875.

Prado Acosta, M., Valdman, E., Leite, S.G.F., Battaglini, F. & Ruzal, S.M. 2005. Biosorption of copper by Paenibacillus polymyxa cells and their exopolysaccharide. *World Journal of Microbiology and Biotechnology*. 21(6–7):1157–1163. DOI: 10.1007/s11274-005-0381-6.

Preston, F., Lehne, J. & Wellesley, L. 2019. *An Inclusive Circular Economy Priorities for Developing Countries*. London.

Prokkola, H., Nurmesniemi, E. & Lassi, U. 2020. Prokkola, Nurmesniemi, Lassi - 2020 - Removal of metals by sulphide precipitation using na2s and hs−-solution.pdf. *ChemEngineering*. 4(51).

Pumera, M. 2011. Graphene in biosensing. *Materials Today*. 14(7–8):308–315. DOI: 10.1016/S1369-7021(11)70160-2.

Qian, K., Kumar, A., Patil, K., Bellmer, D., Wang, D., Yuan, W. & Huhnke, R.L. 2013. Effects of biomass feedstocks and gasification conditions on the physiochemical properties of char. *Energies*. 6(8):3972–3986. DOI: 10.3390/en6083972.

Radmehr, V., Koleini, S.M.J., Khalesi, M.R. & Tavakoli, M.R. 2012. Ammonia Leaching in the Copper Industry : a Review. *XXVI International Mineral Processing Congress (IMPC)*. (487):2512–2523.

Ren, Y., Zhang, M. & Zhao, D. 2008. Synthesis and properties of magnetic Cu(II) ion imprinted composite adsorbent for selective removal of copper. *Desalination*. 228(1–3):135–149. DOI: 10.1016/j.desal.2007.08.013.

Renu, Agarwal, M. & Singh, K. 2016. Heavy metal removal from wastewater using various adsorbents: a review. *Journal of Water Reuse and Desalination*. 7(4):387–419. DOI: 10.2166/wrd.2016.104.

Rhazi, M., Desbrières, J., Tolaimate, a, Alagui, a & Vottero, P. 2000. Investigation of different natural sources of chitin: influence of the source and deacetylation process on the physicochemical characteristics of chitosan. *Polymer International*. 49(4):337–344. DOI: 10.1002/(SICI)1097-0126(200004)49:4<337::AID-PI375>3.0.CO;2-B.

Rhazi, M., Desbrières, J., Tolaimate, A., Rinaudo, M., Vottero, P., Alagui, A. & El Meray, M. 2002. Influence of the nature of the metal ions on the complexation with chitosan. Application to the treatment of liquid waste. *European Polymer Journal*. 38(8):1523–1530. DOI: 10.1016/S0014-3057(02)00026-5.

Rigby, G.W. 1936. *Patent No. US 2047226 A*. USA.

Romera, E., González, F., Ballester, A., Blázquez, M.L. & Muñoz, J.A. 2007. Comparative study of biosorption of heavy metals using different types of algae. *Bioresource Technology*. 98(17):3344–3353. DOI: 10.1016/j.biortech.2006.09.026.

Şahan, T., Ceylan, H., Şahiner, N. & Aktaş, N. 2010. Optimization of removal conditions of copper ions from aqueous solutions by Trametes versicolor. *Bioresource Technology*. 101(12):4520–4526. DOI: 10.1016/j.biortech.2010.01.105.

Schluep, M., Wasswa, J., Kreissler, B. & Nicholson, S. 2008. e-WASTE GENERATION AND MANAGEMENT IN UGANDA. *Waste Management*. (October):510–515.

Schluep, M., Rochat, D., Munyua, A.W., Laissaoui, S.E., Wone, S., Kane, C. & Hieronymi, K. 2008. Assessing the e-waste situation in Africa. *Electronics*. (June):8–10.

Schluep, M., Manhart, A., Osibanjo, O., Rochat, D., Isarin, N. & Mueller, E. 2011. *Where are WEee in Africa?* Dübendorf. Available: file:///E:/USUARIO/Downloads/UNEP-CHW-EWASTE-PUB-WeeAfricaReport.English.pdf.

Schmuhl, R., Krieg, H.M. & Keizer, K. 2001. Adsorption of Cu(II) and Cr(VI) ions by chitosan: Kinetics and equilibrium studies. *Water SA*. 27(1):1–7. DOI: 10.1016/j.orgel.2018.04.039.

Senthilkumar, G. & Murugappan, A. 2015. Multicomponent Adsorption Isotherm Studies on Removal of Multi Heavy Metal Ions in MSW Leachate using Fly Ash. *International Journal of Engineering Research & Technology (IJERT)*. 4(08):58–66.

Sharp, R. 2013. A Review of the Applications of Chitin and Its Derivatives in Agriculture to Modify Plant-Microbial Interactions and Improve Crop Yields. *Agronomy*. 3(4):757–793. DOI: 10.3390/agronomy3040757.

Shim, J.W., Park, S.J. & Ryu, S.K. 2001. Effect of modification with HNO3and NaOH on metal adsorption by pitch-based activated carbon fibers. *Carbon*. 39(11):1635–1642. DOI: 10.1016/S0008-6223(00)00290-6.

Simonin, J. & Boute, J. 2016. Intraparticle diffusion-adsorption model to describe liquid/solid adsorption kinetics. *Revista Mexicana de Ingenier´ıa Qu´ımica Vol.* 15(1):161–173.

Singh, A.K., Singh, D.P., Panday, K.K. & Singh, V.N. 1988. Wollastonite as adsorbent for removal of Fe(II) from water. *Journal of Chemical Technology & Biotechnology*. 42(1):39–49. DOI: 10.1002/jctb.280420106.

Singh, V., Joung, D., Zhai, L., Das, S., Khondaker, S.I. & Seal, S. 2011. Graphene based materials: Past, present and future. *Progress in Materials Science*. 56(8):1178–1271. DOI: 10.1016/j.pmatsci.2011.03.003.

Sist, C. & Demopoulos, G.P. 2003. Nickel Hydroxide Precipitation from Aqueous Sulfate Media. *JOM - Journal of the Minerals, Metals and Materials Society*. (August):43–46.

Skopp, J. 2009. Derivation of the freundlich adsorption isotherm from kinetics. *Journal of Chemical Education*. 86(11):1341–1343. DOI: 10.1021/ed086p1341.

Sommer, L. 1989. *Analytical absorption spectrophotometry in the visible and ultraviolet the principles*. V. 7. DOI: 10.1016/B978-0-444-98882-9.50007-4.

Srivastava, V.C., Mall, I.D. & Mishra, I.M. 2009. Competitive adsorption of cadmium(II) and nickel(II) metal ions from aqueous solution onto rice husk ash. *Chemical Engineering and Processing: Process Intensification*. 48(1):370–379. DOI: 10.1016/j.cep.2008.05.001.

St-Hilaire, S., Cranfill, K., McGuire, M.A., Mosley, E.E., Tomberlin, J.K., Newton, L., Sealey, W., Sheppard, C., et al. 2007. Fish Offal Recycling by the Black Soldier Fly Produces a Foodstuff High in Omega-3 Fatty Acids SOPHIE. *JOURNAL OF THE WORLD AQUACULTURE SOCIETY*. 38(2):309–313.

Straathof, A.J.J. 2011. *The Proportion of Downstream Costs in Fermentative Production Processes*. Second Edi ed. V. 2. Elsevier B.V. DOI: 10.1016/B978-0-08-088504-9.00492-X.

Stumm, W. & Lee, G.F. 1961. Oxygenation of Ferrous Iron. *Industrial & Engineering Chemistry*. 53(2):143–146. DOI: 10.1021/ie50614a030.

Suchiva, K., Chandrkrachang, S., Methacanon, P. & Peter, M.G. 2002. *Proceedings of the 5th Asia Pacific Chitin and Chitosan Symposium & Exhibition*. Bangkok.

Suponik, T. 2010. Ensuring permeable reactive barrier efficacy and longevity. *Archives of Environmental Protection*. 36(3):59–73.

Szalatkiewicz Jakub. 2014. Metals Content in Printed Circuit Board Waste. *Polish Journal of Environmental Studies*. 23(6):2365–2369.

Takeda, M. & Abe, E. 1962. Isolation of crustacean chitin. Decalcification by disodium ethylenediaminotetraacetate and enzymic hydrolysis of incidental proteins. *Norisho Suisan Koshusho Kenkyu Hokoku*. 11:339–406.

Tetteh, A.Y. 1991. Optimization studies on Chitin extraction from crustacean solid wastess. McGill University.

Van Toan, N. & Hanh, T.T. 2013. Application of chitosan solutions for rice production in Vietnam. *African Journal of Biotechnology*. 12(4):382–384. DOI: 10.5897/AJB12.2884.

Trung, T.S. & Bao, H.N.D. 2015. Physicochemical Properties and Antioxidant Activity of Chitin and Chitosan Prepared from Pacific White Shrimp Waste Trang. *International journal of Carbohydrate Chemistry*. 2(4):1–6. DOI: http://dx.doi.org/10.1155/2015/706259 Research.

Tschirner, M. & Simon, A. 2015. Influence of different growing substrates and processing on the nutrient composition of black soldier fly larvae destined for animal feed. *Journal of Insects*

as Food and Feed. 1(4):249–259. DOI: 10.3920/JIFF2014.0008.

Tunali, S., Çabuk, A. & Akar, T. 2006. Removal of lead and copper ions from aqueous solutions by bacterial strain isolated from soil. *Chemical Engineering Journal*. 115(3):203–211. DOI: 10.1016/j.cej.2005.09.023.

United Nations. 2018. *Circular Economy: The New Normal?*

Veeken, A.H.. & Rulkens, W.H. 2014. Innovative developments in the selective removal and reuse of heavy metals from wastewaters . PubMed Commons. (October):12862211.

Veit, H.M., Bernardes, A.M., Ferreira, J.Z., Tenório, J.A.S. & Malfatti, C. de F. 2006. Recovery of copper from printed circuit boards scraps by mechanical processing and electrometallurgy. *Journal of Hazardous Materials*. 137(3):1704–1709. DOI: 10.1016/j.jhazmat.2006.05.010.

Viadero, R.C., Wei, X. & Buzby, K.M. 2006. Characterization and dewatering evaluation of acid mine drainage sludge from ammonia neutralization. *Environmental Engineering Science*. 23(4):734–743. Available: http://0-ovidsp.ovid.com.wam.city.ac.uk/ovidweb.cgi?T=JS&PAGE=reference&D=emed7&NEWS=N&AN=2006391381.

Vijayaraghavan, K., Jegan, J.R., Palanivelu, K. & Velan, M. 2005. Nickel Recovery from Aqueous Solution Using Crab Shell Particles. *Adsorption Science & Technology*. 23(4):303–311. DOI: 10.1260/0263617054770002.

Wan, M.-W., Petrisor, I.G., Lai, H., Kim, D. & Yen, T.F. 2004. Copper adsorption through chitosan immobilized on sand to demonstrate the feasibility for in situ soil decontamination. *Polymers*. 55:249–254. DOI: 10.1016/j.carbpol.2003.09.009.

Wang, Y.-S. & Shelomi, M. 2017. Review of Black Soldier Fly (Hermetia illucens) as Animal Feed and Human Food. *Foods*. 6(10):91. DOI: 10.3390/foods6100091.

Wang, B., Bai, Z., Jiang, H., Prinsen, P., Luque, R., Zhao, S. & Xuan, J. 2019. Selective heavy metal removal and water purification by microfluidically-generated chitosan microspheres: Characteristics, modeling and application. *Journal of Hazardous Materials*. 364(October):192–205. DOI: 10.1016/j.jhazmat.2018.10.024.

Wang, J., Bai, J., Xu, J. & Liang, B. 2009. Bioleaching of metals from printed wire boards by Acidithiobacillus ferrooxidans and Acidithiobacillus thiooxidans and their mixture. *Journal of Hazardous Materials*. 172(2–3):1100–1105. DOI: 10.1016/j.jhazmat.2009.07.102.

Wang, P.L., Ponou, J., Seiji, M., Katsunori, O., Gjergj, D., Tatsuki, N. & Toyohisa, F. 2014. Selective Precipitation of Copper and Zinc over Iron from Acid Mine Drainage by Neutralization and Sulfidization for Recovery. *J. Soc. Mater. Eng. Resour*. 20(2):136–140. DOI: 10.5188/ijsmer.20.136.

Waśko, A., Bulak, P., Polak-Berecka, M., Nowak, K., Polakowski, C. & Bieganowski, A. 2016. The first report of the physicochemical structure of chitin isolated from Hermetia illucens. *International Journal of Biological Macromolecules*. 92(December 2017):316–320. DOI: 10.1016/j.ijbiomac.2016.07.038.

Watling, H. 2016. Microbiological Advances in Biohydrometallurgy. *Minerals*. 6(49):1–19. DOI: 10.3390/min6020049.

Weber Jr, W.J., Morris, J.C. & Sanit, J. 1963. Kinetics of Adsorption on Carbon from Solution. *Journal of the Sanitary Engineering Division*. 89:31–38.

Whistler, R.S. & BeMiller, J.N. 1962. Chitin. *J. Org. Chem*. 27:1161–1163.

Willner, J. & Fornalczyk, A. 2013. Extraction of metals from electronic waste by bacterial

leaching. *Environment Protection Engineering*. 39(1):197–208. DOI: 10.5277/EPE130115.

Wong, C.Y., Rosli, S.S., Uemura, Y., Ho, Y.C., Leejeerajumnean, A., Kiatkittipong, W., Cheng, C.K., Lam, M.K., et al. 2019. Potential protein and biodiesel sources from black soldier fly larvae: Insights of larval harvesting instar and fermented feeding medium. *Energies*. 12(8). DOI: 10.3390/en12081570.

Wong, S.S., Joselevich, E., Wololly, A.T., Cheung, C.L. & Lieber, C.M. 1998. Covalently functionalized nanotubesasnanometre- sizedprobes in chemistryandbiology. *Nature*. 97(2):538–540. DOI: 10.1073/pnas.97.2.538.

Wood, A.R. 2017. Fungi and invasions in South Africa. *Bothalia*. 47(2):1–16. DOI: 10.4102/abc.v47i2.2124.

World Economic Forum. 2018. *Recovery of Key Metals in the Electronics Industry in the People' s Republic of China : An Opportunity in Circularity*.

Xu, Y., Li, J. & Lililua. 2016. Current Status and Future Perspective of Waste Printed Circuit Boards Recycling. *Procedia Environmental Sciences*. 31(0):162–170. DOI: http://dx.doi.org/10.1016/j.proenv.2012.10.081.

Xu, Z., Cai, J. & Pan, B. 2013. Mathematically modeling fixed-bed adsorption in aqueous systems. *Journal of Zhejiang University SCIENCE A*. 14(3):155–176. DOI: 10.1631/jzus.A1300029.

Yakout, S.M. & Elsherif, E. 2010. Batch kinetics, isotherm and thermodynamic studies of adsorption of strontium from aqueous solutions onto low cost rice-straw based carbons. *Carbon - Science and Technology*. 3(1):144–153. DOI: 10.1080/07352680590910410.

Yang, Y., Chen, S., Li, S., Chen, M., Chen, H. & Liu, B. 2014. Bioleaching waste printed circuit boards by Acidithiobacillus ferrooxidans and its kinetics aspect. *Journal of Biotechnology*. 173(1):24–30. DOI: 10.1016/j.jbiotec.2014.01.008.

Yen, M. & Mau, J. 2006. Preparation of fungal chitin and chitosan from shiitake stipes. *Fung. Sci.* 21((1,2)):1–11.

Yi, L. 2015. *A study on the potential of insect protein and lipid as a food source*. Available: http://edepot.wur.nl/330195.

Young, C., Taylor, P., Anderson, C. & Choi, Y. 2008. *Hydrometallurgy 2008, Preceedings og the Sixth international Symposium*. Littleton: Society for Mining, Metallurgy, and Exploration, Inc.

Yu, J., Tong, M., Sun, X. & Li, B. 2008. Enhanced and selective adsorption of Pb2+ and Cu2+ by EDTAD-modified biomass of baker's yeast. *Bioresource Technology*. 99(7):2588–2593. DOI: 10.1016/j.biortech.2007.04.038.

Yunus, P.A. & Sengupta, B. 2016. E-Waste Indian Perspective And Recovery of Valuable Metals From E-Waste-A Review. *International Refereed Journal of Engineering and Science (IRJES)*. 5(4):70–80.

Zamzow, M.J., Eichbaum, B.R., Sandgren, K.R. & Shanks, D.E. 1990. REMOVAL OF HEAVY METALS AND OTHER CATIONS FROM WASTEWATER USING ZEOLITES. *Separation Science and Technology*. 25(February 2013):13–15. DOI: 10.1080/01496399008050409.

Zhang, M., Haga, A., Sekiguchi, H. & Hirano, S. 2000. Structure of insect chitin isolated from beetle larva cuticle and silkworm (Bombyx mori) pupa exuvia. *International Journal of Biological Macromolecules*. 27(1):99–105. DOI: 10.1016/S0141-8130(99)00123-3.

Zhou, D., Zhang, L., Zhou, J. & Guo, S. 2004. Cellulose/chitin beads for adsorption of heavy

metals in aqueous solution. *Water Research*. 38(11):2643–2650. DOI: 10.1016/j.watres.2004.03.026.

Appendix:

A1 Literature Review Figures and Tables

Table A1. 1: Fungal biomass, yeast, algal biomass, bacteria, chitosan and chitin, zeolites, clay, peat, fly ash, industrial waste, activated carbon, magnetic adsorbents and alumina copper adsorption capacities and best model fit, process pH, initial copper concentration, contact time and adsorbent dose for bio-sorbents.

	Adsorbent	Initial metal concentration (mg/L)	pH	Best model fit	Contact time (min)	Adsorbent dose (g/L)	Adsorption capacity (mg/g)	Reference
Fungal biomass	Aspergillus niger	10-100	6	Langmuir and Freundlich			23.6	(Mukhopadhyay, 2008)
	Mucor rouxii	10-1000	5-6	Langmuir	4320	0.25	52.6	(Majumdar et al., 2008)
	Rhizopus oryazae filamentous fungus	20-200	4-6	Langmuir	200	1	19.4	(Bhainsa & D'Souza, 2008)
	Trametes versicolor	37-80	5.5 1	Plackett-Burman	80	1	61.0	(Şahan et al., 2010)
	Aspergillus niger	10-100	6	Langmuir and Freundlich	30	2-5	23.6	(Mukhopadhyay et al., 2007)
Yeast	Caustic-treated Saccharomyces cerevisiae yeast biomass	16-18	5	Langmuir and Freundlich	2160	2	9.01	(Lu & Wilkins, 1996)
	Saccharomyces cerevisiae biomass	25-200	3-4	Freundlich, Langmuir, Redlich-Peterson		15	2.59	(Cojocaru et al., 2009)
	Baker's yeast	100	2.7-6	Langmuir	250	1	65.0	(Yu et al., 2008)
Algal biomass	Padina sp.	127	5	Langmuir	30	2	50.9	(Kaewsarn P., 2002)
	Macroalga, Sargassum muticum	15-190	4.5	Modified competitive Langmuir	240	5	71.0	(Herrero et al., 2011)
	Cystoseira crinitophylla biomass	25, 40,50	4.5	Langmuir and Freundlich	720	2.5	160	(Christoforidis et al., 2015)
	Sargassum, Chlorococcum	1-100	4.5	Langmuir and Freundlich	300	0.1	71.4	(Jacinto et al., 2009)
	Codium vermilara	10-150	5	Langmuir	120	0.5	16.5	(Romera et al., 2007)
	Dried micro-algal/ bacterial biomass	10-1000	4	Langmuir	120	0.4	31.0	(Loutseti et al., 2009)
Bacteria	Paenibacillus polymyxa	25-5000	6	Langmuir	120		112	(Prado Acosta et al., 2005)
	Pseudomonas stutzeri	30-100	5	Langmuir and Freundlich	30	1	36.2	(Hassan et al., 2009)
	Sphaerotilus natans (Gram-negative bacteria)			Langmuir	30	1	44.5	(Pagnanelli et al., 2003)
	Bacillus sp. (bacterial strain isolated from soil)	100	5	Langmuir	30	2	16.3	(Tunali et al., 2006)
	Sphaerotilus natans	100	6	Langmuir	150	3	60.0	(Beolchini et al., 2006)
Chitosan and chitin	Chitosan						222	(Findon et al., 1993)
	Non-cross-linked chitosan						86.0	(Schmuhl et al., 2001)
	Cellulose/chitin beads						19.1	(Zhou et al., 2004)

	Chitosan immobilized on sand						260	(Wan et al., 2004)
	chitosan						76.2	(Rhazi et al., 2002)
Zeolites	Clinoptilolite						1.64	(Zamzow et al., 1990)
	Chabazite						5.10	(Ouki & Kavannagh, 1997)
	Chabazite–phillipsite						0.370	(Ibrahim et al., 2002)
Clay	Fly ash-wollastonite						1.18	(Panday et al., 1986)
	bentonite clay						11.9	(Bertagnolli et al., 2011)
	Bofe bentonite calcinated clay						19.1	(de Almeida Neto et al., 2014)
Peat	Eutrophic peat						19.6	(Chen et al., 1990)
	Oligotrophic peat						12.1	(Gosset et al., 1986)
Fly ash	Fly ash						1.39	(K.K.Panday et al., 1985)
	Fly ash–wollastonite						1.18	(Singh et al., 1988)
Industrial waste	Waste slurry						21.0	(Lee & Davis, 2001)
	Blast-furnace slag sawdust						13.8	(Ajmal et al., 1998)
Activated carbon	GAC						38.0	(Monser & Adhoum, 2002)
	As-received ACF						9.00	(Shim et al., 2001)
	Oxidized ACF						30.0	(Babić et al., 2002)
Magnetic adsorbents	Cu(II) ion imprinted composite adsorbent (Cu(II)-MICA).						71.4	(Ren et al., 2008)
	hyaluronic acid supported magnetic microspheres			Freundlich			12.2	(Lan et al., 2013)
	pectin-coated iron oxide magnetic nanocomposite			Langmuir and Freundlich			49.0	(Gong et al., 2012)
Alumina	γalumina nanoparticles			Freundlich			31.3	(Fouladgar et al., 2015)
	alumina adsorbents with 1-nitroso-2-napthol as a cation exchanger						28.6	(Mahmoud et al., 2010)
	aminated mesoporous alumina						7.92	(Lee & Davis, 2001)

A2 Method developments

The need to reduce cost and time in the quantification of metals in solution led to research into spectrophotometric assays that can be used in the quantification of metals in the model leachate solution during the adsorption, desorption and precipitation studies. Spectrophotometry is regarded as a cheaper and more rapid method for the quantification of metals in solution than Inductively Coupled Plasm Spectrometry (ICPS) and Atomic Emission Spectrometry (AES) (Sommer, 1989). The model leachate solution contains iron, copper and aluminum. Spectrophotometric assays for the three metals were adapted/developed to be applicable to the model leachate solution. The criterion in the choice of these assays was their ability to work in acidic conditions and to quantify metals in the presence of other metals.

A2.1 Adaptation of a spectrophotometric copper assay

A spectrophotometric copper assay was adapted from Ahmed et al (2004) using 2,5-Dimercapto-1,3,4-thiadiazole (DMTD) as a reagent in the spectrophotometry determination of copper (II). Ahmed et al (2004), showed that the method was based on the complex formation of copper (II) with DMTD in acidic medium at room temperature. The complex formed was yellow-orange and had a maximum absorption wavelength at 390 nm obeying Beer's law at a copper concentration range of 0.1 to 20 ppm and 0.1 to 10 ppm in the presence of masking agents. Interference due to zinc (II), cadmium (II), nickel (II), cobalt (II), chromium (III) and several anions was masked using 1g/L citric acid, 0.2 g/L Potassium sodium tartrate and 0.1 g/L 1,10-phenanthroline. The method was adapted as described in Ahmed et al (2004). Calibration curve of the Copper-DMTD assay without and with masking agents are shown in Figure A3. 1 and Figure A3. 2. Table A2. 1 shows the application of the Copper-DMTD assay in a model PCB leachate solution with varying metal concentrations.

Table A2. 1: Concentration of Copper found using Copper-DMTD assay with masking agents on the PCB model leachate solution with varying metal concentrations.

Sample No.	Cu^{2+} (mg/L)	Fe^{2+} (mg/L)	Al^{3+} (mg/L)	Ni^{2+} (mg/L)	Zn^{2+} (mg/L)	Concentration Cu^{2+} found (mg/L)	Relative error (%)
1	2.00	0	0	0	0	2.06	2.82
2	2.00	62	76.1	16.3	28.9	2.02	0.76
3	2.00	40	76.1	16.3	28.9	1.91	-4.65
4	2.00	45	20	10	26	1.90	-5.01

The Copper-DMTD assay was able to quantify the copper in the Model leachate solution with relative errors between -5.01 % to 2.82 % indicating high accuracy. The Copper-DMTD was therefore adopted for the quantification of copper concentration in the adsorption, desorption and precipitation studies.

A2.2 Adaptation of a spectrophotometric aluminium assay

A spectrophotometric aluminium assay was adapted from Ahmed & Hossan (1995) using Morin as a reagent in the spectrophotometry determination of aluminium. Ahmed & Hossan (1995) showed that the method was based on the complex formation of aluminium with Morin in acidic medium at room temperature. The complex formed was deep yellow and had a maximum absorption wavelength at 421 nm obeying Beer's law at an aluminium concentration range of 0.005 to 3 ppm in the absence/presence of masking agents. Interference due to zinc (II), cadmium (II), nickel (II), cobalt (II), chromium (III) and several anions was masked using 10 g/L Potassium sodium tartrate and 0.1 g/L. The method was adapted as described in Ahmed & Hossan (1995). Calibration curves of the Aluminium-Morin assay without and with masking agents are shown in Figure A3. 3 and Figure A3. 4. Table A2. 2 shows the application of the Copper-DMTD assay in a model PCB leachate solution with varying metal concentrations.

Table A2. 2: Concentration of Aluminium found using Aluminium-Morin assay with masking agents on the PCB model leachate solution with varying metal concentrations.

Sample No.	**Cu^{2+} (mg/L)**	**Fe^{2+} (mg/L)**	**Al^{3+} (mg/L)**	**Ni^{2+} (mg/L)**	**Zn^{2+} (mg/L)**	**Concentration Al^{3+} found (mg/L)**	***Relative error (%)***
1	0	0	1.5	0	0	1.51	0.528
2	34.9	62	1.5	16.3	28.9	1.55	3.29
3	34.9	40	1.5	16.3	28.9	1.49	-0.805
4	34.9	45	1.5	10	26	1.52	1.38

The Aluminium-Morin assay was able to quantify the aluminium in the Model leachate solution with relative errors between -0.67 % to 3.33 % indicating high accuracy. The Aluminium-Morin assay was therefore adopted for the quantification of aluminium concentration in the adsorption, desorption and precipitation studies.

A2.3 Adaptation and development of a spectrophotometric iron assay

A spectrophotometric iron assay was adapted from Govender et al. (2012) using hydrochloric acid as a reagent in the spectrophotometry determination of aluminium. Govender et al. (2012) showed that the method was based on the complex formation of iron with chloride ions in acidic medium at room temperature. The complex formed was yellow and had a maximum absorption wavelength at 340 nm obeying Beer's law at an iron concentration range of 0 to 75 ppm. The assay could be used to quantify both ferric and total iron concentration. Govender et al. (2012) showed that the assay is precise and accurate even in the presence of up to 10 g/L of copper at 340 nm however the interference of aluminium, zinc and nickel were not investigated. Figure A2. 1 shows the absorbance spectra of the ferric chloride assay with 50 mg/L ferric iron in the absence and presence of the PCB leachate metals (copper, aluminium, zinc and nickel). Presence of copper, aluminium, zinc and nickel resulted in a shift in the maximum absorbance in the ferric chloride assay to 285 nm. The shift indicates interference by the present metals on the ferric chloride assay motivating for the need for masking agents. Masking agents used in Ahmed et al (2004) were adopted. The method was adapted as described in Govender et al. (2012) however 1 mL of masking agents of 1g/L citric acid and

0.2 g/L Potassium sodium tartrate were added. Calibrations of the Iron-Chloride assay without masking agents and with masking agents are shown in Figure A3. 5 and Figure A3. 6.

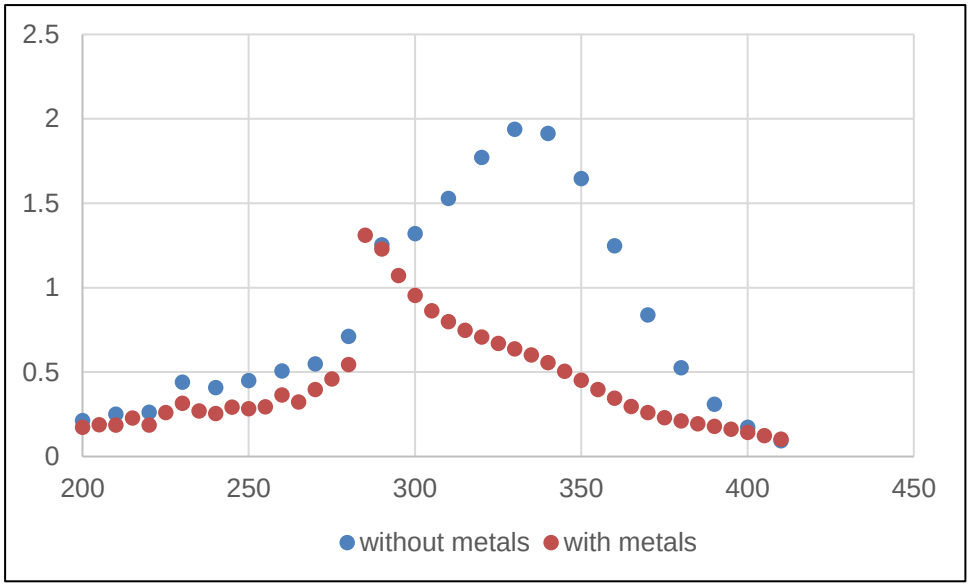

Figure A2. 1: : Absorbance spectra of the ferric chloride assay with 50 mg/L ferric iron in the absence and presence of the PCB leachate metals (copper, aluminium, zinc and nickel)

Table A2. 3 shows the application of the Ferric-Chloride assay in a model PCB leachate solution with varying metal concentrations.

Table A2. 3: Concentration of iron found using Ferric-Chloride assay with masking agents on the PCB model leachate solution with varying metal concentrations

Sample No.	Cu^{2+} (mg/L)	Fe^{2+} (mg/L)	Al^{3+} (mg/L)	Ni^{2+} (mg/L)	Zn^{2+} (mg/L)	Concentration Fe^{3+} found (mg/L)	Relative error (%)
1	0	10	0	0	0	10.0	-0.32
2	100	10	40	16.3	28.9	10.5	5.04
3	40	10	100	16.3	28.9	10.5	5.03
4	100	10	180	10	26	10.3	3.27

The Ferric-Chloride assay was able to quantify the iron in the model PCB leachate solution with relative errors between 2 % to 5 % indicating accuracy high accuracy. The Ferric-Chloride assay was therefore adopted for the quantification of ferric and total iron concentration in the adsorption, desorption and precipitation studies.

A3 Spectrophotometry calibration curves

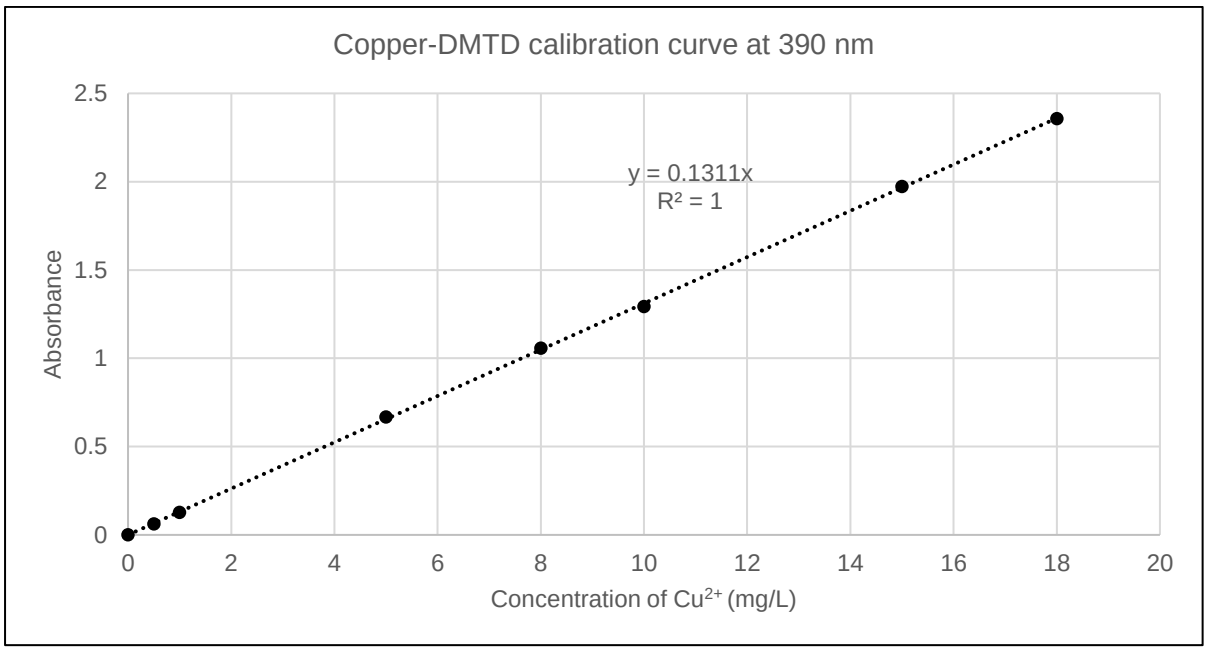

Figure A3. 1: Calibration curve for the Copper (II)-DMTD assay (without masking agents)

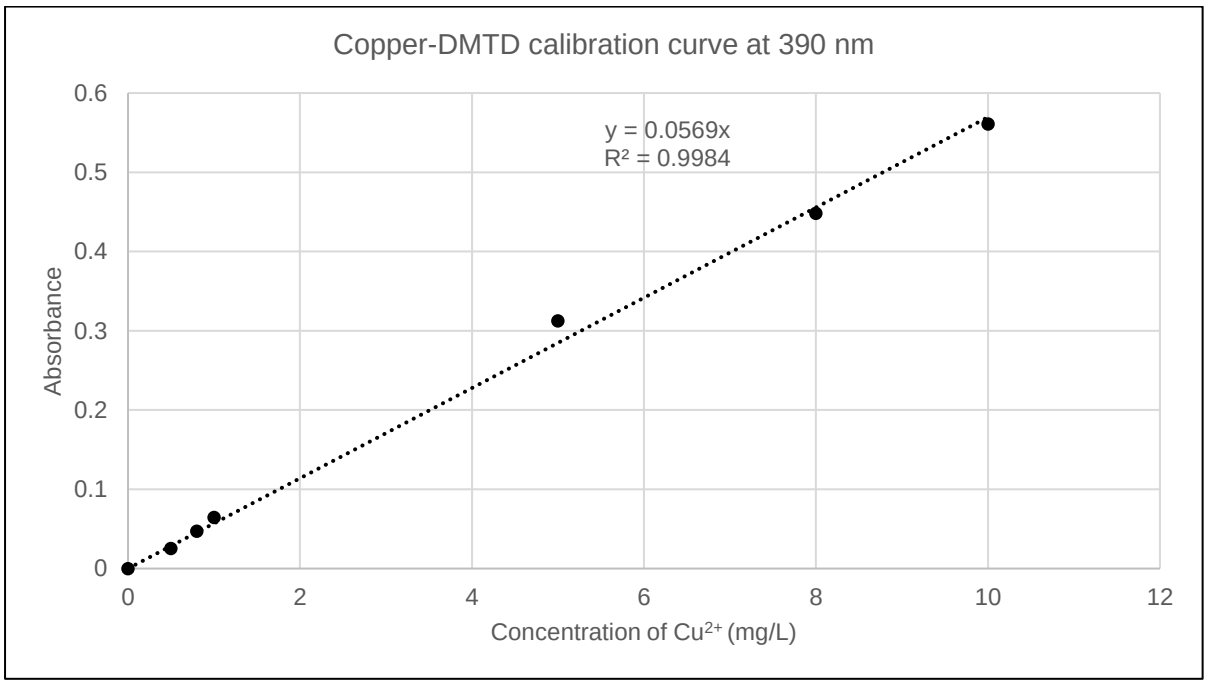

Figure A3. 2: Calibration curve for the Copper (II)-DMTD assay (with masking agents)

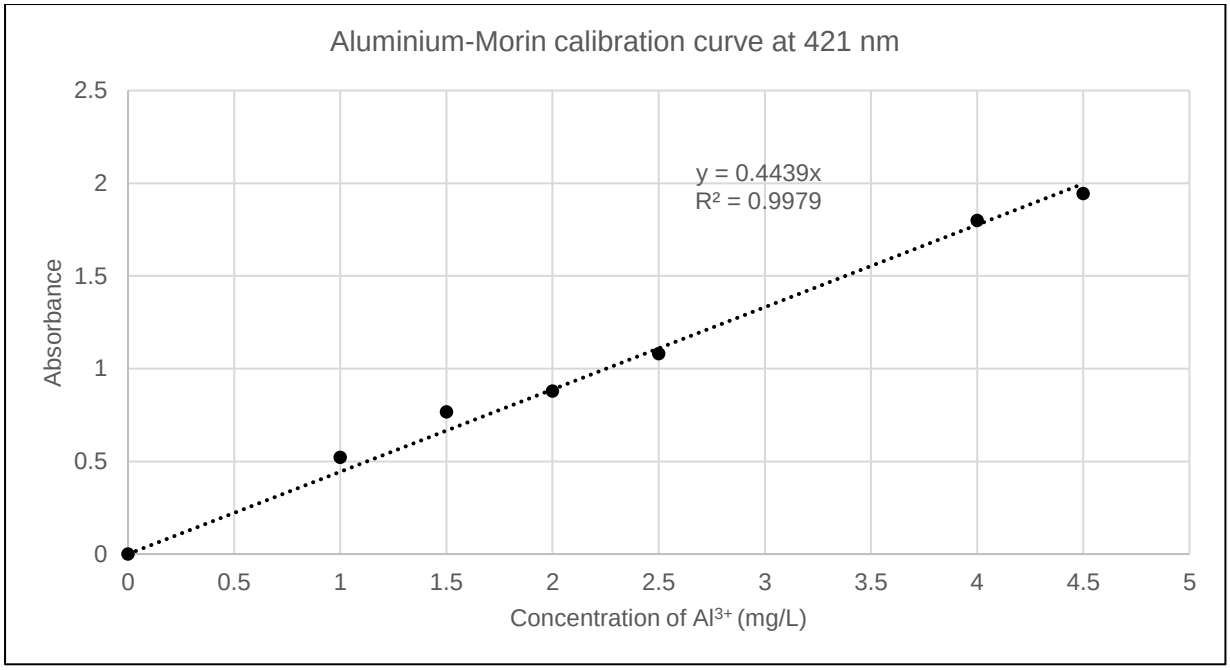

Figure A3. 3: Calibration curve for the Aluminium-Morin assay (without masking agents)

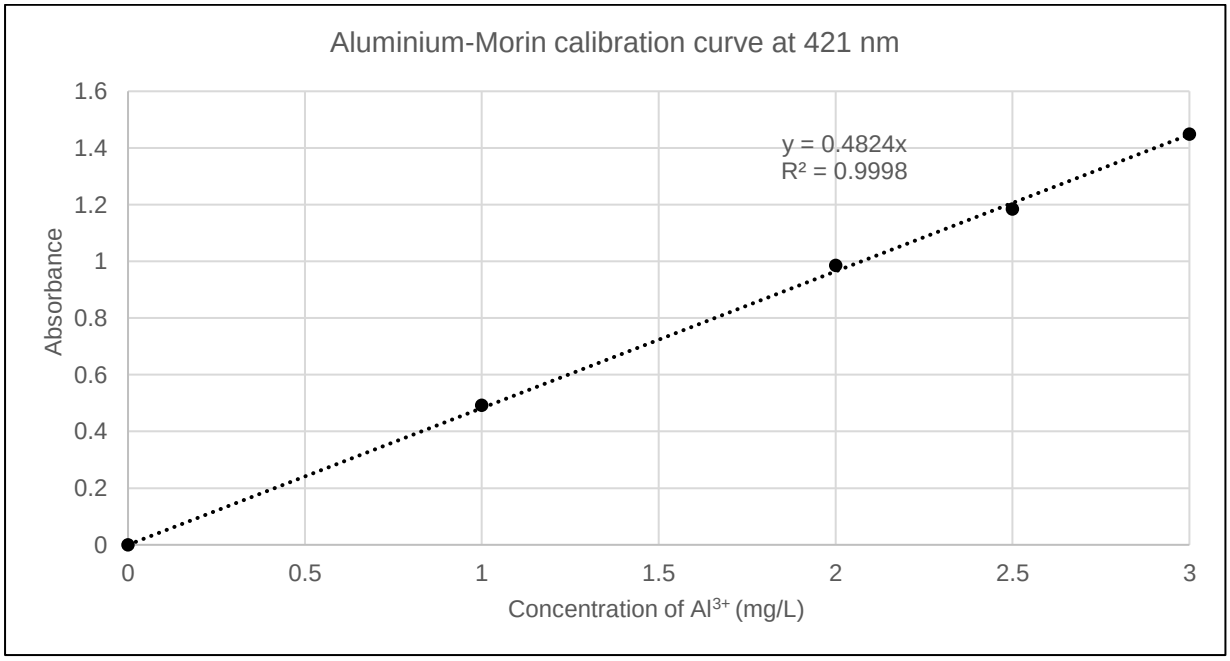

Figure A3. 4: Calibration curve for the Aluminium-Morin assay (with masking agents)

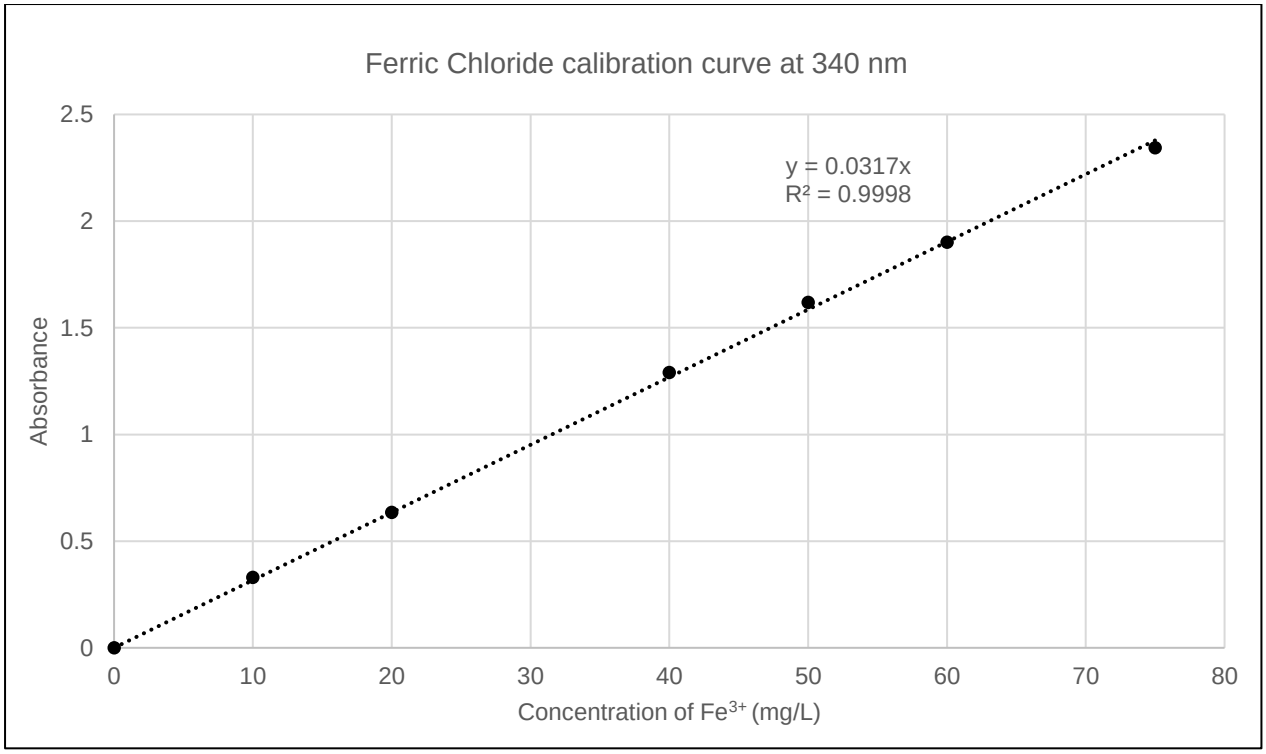

Figure A3. 5: Calibration curve for the Ferric-Chloride assay (without masking agents)

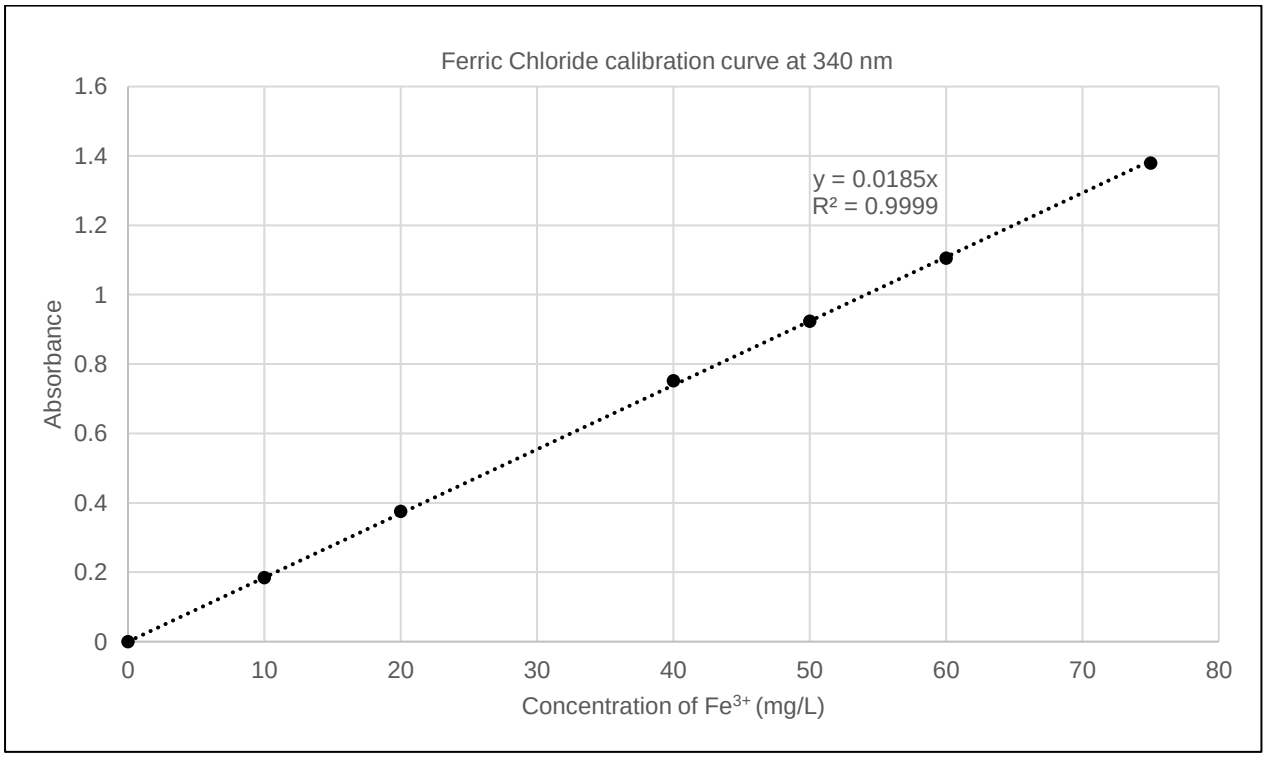

Figure A3. 6: Calibration curve for the Ferric-Chloride assay (with masking agents)

A4 Chitin and chitosan cost of production

Table A4. 1: Chitin 1, Chitin 2, Chitin 3, Chitin 4 demineralization, deproteination, decolorization yield and cost of process step.

	Chitin 1	Chitin 2	Chitin 3	Chitin 4
Raw material used (kg)	40	40	16	
Yield from demineralization (%)	40	40	(N/A)	(N/A)
Yield from deproteination (%)	11.9	11.9	25.3	(N/A)
Yield from decolorization (%)	84.2	(N/A)	(N/A)	(N/A)
Yield (%)	4	4.75	25.3	100
Cost of demineralization ($/kg)	1.66	1.66	0	0
Cost of deproteination ($/kg)	3.64	3.64	1.75	0
Cost of decolorization ($/kg)	15.44	0	0	0
Cost of chitin production ($/kg)	20.74	5.30	1.75	0.00
Cost of chitin production (ZAR/kg)	290	74	25	0

Table A4. 2: Chitin 3 (1 h Deprot), Chitin 3 (2 h Deprot), Chitin 3 (4 h Deprot) demineralization, deproteination, decolorization yield and cost of process step.

	Chitin 3 (1 h Deprot)	Chitin 3 (2 h Deprot)	Chitin 3 (4 h Deprot)
Yield from deproteination (%)	50.6	35	31.3
Yield (%)	50.6	35	31.3
Cost of deproteination ($/kg)	0.91	1.36	1.64
Cost of major electricity usage ($/kg)	0.0715	0.143	0.286
Cost of chitin production ($/kg)	0.910	1.36	1.64
Cost of chitin production (ZAR/kg)	13	19	23

Table A4. 3: Chitosan 2, Chitosan 3, Chitosan 4 demineralization, deproteination, de-acetylation yield and cost of process step

	Chitosan 2	Chitosan 3	Chitosan 4
Raw material used (kg)	40	16	16
Yield from demineralization (%)	40	(N/A)	(N/A)
Yield from deproteination (%)	11.9	25.3	(N/A)
Yield from decolorization (%)	(N/A)	(N/A)	(N/A)
Yield from deacetylation (%)	21.2	31.1	17.5
Yield (%)	1.01	7.87	17.5
Cost of demineralization ($/kg)	1.66	0	0
Cost of deproteination ($/kg)	3.64	1.75	0
Cost of deacetylation ($/Kg)	20.1	13.7	24.36
Cost of major electricity usage ($/kg)	0.572	0.572	0.429
Cost of chitin production ($/kg)	25.99	16.06	24.79
Cost of chitin production (ZAR/kg)	364	225	347.046

A5 Metal concentration and pH-time graphs

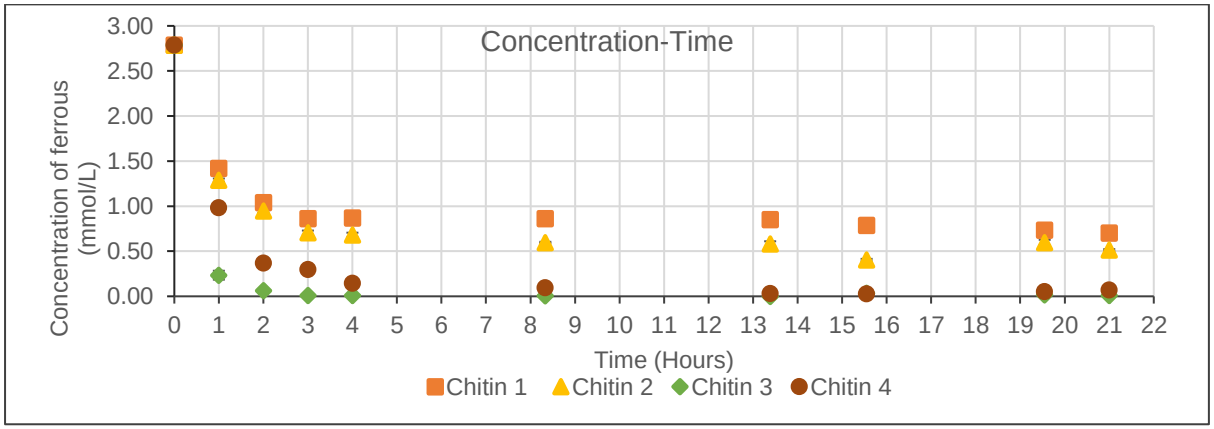

Figure A5. 1: Chitin 1, Chitin 2, Chitin 3, Chitin 4 ferrous adsorption concentration time graph

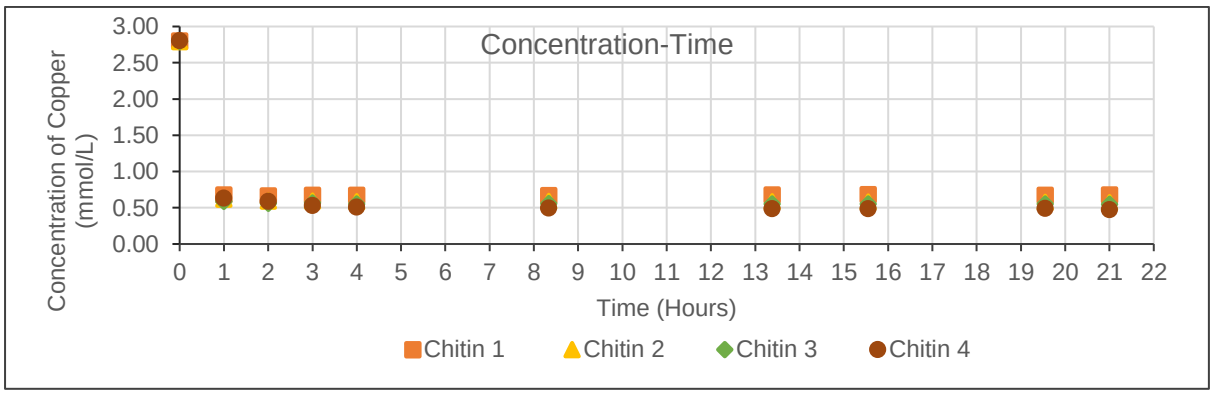

Figure A5. 2: Chitin 1, Chitin 2, Chitin 3, Chitin 4 copper adsorption concentration time graph

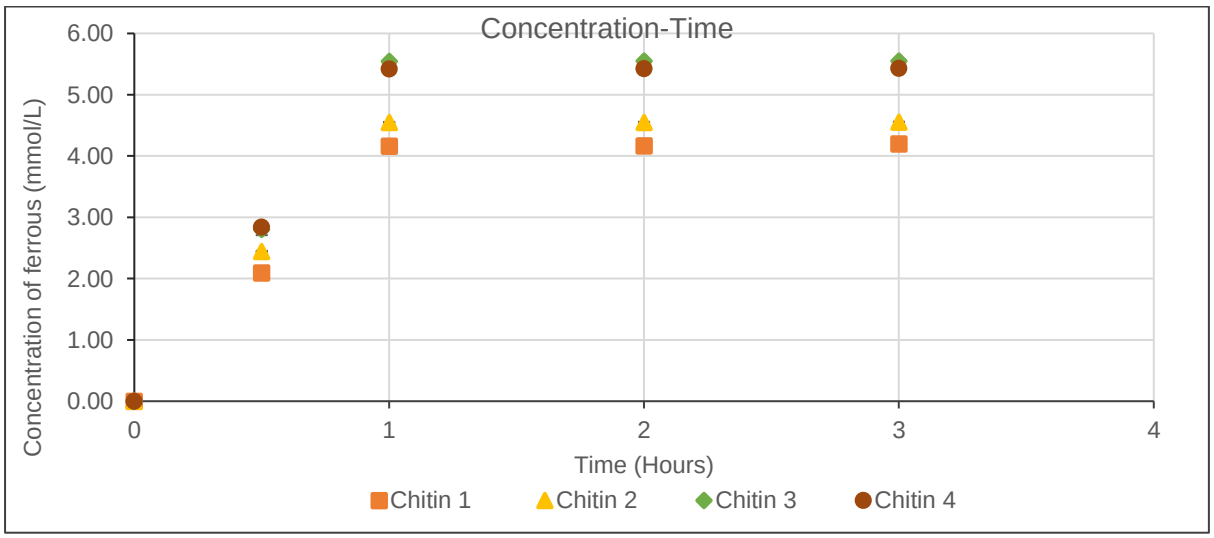

Figure A5. 3: Chitin 1, Chitin 2, Chitin 3, Chitin 4 ferrous desorption concentration time graph

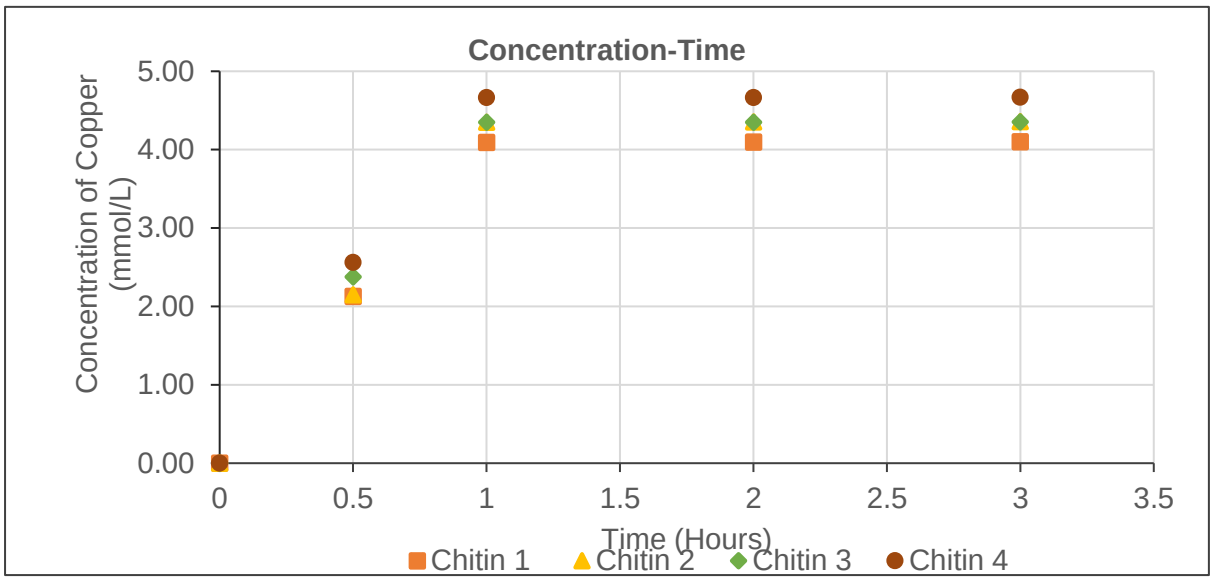

Figure A5. 4: Chitin 1, Chitin 2, Chitin 3, Chitin 4 copper desorption concentration time graph

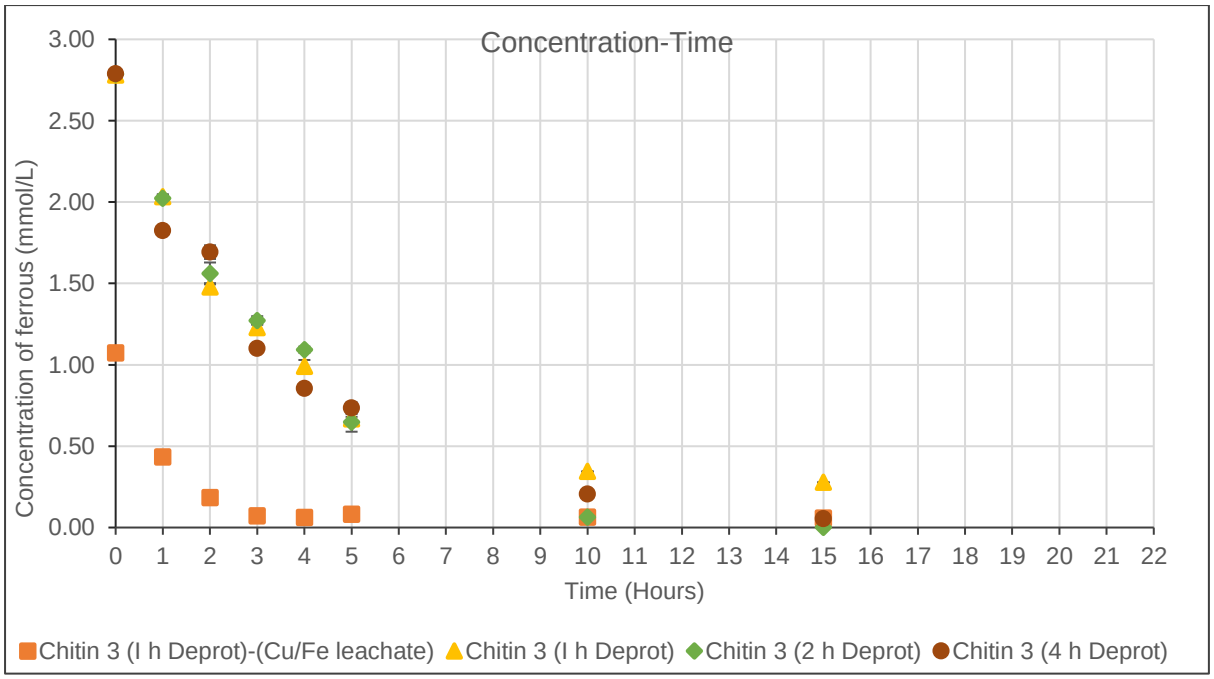

Figure A5. 5: Chitin 3 (1 h Deprot)-(Cu/Fe leachate), Chitin 3 (1 h Deprot), Chitin 3 (2 h Deprot), Chitin 3 (4 h Deprot) ferrous adsorption concentration time graph

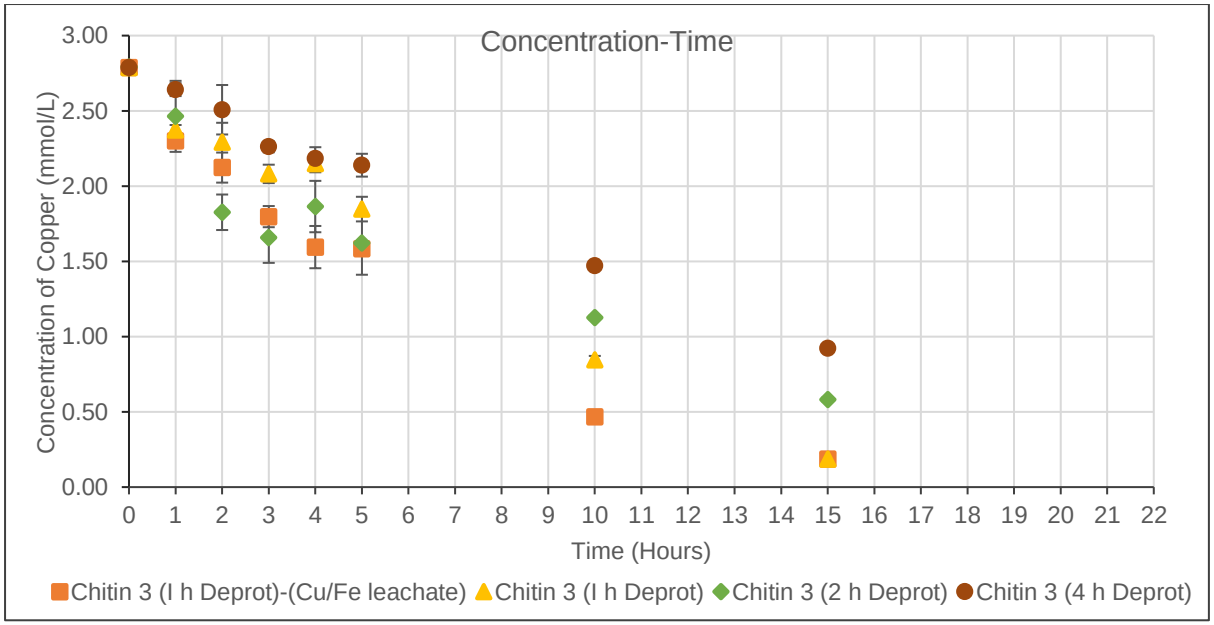

Figure A5. 6: Chitin 3 (1 h Deprot)-(Cu/Fe leachate), Chitin 3 (1 h Deprot), Chitin 3 (2 h Deprot), Chitin 3 (4 h Deprot) copper adsorption concentration time graph

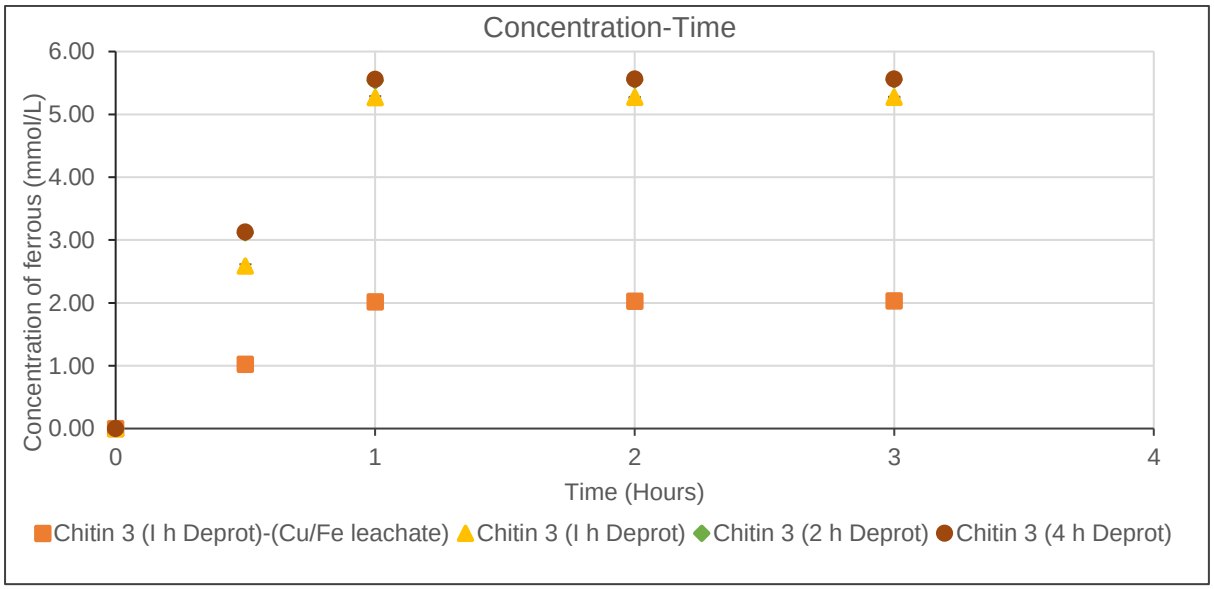

Figure A5. 7: Chitin 3 (1 h Deprot)-(Cu/Fe leachate), Chitin 3 (1 h Deprot), Chitin 3 (2 h Deprot), Chitin 3 (4 h Deprot) ferrous desorption concentration time graph

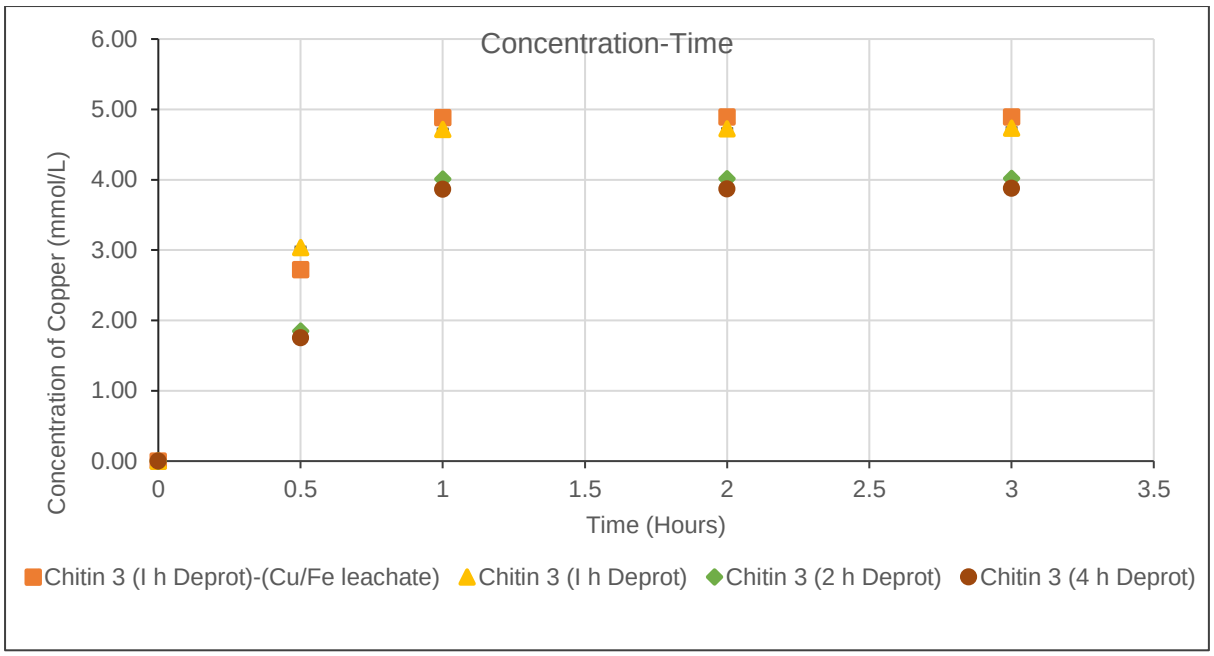

Figure A5. 8: Chitin 3 (1 h Deprot)-(Cu/Fe leachate), Chitin 3 (1 h Deprot), Chitin 3 (2 h Deprot), Chitin 3 (4 h Deprot) copper desorption concentration time graph

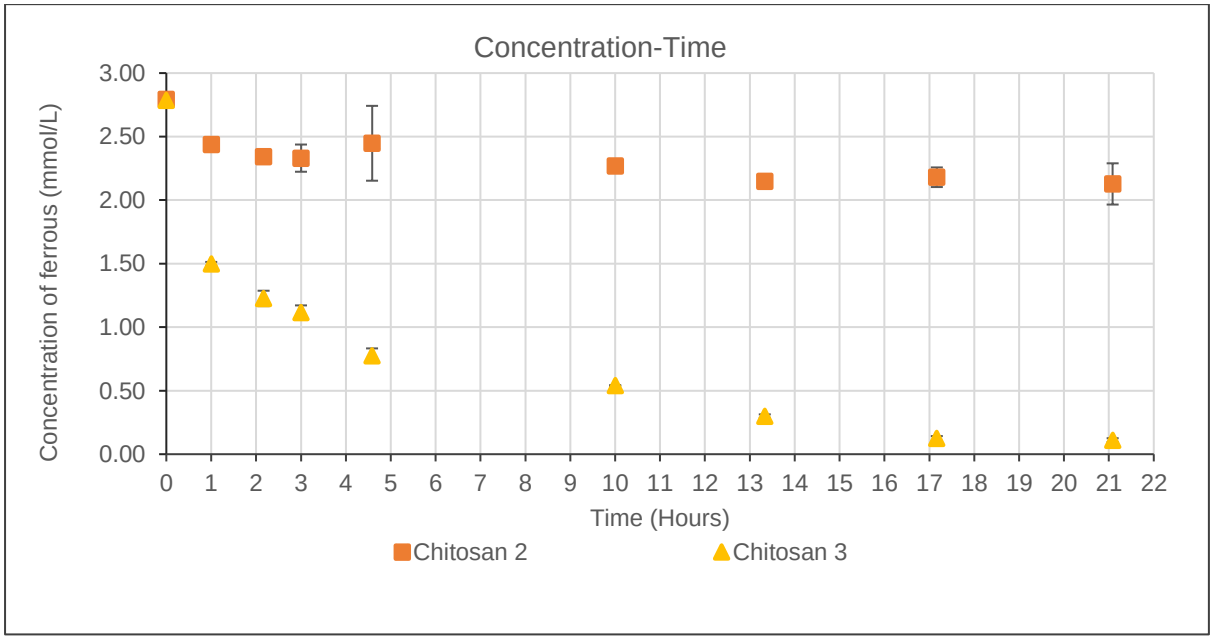

Figure A5. 9: Chitosan 2, Chitosan 3, Chitosan 4 ferrous adsorption concentration time graph

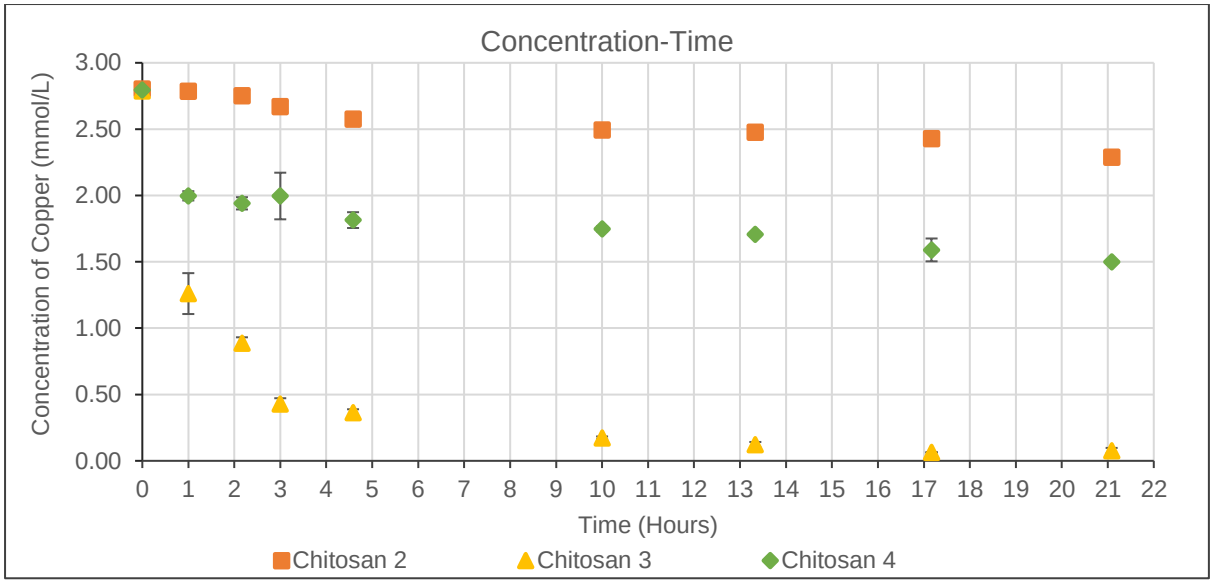

Figure A5. 10: Chitosan 2, Chitosan 3, Chitosan 4 copper adsorption concentration time graph

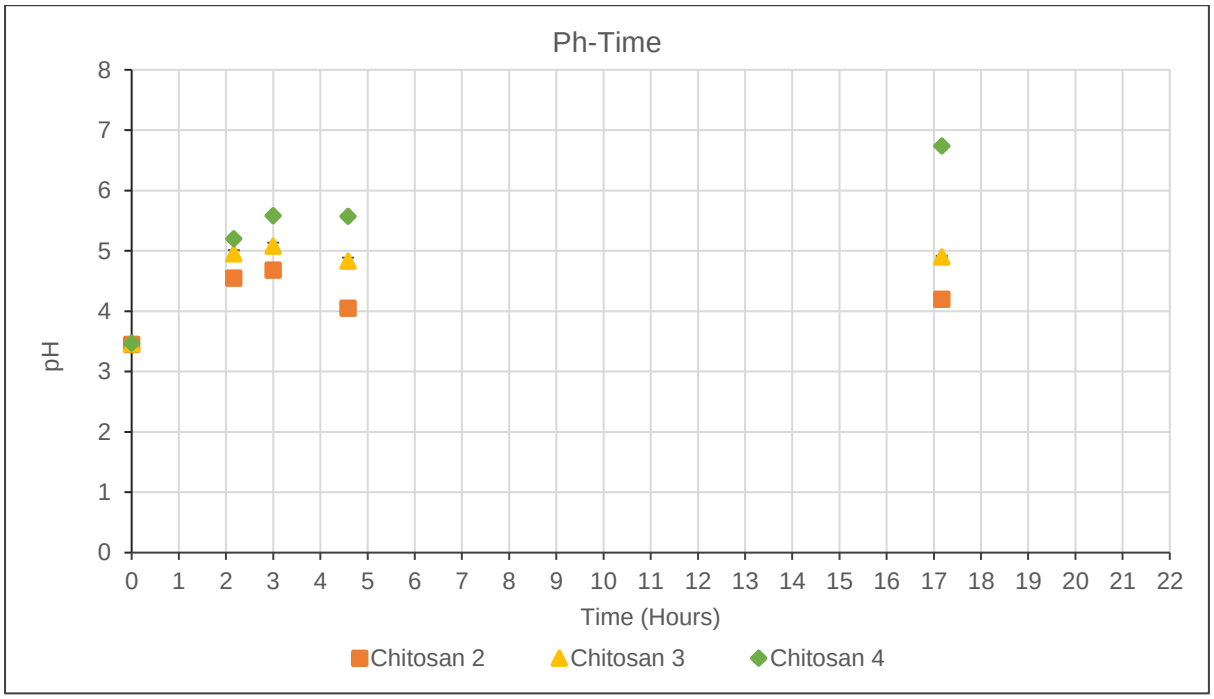

Figure A5. 11: Chitosan 2, Chitosan 3, Chitosan 4 ferrous and copper adsorption pH time graph

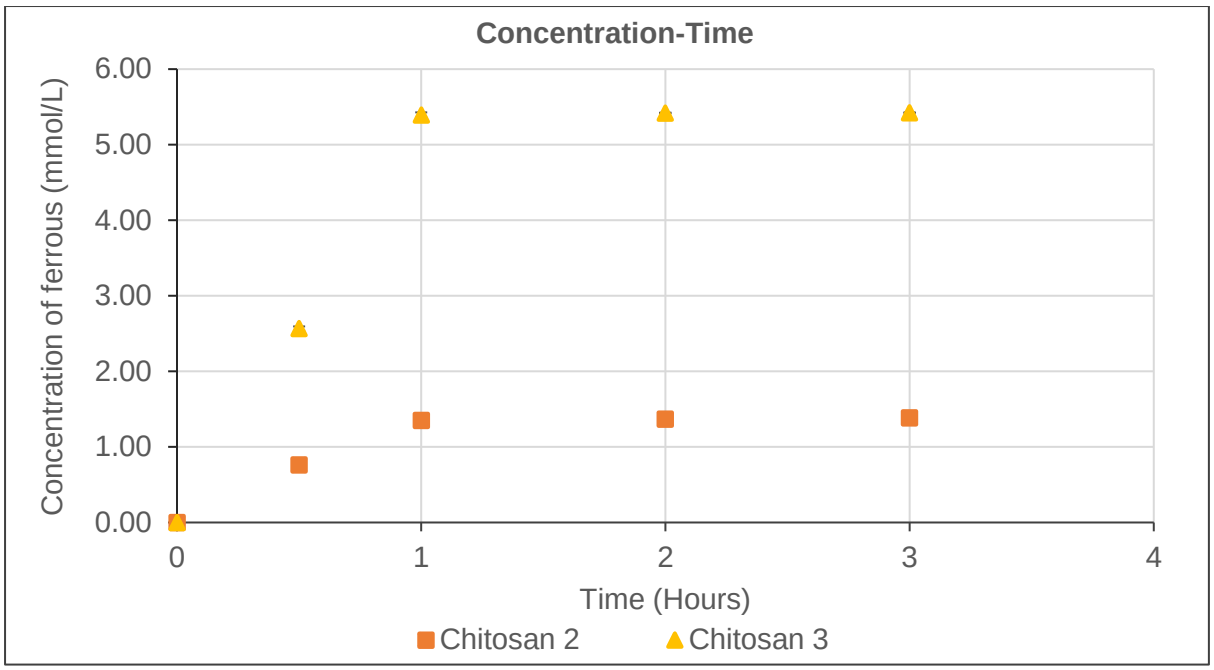

Figure A5. 12: Chitosan 2, Chitosan 3, Chitosan 4 ferrous desorption concentration time graph

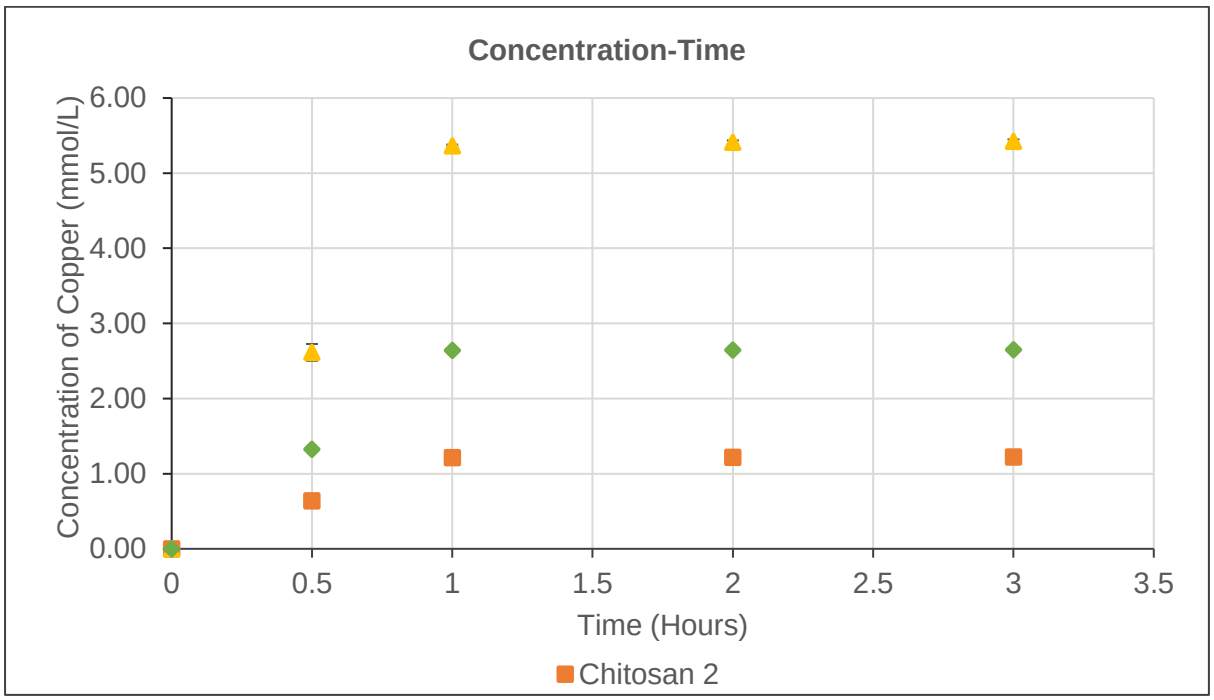

Figure A5. 13: Chitosan 2, Chitosan 3, Chitosan 4 copper desorption concentration time graph

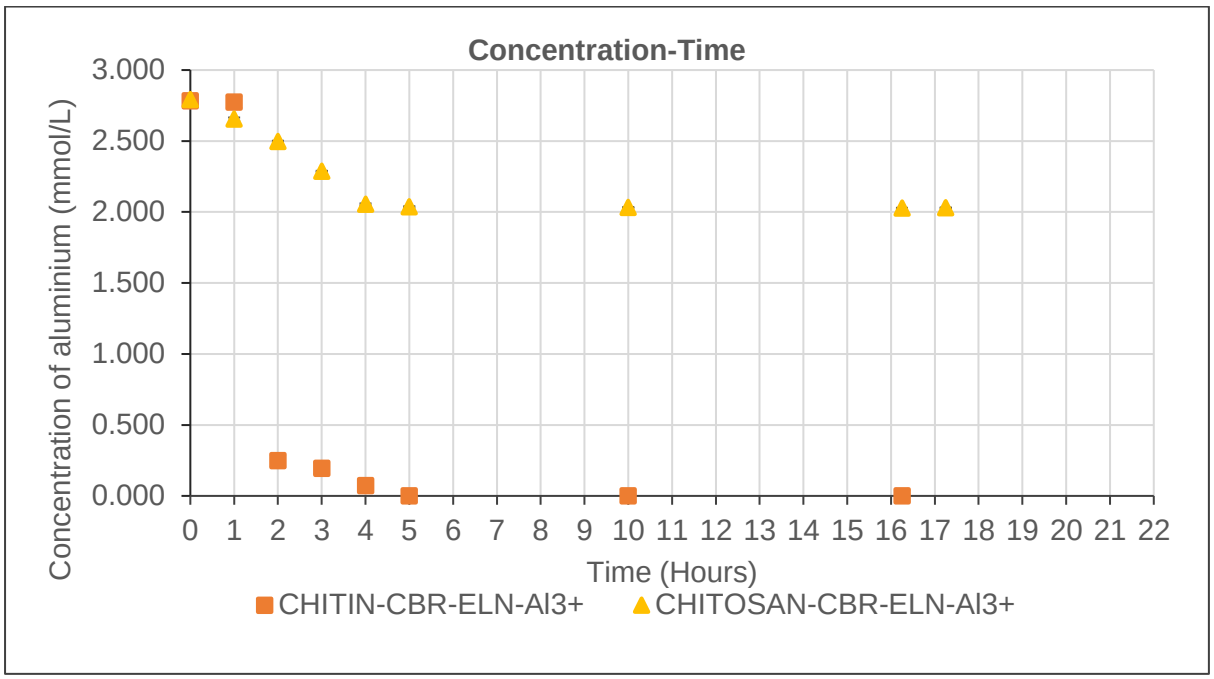

Figure A5. 14: CHITIN-CBR-ELN and CHITOSAN-CBR-ELN aluminium adsorption concentration time graph

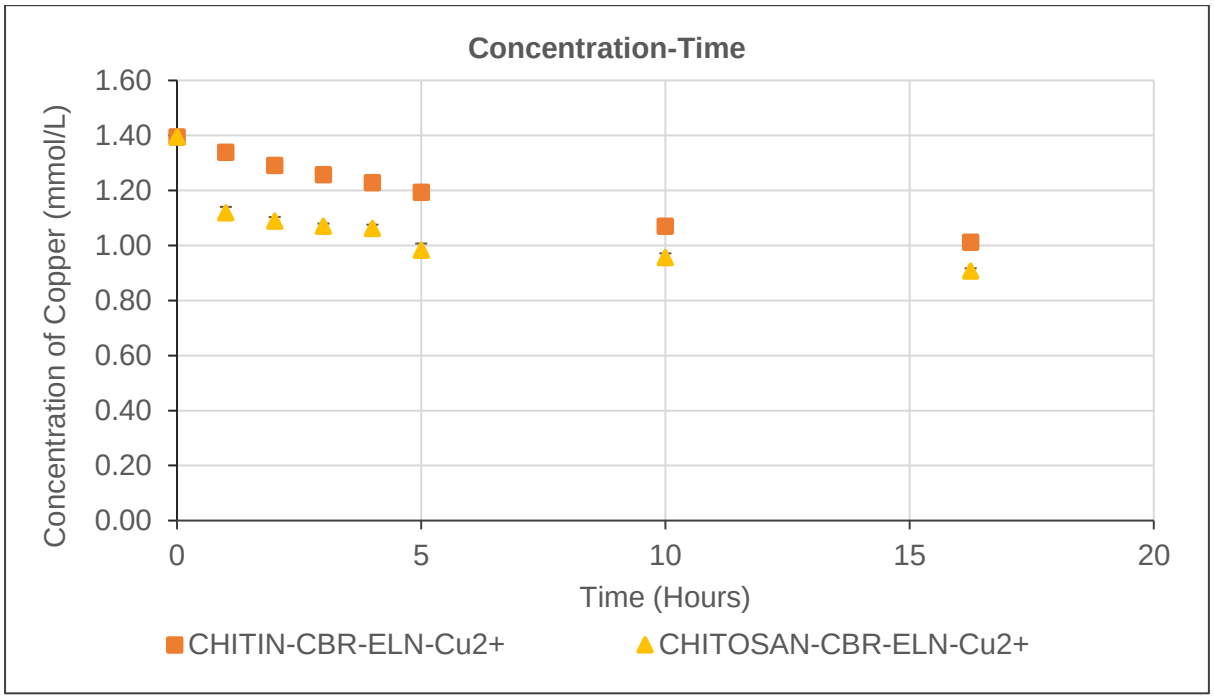

Figure A5. 15: CHITIN-CBR-ELN and CHITOSAN-CBR-ELN copper adsorption concentration time graph

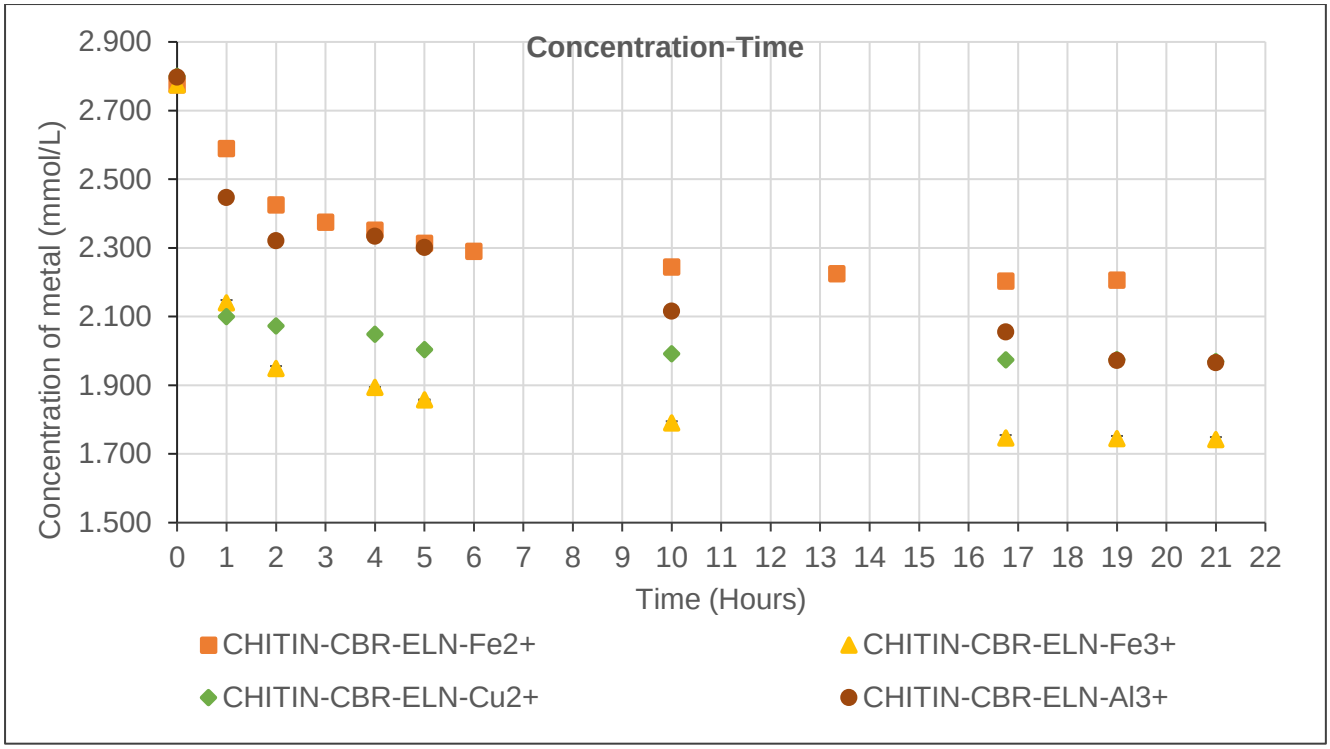

Figure A5. 16: CHITIN-CBR-ELN ferrous, ferric, copper aluminium adsorption concentration time graph

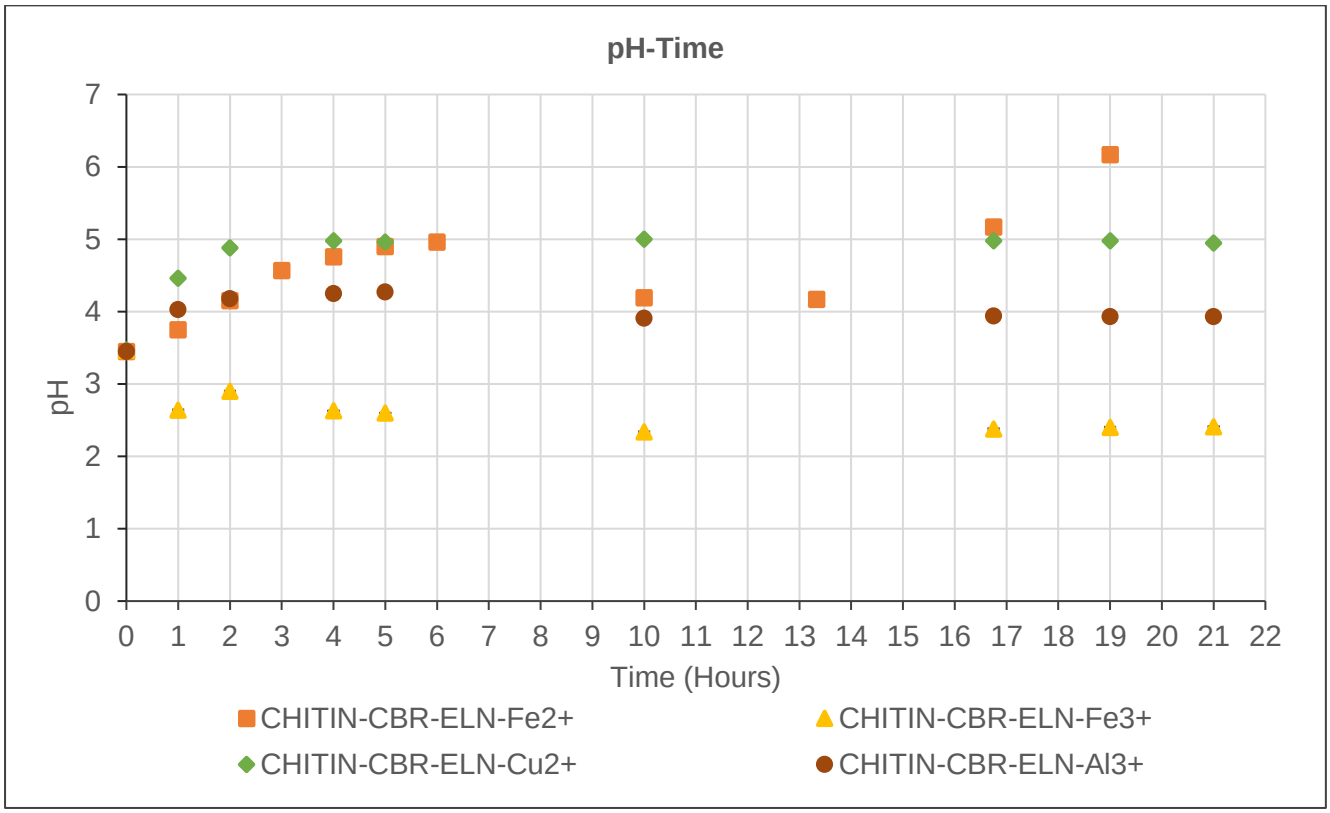

Figure A5. 17 CHITIN-CBR-ELN ferrous, ferric, copper aluminium adsorption pH time graph

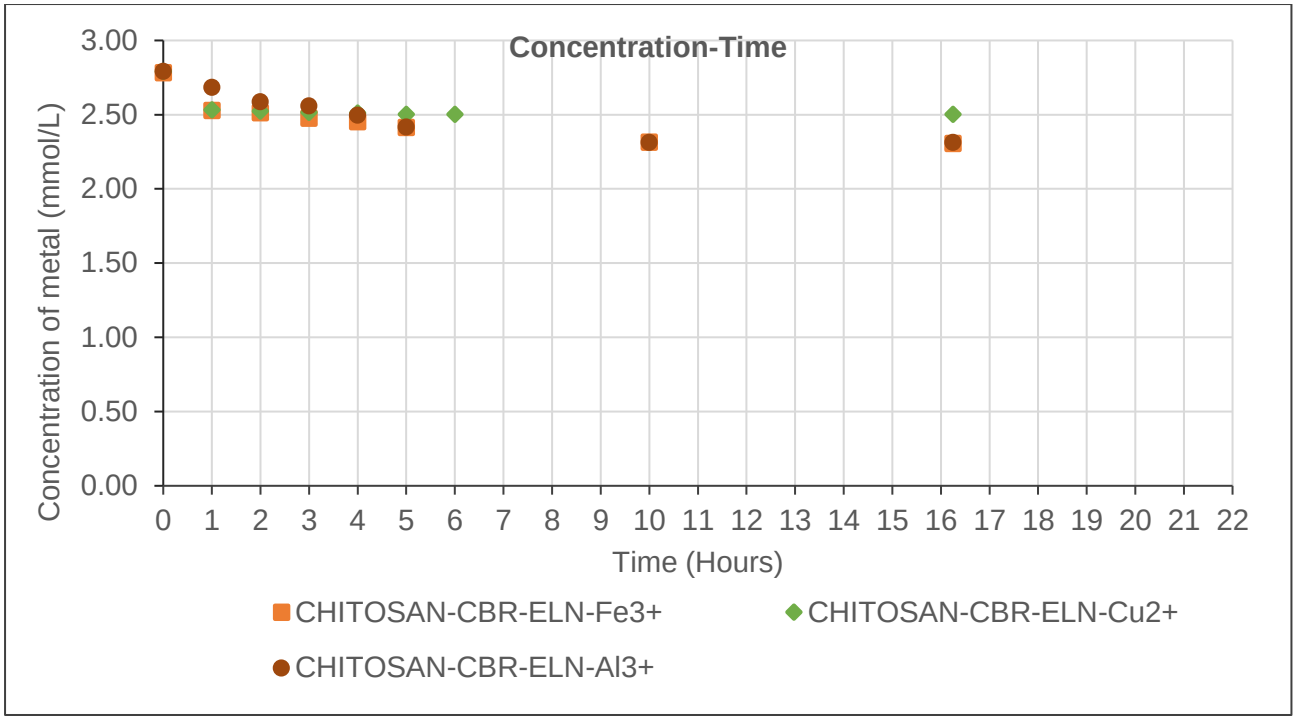

Figure A5. 18: CHITOSAN-CBR-ELN ferrous, copper aluminium adsorption concentration time graph

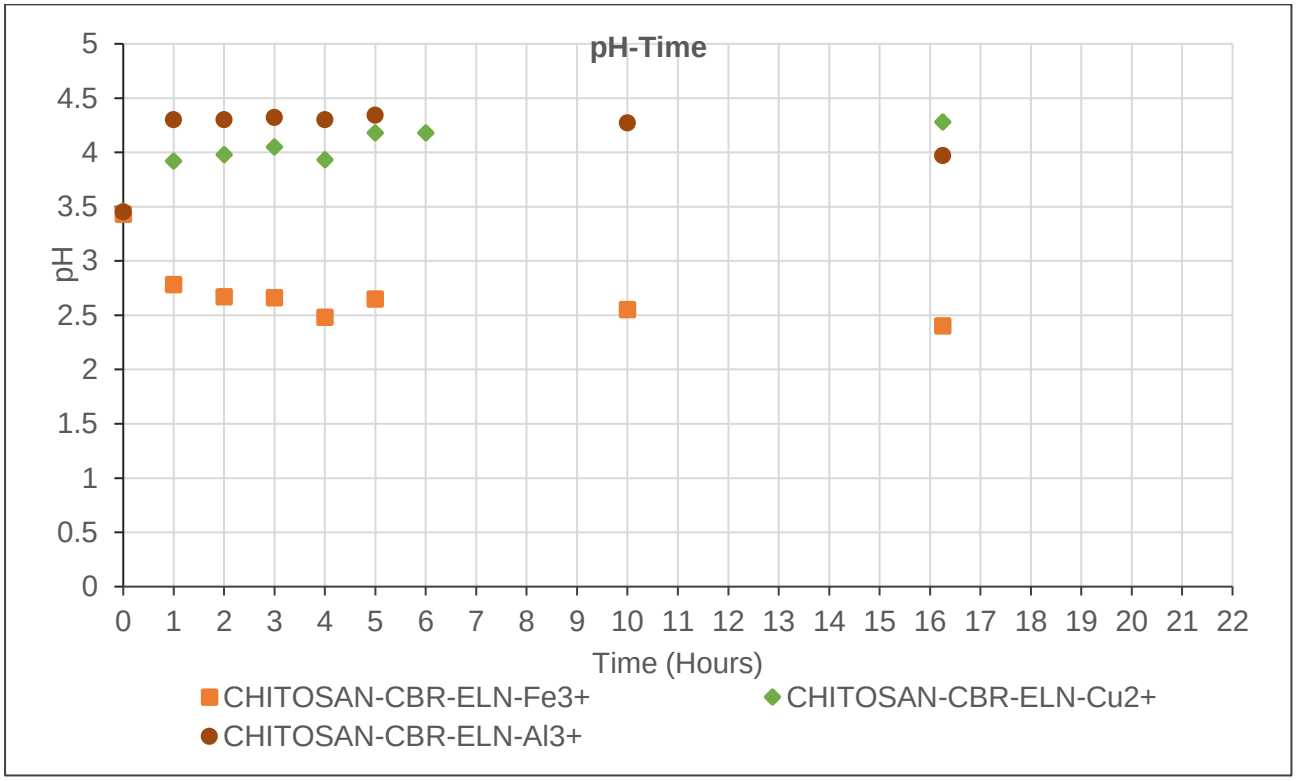

Figure A5. 19: CHITOSAN-CBR-ELN ferrous, copper aluminium adsorption pH--time graph

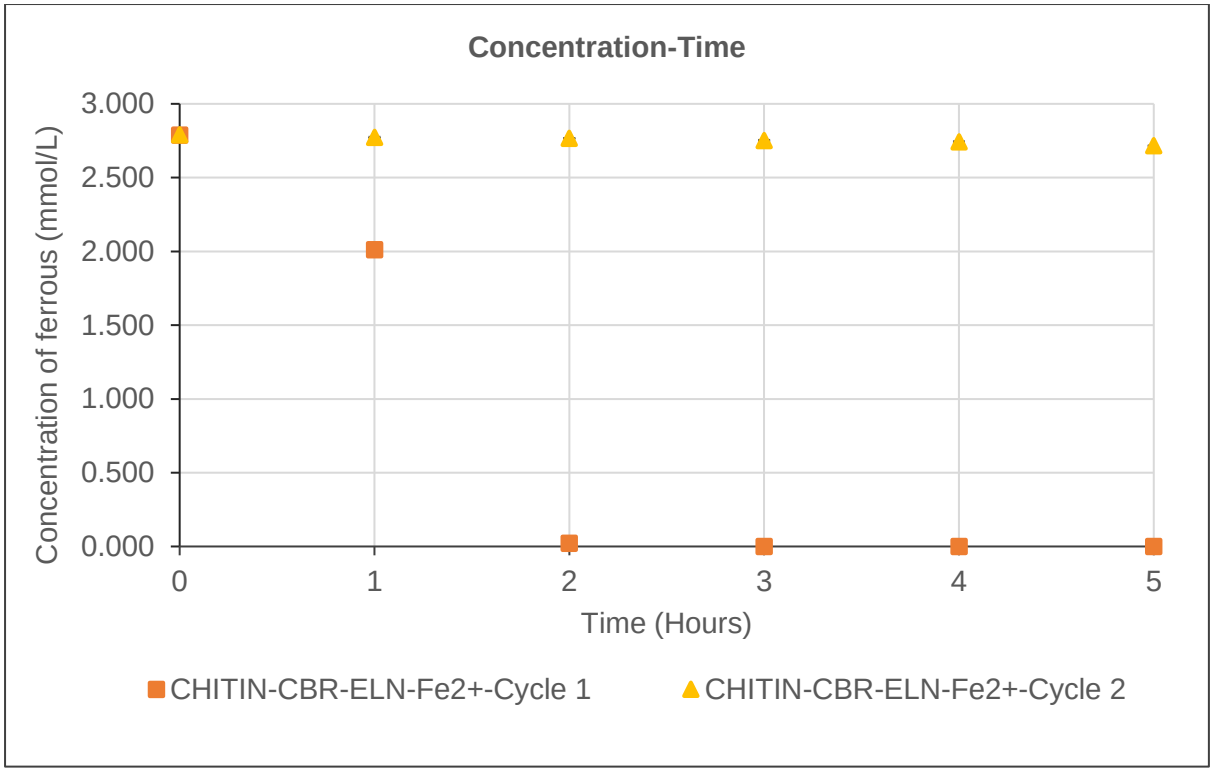

Figure A5. 20: CHITIN-CBR-ELN ferrous adsorption in 2 consecutive adsorption cycles concentration time graph

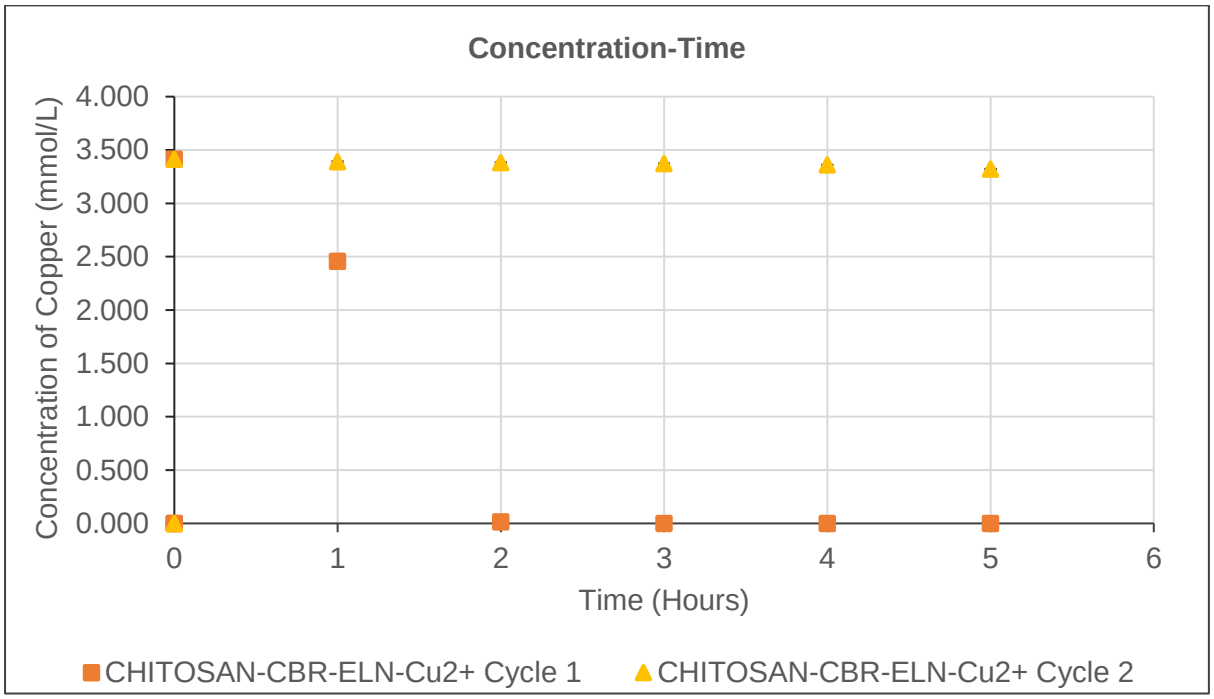

Figure A5. 21: CHITOSAN-CBR-ELN copper adsorption in 2 consecutive adsorption cycles concentration time graph

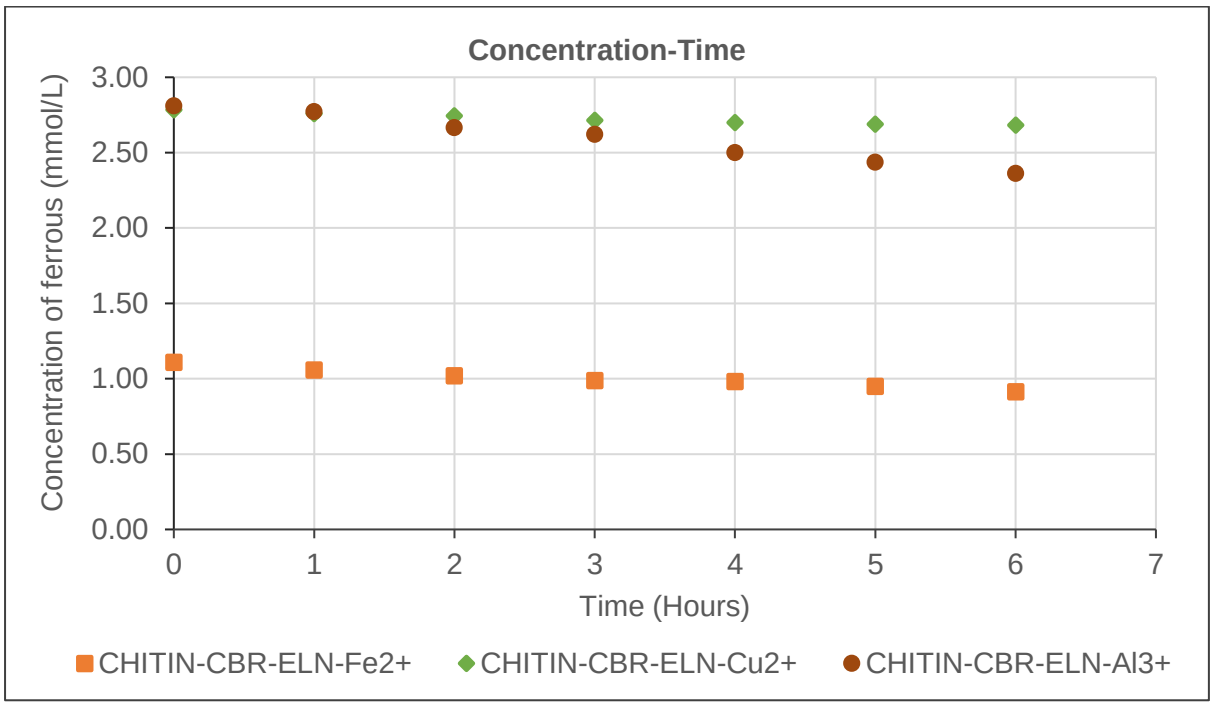

Figure A5. 22: CHITIN-CBR-ELN model leachate solution adsorption concentration time graph

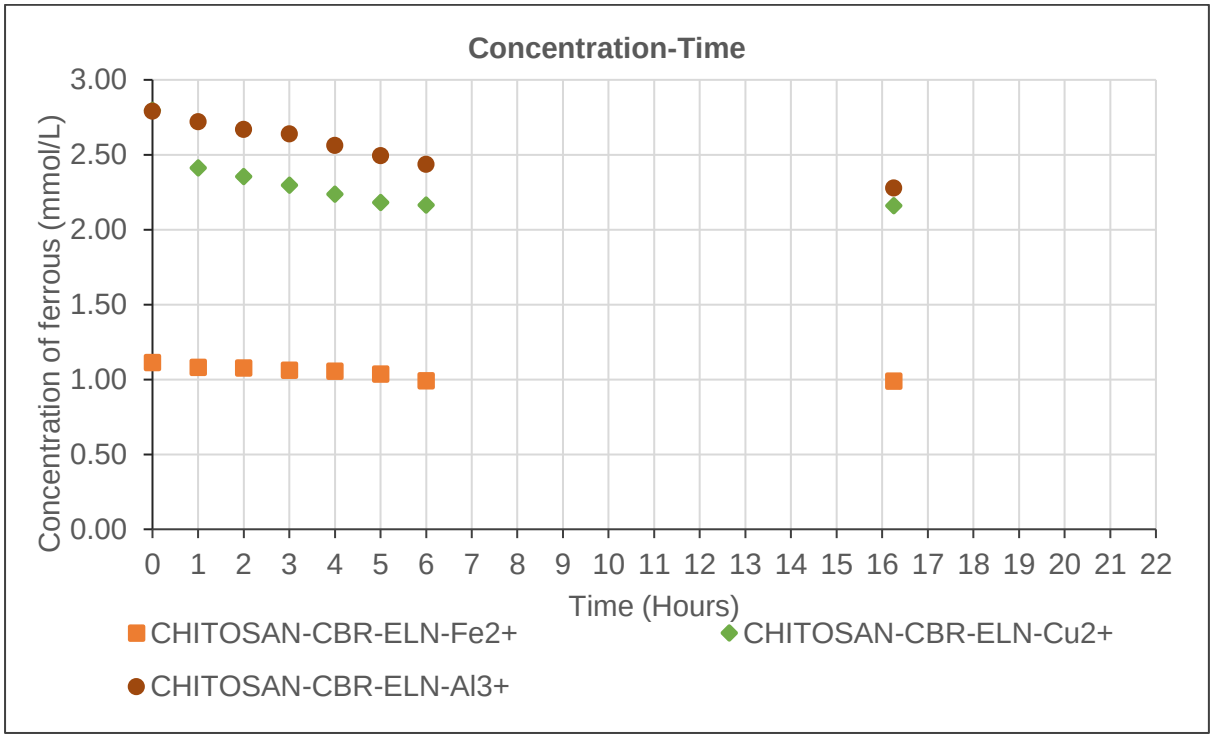

Figure A5. 23: CHITOSAN-CBR-ELN model leachate solution adsorption concentration time graph

A6 Metal Adsorption isotherms

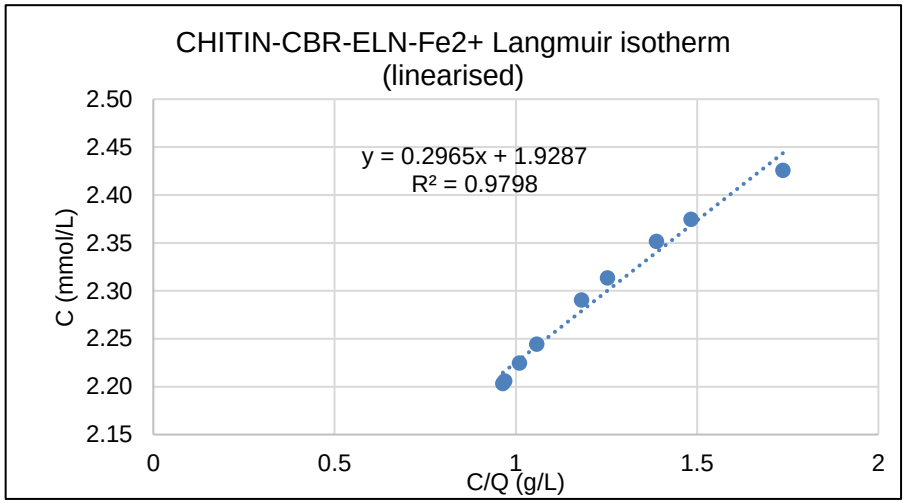

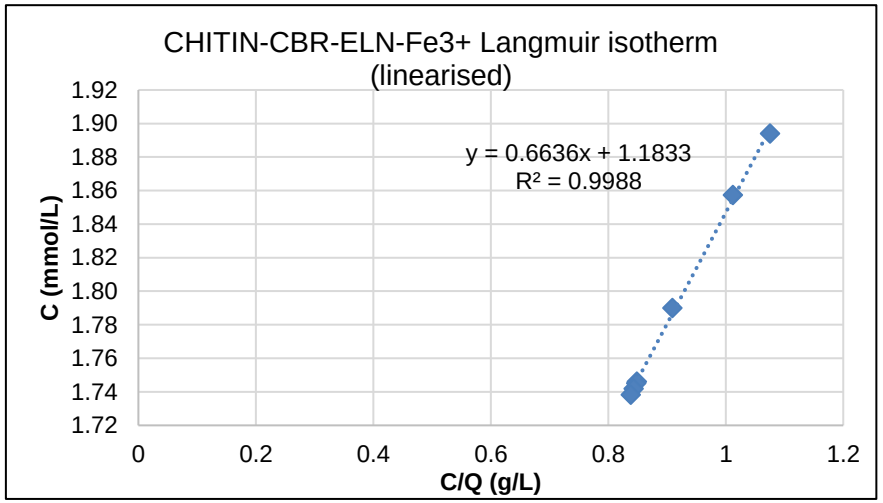

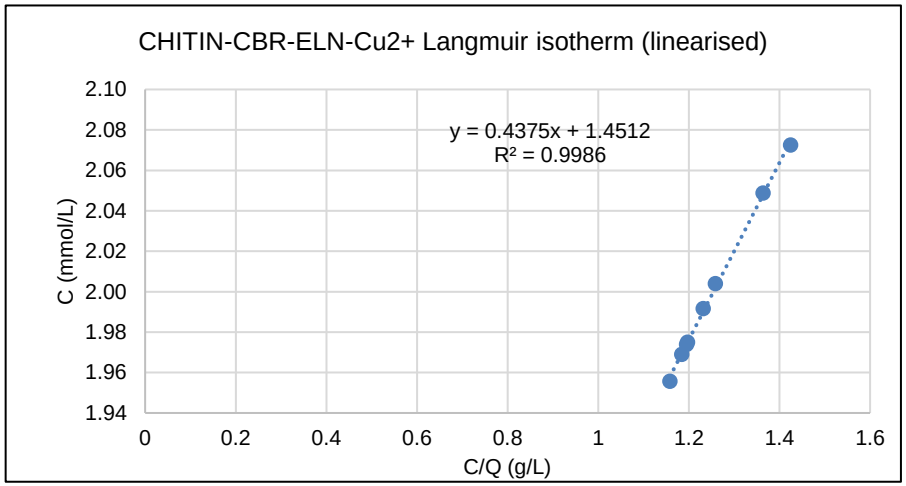

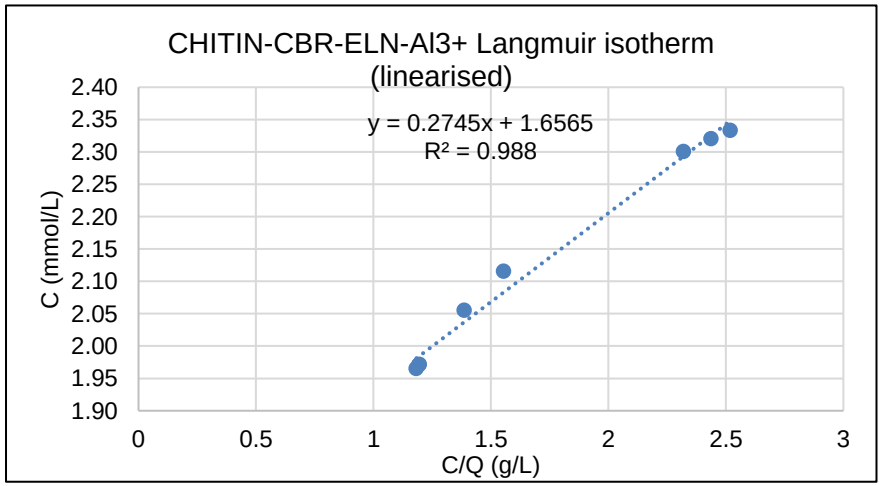

Figure A6. 1 Langmuir isotherm linear fit for adsorption of ferrous, ferric, copper and aluminium onto CHITIN-CBR-ELN

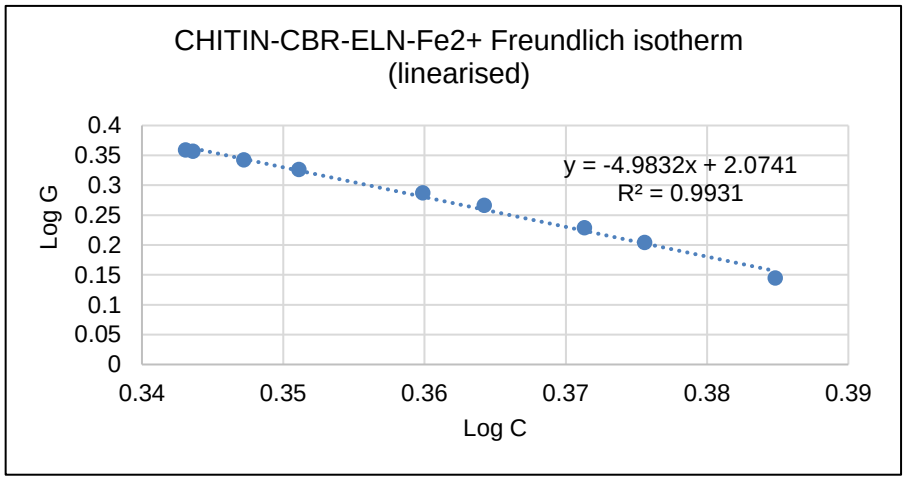
CHITIN-CBR-ELN-Fe2+ Freundlich isotherm
(linearised)
y = -4.9832x + 2.0741
R² = 0.9931
Log G
Log C
0.4
0.35
0.3
0.25
0.2
0.15
0.1
0.05
0
0.34
0.35
0.36
0.37
0.38
0.39

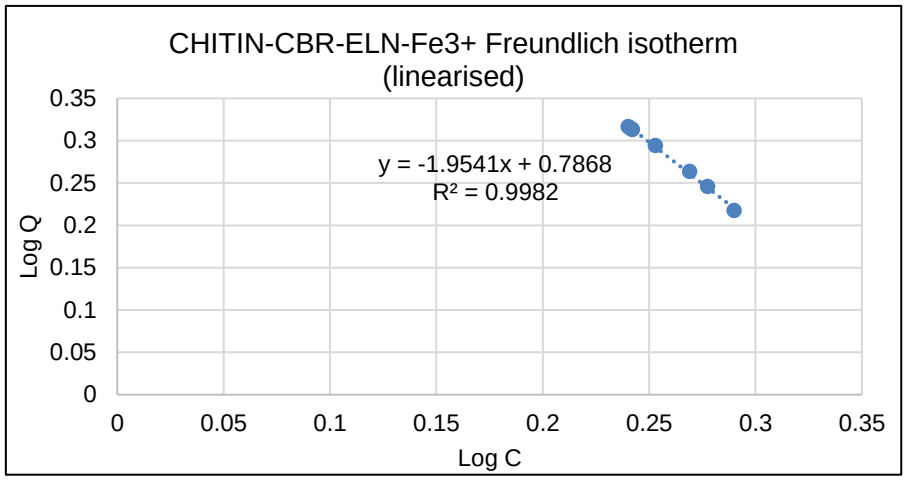
CHITIN-CBR-ELN-Fe3+ Freundlich isotherm
(linearised)
y = -1.9541x + 0.7868
R² = 0.9982
Log Q
Log C
0.35
0.3
0.25
0.2
0.15
0.1
0.05
0
0
0.05
0.1
0.15
0.2
0.25
0.3
0.35

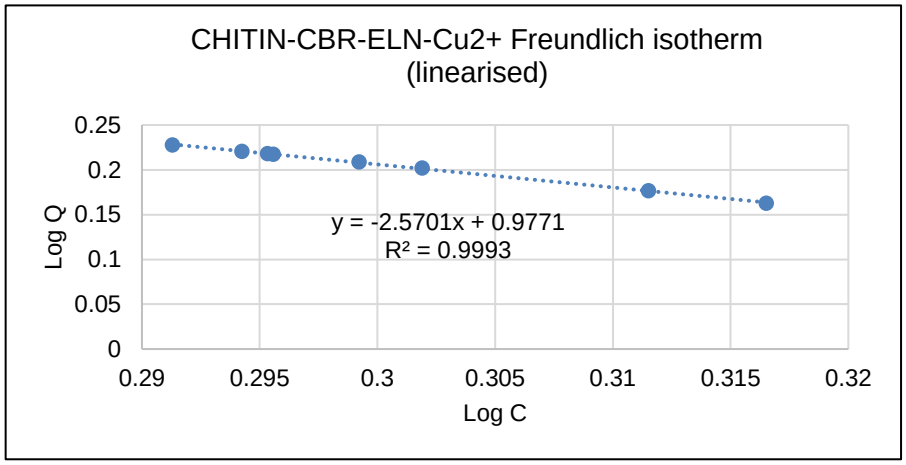
CHITIN-CBR-ELN-Cu2+ Freundlich isotherm
(linearised)
y = -2.5701x + 0.9771
R² = 0.9993
Log Q
Log C
0.25
0.2
0.15
0.1
0.05
0
0.29
0.295
0.3
0.305
0.31
0.315
0.32

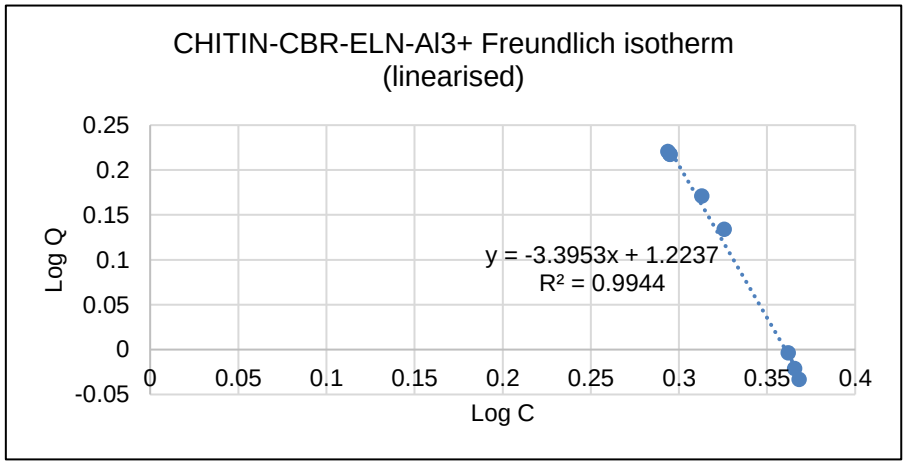
CHITIN-CBR-ELN-Al3+ Freundlich isotherm
(linearised)
y = -3.3953x + 1.2237
R² = 0.9944
Log Q
Log C
0.25
0.2
0.15
0.1
0.05
0
-0.05
0
0.05
0.1
0.15
0.2
0.25
0.3
0.35
0.4

Figure A6. 3: Freundlich isotherm linear fit for adsorption of ferrous, ferric, copper and aluminium onto CHITIN-CBR-ELN

Figure A6. 4: Freundlich isotherm linear fit for adsorption of ferrous, ferric, copper and aluminium onto CHITIN-CBR-ELN

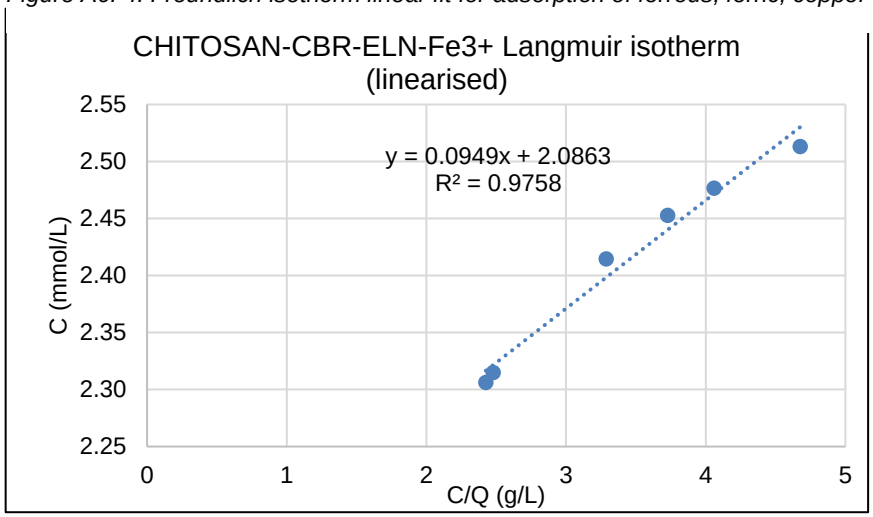

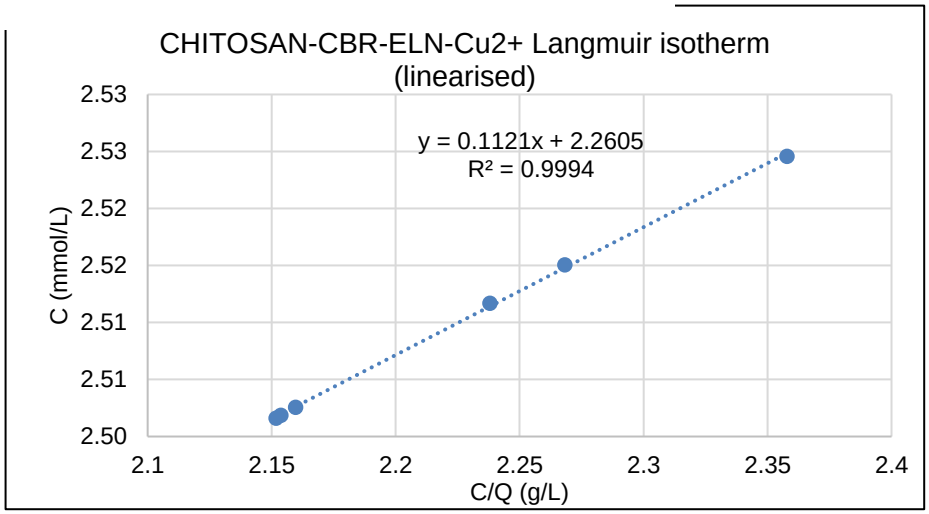

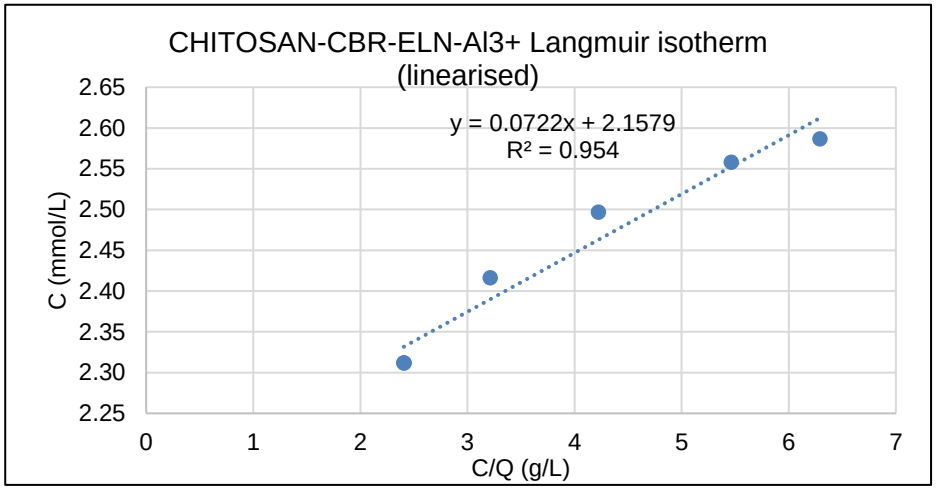

Figure A6. 5: Langmuir isotherm linear fit for adsorption of ferrous, ferric, copper and aluminium onto CHITOSAN-CBR-ELN

Figure A6. 6: Langmuir isotherm linear fit for adsorption of ferrous, ferric, copper and aluminium onto CHITOSAN-CBR-ELN

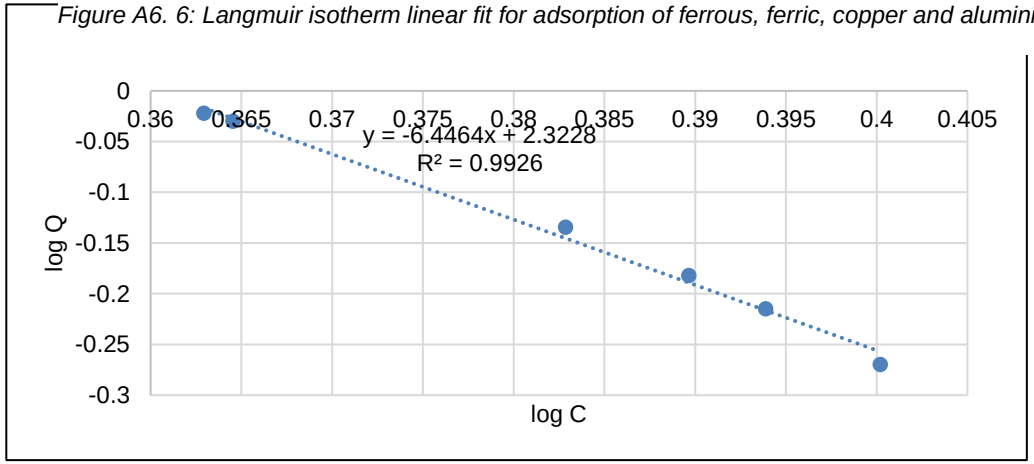

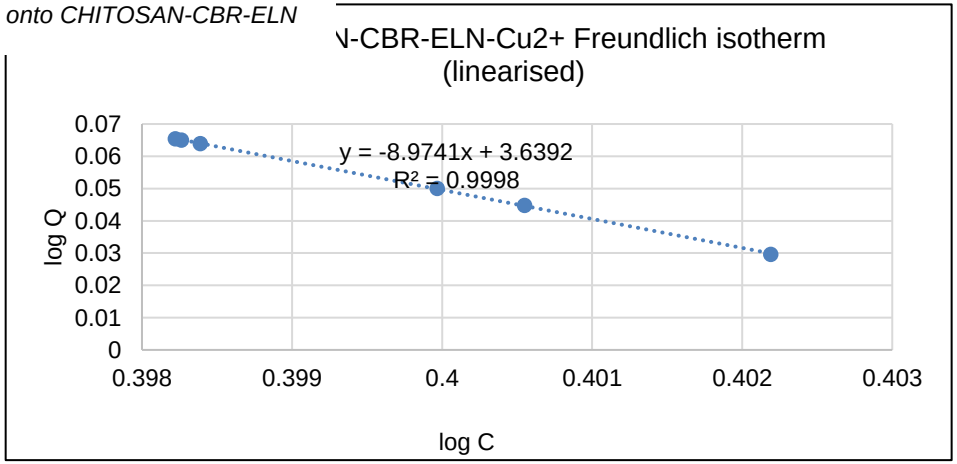

Figure A6. 7: Freundlich isotherm linear fit for adsorption of ferrous, ferric, copper and aluminium onto CHITOSAN-CBR-ELN ised)

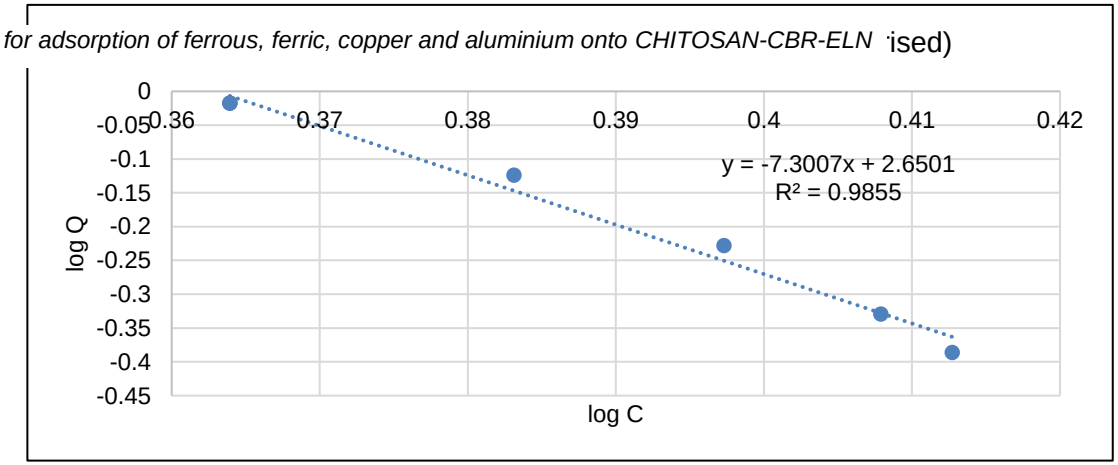

A7 Adsorption reaction kinetics

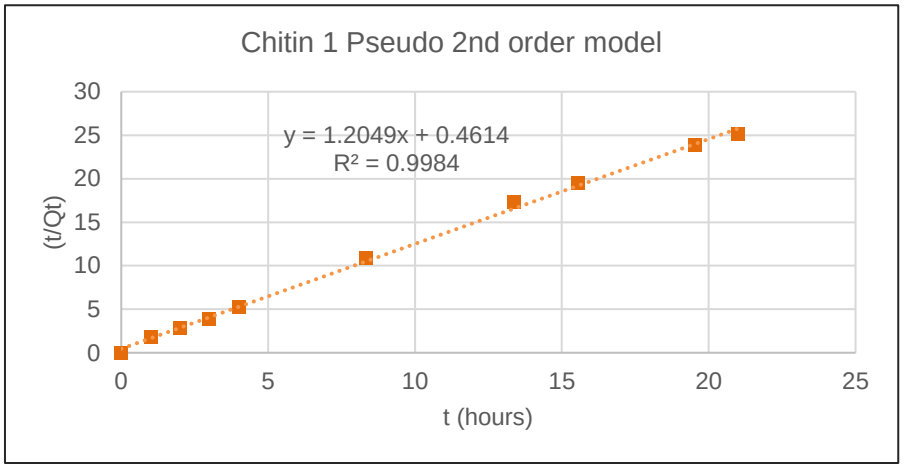

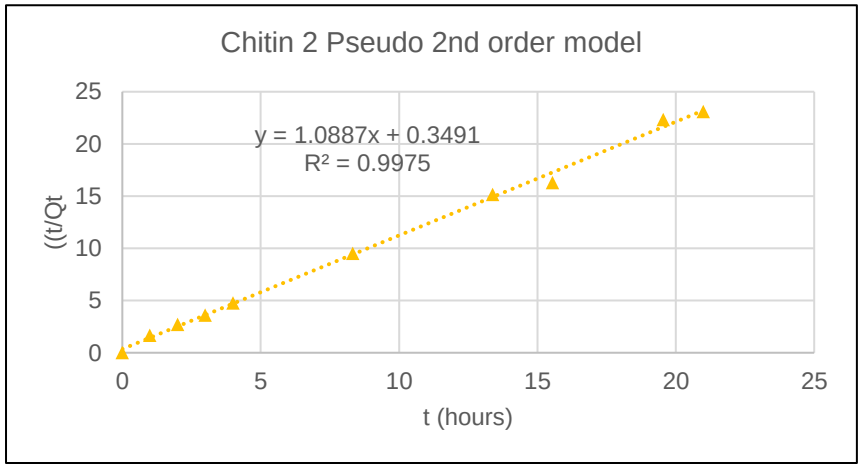

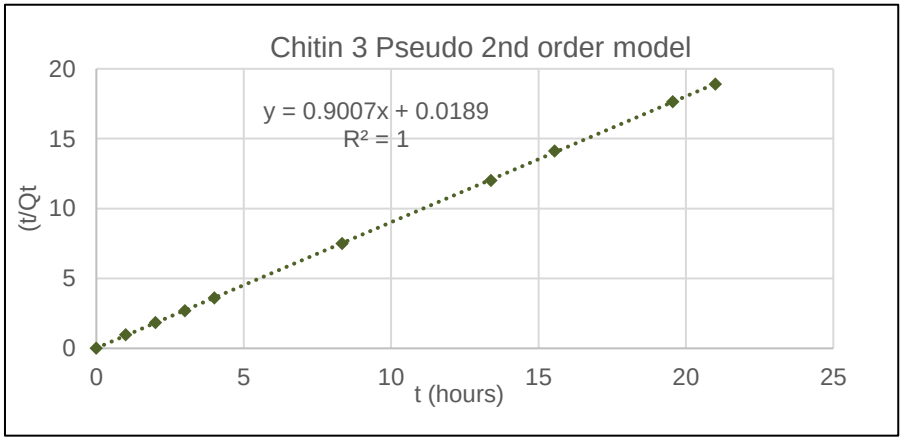

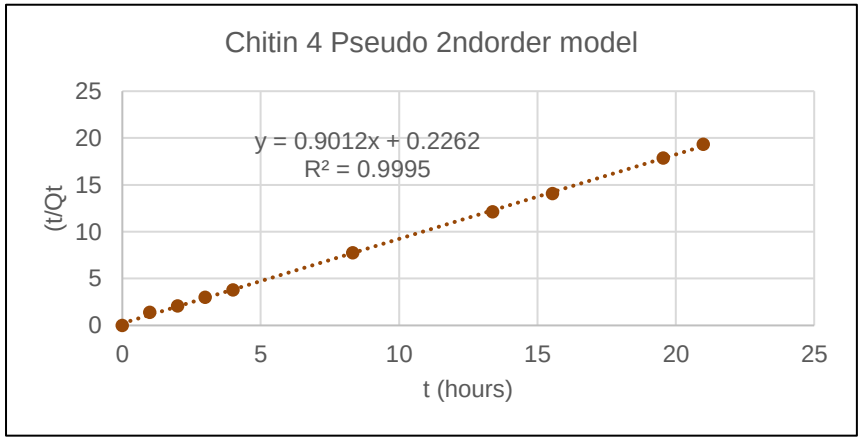

Figure A7. 1: Chitin 1, Chitin 2, Chitin 3 and Chitin 4 ferrous adsorption Pseudo 2nd order kinetic model linear fit.

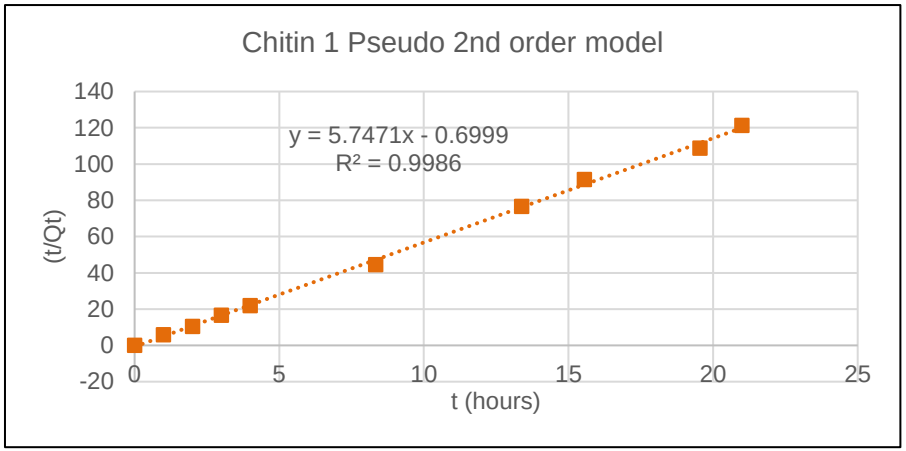

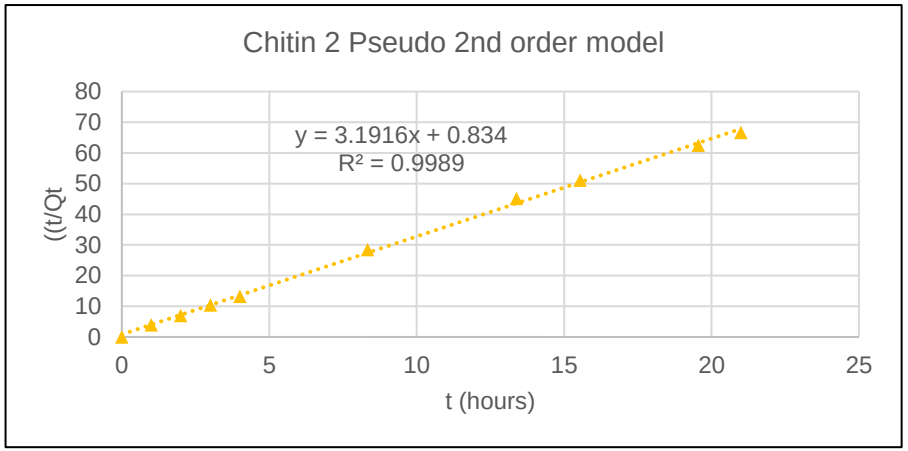

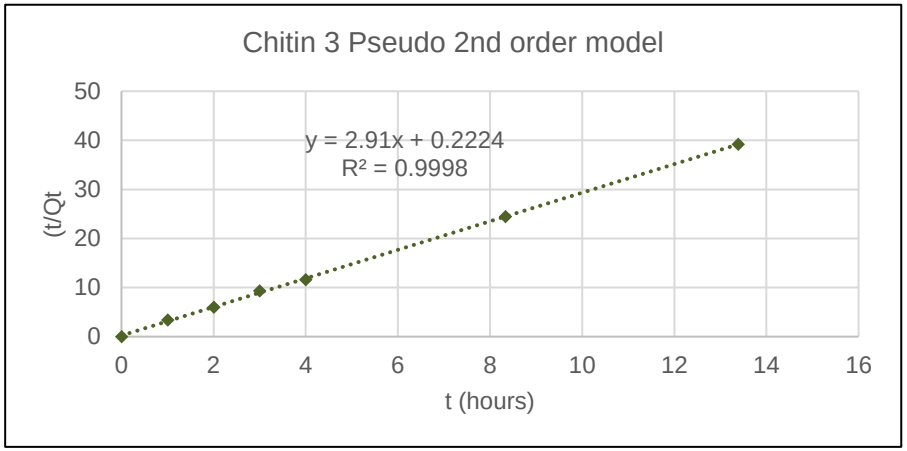

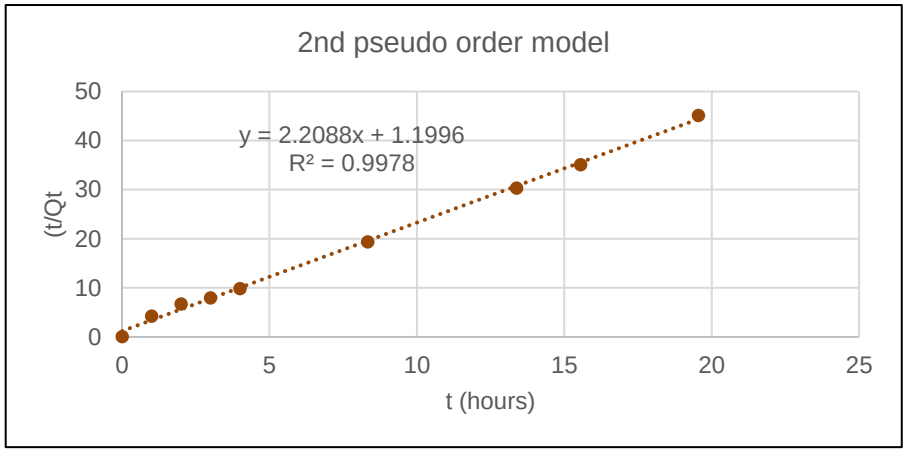

Figure A7. 2: Chitin 1, Chitin 2, Chitin 3 and Chitin 4 copper adsorption Pseudo 2nd order kinetic model linear fit.

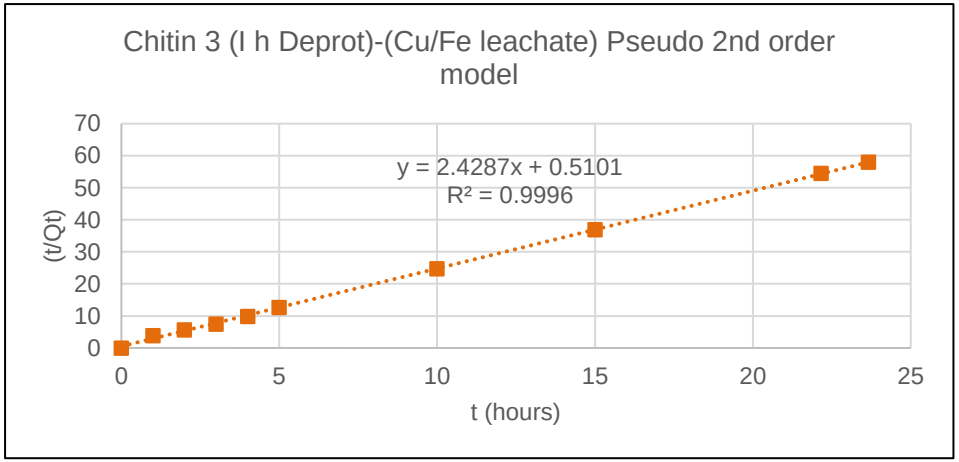

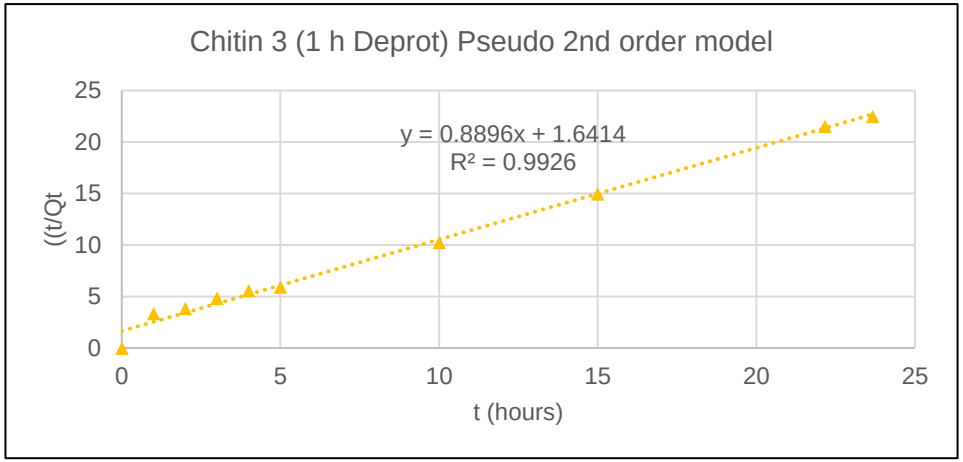

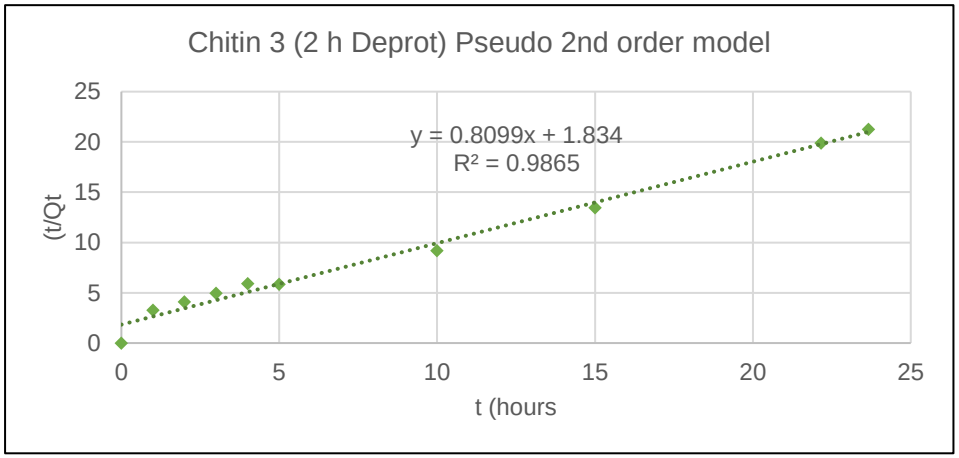

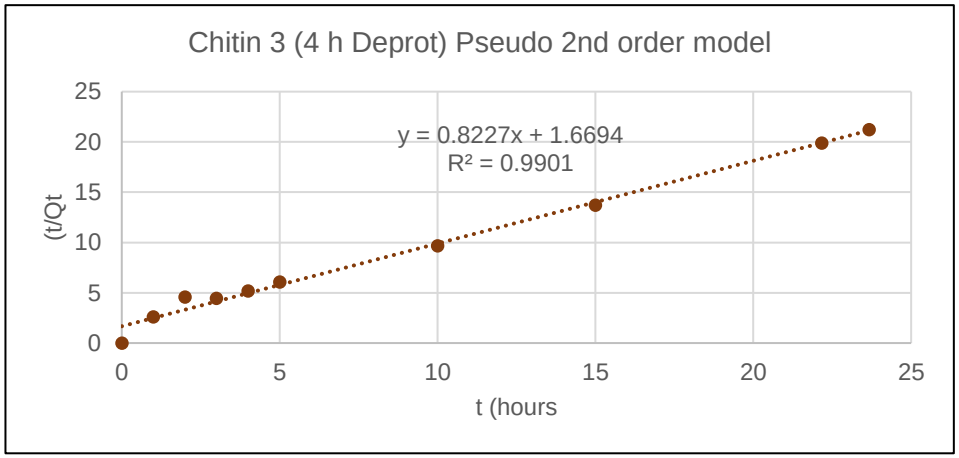

Figure A7. 3: Chitin 3 (1 h Deprot)-(Cu/Fe leachate), Chitin 3 (1 h Deprot), Chitin 3 (2 h Deprot) and Chitin 3 (4 h Deprot) ferrous adsorption Pseudo 2nd order kinetic model linear fit.

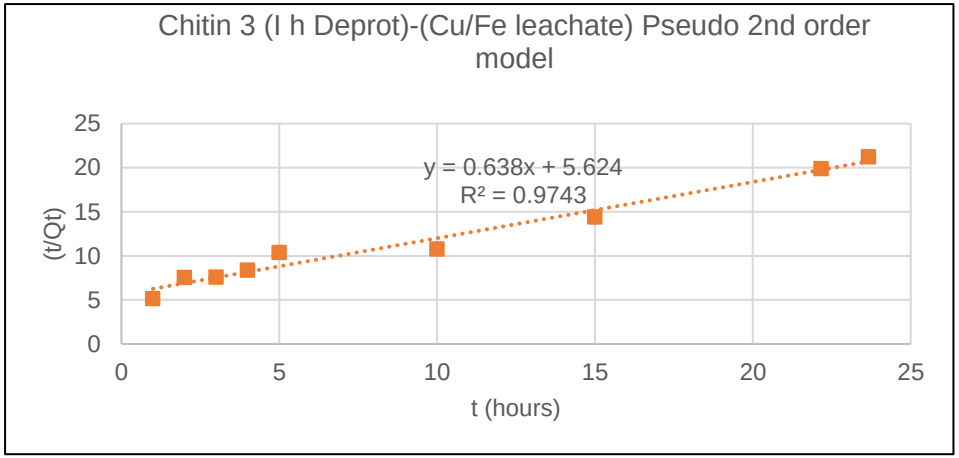

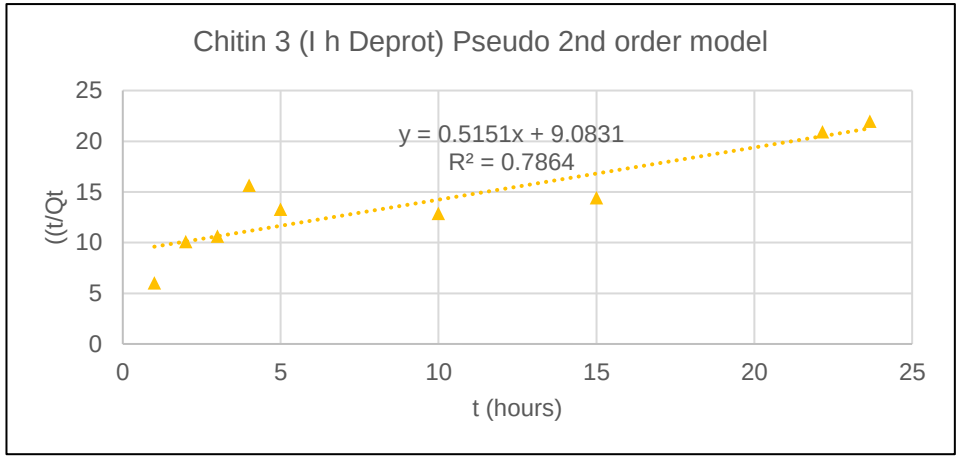

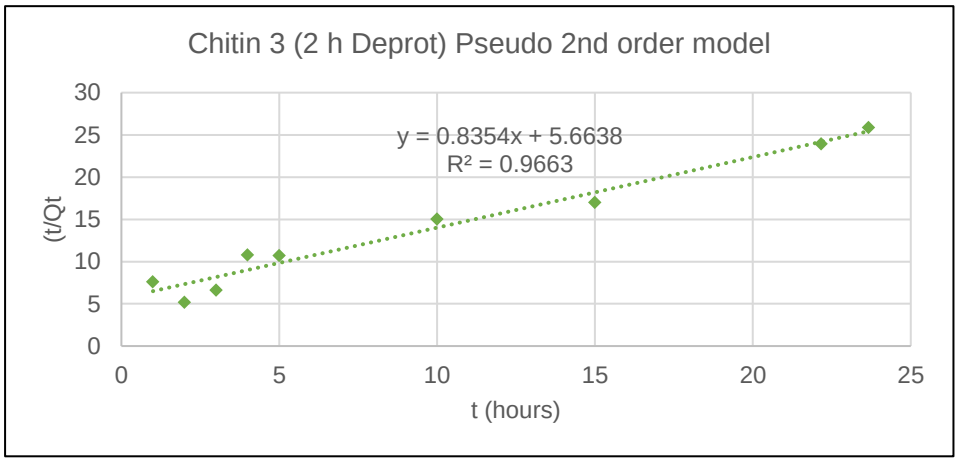

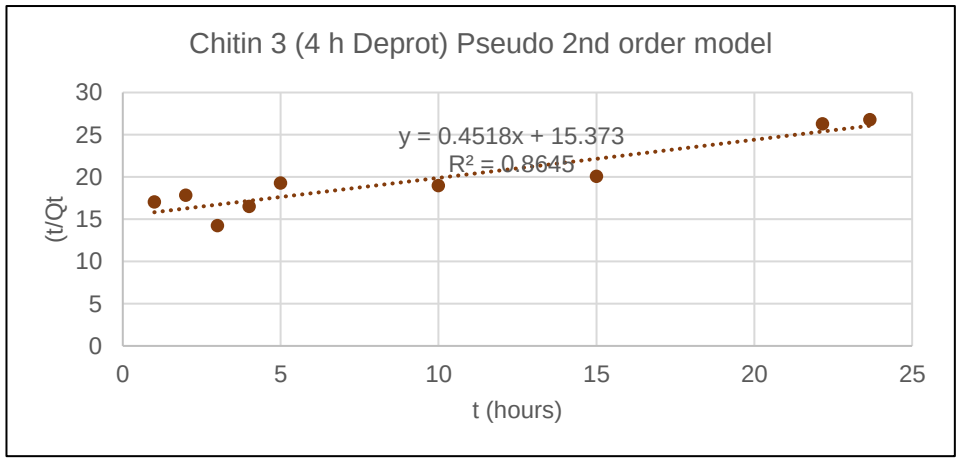

Figure A7. 4: Chitin 3 (1 h Deprot)-(Cu/Fe leachate), Chitin 3 (1 h Deprot), Chitin 3 (2 h Deprot) and Chitin 3 (4 h Deprot) copper adsorption Pseudo 2nd order kinetic model linear fit.

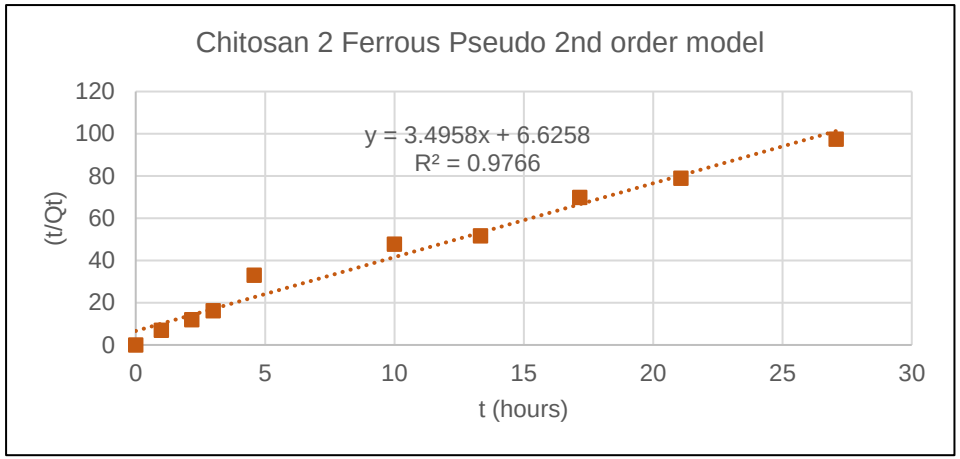

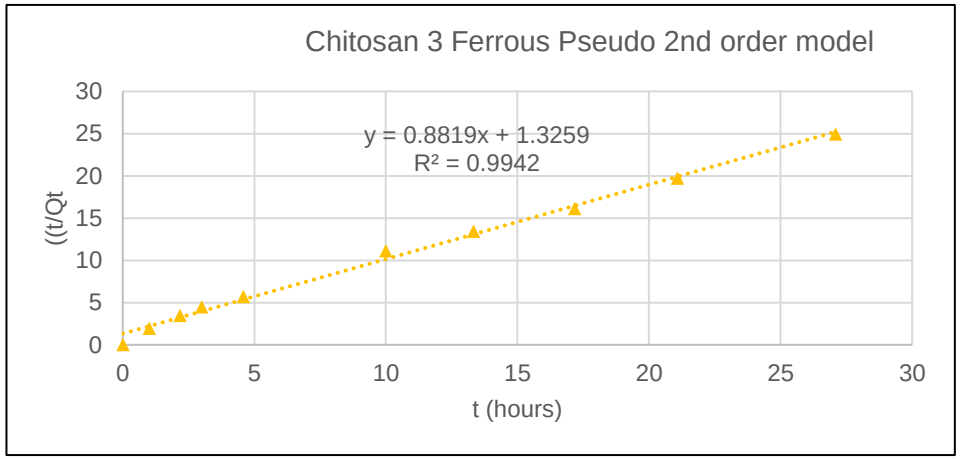

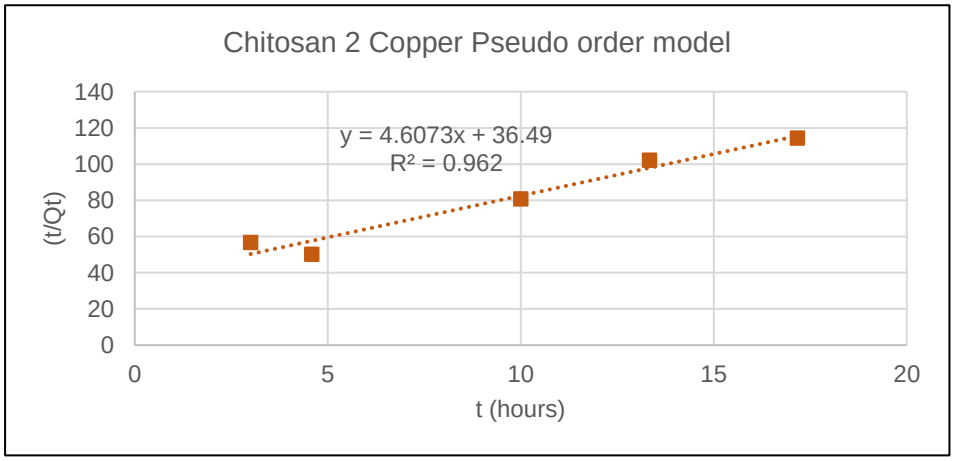

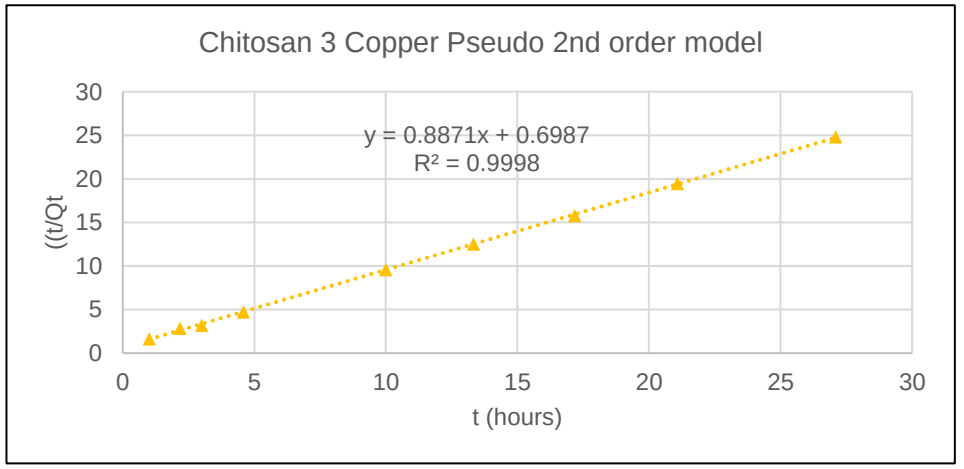

Figure A7. 5: Chitosan 2, Chitosan 3 ferrous and copper adsorption Pseudo 2nd order kinetic model linear fit.

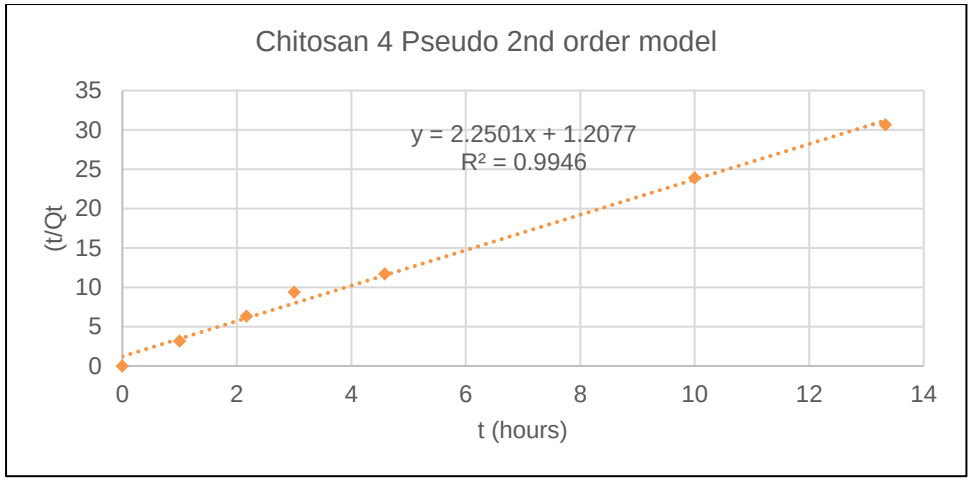

Figure A7. 6: Chitosan 4 copper adsorption Pseudo 2nd order kinetic model linear fit

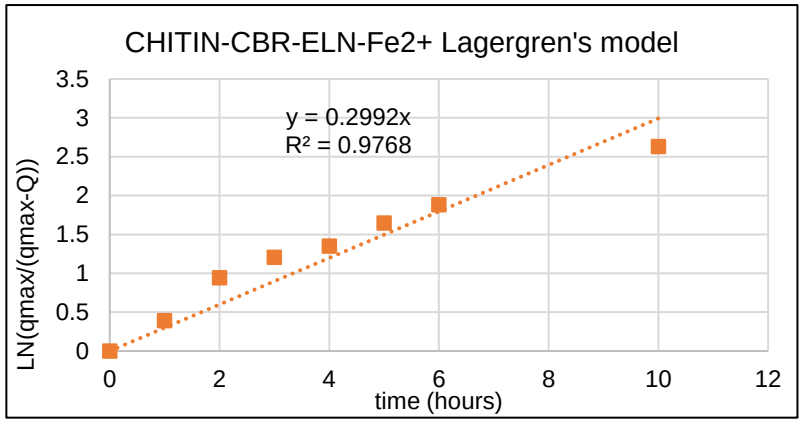

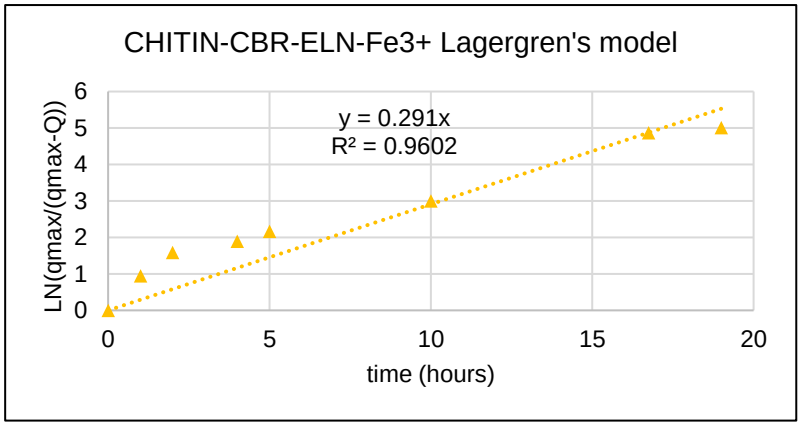

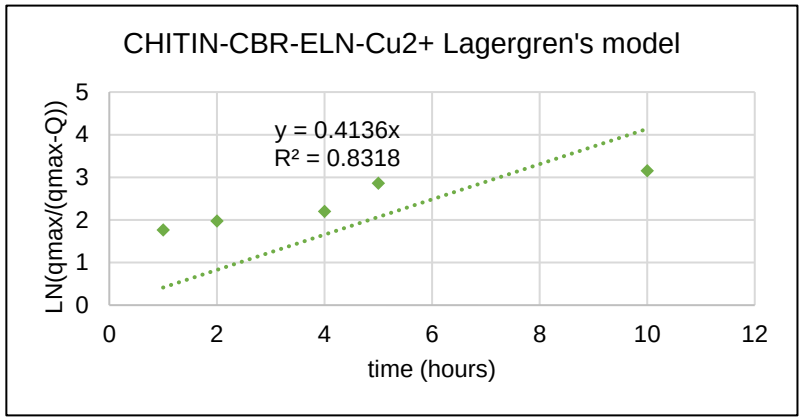

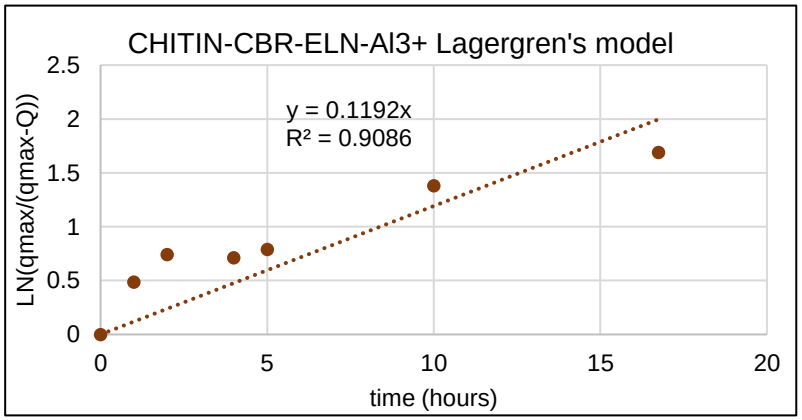

Figure A7. 7: CHITIN-CBR-ELN ferrous, ferric, copper and aluminium adsorption Pseudo1st order kinetic model linear fit

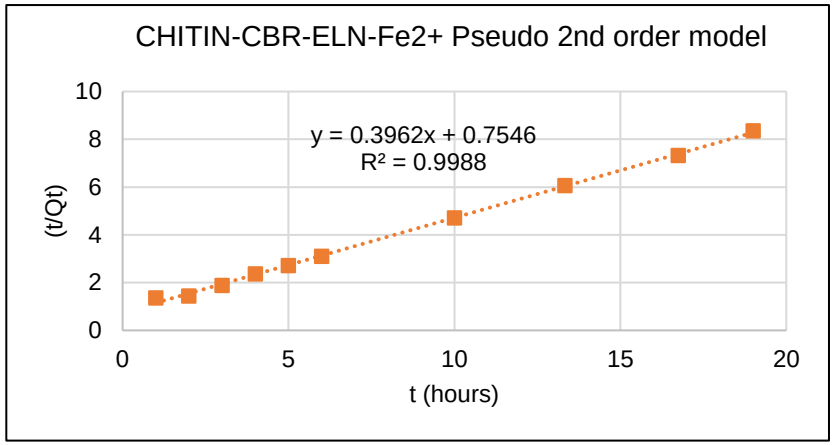

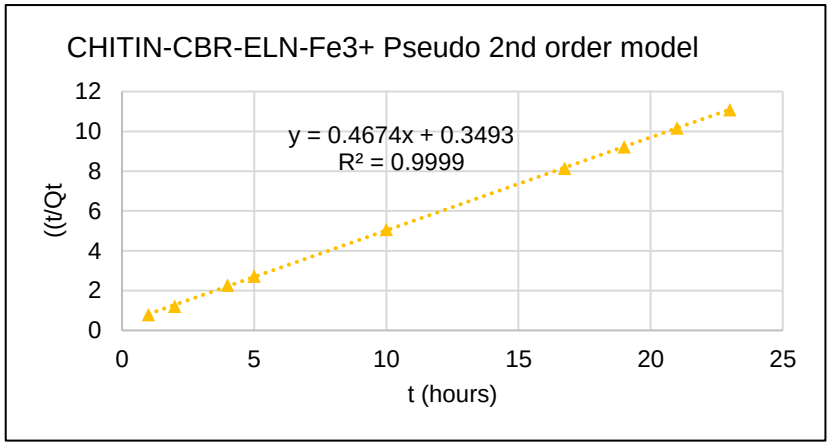

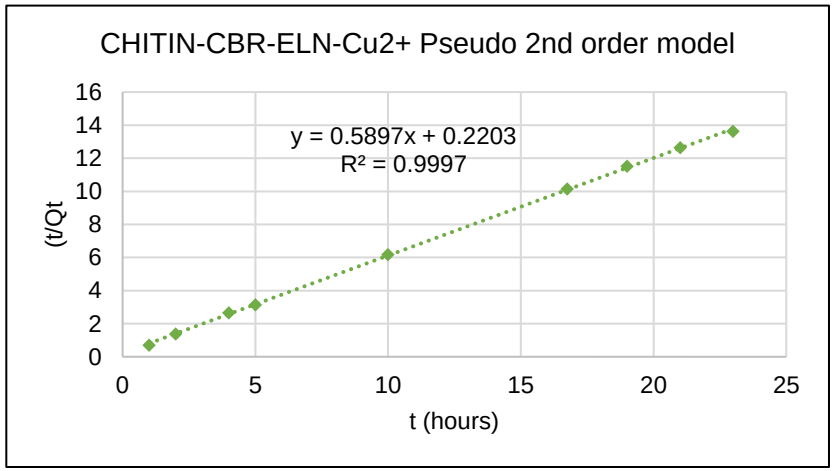

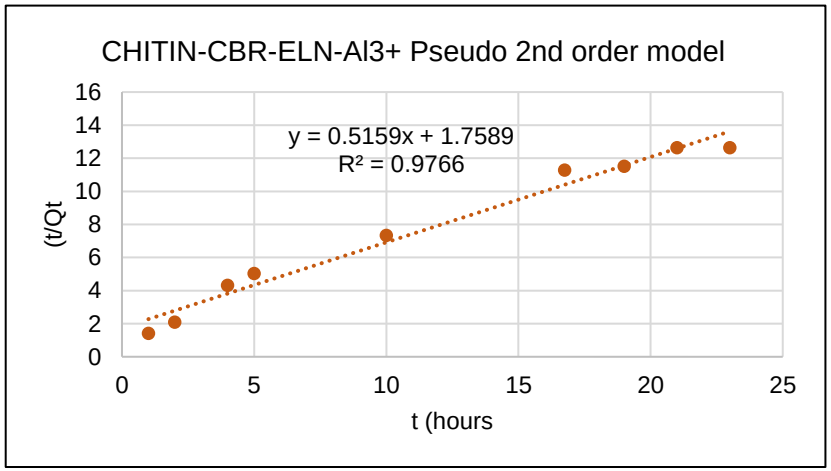

Figure A7. 8: CHITIN-CBR-ELN ferrous, ferric, copper and aluminium adsorption Pseudo 2ndt order kinetic model linear fit

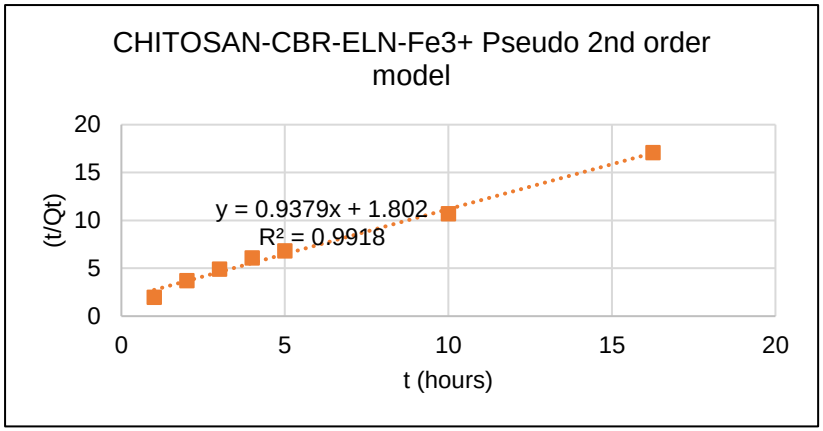

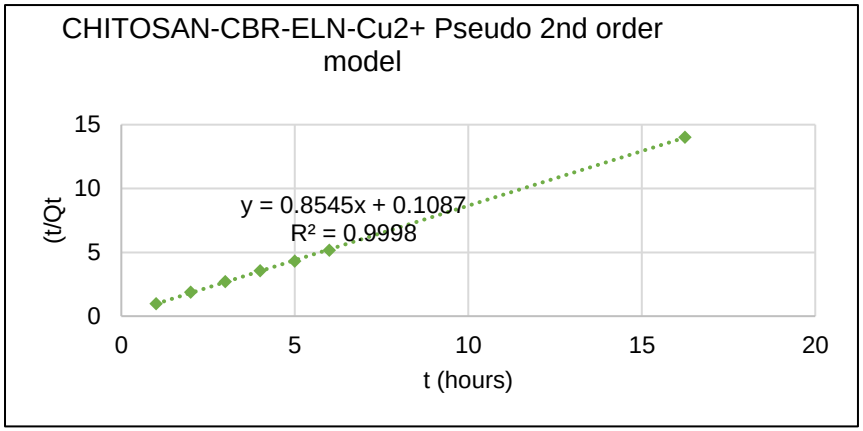

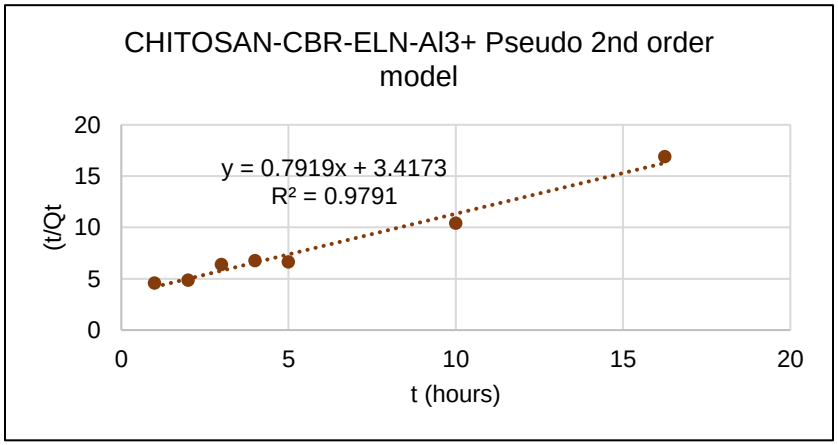

Figure A7. 9: CHITOSAN-CBR-ELN ferric, copper and aluminium adsorption Pseudo 2ndt order kinetic model linear fit